Characterisation and *in vitro* simulation of the natural hip

Rachel Louise Pallan
(CEng, MEng, Hons)

Submitted in accordance with the requirements for the degree of
Doctor of Philosophy

The University of Leeds

School of Mechanical Engineering

September 2016

The candidate confirms that the work submitted is his/her own and that appropriate credit has been given where reference has been made to the work of others.

Acknowledgements

I can honestly say I have never been happier than the moments I have just spent writing the last few words of my thesis. To say it has been a challenge is an understatement. It's been a rollercoaster where I have both hated and loved this PhD. I can't even put into words the gratitude I have for the people who kept me sane throughout this journey and for laughing with me, not at me, during my many failed attempts at science.

I would like to acknowledge the EPSRCs support of the DTC who fully funded my research under the supervision of Dr S Williams, Prof J Tipper and Prof J Fisher. Therefore, my first thanks, out of a long list, goes to my supervisor, Sophie Williams. She has shown immense support and patience throughout my PhD, without her guidance and knowledge this work would not have been possible. She has been a fantastic mentor who has believed in me and encouraged me throughout this journey and has even taught me a few dance moves along the way. There has never been a moment where she hasn't made time for me and her enthusiasm has never faltered, for that I am truly grateful. I would also like to thank my co-supervisors Joanne Tipper and John Fisher, for their guidance and support. Their time and commitment has been greatly appreciated throughout the years.

I would also like to thank all members of the iMBE, at some point; somehow, they have all played a role in supporting me and the work I have carried out at the University of Leeds. Special thanks go out to Hazel Fermor, Abdel Abdelgaied, Tony Herbet and Dawn Groves for their training and assistance as well as the technicians who have fixed and made numerous components for me.

My family have been unbelievable throughout this journey and have provided a never ending source of support and encouragement. They have never doubted me and have been there for every obstacle I have overcome to allow me to do what I could have only dreamt of. I would like to thank them from the bottom of my heart, without them I would not have been where I am today. To Rob, I am truly grateful for driving the numerous miles you did over the four years to come and see me, for loving the many sides of me you have seen throughout my PhD and for keeping me company on the flight to Las Vegas for ORS. To my friends, I am truly grateful for never complaining at my absence and especially Viv, who for the last 17 years has not only been by my side supporting me has waited for me to finish writing my thesis so we can plan her wedding.

Abstract

Abnormal hip joint morphology, associated with diseases such as femoroacetabular impingement (FAI) or developmental dysplasia of the hip (DDH), is thought to be a precursor of osteoarthritis (OA) in the hip. Changes in joint morphology alter the loading pattern through the hip, which results in damage to the tribological interface, including labral tears and/or labral-cartilage separation. Evidence shows that early intervention to repair the labrum is more beneficial than labral excision; however scientific understanding of the tissue and the effect of surgical treatments are limited. It is hypothesised that an *in vitro* natural hip simulation system could be used in biomechanical testing of hip joint tissues as well as generating labral damage which could be used to assess current and new surgical treatment methods for the labrum.

Initial quantitative assays revealed human and porcine labral tissue to have higher collagen content but lower water and GAG content than articular cartilage. Histological staining identified the structure of collagen within the labrum and cartilage, as well as the dispersion of GAGs, in human and porcine tissue. Slight differences were seen between the two species with the human labrum containing more connective tissue compared to the porcine labrum, which was primarily composed of fibrocartilage, and less GAGs. Mechanical tests identified little variation between the compressive properties of the human and porcine labrum however, larger differences were identified in the tissues tensile properties, where by the human labrum was stronger than the porcine labrum. Labral tissue was also found to be weaker in compression in comparison to cartilage tissue.

An *in vitro* natural hip model was successfully developed using clinically relevant conditions. The cup inclination angle was set at 45 °, a full ISO14242 gait cycle was applied to the joint with a peak load of 750 N, to account for porcine tissue. No labral or cartilage damage was observed after 10800 cycles. *In vitro* labral damage was also successfully developed, by increasing the acetabular cup angle to 60 ° and increasing the load by 50 %. The model was run through the full gait cycle for a minimum of 10800 cycles. Damage was classified using the Outerbridge and Lage systems. All types of labral damage outlined in the Lage classification system were identified within the model. Labral damage was found to progress from labral flattening, to radial fibrillation followed by longitudinal peripheral tears.

The methodology and findings within this study can be used in future studies and can be advanced to mechanically test the soft tissues of the hip in situ, as well as the effect of labral damage on the functions of the hip joint and potential labral treatments.

Table of contents

List of figures

List of tables

Abbreviations

2D	Two-dimensional
3D	Three-dimensional
AA	Abduction-adduction
ANOVA	Analysis of variance
AP	Anterior-posterior
BSA	Bovine serum albumin
BW	Body weight
C/B	Cartilage bruising
C/C	Colour change
C/D	Cartilage damage
Ce/D	Cement damage
CL	Confidence limit
CoCr	Cobalt-chromium
CoR	Centre of rotation
CT	Computed tomography
DAB	Diaminobenzidine
DIR	Displacement including instantaneous response
DDH	Developmental dysplasia of the hip
DSR	Displacement from shaft release
ECM	Extracellular matrix
DMB	Dimethylene blue
EDTA	Ethylenediaminetetraacetic acid
FAI	Femoroacetabular impingement

FE	Flexion-extension
FEA	Finite element analysis
GAG	Glycosaminoglycan
H&E	Haematoxylin and eosin
IE	Internal-external rotation
ISO	International Organization for Standardization
L/D	Labral damage
L/F	Labral flattening
L/P	Labral peripheral
LVDT	Linear variable differential transformer
NBF	Neutral buffered formalin
ML	Medial-lateral
MRI	Magnetic resonance imaging
OA	Osteoarthritis
PBS	Phosphate buffered saline
PMMA	Polymethylmethacrylate
R/F	Radial fibrillation
SEM	Scanning electron microscopy
S/W	Stripe wear
TAL	Transverse acetabular ligament
TBS	Tris buffered saline
UK	United kingdom
UTS	Ultimate tensile stress

Chapter 1

Introduction

1.1 General introduction

The hip joint is the second largest weight bearing joint in the body, and is highly adapted to its function to allow for load transmission and large ranges of motion to the lower body (Clarkson 2005; Al-Obaid et al. 2007). The morphology of the hip joint plays a key role in its stability, hence when modifications to the structure occur, it can result in catastrophic damage (Bredella 2011). The soft tissues within the hip also aid in its ability to function. The composition of articular cartilage varies compared to that of the closely associated acetabular labrum, giving them the ability to perform specific functions. The articular cartilage's function is to aid in the movement of the hip whilst minimising contact stresses, whereas the labrum's function is to increase stability and seal the joint (Petersen et al. 2003; Athanasiou et al. 2009; Link 2011). Damage can occur independently to the bony structure of the hip or to the soft tissues within the joint. Soft tissue damage to the articular cartilage or labral tissue within the hip joint can be a direct result of the abnormalities in the bony structure; leading to abnormal joint loading, or as a result of trauma or disease which independently affects the tissue (Ferguson et al. 2003; Berry & Lieberman 2012).

OA is the most common joint disease, affecting around 8.5 million people in the UK in 2012 (Smith 2012), however little is known about the etiology of the disease. FAI and DDH are both associated with the initiation of OA and characterised by alteration in geometry and altered contact mechanics. They cause damage to the soft tissues of the hip due to altered mechanical stresses (Ferguson et al. 2003; Ganz et al. 2008; Talmage 2009). It is therefore crucial to gain an understanding of how the morphology of the hip impacts on soft tissue damage, in order to develop an understanding of the causes of hip joint diseases.

1.2 The human hip

In the human body, the hip joint is significantly larger and more stable than many other joints and has the ability to allow for large ranges of motion (Frankel & Pugh 1984; Nordin & Frankel 2001). It is composed of two bones; the head of the femur and the acetabulum of the pelvis, connected together by internal and external ligaments (Figure 1-1). Due to the femoral head and acetabulum's conformity, they form a moderately stiff ball and socket joint, providing the hip with its intrinsic stability (Frankel & Pugh 1984). In order to produce the large ranges of motion required for everyday activities such as walking, sitting, bending and squatting, the joint must be precisely aligned and controlled (Frankel & Pugh 1984; Nordin & Frankel 2001).

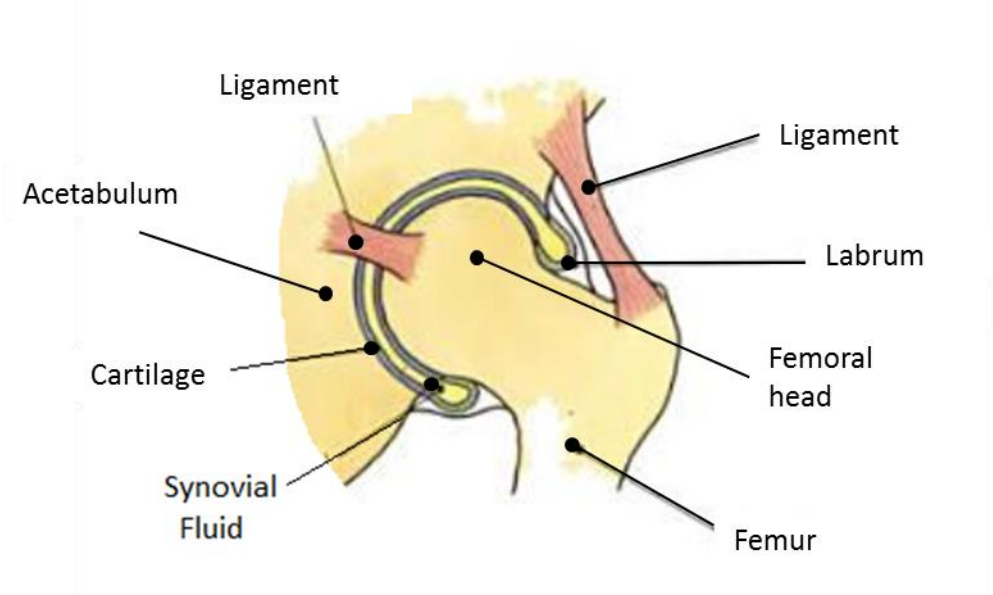

Figure 1-1 The synovial hip joint. The capsule surrounding the hip joint. Diagram adapted from Johnson et al. (2004).

The role of the hip joint is to allow for large ranges of motion whilst withstanding high mechanical loads (Whiting et al. 2006). It is capable of this due to the aid of the soft tissues within the joint. The articulating surfaces of the hip joint are protected by a smooth layer of articular cartilage, both cushioning the bone and allowing for effortless movement (Drake et al. 2012). As well as articular cartilage, there is a fibrocartilaginous lip around the acetabulum, known as the labrum, creating a deeper socket, to provide further stability (Figure 1-1, Ferguson et al. 2001). The labrum transitions directly into the articular cartilage, known as the labral-cartilage junction, and directly to the acetabular rim, on both the articulating and non-articulating surfaces (Lewis & Sahrmann 2006). The hip joint is surrounded by a loose joint capsule, known as a synovial membrane, giving the hip joint its name as a synovial joint. Synovial fluid is produced by the synovial membrane, which has the ability to absorb and secrete, and is responsible for the supply of nutrients to articular cartilage.

1.2.1 Healthy hip joint anatomy

The conformity of the hip joint plays an important role in the stability of the joint (Radin 1980). The acetabulum is a concave surface making the 'socket' component of the ball and socket configuration, whilst the femoral head is a conforming convex surface, producing the 'ball' component of the ball and socket configuration. The femoral head is two-thirds of a sphere and is slightly compressed in an approximate anterior-posterior (AP) direction, whilst the acetabulum is shaped like a horse-shoe (Figure 1-2, Rydell 1973; Radin 1980; Nordin & Frankel 2001). The femoral neck is approximately 30-40mm long and lies in the lateral direction to the head. At its medial end the femoral neck is virtually cylindrical, with its shape becoming increasingly elliptical towards its distal end (Rydell 1973).

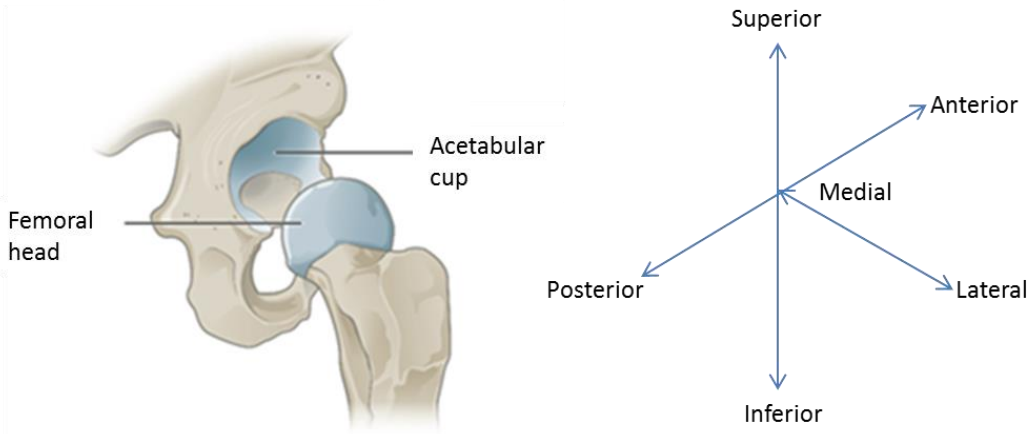

Figure 1-2 Anatomical terms of location of the hip. A posterior view of the pelvis and acetabulum and their orientation within the body. Image adapted from OpenStax College, (2013)

The acetabulum and femoral head provide the hip joint with some elasticity due to their trabecular bone composition. The deformable bone allows the joint to undergo essential spreading during loading, reducing the stress placed on the articular cartilage to a tolerable magnitude. When the acetabulum is unloaded its diameter is smaller than that of the femoral head, allowing it to undergo elastic deformation to become congruous around the femoral head during loading, resulting in maximum contact area and congruence, as seen in Figure 1-3. In a congruous hip the contact area is formed around the periphery of the anterior, superior and posterior articular surface of the acetabulum. If the joint was congruent under no load, during loading the acetabulum and femoral head would be incongruent, resulting in a reduced contact area against the acetabulum and increased force (Radin 1980; Konrath et al. 1998; Nordin & Frankel 2001).

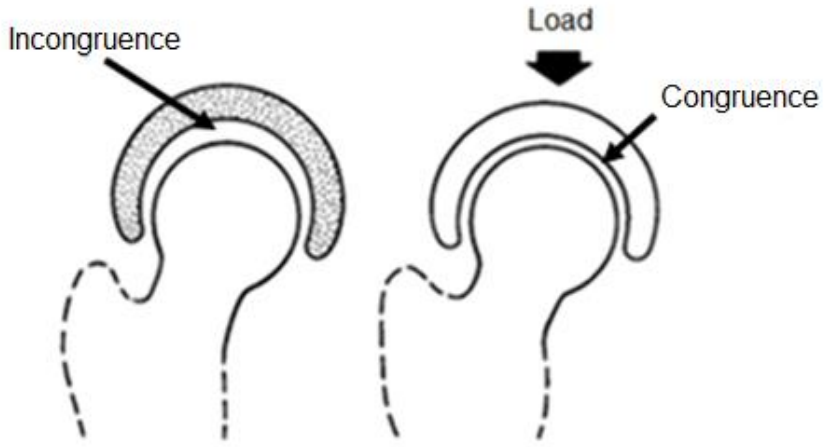

Figure 1-3. **Elastic deformation of the acetabulum.** The acetabulum is seen before and after deformation, where it deforms around the femoral head congruently, image adapted from Radin, (1980).

1.2.2 Healthy hip joint biomechanics

There has been a great deal of research into the kinematics and kinetics of the hip, providing surgeons with a greater understanding of the vast mechanical disorders of the hip and enabling them to develop successful surgical treatments to improve or restore natural function. Research into the biomechanics of the hip produces a clear understanding of the mechanical characteristics of the joint structure, the key relationships between the internal and external loads, and the direction of the joint and muscles forces (Frankel & Pugh 1984).

1.2.2.1 In vivo kinematics of the healthy hip joint

The natural hip joint allows for almost unrestricted rotation, with a gliding surface motion of the femoral head articulating against the acetabulum and labral tissue (Monkhouse 2007; Loudon et al. 2013). The rotation of the femoral head in the acetabulum can be characterised in three planes (sagittal, frontal and transverse, Figure 1-4) around the femoral head's centre of rotation (CoR). Rotation is greatest in the sagittal plane, followed by the transverse and frontal plane (Table 1-1, (Nordin & Frankel 2001; Khurana 2009). Although rotation is relatively unlimited, subluxation (dislocation) of the hip joint and translation in the anterior/posterior and medial/lateral direction is limited (Stewart & Hall 2006).

Table 1-1 **Full ranges of motion of the natural hip joint** (Nordin & Frankel; 2001).

Plane	Direction	Range
Sagittal	Flexion	0°-140°
Sagittal	Extension	0°-15°
Frontal	Abduction	0°-30°
Frontal	Adduction	0°-25°
Transverse	Internal Rotation	0°-90°
Transverse	External Rotation	0°-70°

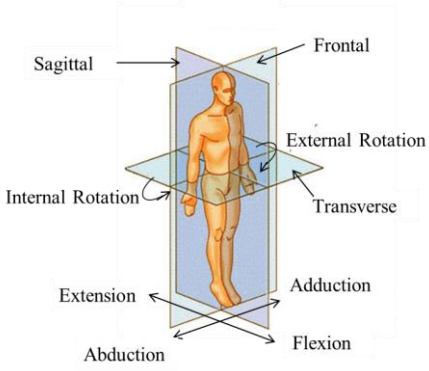

Figure 1-4 Anatomical planes and rotations of the natural hip joint. Sagittal, transverse and frontal plane of the human body with flexion-extension, abduction-adduction and internal-external motion.

The range of motion that the hip is capable of producing far exceeds the requirement of daily activities. Activities such as walking and climbing stairs require relatively small ranges of motion; however activities such as tying shoes, sitting and squatting are a lot more demanding on the hip (Table 1-2, Stewart & Hall 2006). During gait, the hip joint undergoes maximum flexion in the late swing phase, as the leg moves forward for heel strike and experiences maximum extension at toe-off. Maximum adduction and internal rotation is experienced during the stance phase and abduction and external rotation during the swing phase (Figure 1.6, Nordin & Frankel 2001).

Table 1-2 **Ranges of motion of the hip during daily activities.** Table adapted from Nordin & Frankel (2001); Stewart & Hall (2006).

Plane	Walking	Climbing Stairs	Tying Shoes	Sitting	Squatting
Sagittal	30°	67°	129°	104°	122°
Frontal	9°	16°	18°	20°	28°
Transverse	7°	18°	13°	17°	26°

1.2.2.2 In vivo kinetics of the healthy hip joint

Kinetic studies on the hip joint have enabled the moments and forces, produced by external loads, body weight (BW) and muscle action, to be determined. A clearer understanding of the *in vivo* forces acting on the hip can aid in minimising abnormal loading of the hip, which can result in degenerative joint diseases, as well as developing clinical solutions for surgical procedures to reduce or eliminate pre-existing hip conditions (Komistek et al. 2005).

During everyday activities the hip supports large loads, requiring large muscle groups to stabilise the joint. The determination of the loading across the hip can be complex due to the vast ranges of movement the hip is capable of producing, as well as the large number of muscle groups involved in the movements. Although there are a range of methods for determining the joint reaction forces of the hip, a simplified free-body technique for coplanar forces or a mathematical model of the equilibrium equations have proven popular. Kinetic studies can be separated into two types; static forces that act during one-legged or two-legged stance and forces that act during dynamic motion (Paul 1966; Nordin & Frankel 2001).

During two-leg stance, the centre of gravity passes posterior to the pubis symphysis and close to the frontal plane between the centre of the two femoral heads (Figure 1-5). As the centre of gravity is essentially through the middle of the body, theoretically an erect stance is possible with little or no muscular force. This is possible due to the stabilising of the joint capsule and capsular ligaments. During two-leg stance the hips support 62% of the BW; hence if the body is symmetrical, each hip will carry 31% of the BW (Maquet 1985; Nordin & Frankel 2001).

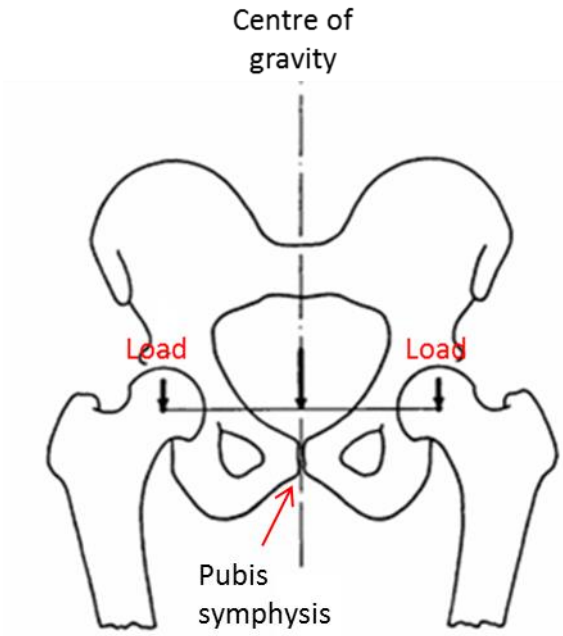

Figure 1-5 Centre of gravity through the pelvis during stance. The centre of gravity is located close to the frontal plane through the centre of the two femoral heads, taken from Maquet (1985)

During single-leg stance, an individual hip will carry 81% of the total BW, resulting in an eccentric load on the hip, causing the pelvis to tilt and the hip to become adducted. The centre of gravity becomes altered in all three planes, causing forces from the muscles to counteract the moments around the hip, resulting in a joint reaction force. An alteration in the centre of gravity,

and hence the lever arm length of the gravitational force, determines the magnitude of the moments about the hip, and therefore the joint reaction force (Maquet 1985; Nordin & Frankel 2001).

There have been several studies on the loads of the hip joint during dynamic activity, with a range of magnitudes for peak joint loading (Maquet 1985; Nordin & Frankel 2001; Stewart & Hall 2006). A study by Paul (1976) calculated the resultant hip joint forces during the gait cycle at slow (1.10 m/s), medium (1.48 m/s), and fast (2.01 m/s) pace walk in 36 subjects. Two peak forces were identified just after heel-strike and just before toe-off. At a slow pace, peak loads of approximately 3 and 4 times body weight were identified at heel strike and toe-off respectively. At a medium pace average peaks at 4 and 5 times body weight were identified and at a face pace peak loads were as high as approximately 7 and 8 times body weight during heel strike and toe-off respectively (Figure 1-6).

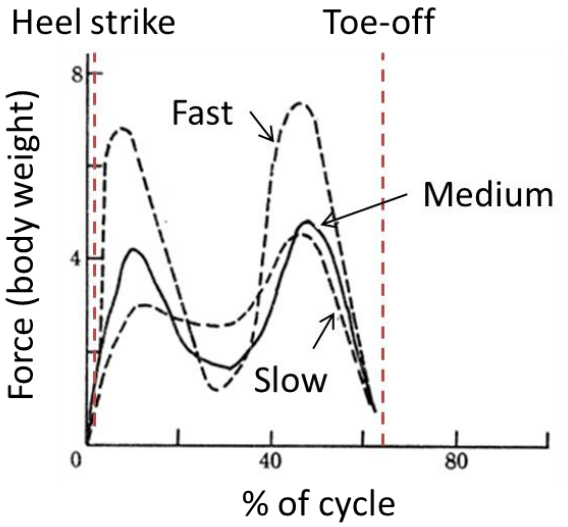

Figure 1-6 Hip joint reaction forces during gait. The resultant hip joint forces during gait are shown for a range of walking paces, adapted from (Paul, 1976).

1.2.3 Abnormal hip joint biomechanics

There are many different conditions that result from abnormal biomechanics of the hip. Any disorders of the hip can alter the stress distribution through the cartilage and bone. Any damage that occurs in the hip can be further progressed due to the large forces that occur at the joint. Abnormalities in the hip joint often result in OA (Frankel & Pugh 1984; Nordin & Frankel 2001).

Alterations in the femoral neck-to-shaft angle are known as either coxa valga or coxa vara conditions, which alter the lever arm of the abductor muscles resulting in elevated joint reaction forces. An alteration to the acetabular anteversion angle can result in exposure of the femoral head, causing the hip to compensate with either internal or external rotation to avoid dislocation.

Incongruity of the femoral head and acetabulum leads to an increase in load due to a smaller surface contact area, resulting in abnormal compression or distraction of the articular cartilage (Radin 1980; Nordin & Frankel 2001). If the trabecular bone of the hip undergoes extreme deformation, microfractures result and when combined with prolonged abutment, bone remodelling and stiffening of the underlying network may appear. Bony abnormalities are seen in diseases such as DDH and FAI discussed later in this report (Radin 1980).

1.3 Cartilage

Cartilage is a flexible, connective tissue, defined in three categories; elastic cartilage such as the ear, hyaline cartilage found in synovial joints, and fibrocartilage such as the meniscus in the knee. Differences in cartilage composition and structure are most recognisable by their extracellular matrix (ECM); with hyaline cartilage consisting mainly of cartilage-specific collagen type II, fibrocartilage containing a mixture of collagen type I and II, and elastic cartilage containing elastic fibres. The significant difference between cartilage and any other connective tissue is its lack of blood vessels, resulting in low potential for self-renewal and is dependent on diffusion for nutrients and waste extraction. Cartilage also lacks nerves; hence early diagnosis of damage is often prohibited due to damage being asymptomatic (Yannas 2005; Bucholz 2012; Eroschenko et al. 2012).

Articular cartilage is a form of hyaline cartilage, enveloping the articulating surfaces of synovial joints. It is a highly resilient, complex, composite tissue, which is smooth and stiff in texture and pale whitish-blue in colour. Articular cartilage has a thickness ranging from 1.15mm to 1.78mm across the surface of the femoral head and acetabulum (Mechlenburg et al. 2007). Its function is to "provide a low-friction, wear-resistant surface that can withstand large loads during constant use" by increasing the contact area to disperse the load. During load support and transfer, articular cartilage allows for translation and rotation between bones (Athanasiou, et al. 2009).

Due to articular cartilage's high metabolic nature it can adapt to a weakened condition, however once its collagen network becomes disorganised the changes that occur are thought to be permanent. Articular cartilage's function is highly demanding and due to a lower regenerating capacity than degradation rate, articular cartilage frequently fails to cope with the demand placed upon it.

1.3.1 Cartilage macrostructure

Articular cartilage has a specialised composition, with a highly anisotropic, inhomogeneous structure. Its uniquely organised formation enables it to endure high mechanical loads for many years and possibly over the lifespan of an individual. The structure of the tissue varies greatly from the articular surface down to the bone interface, with changes occurring in the collagen fibril network organisation, the concentration of its nutrients, cell morphology, and its mechanical properties.

Articular cartilage can be characterised by four main regions; the superficial zone, the middle (or transitional) zone, the deep zone and the calcified cartilage zone (Figure 1-7). By far, the largest of the four zones is the middle zone, accounting for 40-60% of the total thickness, with the deep zone and superficial zone decreasing in size, accounting for 30% and 10-20%

respectively. The calcified cartilage zone can account for up to 8% of cartilage thickness (Müller-Gerbl et al. 1987; Narayan 2009). The calcified cartilage zone is used to anchor the base of the articular cartilage to the subchondral bone and is separated from the deep zone by the tide mark (Julkunen et al. 2007; Narayan 2009). There is great debate over the function of this zone with Williams et al (2007) stating that it is predominantly thought to prevent nutrients from exiting the underlying bone, making articular cartilage dependent on synovial fluid for its nutrient supply; however Y. Zhang et al. (2012) believes the role of the calcified cartilage zone to be for force transmission and nutrient diffusion. The superficial zone has a significant role in providing the mechanical properties of articular cartilage and it is often this zone where earliest degenerative signs appear.

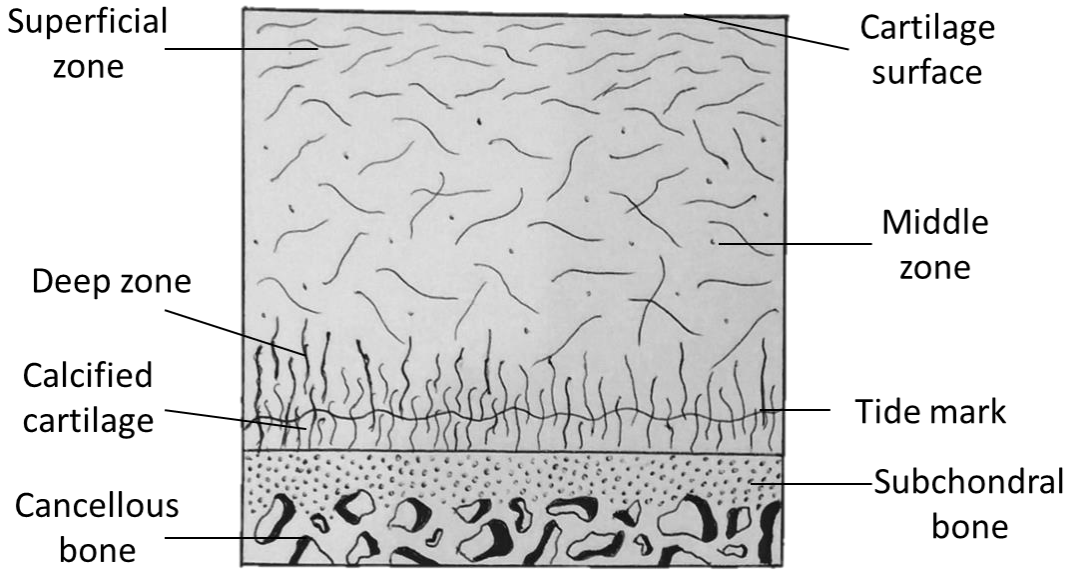

Figure 1-7 Zones of articular cartilage. Articular cartilage zones showing collagen fibrils and alignment adapted.

1.3.2 Cartilage microstructure

Cartilage has a fibrous structure, composed of collagens, proteoglycans, interstitial water and chondrocytes as well as minor components such as non-collagenous proteins. Collagens, proteoglycans and other proteins contribute to 20-40% of cartilages wet weight with the remainder being taken up by interstitial water (Table 1-3). Collagen fibres are cross-linked with a proteoglycan gel to provide support and structure to the tissue, as well providing a framework for other macromolecules and water to bind to.

Table 1-3 **Approximate fractional composition of articular cartilage**. Composition of articular cartilage broken down by percentage of total tissue volume, taken from Link (2011).

Content	Fraction (%)
Water	80
Collagen Type II	10
Proteoglycans	8
Other Cartilage-specific Collagens (IX, X, XI)	<1
Other Proteins	<1
Inorganic Salts	<1

1.3.2.1 Collagen

Collagen has an axial, periodic structure, constructed of long fibrils. Fibrils are responsible for proving and maintaining the structure of the biomechanical matrix which cells and macromolecules adhere to (Kadler et al. 1996). Within articular cartilage, collagen fibres account for 60% of cartilages dry weight and are the main component of the ECM (Johnson et al. 2007). Their arrangement produces an orientated fibril network, providing the tissue with its elastic properties; such as tensile strength and stiffness. The principle collagen found in articular cartilage is type II collagen, accounting for 90-95% of the total collagen content, however smaller concentrations of other collagens such as collagen VI, IX, X and XI are also present. The core for type II collagen fibrils is produced by the XI collagen, which is thought to be responsible for controlling fibril growth. IX collagen is periodically connected to type II collagen via covalently cross-linked bonds. It is thought to have a significant function in the binding of proteoglycans to the matrix and in the structural integrity of collagen fibril formation, hence disruption to the type IX-type II bond may initiate cartilage degeneration. Type VI collagen is located, in small quantities, in the pericellular region of the chondrocytes. It is thought to function alongside collagen IX as an adhesion molecule for the chondrocytes, enhancing stability of the ECM. Minor collagens such as types X, XII and XIV are thought to assist in the formation and stability of the primarily assembled principle type II collagen. Type X collagen is thought to be specifically related to controlling the mineralisation of the cartilage matrix, whilst types XII and XIV are thought to provide cohesions between the extrafibrillar matrix and collagen fibres (Martin et al. 1998; Seibel 2006).

Throughout the structure of cartilage, collagen fibres vary in formation as well as size, with the smallest fibres located in the superficial zone. Here the collagen fibres are orientated parallel to the cartilage surface, with an unconfined direction within this plane. This in-plane orientation is thought to develop due to the joint movements and principle stress directions, effectively resisting the loads the cartilage is placed under (Mononen et al. 2012). Deeper into the tissue,

around the transitional zone, fibres become more random in orientation, arching from parallel to the surface to radial in orientation as well as becoming larger in diameter compared to those in the superficial and deep zone. In the deep zone, collagen fibres are largest in order to anchor the cartilage to the subchondral bone and are primarily located perpendicular to the surface (Mow & Huiskes 2004; Narayan 2009; Mononen et al. 2012).

1.3.2.2 Proteoglycans

Proteoglycans are dispersed throughout the fibril network of the ECM. They consist of a protein core of hyaluronan, to which multiple highly anionic GAG side chains are covalently bonded (Lohmander 1988; Yanagishita 1993). Proteoglycans account for around 20% of the tissue's dry weight and have a highly negative fixed charge, allowing them to bind and retain water within the matrix. Proteoglycans negative charge provides an osmotic pressure, allowing the tissue to resist compressive loads, whilst the connection to the water molecules regulates internal fluid transportation, giving the tissue its time-dependent viscous properties (Lohmander 1988; Bader et al. 1992). The highest concentration of proteoglycans is found in the deep zone with concentrations decreasing up to the superficial region.

Cartilage tissue's major biological function is developed from the physiochemical properties of the GAG, providing hydration and swelling pressure to give the tissue rigidity and structural integrity (Yanagishita 1993). There are different varieties of GAGs, aggrecan is composed of mainly chondroitin sulfate and keratin sulfate, which are two of the most abundant GAGs, found in articular cartilage. They play an important role in the hydration of the tissue and give cartilage its gel-like properties and resistance to deformation (Yanagishita 1993).

1.3.2.3 Interstitial water

Interstitial water is by far the most abundant component of articular cartilage, accounting for around 68-85% of the tissue. It has many significant functions within the tissue, with its primary role to provide lubrication whilst supporting a load. It is also responsible for the swelling of proteoglycans and chondrocytes, as well as providing nutrition and transportation of waste products from the tissue (Lohmander 1988; Narayan 2009; Link 2011). There are two distinct areas in which interstitial water is associated; around 30% of the water is located intrafibrillarly, within the collagenous network whilst the remaining 70% is associated with the proteoglycans, extrafibrillarly, where it can freely exchange during joint loading and unloading (Elices 2000). Interstitial water concentration is most abundant in the superficial surface zone and linearly decreases down to the deep zone. Its volume at any given time is governed by the swelling pressure, produced by the fixed charge density of the surrounding proteoglycans and decreases over time with age. Interstitial water is secured in place due its positive charge, attracting the

highly negatively charged proteoglycans, found within the tissue (Figure 1-8, Elices 2000; Cole & Malek 2004; Mow & Huiskes 2004).

During mechanical loading, fluid flow is restricted through the ECM, due to its small pore sizes and the interaction between the oppositely charged GAGs and water molecules. The intrafibrillar water becomes trapped in the collagenous network, increasing the density of the fixed charges and generating a pressure gradient in the interstitial fluid. This increase in interstitial osmotic pressure or charge-charge repulsion is critical for the tissues ability to support up to 95% of the load applied to it. The further 5% of the load is supported by the stiffness of the ECM (Elices 2000; Mow & Huiskes 2004; Little et al. 2011).

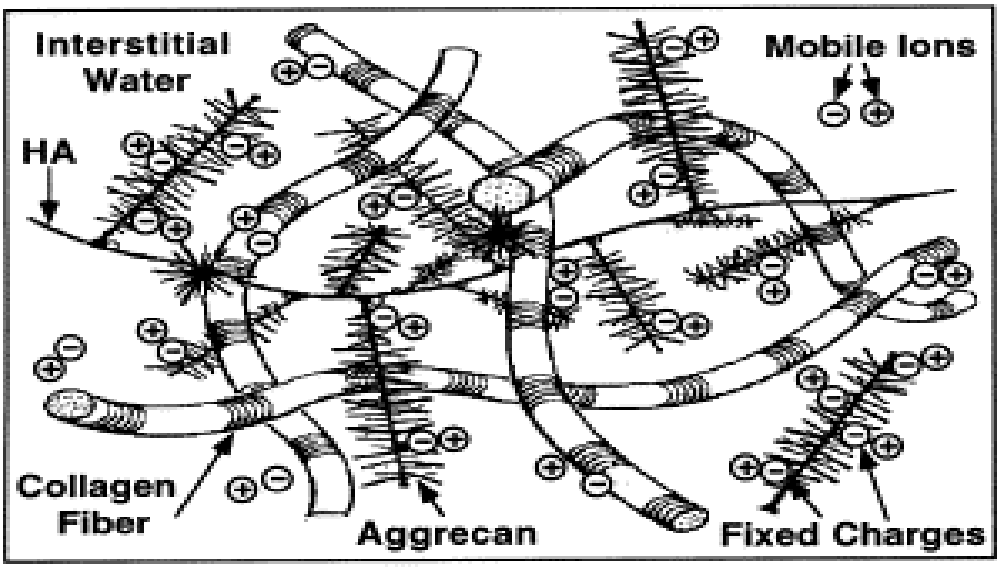

Figure 1-8 Microstructural organisation of articular cartilage. The relationships between interstitial water, collagen fibres and aggrecan, taken from Mow et al. (1998)

When a load is applied to the cartilage, it is immediately supported by the interstitial water throughout the tissue, the cartilage then undergoes slight deformation caused by stress relaxation. If the cartilage remains under load, the interstitial water is forced out of the tissue by creep deformation, further deforming the cartilage. Cartilage deformation reduces contact stresses by increasing the contact area of the tissue. Once the fluid has fully dispersed, the load becomes supported by the collagen fibres in the ECM. When the load is removed, the structure of the matrix returns the cartilage to its original shape and interstitial fluid is restored to its normal level (Mow & Huiskes 2004).

1.3.2.4 Chondrocytes

Chondrocytes are the only cell type found in articular cartilage. They are highly specialised and sparsely distributed throughout the tissue, accounting for around 5% of the tissue weight

(Stockwell 1979; Mirzayan 2006). They are surrounded by the ECM, preventing cell-cell contacts, and receive their nutrients via diffusion from the synovial fluid (Ikada 2006; Nissi 2008). Chondrocytes have a peak metabolic activity rate during growth, in which they undergo replication. Once the cell matures and reaches adolescence, cell division declines and its metabolic activity reduces. Chondrocytes are the only living mediators able to detect and respond to mechanical changes in the tissue. They are able to receive and read a range of environmental signals transmitted from the mechanical loading of the ECM which mediates its function (Stockwell 1979; Nordin & Frankel 2001; Nissi 2008).

Chondrocytes perform both anabolic and catabolic activity in order to maintain the homeostasis of the complex structure of articular cartilage. They are responsible for the synthesis, maintenance and the renewal of all components of the ECM such as collagen, proteoglycans and glycoproteins, as well as being largely responsible for the degradation and turnover of the matrix (Lohmander 1988; Cole & Malek 2004; Mirzayan 2006; Goldring & Marcu 2009; Ottenbrite et al. 2010).

Chondrocytes are distributed throughout the ECM of the tissue and follow the alignment of collagen fibres; with a thin layer of cells parallel to the surface in the superficial zone, randomly orientated cells in the middle zone and vertical columns of cells perpendicular to the subchondral bone in the deep zone (Nissi 2008). Their size, shape and number vary at different cartilage depths, with the cells increasing in size and gaining sphericity from the surface zone down to the subchondral bone. In the upper regions of the tissue, chondrocytes are more elliptical in shape, with their flattest side parallel to the articular surface. Their change in shape and distribution result in metabolic specialisation and create depth-related differences, seen in the various cartilage zones. Chondrocytes can be categorised into four defined groups of spatially organised arrangements, including singles, pairs, strings and clusters. The chondrocyte organisations are orientated parallel to the articular cartilage surface, in the superficial region. Within various joints of the body, the arrangements vary, however within a single joint type; one pattern dominates over the other four in the superficial zone. Studies by Rolauffs et al. (2008 and 2010) have identified the dominant pattern in the knee, ankle, shoulder and elbow, however no studies were identified which determined the spatial pattern in the hip joint.

1.3.3 Cartilage mechanical properties

The mechanical properties of articular cartilage are governed by two main factors; the intrinsic mechanical properties of the constituents, as well as the interaction of these constituents during deformation (Armstrong & Mow 1982). Due to cartilage's non-uniform zones and anisotropic structure, the tissue's mechanical properties vary across the different zones. Articular cartilage also demonstrates different mechanical properties under compression, tension and shear, as well as under creep and stress relaxation (Little et al. 2011).

1.3.3.1 Compressive properties

During motion, the articular cartilage in the hip undergoes compression; when under sustained loading its volume decreases as the pressure placed on it increases. In instantaneous compressive loading, the fluid phase is able to support the load applied by the hip, due to small pore sizes within the matrix, hence protecting the underlying bone of the femoral head and acetabular cup. This reduces the porosity and inhibits water from rapidly exiting the tissue, which in turn increases the density of proteoglycans, increasing the negatively charged concentration. The middle zone of articular cartilage provides the highest resistance to compression, due to its high proteoglycan content, hence it plays a crucial role in joint loading (Little et al. 2011).

1.3.3.2 Tensile properties

Articular cartilage can be placed under tension when two cartilage surfaces slide against each other or when the cartilage is compressed pulling on the surrounding tissue (Callaghan 2003, (Athanasiou, et al. 2009). Articular cartilage gains its tensile properties from both flow-dependent and flow-independent viscoelastic mechanisms (Mirzayan 2006). Its non-linear properties are greatly governed by the collagen fibres within the tissue. During low tensile forces, collagen fibres become straightened, causing them to realign in the direction of loading, demonstrated by the toe-region in stress-strain curves (Figure 1-9). As the tensile force increases, the cross-linked fibres become stretched, increasing the stiffness of the tissue, which can be seen in the linear region of a stress-strain curve (Figure 1-9, Mirzayan 2006; Athanasiou et al. 2009; Little et al. 2011). The tensile properties of articular cartilage are altered by many factors including; depth and orientation within the tissue, collagen fibre density, fibre diameter, level of cross-linking and the strength of the ionic bonds between the collagen and proteoglycan network. The tensile properties of cartilage also differ depending on loading direction, producing higher tensile strengths when orientated along split-lines (parallel to the predominant collagen fibre direction).

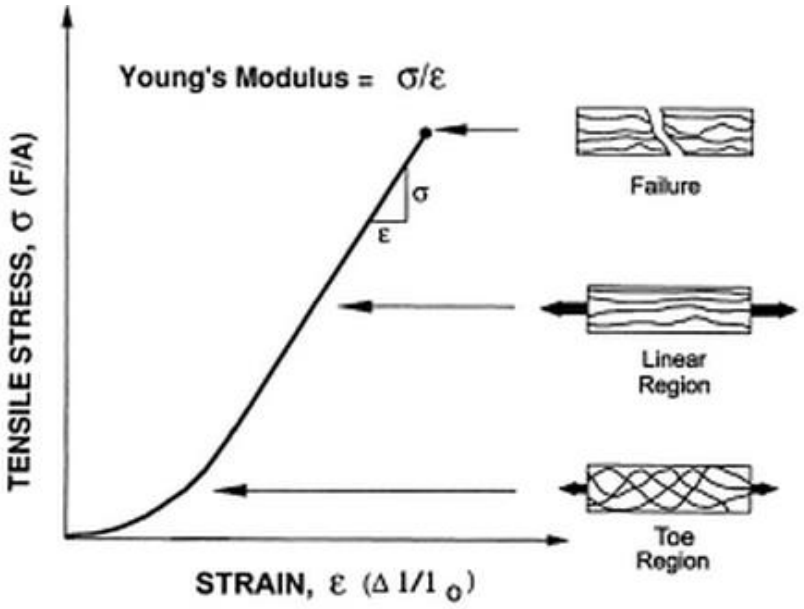

Figure 1-9 Stress-strain curve of articular cartilage. The stress-strain curve of articular cartilage under tensile stress, taken from Mirzayan (2006).

1.3.3.3 Shear properties

Articular cartilage experiences shear stresses throughout its zones. These stresses are generated by typical rotational and translational movement, during everyday activities such as walking and running (Athanasiou, et al. 2009; Little et al. 2011). Shear properties of articular cartilage, at equilibrium, are inhomogeneous and largely governed by the interactions between the solid components, without significant influence from the fluid phase. The tissue becomes physically stretched by pure shear forces, with no compression and is largely unaffected by fluid pressurisation. Proteoglycans within the tissue, expand the collagen matrix producing a tensile pre-stress in the collagen fibres. This interaction allows cartilage to resist shear deformation, hence when proteoglycans are degraded; the shear modulus is greatly reduced (Zhu et al. 1993; Buckley et al. 2008; Little et al. 2011). The static equilibrium shear modulus for human articular cartilage can range from 0.05 to 0.25 MPa, whereas the tissue's dynamic shear moduli can range from 0.1 to 4MPa (Buckley et al. 2008). During shear, the solid matrix of articular cartilage demonstrates intrinsic, viscoelastic properties, which are dependent on compressive strains (Zhu et al. 1993). Shear forces can affect the viscosity of synovial fluid within the joint, when the shear rate increases the viscosity of the fluid is reduced, affecting the load it can support (Mirzayan 2006).

1.3.3.4 Viscoelasticity

Articular cartilage's response to a constant (time-independent) load or constant deformation varies over time, giving it its viscoelastic properties. They are the result of the frictional drag, generated from the flow of the interstitial fluid (known as biphasic viscoelasticity) or the macromolecular movement of the ECM (known as flow-independent viscoelasticity) (Nordin & Frankel 2001). The viscoelasticity of articular cartilage is also dependent on the interactions between the collagen matrix and proteoglycans. When the tissues GAG content is reduced, collagen fibres become more aligned, affecting the rate of deformation, or creep, when under tension (Athanasiou, et al. 2009). Due to cartilage's elastic properties it has the capability to deform, internally storing energy and then returning to its original form. As well as elasticity, the rate at which the tissue reversibly deforms is governed by fluid flow, preventing the tissue from instantaneously returning to its pre-loaded state. There are two central responses of articular cartilage's viscoelastic nature; known as creep and stress relaxation (Nordin & Frankel 2001).

1.3.3.5 Creep

Creep occurs in articular cartilage when the tissue is placed under a constant compressive stress. Initially the tissue will undergo rapid deformation, followed by a slow (time-dependent) progressive additional deformation, as the fluid is forced out of the tissue. The strain placed on the tissue will continue to increase, until the point where the fluid is fully discharged from the tissue, given a large enough load is placed on the tissue. The creep rate of the tissue is dependent on the time it takes to reach a constant strain, governed by the size of the compressive load placed upon it (Nordin & Frankel 2001; McGinnis 2005; Little et al. 2011).

1.3.3.6 Stress relaxation

When articular cartilage is subjected to a constant deformation, it undergoes a constant strain; however it does not endure a constant stress. In contrast, the application of the strain will create a rapid increase in stress levels (seconds), followed by a slow (hours) decrease in stress, known as relaxation. Stress relaxation, is more simply, the time the tissue takes to react to an applied load or displacement and reach an equilibrium state.

The time taken for the tissue to reach an equilibrium state is dependent on the load or displacement that is applied to it and varies as a result of the ECM deforming, decreasing the average pore size within it. As a result, this increases the diffusional drag between the ECM and the interstitial fluid. Like creep, stress relaxation largely results from fluid discharging from the tissue (Nordin & Frankel 2001; McGinnis 2005; Little et al. 2011).

1.3.4 Cartilage damage

Different components of the ECM are constantly being turned over throughout the lifetime of articular cartilage. Under physiological conditions, a balance is maintained by the chondrocytes, between synthesis and degradation. However, cartilage has a limited capacity for repair and regeneration and while under pathological conditions the balance may incline towards an overall loss of matrix components from the tissue (Lohmander 1988; Nordin & Frankel 2001). Articular cartilage is highly adapted for its function within a synovial joint and can withstand a wide range of static and dynamical loads. It has an optimum range of functional use, if cartilage is under used, in cases such as immobilisation, or overused in cases such as excessive loading; the quality of the tissue is reduced and begins to break down. Although cartilage can adapt to changes in its mechanical environment, due to its avascular and aneural properties, in many instances, the adaptation is degenerative, leading to joint diseases such as OA (Whiting & Zernicke 2008).

1.3.4.1 In vivo cartilage damage

Articular cartilage can degrade by two ways; fatigue wear or interfacial wear. Fatigue wear results from the cyclic stresses and strains generated within the cartilage, caused by the repetitive loading of joint motion. The wear occurs at the surface of the articular cartilage and is not affected by the lubrication in the joint. The large cyclic stresses and strains can result in damage within the bulk material, where microscopic damage accumulates and progresses to the surface. Interfacial wear is caused by the contact of the two articulating surfaces either as a result of the more common adhesive wear or due to abrasion. Adhesion occurs when a junction is created by the articular cartilage of two surfaces coming into contact, causing fragments of the cartilage to be torn off. Abrasive wear occurs when there is a difference in the hardness of two materials which come into contact. This can occur when fragments of loose particles such as bone cut into the softer articular cartilage (Nordin & Frankel 2001; Mow & Huiskes 2004; Katta et al. 2008).

In the majority of circumstances it is difficult to identify the etiology of the degradation process and which of the biological or mechanical degradation processes precedes the other (Katta et al. 2008). There are many factors that can be responsible for the initiation or progression of cartilage wear, including but not limited to, trauma, abnormal biomechanical loading, altered mechano-chemical transduction by chondrocytes, chondrocyte senescence, metabolic disorders, proteolytic enzymes, pathological changes in the collagen-proteoglycan matrix, and loss of lubrication mechanisms or a combination of the above (Katta et al. 2008). When articular cartilage becomes damaged, even by a relatively small amount, it can have a largely detrimental effect on the joint, due to the hydrodynamics of the thin lubricant film (Mow & Huiskes 2004).

As well as mechanical factors, degeneration occurs due to a deterioration of the superficial proteoglycan concentration, increase in water content and separation and disorganisation of the superficial collagen fibrils (Arokoski et al. 2000). Degeneration results from a change in biological factors, such as an elevated expression and activity of proteolytic enzymes. These enzymes, which normally function in the formation, remodelling and repair of the tissue, transform from an anabolic state to a catabolic state as a result of abnormal joint loading. During tissue degeneration, chondrocytes respond to proinflammatory cytokines, by producing more proteinases, which degrade cartilage collagens and proteoglycans (Goldring & Marcu 2009). Loss of proteoglycans decreases the fluid pressurisation, resulting in the inability of the fluid to bear the load. This causes an alteration in the loading pattern, resulting in an intensified load on the collagen fibres in the ECM. Many believe that after the strength of the superficial zone of the cartilage is lost, the remaining cartilage zones have to endure abnormally high strains. Over time, this can lead to cartilage degradation and extensive bone remodelling, and further, the total loss of the tissue due to cartilage's low rate of renewal (Arokoski et al. 2000; Julkunen et al. 2007; Athanasiou 2009; Narayan 2009). Once the structure of the collagen-proteoglycan network becomes damaged, it is unable to produce normal mechano-electrochemical stimuli, resulting in abnormal ECM remodelling by the chondrocytes and inhibits normal tissue function (Nordin & Frankel 2001).

The rate at which the articular cartilage degenerates is thought to be governed by multiple factors such as; the magnitude of the imposed stresses, the total number of sustained peaks, a change in the intrinsic molecular and microscopic structure of the collagen-proteoglycan matrix, a change in the intrinsic mechanical properties of the tissue, and the type of loading. Failure initiation appears to be highly dependent on the "loosening" of the collagen network, causing the proteoglycans to abnormally expand, resulting in a swelling of the tissue. As the collagen network "loosens", the tissue becomes more relaxed and permeable, altering the function of the tissue (Nordin & Frankel 2001).

1.3.4.2 In vitro cartilage damage

Although thought to be a crucial factor in hip joint damage, there have been fairly limited studies on the effects of varying contact stresses on the friction and wear of articular cartilage. The *in vitro* studies available found that the coefficient of friction decreased as the contact stress was increased (Katta et al. 2008). However, a study by Katta et al, (2008) found that this was only valid to a certain stress level, when rehydration of the cartilage was possible. A further study by Katta et al. (2008) found that during biphasic lubrication conditions, when the cartilage could rehydrate, friction levels remained very low. *In vitro* studies have also found long-term or static loading within the physiological range can cause articular cartilage to compress by 15%-

45%, whereas short-duration (high-frequency) loading only results in a minimal cartilage compression (Grodzinsky et al. 2000).

1.4 Acetabular labrum

The human acetabular labrum is a fibrocartilaginous lip, which is attached to the transverse acetabular ligament (TAL), bridging the acetabular notch and forming a complete circle around the acetabulum (Figure 1-10). It increases the size of the acetabulum by 33 %, as well as providing around 22 % of the articulating surface of the hip. Commonly, the human labrum is anteriorly triangular in cross-section with a more bulbous lip posteriorly; however, it has been reported to vary greatly in shape, ranging from triangular to rounded or flat.

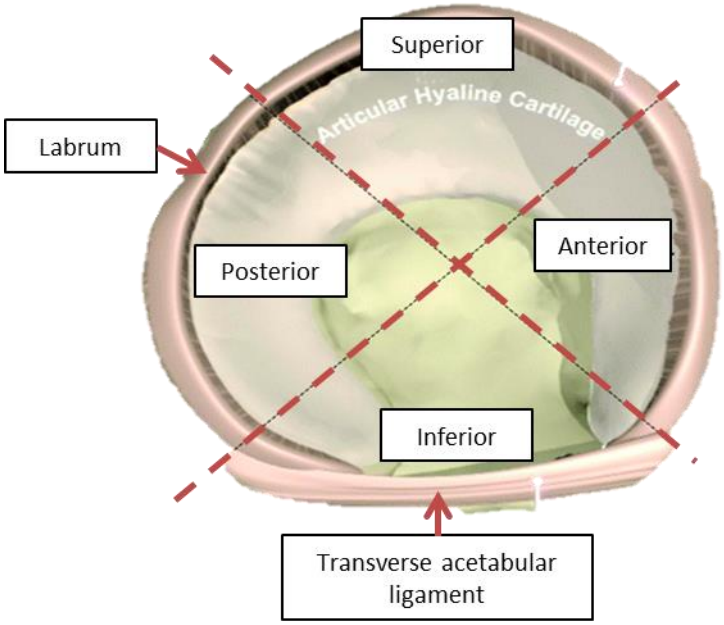

Figure 1-10 Regions of the acetabular labrum. The orientation of labrum within the human body taken from Lewis & Sahrmann (2006).

The labrum has an approximate height of 5.5 mm and a width of 4.7 mm, at its base (Figure 1-11). The base of the acetabular labrum is attached to the circumference of the osseous acetabular margin, with its apex forming the free edge, turned against the femoral head. It connects to the articular cartilage through a transition zone, of approximately 1 to 2mm thick, with a well-defined tide-mark. A thin section of bone extends from the hip into the middle of the labrum. On the external side of the labrum, a narrow synovial lined recess separates it from the joint capsule (Konrath et al. 1998; S J Ferguson et al. 2000; Narvani 2003; Petersen et al. 2003; Kelly et al. 2005; Manaster & Zakel 2006; Bowman et al. 2010; Henak et al. 2011).

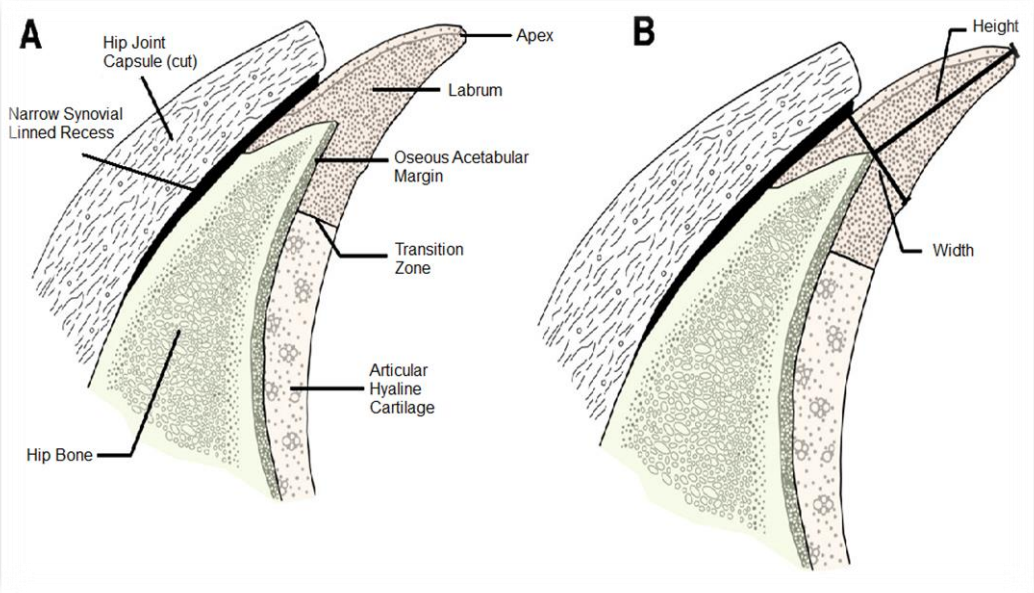

Figure 1-11 Acetabular labral fixations and dimensions Diagram A shows the attachment sites of the acetabular labrum. Diagram B shows the dimensions of the acetabular labrum. Diagram adapted from Lewis & Sahrmann (2006)

1.4.1 Labrum macrostructure

The structure of the acetabular labrum varies greatly across the tissue, similar to that of the meniscus in the knee. Collagen fibres are primarily orientated parallel to the acetabular rim, in a circular fashion on both the internal and external circumferences, with a handful of fibres scattered obliquely to the leading fibre orientation (S.J. Ferguson et al. 2000; Petersen et al. 2003). The acetabular labrum is composed of three zones; the superficial zone, formed by a network of delicate fibrils, a deeper middle zone consisting of a layer of lamellar-like collagen fibril bundles, intersecting at various angles and a third, external deep zone, composed of highly orientated, circumferential fibres (Figure 1-12, Ferguson et al. 2000; Petersen et al. 2003). The anterior and posterior sections of the acetabular labrum are continuously connected to the transverse ligament, with the fibrils of the three layers diffusing directly into it (Petersen et al. 2003). It is hydrated with a water content of around 70% (S J Ferguson et al. 2000; Ferguson et al. 2001; Narvani 2003).

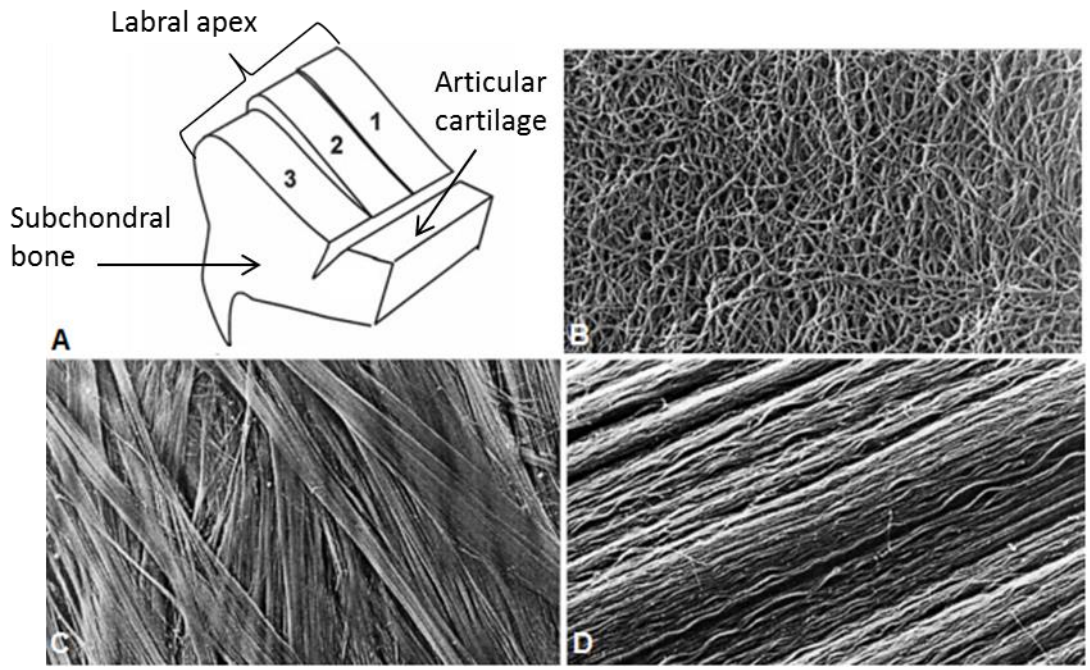

Figure 1-12 Labral collagen fibre alignment diagram A – Schematic of the three zones within the acetabular labrum. B – SEM of internal superficial zone (layer 1) with a network of delicate collagen fibrils. C – SEM of middle zone (layer 2) consisting of a layer of lamellar-like collagen fibre bundles, intersecting at various angles. D – SEM of external and deep zone (layer 3) with highly orientated circumferential fibres. Image taken from Petersen et al. (2003)

1.4.2 Labrum microstructure

Many studies of the labrum state that it is exclusively composed of fibrocartilage; however a study by Petersen et al (2003) states the labrum consists of fibrocartilage and dense connective tissue. Dense connective tissue composes the external region, directed towards the joint capsule, whereas the inner region, directed towards the femoral head, is composed of a thin layer of fibrocartilage. The fibrocartilaginous layer is approximately 200 to 300 µm thick and contains chondrocytes embedded between the collagen fibrils. There is a continuous transition from the fibrocartilage tissue to the dense connective tissue. Between the joint capsule and the labrum there is a small recess, in this region the labrum is covered by a layer of loose, well vascularised, connective tissue and fat, approximately 200µm thick. The transition between the labrum and the articular cartilage also resembles fibrocartilage with isogenic groups of chondrocytes present (Narvani 2003, Petersen et al. 2003).

1.4.2.1 Collagen

The acetabular labrum is predominantly composed of thick, circumferential, type I collagen fibre bundles. Type I collagen fibres are located alongside type II collagen in the dense connective tissue as well as types II and III in the fibrocartilaginous zones (S J Ferguson et al.

2000; Ferguson et al. 2001; Narvani 2003; Petersen et al. 2003; Henak et al. 2011). Petersen et al (2003) found that type II collagen is constrained to the pericellular matrix of chondrocytes. The surface of the acetabular labrum is covered by a 10 µm-wide, network of randomly orientated collagen fibrils approximately 30nm in diameter. Below the superficial layer, collagen fibrils increase in size to approximately 100-130 nm in diameter, forming tight lamellar bundles around 40µm-wide (Petersen et al. 2003). These collagen fibres have the ability to withstand deformation under the pressure applied by the fluid in the joint space (Ferguson et al. 2000).

1.4.2.2 Blood and nerve supply

Unlike articular cartilage, the labrum has been shown to possess a slight vascular and nerve supply. Although largely avascular, a greatly reduced number of blood vessels, originating from the capsular periphery, infiltrate into the central articular-sided region of the labrum, providing nutrients to the joint (Figure 1-13, Kelly et al. 2005). Laminin found in the walls of blood vessels has been reliably located in the peripheral third of the labrum, with the inner two thirds of the tissue presented as avascular (Petersen et al. 2003).

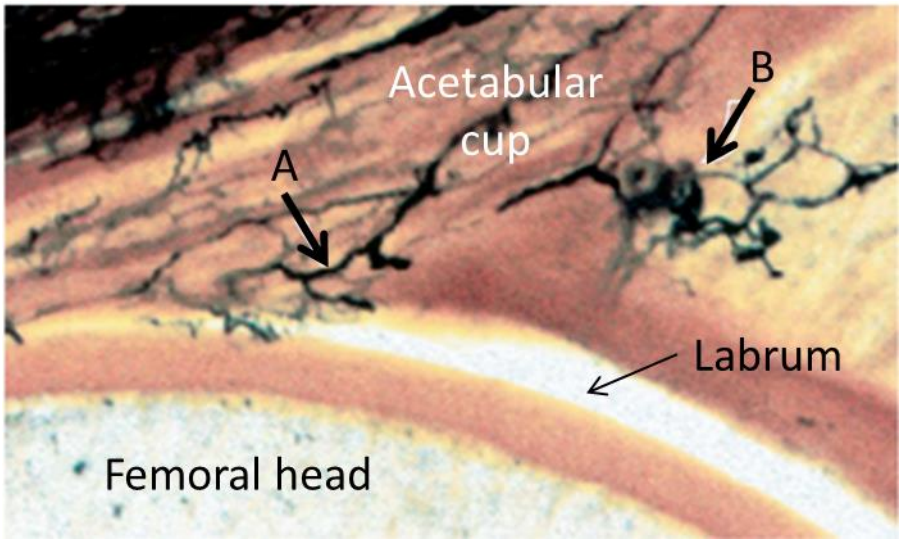

Figure 1-13 The blood supply to the acetabular labrum. The blood supply to the labrum from the joint capsule (A) and the bony acetabulum (B), taken from Kelly et al. (2005).

It is thought that younger patients may have a higher vascular penetration throughout the tissue, but still show regional differences, similar to that of other intra-articular structures such as the meniscus, in the knee. Due to high levels of labral tears in the anterosuperior region, it is thought that they may reflect an area of relative hypovascularity (Kelly et al. 2005). Upon histological examination, free nerve-endings and sensory end organs have been observed in all

areas of the tissue; however they are more dominant in the superficial layers and in the superior and anterior quarters. It has been suggested that these nerve endings may be involved in proprioceptive and nociceptive mechanisms (Konrath et al. 1998; Narvani 2003; Kelly et al. 2005).

1.4.3 Labrum mechanical properties

Although diffused into the acetabular cartilage, the labrum has its own unique mechanical properties. Two different forces play a key role in the formation of labral tissue; dense connective tissue is a result of a functional adaptation to tensile stresses, whereas fibrocartilage tissue is formed by intermittent, compressive and shear forces (Ferguson et al. 2001; Petersen et al. 2003). A distinct difference in the labrum, compared to that of articular cartilage, is its lack of a bony bearing, therefore, when a force is applied to the tissue surface, the labrum is pushed away from the acetabular rim (Petersen et al. 2003). Many of the acetabular labrum's mechanical properties were developed from bovine models, however, Joshi et al. (1995) found no variations in the mechanical properties of human and bovine meniscal tissue, which is morphologically similar to the labrum .

1.4.3.1 Tensile properties

When acetabular labral tissue is placed under tension, the tissue has a higher stiffness compared to that of the adjoining articular cartilage. Posteriorly, the tissue also has an increased stiffness and strength compared to that of the superior region (Ferguson et al. 2001; Petersen et al. 2003). The tensile stress-strain curve for labral tissue follows the same curve of various soft tissues, such as the meniscus in the knee and acetabular cartilage (Figure 1-14). The toe region of the graph relates to the sequential recruitment and stretching of crimped collagen fibres, followed by a near-linear region, suggesting the collagen fibres have been recruited and uniformly expanded (Ferguson et al. 2001). A study by Ferguson et al (2001) found that labral tissues, with a more uniform appearance (with most of the fibres aligned along the length of the tissue) had the highest moduli and tensile strength and failed at much higher stress levels, under quasi-static test conditions. Due to labral tissues thick collagen fibre bundles, it has the ability to resist stretching around its circumference, however it may be susceptible to shearing forces (Shibutani 1988).

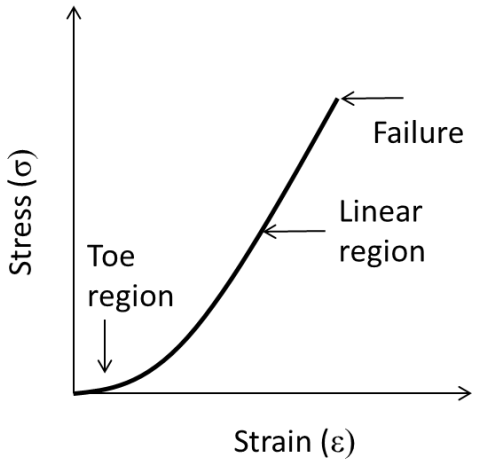

Figure 1-14 Typical stress-strain curve for a soft tissue. Graph showing the different regions of a stress strain curve, the initial toe region followed by the linear region and failure.

1.4.3.2 Compressive properties

There is limited knowledge regarding the compressive modulus of acetabular labrum; however, a study by Ferguson et al. (2001) found the compressive strength of the bovine labrum to be around 0.16 MPa under confined compression.

1.4.3.3 Permeability

The acetabular labrum has a greatly decreased permeability, compared to the adjoining articular cartilage and compared to that of the meniscus in the knee, providing it with an increased resistance to fluid flow. There is a notable variance in the permeability of the labrum, with higher resistance to interstitial fluid flow across the rim of the labrum compared to around the rim. The tissues permeability affects the tissues response to creep, due to its prolonged time requirement to reach an equilibrium displacement. It is also possible that the tissues low permeability functions in the shock absorbing capability of the tissue, reducing impact and risk of dislocation (Ferguson et al. 2001).

1.4.4 Labrum function

Overall, there is relatively little knowledge on the mechanical function of the labrum. However, it is thought that one of its main functions is to aid in joint stability (Ferguson et al. 2000). The labrum is known to deepen the acetabular socket, which increases the coverage of the femoral head, enhancing joint stability. It is similar to that of the glenoid labrum in the shoulder joint, however it is far deeper, providing greater stability.

Several experimental studies have demonstrated a further role of the labrum, in that it can provide a seal against fluid flow, in and out of the intra-articular joint space, enhancing fluid-film lubrication in the hip joint. This is most likely to occur during periods of slow loading, over

prolonged periods of time. The pressurised fluid layer can reduce surface-to-surface contact and limit the rate at which cartilage layers consolidate, by distributing applied loads more evenly across the cartilage surface. Petersen et al (2003) found that without this sealing mechanism, strains found within the cartilage matrix were significantly higher, which could lead to wear and damage of the tissue. The seal of the labrum is highly dependent upon its fit against the femoral head (Konrath et al. 1998; S J Ferguson et al. 2000; S.J. Ferguson et al. 2000; Narvani 2003; Petersen et al. 2003; Kelly et al. 2005; D. Zhang et al. 2012).

Independent of its ability to act as a seal for the intra-articular joint space, due to its relatively low permeability, the labrum is thought to increase resistance of the flow path of interstitial fluid, limiting the rate of fluid expressed from cartilage during loading. This increase in interstitial fluid pressurisation, allows the cartilage to carry greater loads, limiting stresses within the collagenous solid matrix (S J Ferguson et al. 2000; Ferguson et al. 2003). Bowman et al (2010) also states that the acetabular labrum can aid in limiting extreme ranges of motion, preventing dislocation and also compensating for minor incongruities.

The function of the labrum is highly controversial with Konrath et al. (1998) and Henak et al. (2011) stating that the removal of the labrum has no significant effect on stresses within the acetabulum, following finite element analysis and *in vitro* simulation respectively. Hence, suggesting that its function is to stabilise the joint, as opposed to reducing stresses, by distributing loads.

1.4.5 Labrum damage

The acetabular labrum is similar in composition to the meniscus of the knee, however it is believed that it is uniquely adapted to its role within the hip joint. Any damage to the tissue, such as labral alterations or tears (Figure 1-15), may contribute to joint degeneration and possible OA (Ferguson et al. 2000; Ferguson et al. 2003). Labral tears are related to areas of microvascularity and are thought to cause pain due to the stimulation of nerve endings, around the tear. Labral tears are regularly associated with adjacent labral lesions and occasionally osteophyte formation, as well as cystic spaces. When the labral tear becomes completely ruptured and is separated from the edge of the acetabulum it is referred to as an avulsion (Figure 1-16, Narvani 2003; Kelly et al. 2005; Bharam 2006; D. Zhang et al. 2012).

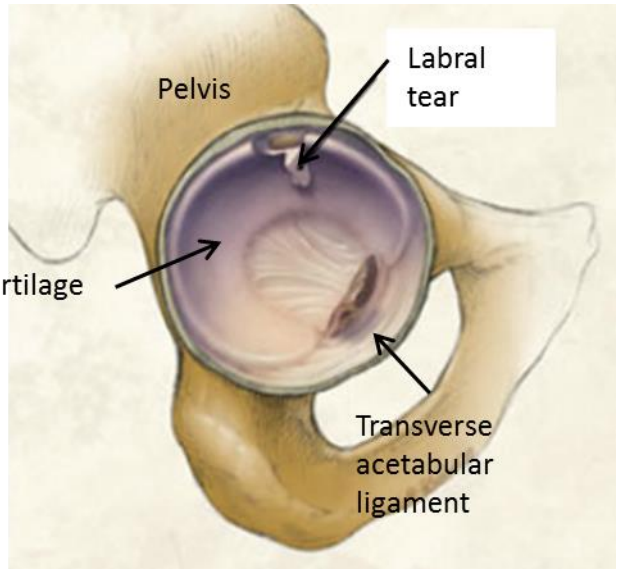

Figure 1-15 Acetabular labral tear. An acetabular labral tear in the superior region, taken from McDermott (2010).

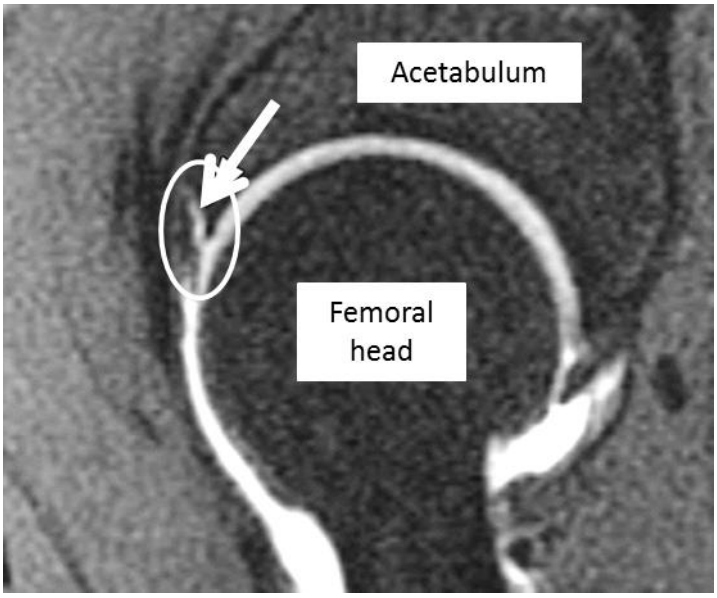

Figure 1-16 Acetabular labral avulsion. An MR arthrography of an acetabular labral avulsion highlighted by the white arrow, taken from Dinauer et al. (2004).

Labral tears can be the result of a sudden isolated event or more commonly, repetitive trauma, generally whilst the hip joint is stressed in rotation. Movements consisting of force adduction, along with either internal or external rotation, can both initiate or promote the aggravation. Hip dislocation and acetabular fractures are also a known cause of labral tears as a result of trauma, as well as repetitive activities leading to possible labral bruising. Additional to trauma, labral tears can be the result of degenerative changes caused by wear and tear, structural abnormalities such as FAI leading to abnormal loading, as well as developmental abnormalities from dysplasia caused by abnormal contact and hip instability. There is often a sharp clicking and

catching sensation associated with labral tears and locking of the joint can also be experienced. Range of motion may not be specifically limited with labral tears however, pain at the extremes may cause movement to be difficult (Narvani 2003).

Labral tears occur along the main circular orientation of the collagen fibrils, directed along the line of greatest tensile strain. The acetabular labrum is more vulnerable to labral tears and lesions in the anterior region, with the majority of tears occurring here. The anterosuperior region is particularly at risk; however, the posterior region can also be susceptible. It is thought that due to presence of blood vessels in the outer one third of the acetabular base, labral tears in this peripheral region have the biological potential to heal (Narvani 2003; Petersen et al. 2003; Kelly et al. 2005; Bharam 2006).

Labral tears are not gender specific and they can occur in all age ranges however, they are a much rarer condition in younger non-active individuals. The most commonly affected groups are athletes as well as the ageing population, with a recent study finding labral tears to be the cause of groin pain in over 20% of athletes, a major concern due to the high risk of morbidity.

Acetabular labral tears can be classified by their nature, Lage et al (1996) was the first person to publish a classification system for hip labral tears using arthroscopic findings (Blankenbaker et al. 2007). It was found that the most frequently occurring tear is a type 1 radial flap (Figure 1-17 A), with 57% of all tears classified as type 1. The tear occurs in the free margin of the labrum and forms a discrete flap. Chronic degeneration can lead to a brush-like, radially fibrillated tear (Figure 1-17 B), classified as type 2. Type 3 occurs at the junction of the labrum and acetabular rim, resulting in a longitudinal peripheral tear (Figure 1-17 C) as opposed to type 4 which consists of an unstable, abnormally mobile tear.

As well as acetabular tears, osteochondral lesions, can differ in severity and can be classified by grades using an x-ray. Grade 1 lesions include an intact cartilage with signal changes in the subchondral bone. Grade 2 occurs once the cartilage becomes partially detached and signal changes in the subchondral bone remain. When a non-displaced fragment becomes entirely detached the lesion is classified as grade 3 and only once the fragment has completely detached and displaced is it classed as grade 4 (Narvani 2003; Kelly et al. 2005; Bharam 2006; Manaster & Zakel 2006).

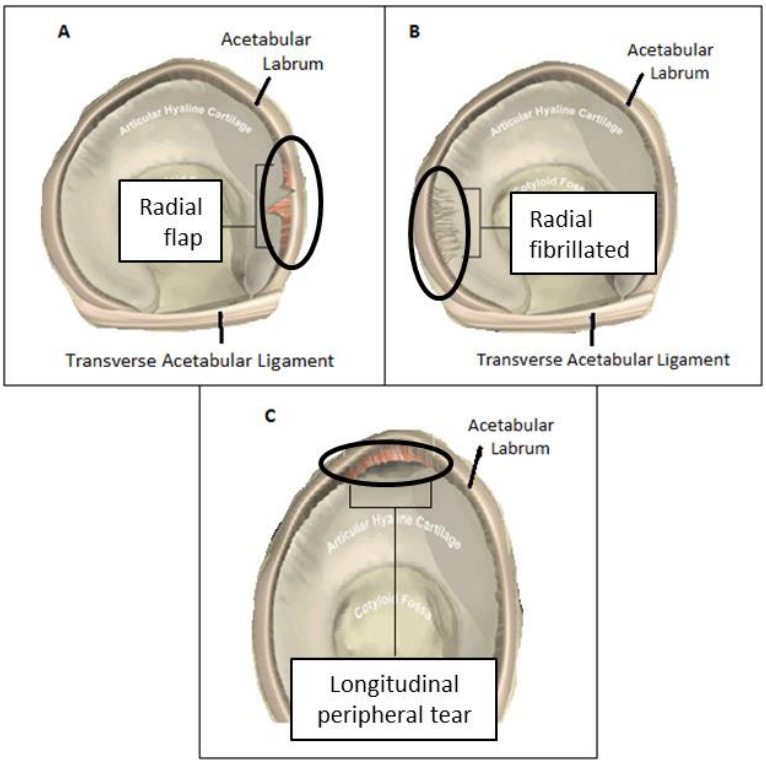

Figure 1-17 Acetabular labral tear classification. A - Radial flap on the anterior region of the labrum. B - Radial fibrillated labrum on the posterior region of the labrum. C - Longitudinal peripheral tear on the superior region of the labrum. Image adapted from Johnson et al. (2007).

Like labral tears, labral lesions have various aetiological factors responsible for them, such as trauma or hip dysplasia, making them uniquely identifiable. Type A lesions are the result of trauma, occurring due to the stresses placed on the labrum. These stresses can either be due to high radial forces, occurring when the femoral head slides against the joint lip, traumatic dislocation or during minor twisting injuries of the leg and hip. These types of lesions primarily occur in younger or middle-ages patients, due to higher level of activities. Labral lesions as a result of hip dysplasia, type B lesions, occur when the femoral head slides against the labrum, which is acting as a barrier, without any sufficient trauma. Both type A and B lesions primarily occur in a circular orientation, following the path of the collagen fibrils (Narvani 2003; Petersen et al. 2003).

Damage to the labrum often needs to be diagnosed in a clinical setting where the combined movement of flexion and rotation that cause the pain, can generally be sufficient diagnosis. More precisely, specific movements and the pain they cause can be used to determine the location of the tear. Pain caused by flexion, adduction and internal rotation are generally signs of anterosuperior tears, passive hyperextension, abduction and external rotation are related to posterior tears, acute flexion combined with external rotation and full abduction, followed by

extension, abduction and internal rotation are specific to anterior tears, whilst extension, abduction and external rotation, moving to a flexed, adducted and internally rotated hip is common in posterior tears (Narvani 2003; Henak et al. 2011).

In artificial hip joint replacements, edge loading has been noted as a cause of damage and possible failure to the joint. Edge loading is a result of misalignment or looseness of the joint, which results in an intensified contact stress (D'Antonio & Dietrich 2006; Knahr 2011; Mellon et al. 2011). Although no studies have reported edge loading to occur in the natural hip, diseases or trauma that result in an altered tribological interface and abnormal loading could possibly result in edge loading and damage to the adjacent tissues, such as the labrum.

1.4.6 Labrum treatment

There are two types of treatment involved in the healing of damaged labral tissue; the first is a conservative, non-operative management, consisting of non-steroidal, anti-inflammatory medication, as well as bed rest with or without traction, followed by protected weight-bearing (Konrath et al. 1998; Narvani 2003). This form of treatment is limited due to the healing capabilities of the tissue being closely associated with the distribution of blood vessels and the majority of labral damage occurring on the avascular articular edge (Narvani 2003; Petersen et al. 2003).

Operative treatment is an alternative option, which includes arthrotomy, arthroscopy and open hip surgery; in which a partial or total labrectomy or debridement is often performed (Figure 1-18). A labrectomy or resection osteoplasty is the excision of the labral tissue (Konrath et al. 1998; Ferguson et al. 2003; Petersen et al. 2003). Although excision of the labrum gives good short term effects with immediate pain relief, it is thought that long term success is limited as the physiological function of the labrum is compromised. This can result in reduced joint stability preventing congruity and unsealing of the joint, as well as leading to increased loads and pressures known to initiate and promote premature OA (Konrath et al. 1998; Ferguson et al. 2003; Petersen et al. 2003). However, more recent studies have shown that labral repair is more beneficial than a labrectomy hence, newer treatments are focusing on labral repair, such as refixation, rather than excision (Figure 1-19).

Figure 1-18 Acetabular labral debridement. Debridement of the torn portion of the labrum, taken from McGinty et al. (2002)

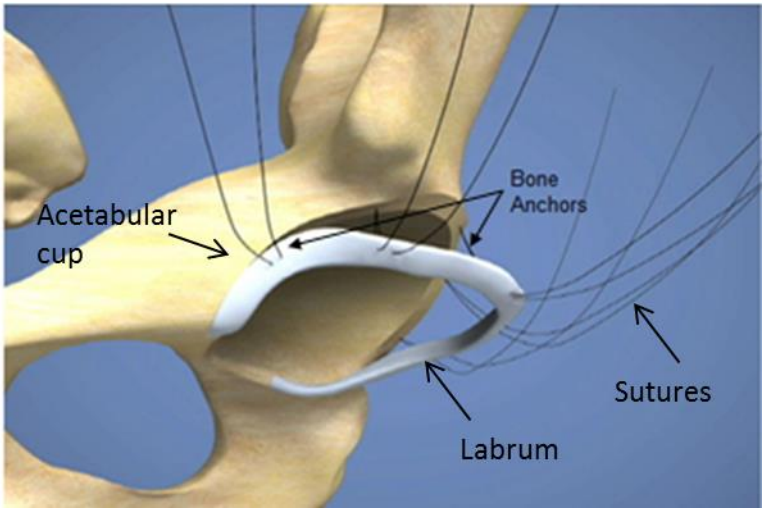

Figure 1-19 Labral refixation. A damaged labrum is reattached to the acetabulum using drilled holes and bone anchors, taken from Ganz (2006)

Diagnosis of damage to the labrum can be undertaken by many methods, with varying results. They include; physical examination, arthrography, magnetic resonance imaging (MRI) with use of a contrast medium, arthroscopy, radiography and computerised tomography (Konrath et al. 1998; Narvani 2003). Many tools, such as radiographs and computed tomography, are used to exclude other types of hip pathology, such as hip dysplasia, arthritis and acetabular cysts, rather than diagnosing the labral damage specifically, hence the reliability of these methods are questionable. Arthrograms can be used alongside other methods to further exclude other types

of hip pathology, but they do not improve the ability of the tools to directly identify labral damage.

MRI works by identifying soft tissues, giving it the ability to directly depict the labral tissue and has shown promise as a more reliable tool in the last two decades. Labral tears can be detected, using MRI, by identifying altered features such as irregular shape, non-triangular cross-section, a thickened labrum lacking a labral recess, increased signal intensities, and detachment from the acetabulum. Limitations with MRI still exist due to the natural variability in normal labral size and shape, as well as differentiating labral tears from the pseudotears caused by normal articular cartilage (Narvani 2003). Insufficient reliability of all of these techniques has been proven by differences to arthroscopic findings in patients with suspected labral damage (Narayan 2009).

Arthroscopy is by far the most advanced and reliable technique for identifying labral damage as it allows the surgeon to look inside the joint using a camera inserted through a small hole in the body, which relays a live image to a screen. Arthroscopy, allows for a comprehensive evaluation of labral anatomy, due to its diagnosis as well as treatment capabilities, however the need for invasive surgery still remains a major disadvantage over other techniques used for diagnosis (Narvani 2003). Due to increased knowledge of the importance of labral function, new surgical techniques to repair or reattach the labrum must be developed to maintain the tissues function within the hip joint (Petersen et al. 2003).

1.5 Tissue degeneration and subsequent diseases

Hip diseases, such as OA, can be initiated by a disruption to the homeostasis of the soft tissues, resulting from a combination of biological mediators and mechanical factors, which can vary according to the specific disease (Goldring & Marcu 2009). There are many factors that can effect cartilage degeneration, including abnormalities of bone, synovial fluid, tendons, ligaments, or soft tissue accessory structures, such as menisci or labra (Ferguson et al. 2003). An abnormal labrum is thought to be an initiator of OA due to altered load transfer and stresses to the cartilage layers (Ferguson et al. 2003). Tissue degeneration is also associated with sclerosis of the subchondral bone and fragmentation of cartilage.

1.5.1 Hip dysplasia

DDH is a condition that causes the hip to be unstable, as a result of the abnormal development of bones and/or supportive soft tissues around the joint, in utero (Talmage 2009). It is predominant in females, thought to be caused by the higher productions of oestrogen that results in more elastic ligaments, which in turn allow the bones to move out of position more easily. DDH is also twice as common in the left hip, possibly caused by the unborn baby lying against the mothers spine on the left side (Hefti 2007; Patient.co.uk 2012). Hip dysplasia is often first recognised in infants; however it is possible for mild hip dysplasia to go unrecognised until adulthood when the condition has developed (Talmage 2009). The severity of the condition is determined by the level of contact between the femoral head and the acetabulum, with mild abnormalities showing incomplete contact (subluxation) and more severe abnormalities building up no contact between the femoral head and acetabulum, known as dislocation (Talmage 2009; Patient.co.uk 2012). Secondary dislocation resulting from dysplasia is caused by the inadequate contouring of the acetabular roof (Morcuende & Weinstein 2002). DDH is a common cause of hip pain in young adults and if left untreated can result in initiation of joint diseases, with around 25 to 50% of patients developing OA by the age of 50 (Morcuende & Weinstein 2002; Manaster & Zakel 2006; Talmage 2009).

1.5.1.1 Characteristics

DDH by anatomical definition is the inadequate development of the femoral head or acetabulum or a combination of the two. It is more common to find the abnormality in the acetabulum, with a shallower socket or irregular orientation of the articular surface (Figure 1-20), however it is possible for the femur to be abnormally rotated, increasing the force through the hip (Morcuende & Weinstein 2002; Talmage 2009; Patient.co.uk 2012). Many patients suffering from DDH develop retroversion of the anterosuperior acetabulum, with inadequate acetabular coverage of the femoral head. A reduced contact area and increased edge loading, promote eccentric and excessive overload of the anterosuperior region (Manaster & Zakel 2006; Parvizi et al. 2006). DDH is also characterised by an associated laxity of the support ligaments around

the hip over time, this combined with the forces of the adjacent muscles, results in an increased freedom of movement of the femoral head within the acetabulum. This increase in freedom allows the femoral head to move out of place within the acetabulum leading to abnormal forces on the joint surface, instability, chronic pain and, eventual degeneration (Morcuende & Weinstein 2002; Talmage 2009).

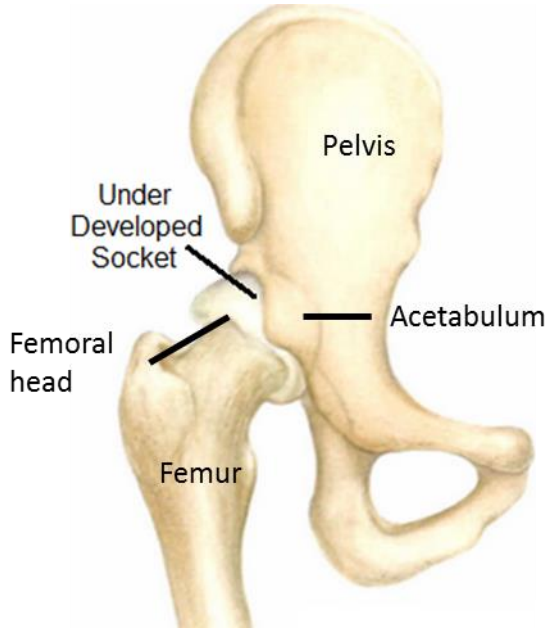

Figure 1-20 Dysplastic hip. The hip anatomy of hip dysplasia, adapted from Bauer et al. (1996).

The rate of deterioration of a patient's hip is determined by two factors; the severity of the subluxation as well as the patients age. Patients suffering from subluxed hips, rather than complete dislocations, develop symptoms at a much younger age; with severe subluxation developing in the second decade of life, moderate at 30-40 years of age and mild subluxation around the menopause (Morcuende & Weinstein 2002). At the point where symptoms are established, the only radiographical signs present may be subchondral sclerosis in the weight-bearing region and more common symptoms of degenerative changes, such as joint space narrowing, osteophyte formation, and subchondral cysts may be identified. Once clinical symptoms and radiographic signs of degenerative joint disease develop, further progression is rapid (Morcuende & Weinstein 2002). The two most noticeable symptoms of DDH are hip pain and/or a limp. Hip pain is generally caused by specific movement and it is primarily felt deep in the front of the groin however, it is also possible to develop pain in the back or side of the hip. In exceptional conditions, it is possible for the patient to feel a popping or clicking sensation during movement. Once symptoms develop, a mild limp may occur, caused by either the pain directly or as a result of weak muscles, limited flexibility or a bony deformity. Patients suffering from DDH, are also at a higher risk of labral tears, labral hypertrophy and labral calcification

(Henak et al. 2011). When symptoms first develop it is normal for them to be mild and only occur occasionally however, overtime they can increase in intensity as well as frequency. The difficulty of diagnosing DDH comes from the similarities of the symptoms to many other hip disorders (HipDysplasia.org 2012).

1.5.1.2 Pathogenesis

Although DDH is known to be caused by an abnormal development of the hip joint, commonly present at birth; the specific cause for the abnormal development is unclear. Various factors are known to increase the chance of a baby developing DDH; family history of the disease, gender (8 in 10 cases of DDH are female, pregnancy conditions (a lack of fluid prevents the baby from moving around), and first born (it is thought that the uterus is tighter, meaning the baby has less room to move) (Morcuende & Weinstein 2002; Patient.co.uk 2012).

1.5.1.3 Treatment

If DDH is diagnosed at a young age, it can be treated with an external brace, such as a Pavlik Harness, worn continuously for around 6 weeks and then weaned for a further 6 weeks. The brace fixes the hips in flexion, with mild abduction and external rotation (Figure 1-21), allowing the capsule to form normally and the acetabulum to deepen. In severe cases such as dislocation, the femoral head must primarily be relocated into the correct position within the acetabulum and then placed in the harness (Patient.co.uk 2012). Mild cases of DDH may be treated with a make-shift brace of two nappies until the hip becomes stabilised. Before placing the baby in a brace, an ultrasound is initially undertaken to confirm the condition and is followed up by further ultrasound treatments during the management of the condition. Early treatment is crucial, in order for normal development of the hip joint (Morcuende & Weinstein 2002; Talmage 2009).

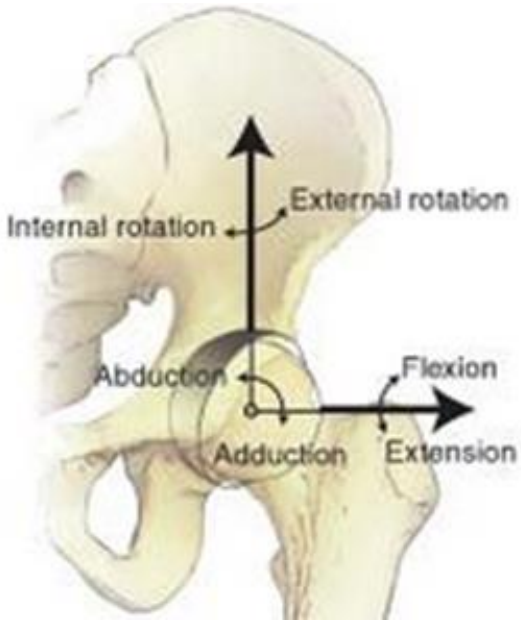

Figure 1-21 The axis and movements of the hip joint. In DDH the hip is held in flexion, mild abduction with external rotation. Image taken from Parvizi et al. (2012).

If DDH is undiagnosed as an infant, adults with mild symptoms can undergo conservative treatments. These can include the use of anti-inflammatory medication, movement alterations to reduce compression on the hip, such as minimising prolonged standing and walking, as well as protecting the joint to prolong its lifespan. In slightly more severe cases, arthroscopy can be an option to remove any debris, such as cartilage fragments, labral tears or inflamed synovial tissues. Severe hip dysplasia is commonly treated with a proximal femoral osteotomy and/or peri-acetabular osteotomy operation, to restore congruence between the femoral head and acetabulum. A proximal femoral osteotomy involves the head of the femur being cut off and repositioned with plates and screws to improve the biomechanical alignment, where as a peri-acetabular osteotomy cuts out and rotates the acetabulum to a position in align with the femoral head (Manaster & Zakel 2006). Final stages result in the need for hip replacement surgery, such as a total hip arthroplasty. Pain management can be undertaken by the use of a walking aid on the contralateral side as well as weight loss in overweight patients (Talmage 2009).

1.5.2 Osteoarthritis

OA is the most prevalent form of joint disease, affecting around 8 million people in the UK alone, and the majority of people over the age of 65, in both males and females equally. It is a chronic condition of the synovial joint, affecting all of the surrounding structures and resulting in damage, thinning and eventual loss of the cartilage tissue. Loss of the cartilage causes the articulating bones to come into direct contact with each other, causing pain and anatomical alterations. OA often has a gradual onset and progressively deteriorates over time and can also

differ in severity. There is a dramatic increase in the number of cases of OA in patients with previous hip conditions or in physically demanding jobs. Due to its high occurrence, it places a large burden on the medical economy (Arden et al. 2008; Arthritisresearchuk.org 2009; Smith 2012).

1.5.2.1 Characteristics

OA generally results in pain and stiffness of the joint, along with loss of function and possible inflammation and swelling (Arden et al. 2008; Conditions & NICE 2008; Arthritisresearchuk.org 2009). Pain is principally felt deep in the front of the groin which may radiate to the anterior and lateral thigh, into the buttock and/or down to the knee (Hochberg et al. 1995; Arthritisresearchuk.org 2009). Inflammation occurs due to the production of extra fluid causing the synovium to swell, in turn resulting in the swelling of the joint. OA is also responsible for fibrillation of the articular cartilage where the collagen fibrils, located in the superficial zone, lose their organisation and functional reliability. As the disease progresses, fibrillation advances deeper through the cartilage zones, altering the stresses and strains, resulting in a decrease of tissue thickness and an increase in surface roughness (Arthritisresearchuk.org 2009; Mononen et al. 2012). In severe cases of OA, the tissue decreases in thickness to the point where the articulating bone surfaces come into direct contact and begin to wear away. The bones may eventually become compressed, shortening the leg on the affected side and/or form osteophytes (Figure 1-22). Osteophytes cause the surface to increase in thickness and grow outwards, forming a bony spur. Loss of cartilage or bone and the formation of osteophytes can result in an alteration to the geometry of the joint, forcing the bone out of its natural position and increasing joint forces (Arden et al. 2008; Arthritisresearchuk.org 2009, Singh & Neutze 2011). Earliest biological signs of OA show an increase in water content and fibronectin with a loss of proteoglycans in the cartilage, affecting the mechanical properties of the tissue (Chevalier 1993).

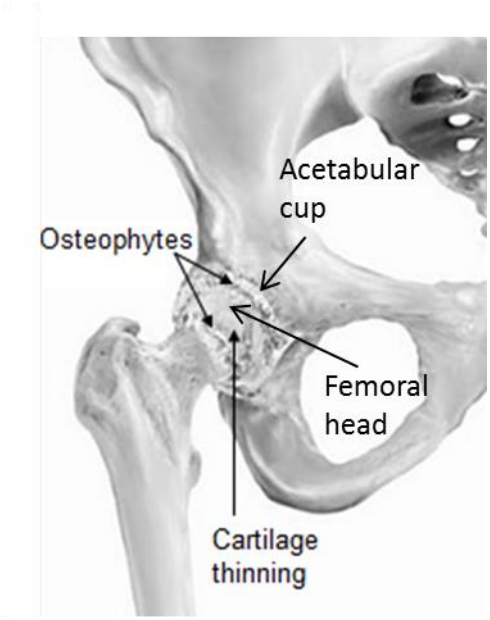

Figure 1-22 Arthritic hip. An osteoarthritic hip with osteophyte formations, adapted from Kennon (2008).

1.5.2.2 Pathogenesis

There is great controversy regarding the aetiology of OA, whether it is solely based on mechanical factors or if biology additionally plays an important role. Moskowitz et al (2006) states the consensus definition of OA as "a result of both mechanical and biological events that destabilise the normal coupling of degradation and synthesis of articular cartilage chondrocytes and ECM, and subchondral bone". Arokoski et al (2000) believes that the development of OA is influenced by both systemic factors and local biomechanical factors. Systemic factors such as age, sex, racial characteristics and genetics influence the foundation for cartilage's properties where as local biomechanical factors including the degree of joint loading, joint injury, elevated weight bearing on account of obesity and joint deformity, impact on the final qualities, the wellbeing and breakdown of articular cartilage (Arokoski et al. 2000). The degree of joint loading can be influenced by different environmental factors such as work or occupational activities as well as obesity being linked to increased mechanical loading. Repetitive impact loading of the joint can result in thickening and stiffening of the subchondral bone causing articular damage. This is more common in athletes where their joints are subjected to overuse and repetition of high level impact forces and torsional loading, increasing their risk of OA (Arokoski et al. 2000; Ferguson et al. 2000).

It is believed that other numerous factors could be responsible for OA in the hip, including the hips tribological function. Cartilage damage is often associated with force transmission such as extensive cartilage loading, leading to high levels of localised stress. Anderst and Tashman (2009) supposed that articular surfaces can be exposed to modified and extreme mechanical

stresses, if instability in the joint is present. Instability is often caused by damage to the surrounding muscles and ligaments or by conditions such as DDH.

There are thought to be two stages associated with OA, the initiation phase and the progression phase, both affected by different factors (Andriacchi et al. 2004). Modification to the position of load bearing areas of articular cartilage to areas infrequently loaded is thought to initiate OA (Andriacchi & Dyrby 2005; Anderst & Tashman 2009). Other than changes in load bearing regions, alterations in sliding, rolling and pivoting contacts may also impact on extensive cartilage loading. After initiation, OA progresses due to a breakdown of the cartilage caused by amplified tangential shear loading. During this progression phase, OA develops in relation to the amount of load applied (Andriacchi et al. 2004). As well as tribological functions, biomechanical factors resulting in cartilage degeneration are generally recognised by concentric or eccentric overload. This is where the joint becomes vulnerable to dynamic instability, localised overload, impingement, or a combination of all factors (Jaberi & Parvizi 2007). It is most often seen in patients with cam impingement (bony growth on the femorl head-neck junction) or DDH, both linked to early onset of OA (Manaster & Zakel 2006; Parvizi et al. 2006). Pistol-grip deformity consists of an aspherical femoral neck and head junction with an increased radius of the femoral epiphysis as it joins the neck (Figure 1-23). Although concentric and eccentric overload provide an explanation for the development of OA in patients with irregular hip joints, it fails to explain the aetiology of the disease in young adults with nondysplastic hips (Leunig et al. 2005; Manaster & Zakel 2006; Ganz et al. 2008). Recently, Ganz et al (2008) discovered that slight morphological abnormalities can result in FAI, thought to be an initiator of OA in young adults.

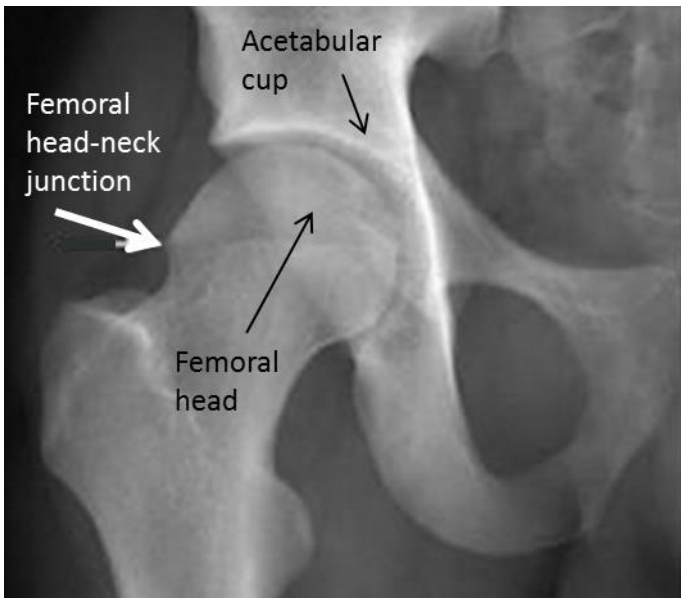

Figure 1-23 Pistol grip deformity. The white arrow highlights the aspherical section of the femoral head-neck junction, taken from Robinson (2010).

Age is also thought to affect the development of OA, as muscles become weaker and the body is less able to heal, joints can become worn out. As well as age, previous injuries or operations to the joint and joint abnormalities or diseases are thought to function in the initiation or progression of OA, these can include damage to the local tissues such as labral tears (Narvani 2003; Arthritisresearchuk.org 2009).

1.5.2.3 Treatments

Treatment of OA in the hip is very similar to that of many other hip joint diseases, where the initial stages include anti-inflammatory medication and minimising weight-bearing activities, followed by arthroscopy to remove tissue debris. The eventual treatment for the chronic disease will result in a joint replacement with a limited life span.

The American College of Rheumatology states that the criteria for diagnosing hip OA must include the presence of pain in the hip and at least two of the following symptoms; a normal erythrocyte sedimentation rate (the rate at which red blood cells sediment, used as a measure of inflammation), the presence of osteophytes or cartilage loss represented by narrowing of the joint space (Arden et al. 2008).

Current literature suggests that there are many different factors influencing the initiation of OA, with one of the most recent developments being FAI. Although FAI is a relatively new area of research, there is a great deal of literature to support the theory. There is however conflicting views on whether cartilage is damaged as a result of degradation to the labrum or vice versa. Therefore, further research is required to gain a full understanding of the condition and how it progresses.

1.5.3 Femoroacetabular impingement

FAI is a morphological abnormality of the bone, found in the proximal femur or acetabulum, resulting in abnormal contact between the femoral neck and acetabular rim. The abnormal contact leads to an impingement of the anterior femoral head-neck junction against the adjacent anterosuperior labrum (Beck et al. 2005; Leunig et al. 2005; Manaster & Zakel 2006; Ganz et al. 2008; Naal et al. 2011). There are two distinct types of impingement, cam and pincer (Figure 1-24), associated with FAI, which differ greatly in patterns of labral and/or chondral injury (Philippon et al. 2007). Differences in cam and pincer impingement are defined by the abnormalities in either the femoral neck or the acetabulum. Abnormalities of the proximal femur and acetabulum can occur independently of one another; however it is not uncommon to find a combination of both abnormalities and impingements (Beck et al. 2005; Manaster & Zakel 2006; Ganz et al. 2008). Degeneration as a result of pincer impingement progresses at a much slower rate to that found in the more destructive cam impingement (Ganz et al. 2008). Young active males are mostly likely to develop cam impingement as opposed to that of pincer

impingement, which is most common in women and elder patient groups (Manaster & Zakel 2006). Anterosuperior impingement is the most frequent impingement which occurs in FAI patients however, it is also possible for posteroinferior impingement to occur. Due to these abnormalities, stresses become localised and hence the load required to initiate damage is minimised, compared to that of general 'wear and tear' in OA (Leunig et al. 2005; Manaster & Zakel 2006; Naal et al. 2011).

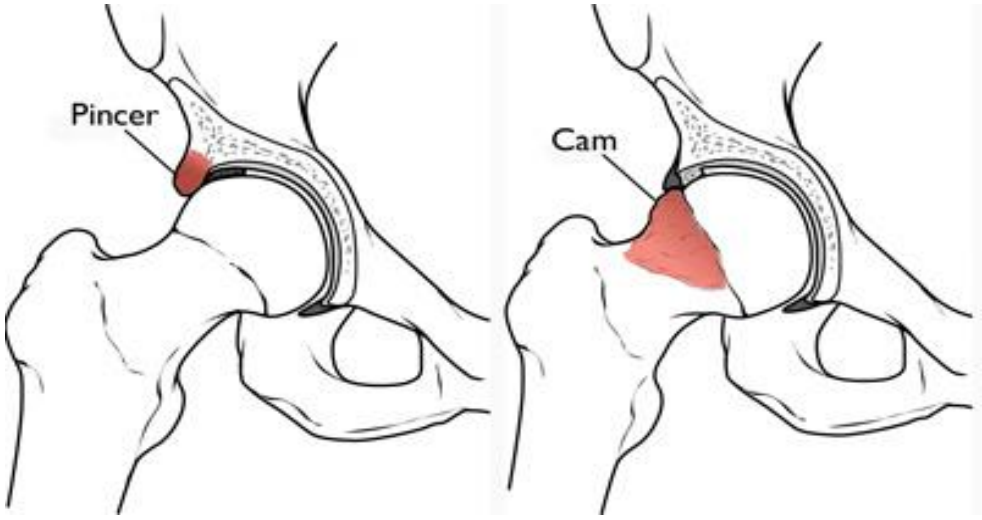

Figure 1-24 Femoroacetabular impingement. Pincer and cam impingement, caused by overhanging anterolateral acetabulum rim and bony prominence at anterolateral head-neck junction respectively, taken from Grana & Fischer (2006).

1.5.3.1 Characteristics

Cam impingement is the result of an abnormal femoral head-neck, due to an insufficient offset, with an increasing radius of the femoral head (Figure 1-24). It causes damage to the cartilage in the anterosuperior region of the acetabular rim and most often occurs when there is a lateral femoral neck "bump" (Beck et al. 2005; Leunig et al. 2005; Manaster & Zakel 2006). During vigorous motions in flexion, adduction or internal rotation, the aspherical section of the femoral head is rotated and driven into the acetabular rim and can be seen as joint space narrowing on an MRI (Leunig et al. 2005; Manaster & Zakel 2006; Ganz et al. 2008). The resulting shear stresses create an outside-in abrasion of the acetabular cartilage and a chondral rupture, leading to a subsequent tear or detachment of the primarily unconcerned labrum (Beck et al. 2005; Manaster & Zakel 2006). The resulting cartilage cleavage can be as deep as 2cm and will become destroyed over time. Cyst development (a swelling of fluid) is often associated with cam impingement and is thought to be a result of the abutment process. Cysts are frequently found in the head or near the head-neck junction (Ganz et al. 2008). Studies by Beck et al. (2005) and Manaster & Zakel (2006) have shown that the labral tear occurs at the articular

margin and not the capsular margin, which suggests that the cartilage is initially damaged followed by the labrum, as a secondary consequence. This theory is further proven by the possibility of chondral damage without the presence of a labral tear in the early stages of FAI (Leunig et al. 2005; Manaster & Zakel 2006). The aetiology of the abnormal femoral head/neck offset is uncertain, however there are various opinions ranging from a subclinical slipped capital femoral epiphysis (a displacement of the capital femoral epiphysis) or a growth disturbance (where the bone grows at different rates), which could result in a delayed separation or eccentric closure of the common physis between the femoral head and greater trochanter. The later would result in an abnormal extension of the femoral head epiphysis and a constant decrease in the head-neck offset (Manaster & Zakel 2006).

Opposed to cam impingement, pincer impingement is characterised by any abnormality that results in an increased coverage of the anterosuperior section of the femoral head by the acetabulum (Figure 1-24, Philippon et al. 2007). The acetabular abnormality can be global or local, similar to that of the focal acetabular retroversion (when the acetabulum is inclined posterolaterally). The abnormality results in a linear contact between the acetabular rim and the femoral head-neck junction, forming an impingement, resulting in labral tears and bony proliferations at the acetabular rim. Ganz et al (2008) disbelieves the theory proposed by Beck et al. (2005) and Manaster & Zakel (2006) and hypothesises that in pincer FAI it is the labrum that is the first structure to fail and only in the late stages of the process cartilage abrasion will occur. Unlike cam impingement, it is possible for the femoral head to be of normal morphology and the abutment caused by an acetabular abnormality, such as a deep socket or a localised overcoverage, as seen in acetabular retroversion (Beck et al. 2005; Leunig et al. 2005; Manaster & Zakel 2006). Continued impact on the femoral head-neck junction produces degeneration of the labrum with intrasubstance ganglion formation (a form of cyst). Further deepening of the acetabulum can result from ossification of the rim, which will increase the over coverage. Bone apposition occurs next to the labrum on the osseous rim causing the labrum to be pushed forward and become thinned, until it eventually becomes indistinguishable (Ganz et al. 2008). Relentless abutment can lead to focal chondral injury and cyst formation from the labral tear or ossification of the acetabular rim. Continued chronic force of the head in the acetabulum can result in chondral damage in the “contre-coup” region of the posterior-inferior acetabulum and/or head, leading to central joint space narrowing (Leunig et al. 2005; Manaster & Zakel 2006). In pincer impingement, chondral lesions can be contained to a small region of the acetabular rim making them less harmful over a prolonged period of time (Leunig et al. 2005).

1.5.3.2 Pathogenesis

Like OA, the causes of FAI are still under debate, however as well as the subtle bony abnormalities, it is thought that FAI can occasionally be the result of extreme ranges of motion

and abnormal stresses, forcing the femoral neck to come into contact with the anterosuperior labrum (Dooley 2008; Naal et al. 2011). FAI can also be caused by trauma or prior surgery or more universally the result of dysplasia (Leunig et al. 2005; Manaster & Zakel 2006).

1.5.3.3 Treatments

Treatments for FAI can vary considerably from conservative to surgical treatments. Pain medication with reduced physical activity is usually the first stage of treatment with physiotherapy also being an option for joint realignment. After conservative treatments, the next stage is generally surgery with either the more common arthroscopy, or in some cases open hip dislocation. Surgeries such as resection osteoplasty of the aspherical section of the femoral head can be used to treat cam impingements or periacetabular osteotomies can be performed to reorient a retroverted acetabulum in pincer impingement. In an osteoplasty procedure the prominent area of bone is removed to restore the femoral neck clearance (Figure 1-25), whereas in periacetabular osteotomies a section of bone around the acetabulum is removed in order to make the joint more stable. If there is any debris from damaged tissues this can be removed during arthroscopy or open hip surgery and labral refixation can also be performed if damage has occurred. If minor surgery is unsuccessful and OA develops, the final option is a hip joint replacement (Pierannunzii & D'ImporzanoMarco 2007).

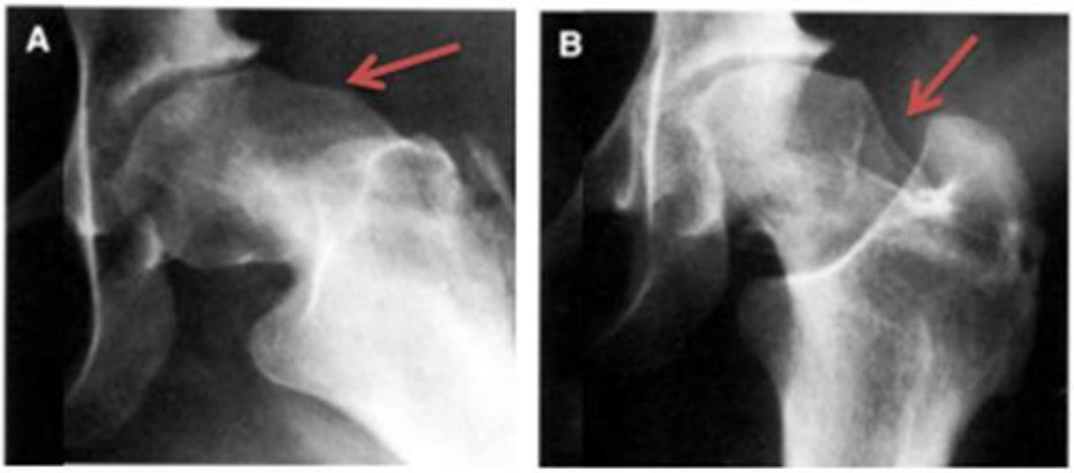

Figure 1-25 Femoral osteoplasty. A - Hip joint prior to an osteoplasty. B - Hip post-surgery. The red arrows highlight the modifications to the femoral head neck. Image taken from Shapiro (2002).

Clohisy et al. (2010) stated that surgical treatment is becoming a lot more frequent for FAI; however there is great debate over the strength of clinical evidence to support the surgery. Short term results, approximately two to three years, have had good patient satisfactory with pain relief and improved function reported however, there is insufficient long term outcome data and hence the overall success rate of these treatments remain unknown (Clohisy et al. 2010).

1.6 Current *in vitro* labral models

As current knowledge of the acetabular labrum is limited, there is a need for the development of a labral model which will allow the function and material properties of the labrum to be determined and labral damage to be investigated. Labral damage models are currently under going research and development to fulfil this clinical niche.

There are two key types of *in vitro* modelling used to gain an understanding of the labrum; computational modelling including two-dimensional (2D) and three-dimensional (3D) models as well as simulation studies using natural hips. Computational models and simulation systems have been used to produce simplified models of the tissue or the joint by making assumptions in order to provide a quicker, easier or cheaper understanding of the issue. It is not always possible to obtain natural tissue due to availability and cost and the body is an intricate system which cannot always be mimicked precisely or patient specifically. Therefore, computational models remove the need for natural tissue as well as being reproducible. Simulation systems allow the movements of the body to be replicated in a simplified manor using natural tissue. Although there are limitations to these studies they are not thought to affect the overall general outcome however, the extent to which they are true needs to take into account these limitations and the effect they will have on the study.

1.6.1 Computational models

Computational models are used in research to model many different types of tissues and joints. The structures can be imported from scans such as computed tomography (CT) or designed within the computer package. They allow varying degrees of simplification to be applied to the model and can be used to compress a time frame, quickly modelling *in vivo* situations which can take several years. Computational models have been developed for the acetabular labrum to determine the effect of the labrum on cartilage consolidation, the role of the labrum in load support, and the location of impingement on the labrum. Several limitations are produced with labral computational models which mainly include the assumption of the material properties including the Young's modulus, permeability and Poisson's ratio, the boundary conditions and the load/motion cycle. A study by S J Ferguson et al. (2000) assumed the underlying bone to be impermeable and rigid and labral and cartilage tissue were assumed to be poro-elastic to represent the biphasic effect of the tissues, where as Henak et al. (2011) represented cortical bone as isotropic linear elastic, cartilage as neo-Hookean hyperelastic and the labrum as transversely isotropic hyperelastic, making comparisons between studies complex.

S J Ferguson et al. (2000) used finite element analysis (FEA) to produce a 2-dimensional (2D) coronal slice of the hip joint to determine the effects of the labrum on cartilage consolidation. A load was applied to the hip joint for 1 hour with and without the labrum attached. It was identified that the labrum reduced fluid flow from the cartilage and slowed down cartilage

consolidation by up to 40 %. Henak et al. (2011) also used FEA as a computational model to assess the role of the labrum in load support across the hip, using CT image data to produce a 3D model of the acetabulum. The hip joint was loaded to represent daily activities. The study identified the normal labrum to support 1-2 % of the total load transferred across the joint where as in a dysplastic hip the labrum supported between 4-11 % of the load. Dy et al. (2012) used CT scans to produce 3D virtual simulations of the hip to simulate hip positions that typically cause labral impingement. The labrum was represented as a curve-fit to the acetabular rim which extruded 5 mm. The hip was placed in a range of flexion angles and internally rotated until the femoral neck impinged upon the labrum. The study identified that damage to labrum could occur in hips with normal morphology however, the presence of morphological features associated with impingement may result in a characteristic pattern or severity of labral damage.

1.6.2 Simulator models

Simulator models have an advantage over computational models as they can use natural tissue and hence the material properties and boundary conditions do not need to be estimated. They allow whole joints to be tested under a range of loading and motion and allow tissues to be tested in situ. Several simulator models have been developed for the acetabular labrum to carry out tribological testing of the tissue and determine the effect of the labrum on cartilage consolidation and rotational restraint of the hip (Van-Arkel et al. 2015; Groves 2016) as well as labral damage models to determine the effect of labral tears on the labral seal and joint stability, and the effects of a full or partial labrectomy on cartilage friction (Ferguson et al. 2003; Safran et al. 2011; Smith et al. 2011; Cadet et al. 2012; Song et al. 2012; Philippon et al. 2014). Similar to computational models, simulator models are still simplified in comparison to *in vivo* tests. General limitations of *in vitro* simulation models include; the load applied to the joint, the motion of the joint, and the duration of the test. Simulator studies in literature simplify the load or motion cycle of the joint, which are likely a result of the limitations of the machines or the test (i.e. inserting devices within the joint would result in damage to the surface during motion). The load is often applied as a constant load or a sinusoidal load, which is simplified compared to the complex load cycle, experienced *in vitro* which constantly changes over the gait cycle. Motion, if applied to the joint, is often applied in a step manner rather than a continuous cycle. A further limitation to using natural tissue for *in vitro* simulation is the duration of the tests; natural tissue decays once its removed from the body and hence the properties of the tissues change over time.

Studies by Song et al. (2012); Philippon et al. (2014); Groves (2016) removed the joint capsule prior to testing. This allowed the articulating surfaces to be analysed for damage in detail, however it resulted in the joint becoming misaligned. Various methods were required by the authors in order to realign the acetabular cup and femoral head using bony landmarks of the hip joint. For the studies where the joint capsules remained intact; Van-Arkel et al. (2015) did not

appear to inspect the joint for damage prior to testing, Cadet et al. (2012) inspected the external joint capsule for damage, Ferguson et al. (2003); Smith et al. (2011) used radiography to assess the bony structures and Safran et al. (2011) used MRI to asses the soft tissues within the hips. By assessing the tissues externally it meant that the joint could be kept intact with the joint fluid and realignment was not required which would reduce errors in the test. Ideally a combination of radiography and MRI would be beneficial to rule out damage to the bony structures as well as the soft tissues however, this is costly and time consuming.

Smith et al. (2011); Song et al. (2012); Philippon et al. (2014); Van-Arkel et al. (2015) applied static loads to the hip joint with a range of magnitudes identified as suitable by the authors for the individual tests. Ferguson et al. (2003); Groves (2016) applied a more advanced dynamic sinusoidal load which roughly mimicked the loading cycle during gait where the fluid is able to flow back into the tissues during unloaded periods. However the simplified load pattern could result in higher or lower loads applied to the joint in incorrect positions, which could result in artificial results such as dislocations or damage at higher loads, or reduced effects at lower loads. Ideally a loading cycle closer to *in vivo* test conditions with a dual-peak load would be beneficial however, this is dependent on the capabilities of the equipment.

Ferguson et al. (2003); Cadet et al. (2012); Philippon et al. (2014) tested the hip joint in a stationary position. During the tests, devices were inserted into the intra-articular space to measure the effect of the fluid seal which would have resulted in damage to the tissue surfaces if a motion had been applied. Safran et al. (2011); Song et al. (2012); Van-Arkel et al. (2015) applied step loads to the tissues where the joints were moved to set positions before the test was started. Groves (2016) applied a pendulum motion to the hip joint in the flexion-extension plane. Ideally tests would be carried out with a gait cycle that closely mimicked that seen *in vivo* with motion in flexion-extension, abduction-adduction and internal and external rotation. This would allow effects to be analysed at the extreme motions and positions that would occur naturally in the body. This is often a limitation of the equipment used and hence a study needs to be developed in which these motions can be applied to the joint in a continuous motion.

The majority of simulator tests were carried out over short periods of time until the test has reached the desired outcome (for example dislocation). The longest test duration (2 hours) was carried out by Groves (2016) where the purpose of the study was to develop an *in vitro* simulation for tribological testing of natural porcine tissue. Hence, a prolonged testing period is required to determine if damage will occur over a realistic time period. Although this is a limitation to the study and longer test periods would be beneficial it is a compromise between duration and sample size as longer test times would result in fewer repeats of each study and potentially degraded tissue if the test is ran for a long enough period.

1.7 Aims & objectives

The primary aim of this study is to develop an *in vitro* natural hip simulation of morphologically abnormal joint diseases to provide scientific understanding to support and assess surgical interventions.

Objectives;

- To determine the structure of the acetabular labrum and labral-cartilage junction in comparison to articular cartilage.

- To assess biological differences in load-bearing and non-load-bearing regions of the acetabular labrum, acetabular cartilage and femoral cartilage.

- To determine the mechanical properties of the acetabular labrum in comparison to acetabular cartilage.

- To compare porcine and human tissue for labrum and labral junction.

- To assess the effects of altered loading (as seen in FAI), to the tribological interface, using an *in vitro* simulation.

Chapter 2

Materials and methods

2.1 Introduction

The functions and constituents of individual tissues in the hip must be fully understood in order to develop a successful *in vitro* simulation system of the hip. This study characterises the cartilage and labral tissue of the hip joint both biologically and mechanically. Figure 2-1 shows the different methodologies used throughout this study to characterise labral and cartilage tissue and develop an *in vitro* simulation of the natural hip joint. The aim of this chapter is to describe the generic equipment, solutions, and methodology used throughout this thesis.

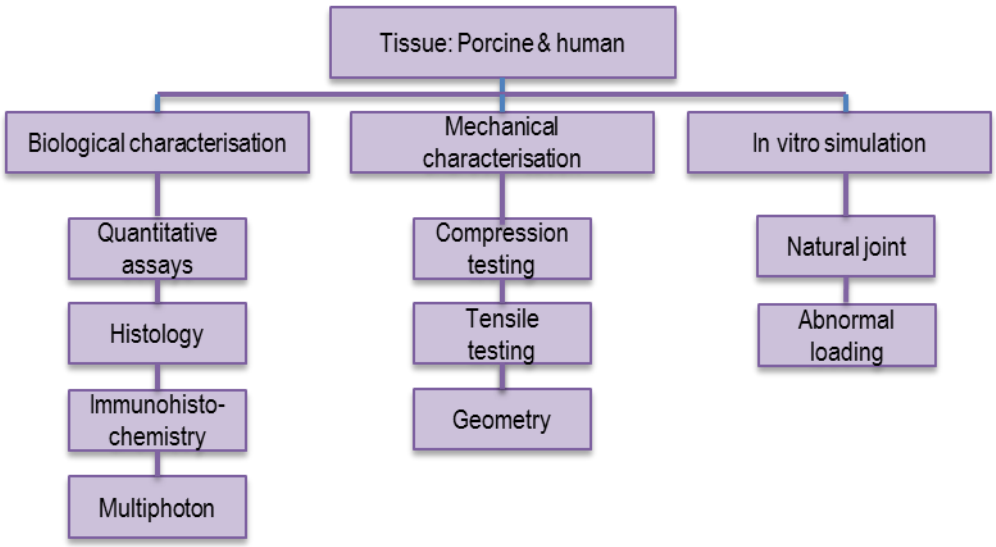

Figure 2-1 Summary of the methods used in this study.

2.2 General materials and methods

This section lists all materials used throughout this study and the general methods that are used during multiple experiments. General methods include methods used to prepare solutions, prepare equipment, and to capture images.

2.2.1 Equipment, reagents and consumables

All reagents, consumables, equipment used, and their suppliers can be found in Appendix A.

2.2.2 Measurement of pH

The pH of various solutions was measured using a pH meter. The pH meter was calibrated using three solutions of known pH (4, 7 and 10), prepared by dissolving buffer tablets in distilled water. To adjust the pH of a solution 1M hydrochloric acid or 1M sodium hydroxide was added drop wise whilst the solution was stirred.

2.2.3 Microscopy

Visualisation of histological and immunohistochemical tissue sections was undertaken using an upright microscope with standard Köhler illumination set up. A polariser was included in the set up for polarised-light microscopy. Images were captured using an attached camera that was controlled by Zen 2012 blue edition imaging software.

2.2.4 Photography

Photography of equipment, tissue, and experiments were carried out using a digital SLR camera. A desk camera stand and tripod were used to hold the camera steady at various positions.

2.2.5 Sterilisation

Equipment and instruments were dry sterilised in an oven for four hours at 180 °C. Items unsuitable for dry sterilisation were moist heat sterilised in an autoclave for 20 minutes at 121 °C and 15 psi. Equipment used for human tissue was soaked in Virkon for 30 minutes prior to dry heat sterilisation.

.

2.3 Tissue acquisition

Porcine and human tissue was used throughout this study. Porcine tissue was supplied by a local abattoir (J Penny, Rawdon, Leeds). Non-transplantable human cadaveric tissue was supplied by Platinum Training and the study was approved by The University of Leeds research ethics committee (MEEC 13-002). Phosphate buffered saline (PBS) was used throughout this study to keep tissue hydrated.

2.3.1 Dissection equipment

The dissection equipment used throughout this study is shown in Figure 2-2. Two, identical dissection sets were used; one for porcine tissue and one for human tissue. A battery powered handheld bone saw was used, in addition to the dissection equipment described, for human tissue.

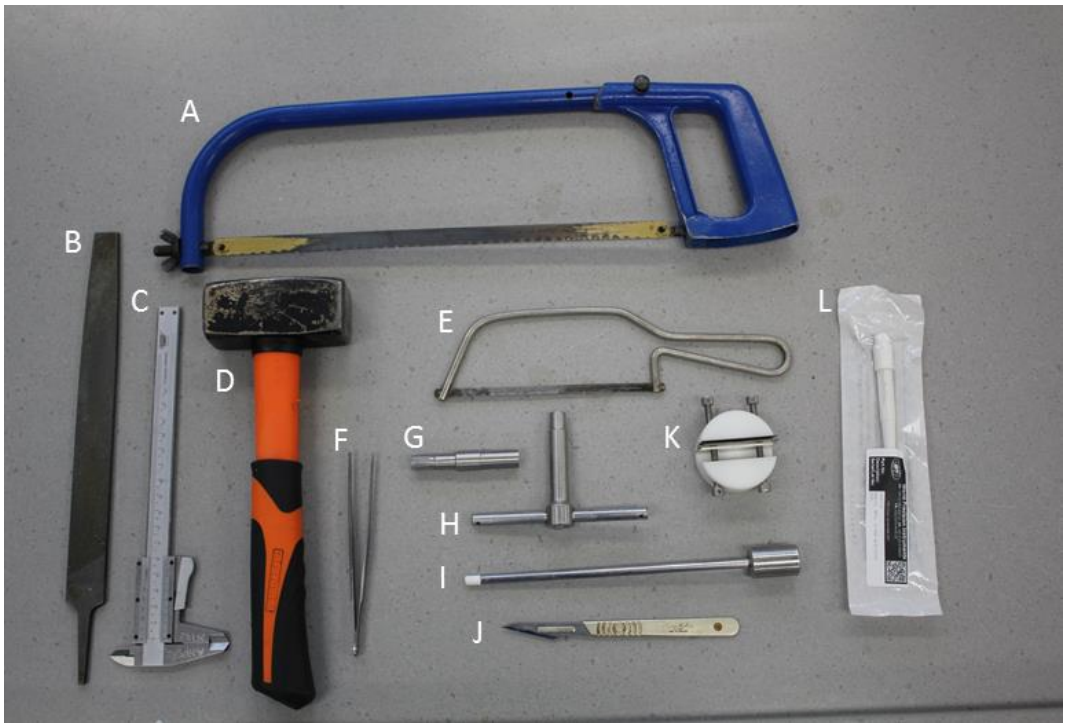

Figure 2-2 Dissection equipment for gross tissue dissection. A – Hack saw. B – File. C – Callipers. D – Hammer. E Hand held bone saw. F – Forceps. G – Serrated corer drill attachment. H – Smooth corer. I – Pin remover. J – Scalpel blade and handle. K – Parallel blades. L – Biopsy punch.

2.3.2 Porcine tissue acquisition

Porcine tissue was acquired from animals approximately six months old, which weighed between 60-100 kg, and was supplied within 24 hours of slaughter. Pigs were slaughtered for human consumption and the age of the animals was determined by availability in the food chain. Joints were used fresh or stored at 4°C overnight for dissection the following day. Hind right legs were used to ensure all repeat experiments were from individual pigs.

Porcine legs were dissected as shown in Figure 2-3 to harvest the whole hip, acetabulum, femoral head and/or soft tissues. Excess flesh, ligamentous tissue, muscle, and fat were removed from the skeletal structures to allow easier access and manoeuvrability of the hip joint Figure 2-3 A-D). The hip joint was exposed by cutting the extracapsular ligaments and joint capsule near the base of the femoral head-neck junction (Figure 2-3 E). The ligamentum teres was severed to separate the femoral head from the acetabulum (Figure 2-3 F–G). Excess joint capsule was removed at the point of connection with the acetabular labrum (Figure 2-3 H-I). Cartilage and labral surfaces were kept hydrated throughout by covering in phosphate buffered saline (PBS) soaked tissue.

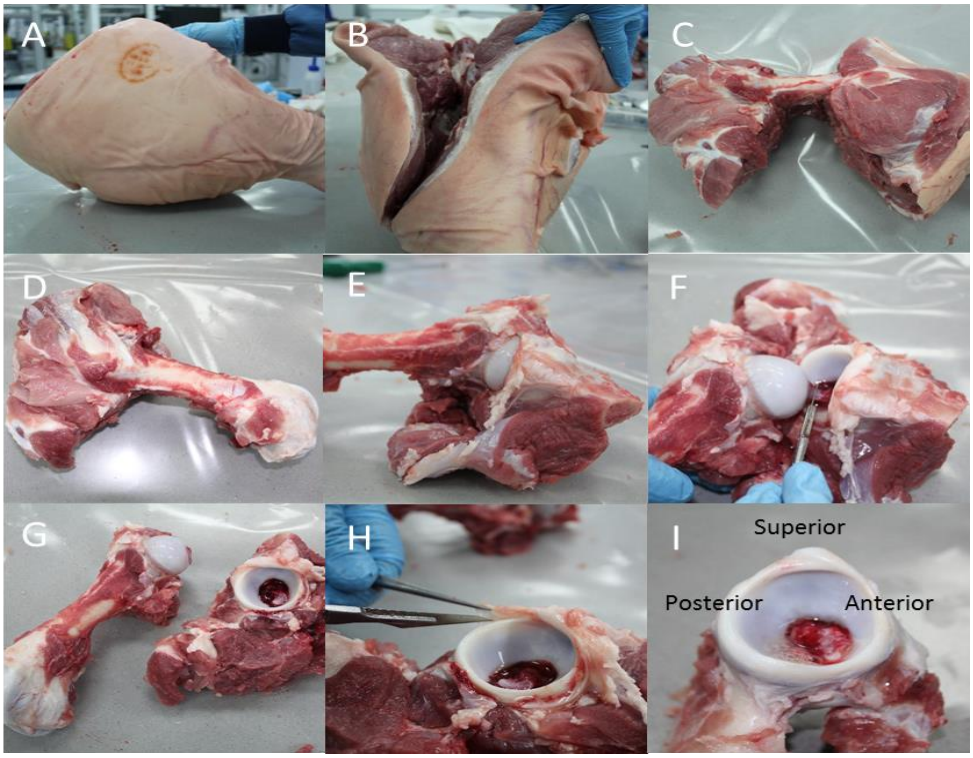

Figure 2-3 General porcine dissection. A – Lateral view of whole porcine leg. B – Initial cut along the length of the femur. C – Removal of soft tissue around the femur. D – Separation of the leg at the knee joint. E – Cut through the joint capsule to expose the femoral head. F – Severing of the ligamentum teres to separate the femoral head and acetabular cup. G – Femoral head and acetabulum. H - Removal of the joint capsule from the acetabulum. I – Acetabular cup with tissue removed.

2.3.3 Human tissue acquisition

Human tissue was acquired from donors with a mean age of 63.7 ± 7.2 years and weight 77.7 ± 31.7 kg. Pelvises were stored at -80 °C until required, upon which they were defrosted at room temperature for 24 hours. Right hips were used to ensure all repeat experiments were from individual donors. Donor demographics are listed below in Table 2-1.

Table 2-1 Human donor demographics.

Number	Donor's Age	Race	Sex	Weight (kg)	Height (cm)	BMI
144	55	White	Female	40	157	16.5
93	70	White	Female	79	152	34.2
556	67	White	Male	117	182	35
071	66	White	Female	64	165	23.6
076	55	White	Male	109	180	33.6
129	69	White	Male	57	154	23.8

Human pelvises were dissected as shown in Figure 2-4. The pelvis was separated into the right hip, left hip, and the spine using a bone saw Figure 2-4 (B-C). Human pelvises were supplied with excess tissue already removed; hence the hip joint capsule was already exposed. The joint capsule was cut at the base of the femoral head and the ligamentum teres was severed to separate the femoral head and acetabulum (Figure 2-4 D-E).Excess joint capsule was removed at the connection with the acetabular labrum (Figure 2-4 F).

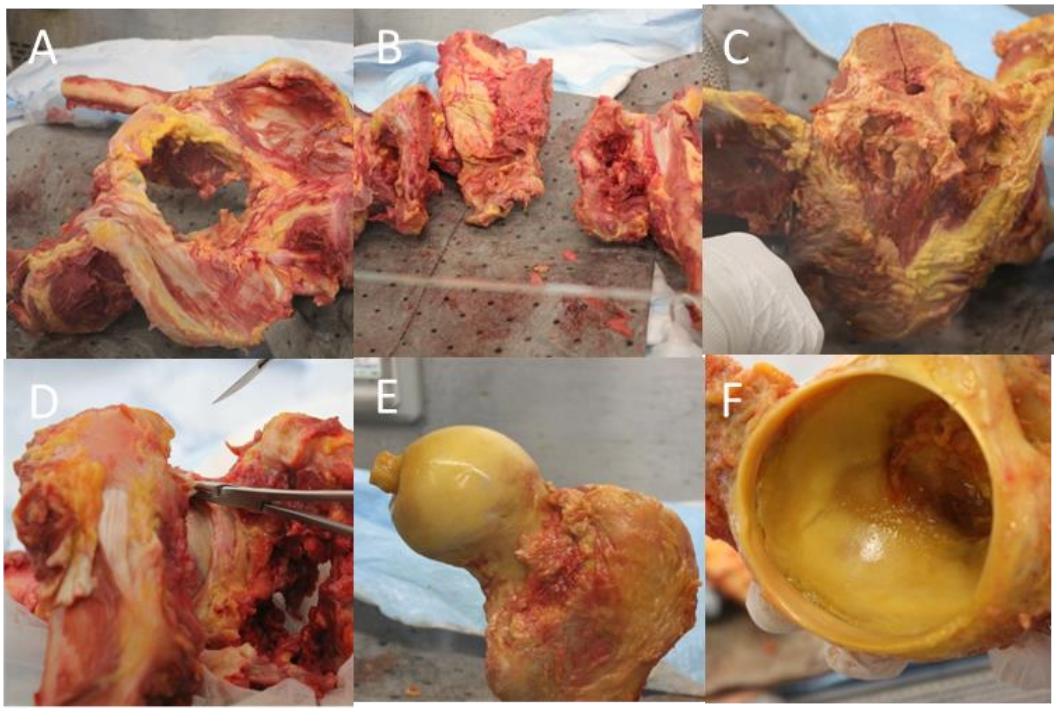

Figure 2-4 General human dissection. A – Whole human pelvis. B – Separation of pelvis into left hip, right hip, and spine region. C – Pelvis cut with bone saw. D – Joint capsule severed. E – Fully exposed femoral head. F – Fully exposed acetabulum.

2.3.3.1 Human tissue ethics and criteria

The following inclusion / exclusion criteria were used to identify suitable donors:

Inclusion:

- Donors who met Platinum Training's requirements regarding tissue donation and have signed a consent form.
- Male or female donors aged 18-70 years.

Exclusion:

- Donors that have suffered from OA in the hip, or suffered a broken hip, or had hip surgery (as described on the donor medical and social history questionnaire).
- Donors with serological results indicating a transmissible disease.

Platinum Training aims to 'provide non-transplantable, human cadaveric tissue for medical research, education and development, and other uses demonstrating scientific merit'. Platinum Training states that it has reviewed the processes by which consent or authorisation for research from the donor or authorising party was obtained (to the best of their knowledge), in accordance with all applicable state and federal laws and regulations prior to recovery and distribution. Platinum Training abides by the Uniform Anatomical Gift Aid Act. Serological test reports

were provided by Platinum Training. Donor samples and associated information was provided with a unique donor identification number to ensure the donors could not be identified by users at The University of Leeds. Samples were stored at -40 °C in a lockable freezer, until required, in accordance with the guidelines set out by the Human Tissue Authority. If a request was received regarding the withdrawal of a donor, those samples would be removed from the study and disposed of in the manner requested by Platinum Training. Any data collected on that donor would be removed from the study and destroyed.

2.3.4 Macroscale measurements

Gross measurements of porcine and human hip joints were carried out to determine the diameter of the acetabulum and the thickness of the labrum in the posterior, superior, and anterior region (n=6). Measurements were repeated three times and the average taken using callipers as seen in Figure 2-5. The acetabulum was measured in the AP direction at the top of the cartilage surface. The labrum was measured from the labral-cartilage junction to the labral apex.

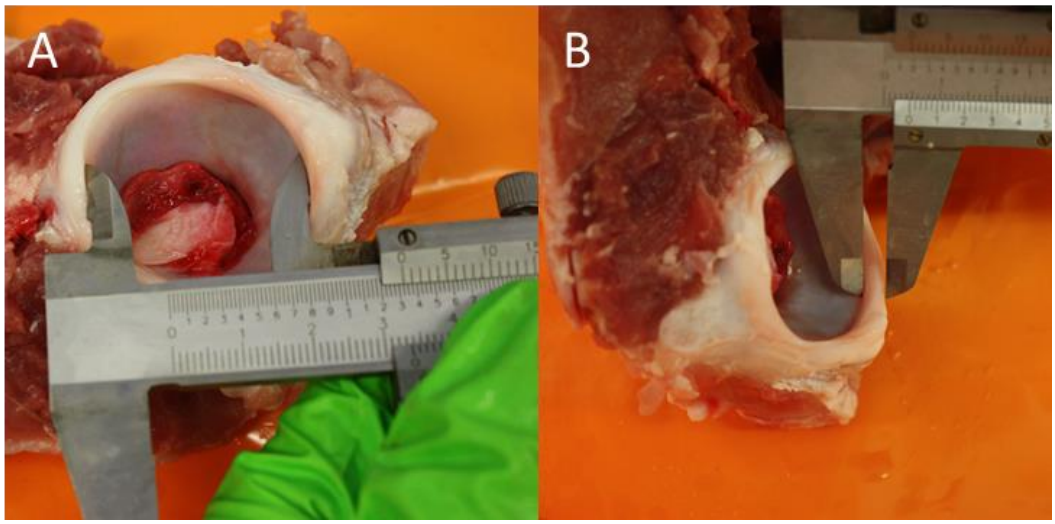

Figure 2-5 Macroscale measurements. A – Measurement of acetabular diameter. B – Measurement of labral thickness. Measurements demonstrated using a porcine acetabulum.

2.3.5 Pin extraction

Labral and osteochondral pins were extracted for use in compression testing, osteochondral pins were also used to acquire tissue for subsequent biochemical assays. Labral and cartilage pins were extracted using two separate methods as described in the below sections.

Labral pin extraction

Labral pins were extracted using a biopsy punch. The pins were cut from the internal to external surface of the superior labrum, above the labral-cartilage junction, and used for compression

testing (Figure 2-6 A). Following extraction the pins were cut to thickness using parallel blades separated by a 3 mm thick metal block (Figure 2-6 C). Pins were extracted and cut to the required thickness whilst the tissue was frozen to allow for more accurate cutting. Sample dimensions (thickness and height) were measured three times using a digital thickness gauge meter and the average taken (Figure 2-6 F).

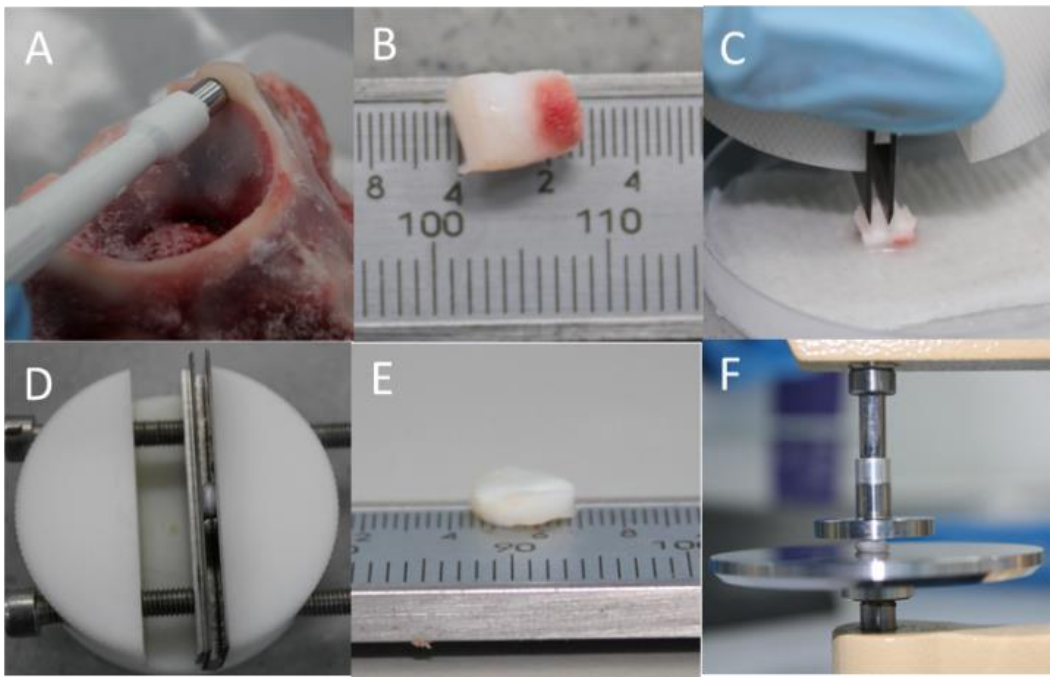

Figure 2-6 Labral pin extraction. A – Biopsy punch used to cut through the labrum. B – Labral pin from biopsy punch (on its side). C – Labral pin cut to thickness using parallel blades. D – Labral pin cut to thickness inside parallel blades. E – Labral pin (on its base). F – Measurement of labral pin thickness with a digital thickness gauge.

Osteochondral pin extraction

Osteochondral pins were extracted for use in compression testing and biochemical assays. The pins were extracted from a flat cartilage surface through to the subchondral bone, approximately 12 mm deep. The pin location was primarily marked with a handheld smooth corer (Figure 2-7 A-B) then cut with a serrated corer of identical diameter using a power drill (Figure 2-7 C). The initial handheld corer was then re-used to loosen the pin and extract it from the joint (Figure 2-7 D). Once the pin was extracted the subchondral bone was filed until parallel with the cartilage surface (Figure 2-7 E-F). Osteochondral pins were taken from the acetabulum and femoral head using the above method, images showing the extraction of an acetabular osteochondral pin are shown in Figure 2-7.

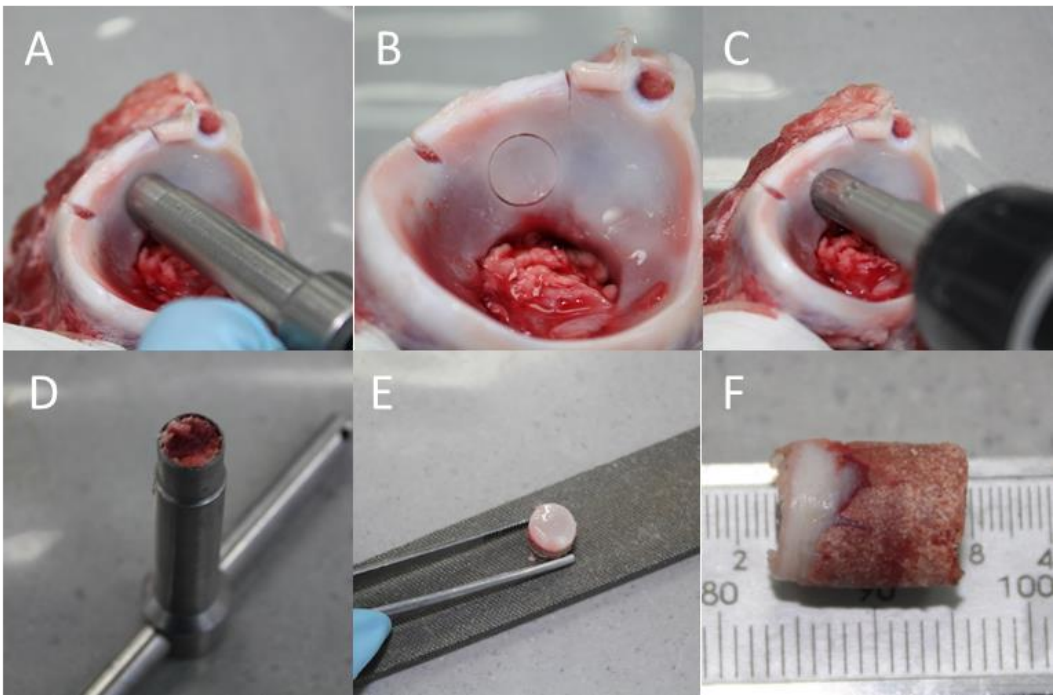

Figure 2-7 Osteochondral pin extraction. A & B – Acetabular cartilage surface marked with smooth corer. C – Cartilage and osteochondral bone cut with serrated corer attached to a power drill. D – Cartilage pin removed with smooth corer. E – Bottom of osteochondral pin flattened with file. F – Osteochondral pin.

2.3.6 Tensile specimen preparation

Labral tissue was prepared for use in the materials testing machine under tensile loading. Labral tissue was removed from the acetabulum along the labral-cartilage interface using a scalpel blade (Figure 2-8 A) and cut to approximately 20mm in length (Figure 2-8 B-C). The tissue was straightened and placed in a petri dish lined with a PBS soaked tissue and placed into a -80 ° freezer. Once frozen, the specimen was cut to width using parallel blades and a spacer (Figure 2-8 D-E). The tissue was rotated length ways 90 ° and placed back onto the PBS tissue and replaced in the -80 ° freezer to ensure the tissue did not defrost. The tissue was cut to thickness (specific to test methodology) using parallel blades and a spacer.

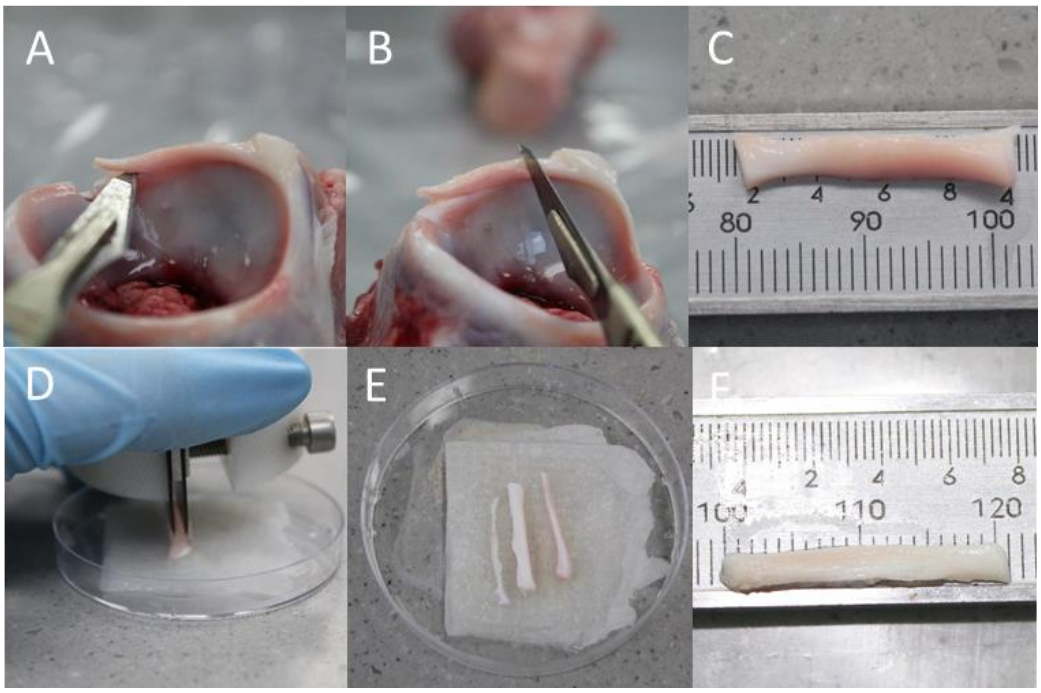

Figure 2-8 Labral tensile specimen preparation. A – Labrum cut along the cartilage-labrum interface. B – Labrum separated from the acetabulum. C – Labral sample before cut to size. D – Labrum cut to required width. E – Labrum cut to required thickness. F – Labral tensile specimen.

2.3.7 Histological and immunohistochemical specimen preparation

Small cross-sections through the acetabulum were used to identify and visualise key structures and constituents within the tissue types. To obtain histology and immunohistochemical sections, cross sections through the acetabulum, including the labrum, cartilage and subchondral bone (Figure 2-9 A-C), were taken from the anterior, superior, and posterior region of the acetabulum for porcine specimens and the anterior region for human specimens (due to limited tissue availability).

In each region two cuts were made, using a scalpel blade, from the apex of the acetabulum down to the subchondral bone, approximately 5mm in width (Figure 2-10 A). The cuts were then extended through the subchondral bone using a hand held bone saw (Figure 2-10 B). A perpendicular cut was then made approximately 20mm up from the base of the acetabulum parallel to the acetabular rim to remove the acetabular sections (Figure 2-10 C). For labral specimens a further cut across the apex of the acetabular labrum was made to remove it from the cartilage and subchondral bone (Figure 2-10 E). Specimens were then placed into plastic cassettes for tissue processing (Figure 2-10 D & F). Images showing the sample preparation are shown in Figure 2-10. To maximise tissue usage, acetabula were used for multiple samples / experiments hence a pin extraction site can also be seen in Figure 2-10 A-B.

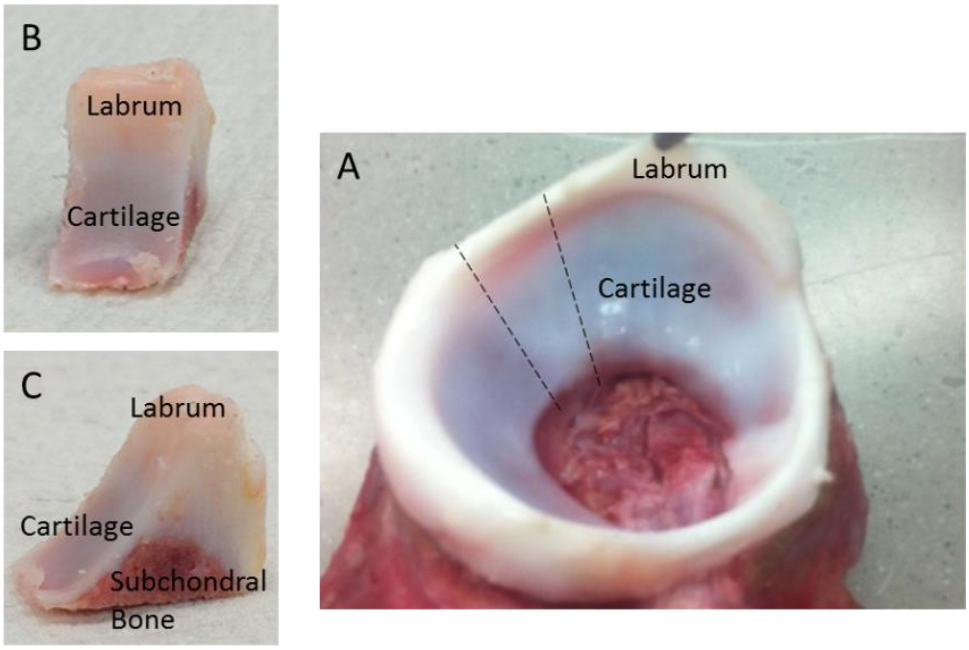

Figure 2-9 Image showing the orientation of a histology or immunohistochemistry specimen. A – Whole acetabulum, dotted lines mark where the section is removed from. B – Front view of a histology / immunohistochemistry section. C – Side view of a histology / immunohistochemistry section.

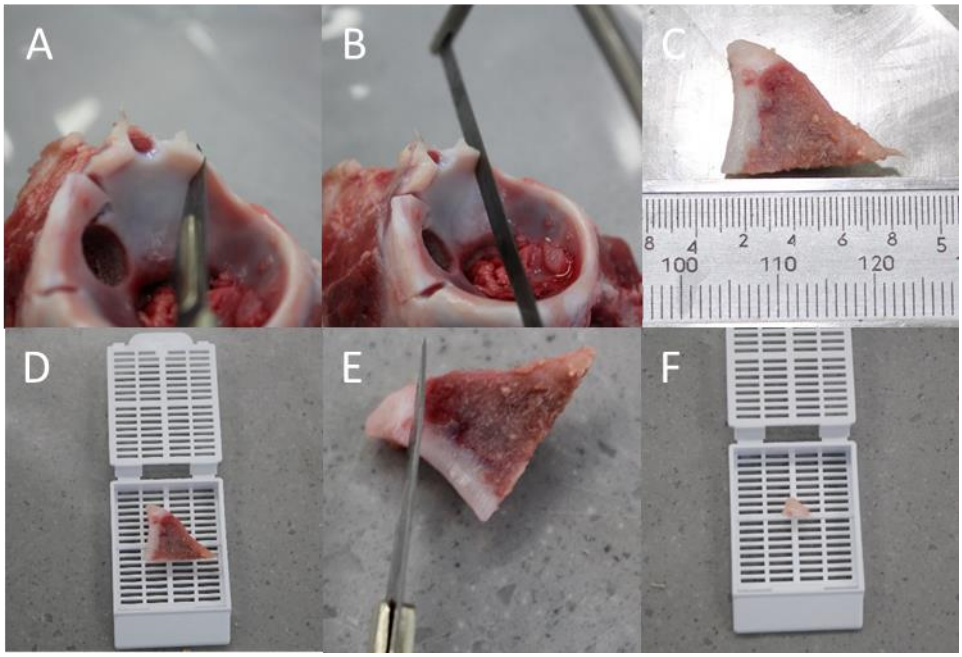

Figure 2-10 Acetabular and labral histological and immunohistochemical specimen preparation. A – Vertical cut through labrum. B – Vertical cut continues through subchondral bone and cartilage. C – Acetabular Specimen. D – Acetabular specimen in plastic cassette for tissue processing. E – Labral specimen cut from acetabular specimen. F – Labral specimen in plastic cassette for tissue processing.

2.3.8 Biochemical assay specimen preparation

Biochemical assays were used to determine the water content and GAG and hydroxyproline concentration, within acetabular cartilage, femoral cartilage, and acetabular labrum across various regions.

Cartilage tissue was removed from the subchondral bone of an osteochondral pin (section 2.3.4) using a scalpel blade as seen in Figure 2-11 A & B. Labral tissue was removed from the acetabulum using a scalpel blade as seen in Figure 2-8 A & B. The tissue was macerated (cut into small pieces, Figure 2-11 C & D) to increase the surface area and placed into pre-weighed bijouxs. Samples were lyophilised (dehydrated using a freezedryer) to a constant weight (±0.0010g) in a freezer dryer at -50 °C, 0.15 to 0.2 mbar for approximately 2 weeks. Samples were weighed before and after lyophilisation to determine the tissues wet and dry weight and every 24 hours to monitor drying. All weight measurements were taken three times and the average calculated.

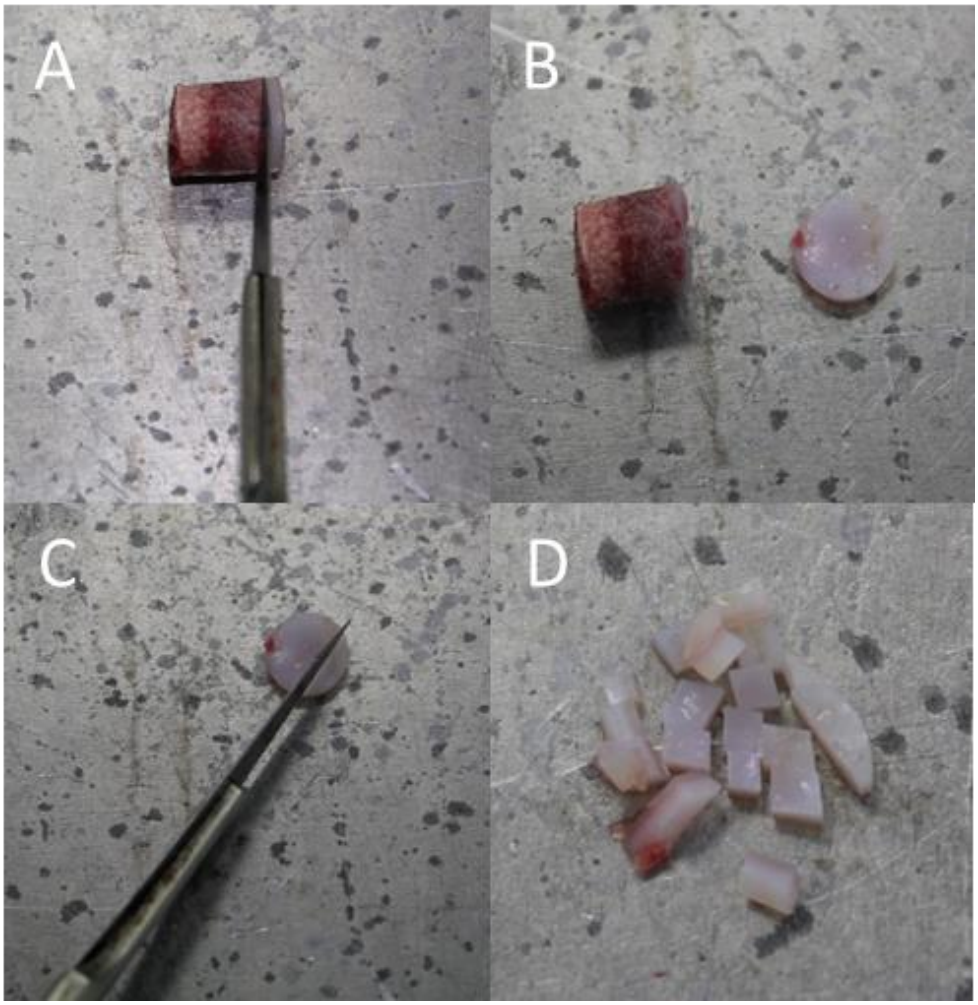

Figure 2-11 Tissue maceration for assays. A – Osteochondral pin. B – Cartilage removed from subchondral bone. Cartilage cut using a scalpel blade. D – Macerated tissue.

2.4 Biochemical assay reagents and methods

2.4.1 Glycosaminoglycan quantification assay

GAG quantification is possible by determining the proteoglycan content within a tissue, as GAGs covalently link to a central core protein to form proteoglycans. The proteoglycans are stained with dimethylene blue (DMB) dye and can be measured using a spectrophotometer to colourimetrically quantify the GAGs.

2.4.1.1 Reagents

The below is a list of chemical solutions used in the glycosaminoglycan assay and the methods used to prepare them.

0.1 M sodium di-hydrogen orthophosphate

Sodium di-hydrogen orthophosphate (0.1 M) solution was prepared by dissolving 3.45 g of sodium di-hydrogen orthophosphate in 250 ml distilled water. The solution was used immediately.

0.1 M di-sodium hydrogen orthophosphate

Di-sodium hydrogen orthophosphate (0.1 M) solution was prepared by dissolving 3.55 g di-sodium hydrogen orthophosphate in 250 ml distilled water. The solution was used immediately.

Digestion buffer

Digestion buffer was prepared by dissolving 0.788 g L-cysteine hydrochloride and 1.8612 g disodium ethylenediaminetetraacetic acid (EDTA) into 1 L of PBS. The solution was then adjusted to pH 6.0. The solution was stored at room temperature for up to six months.

DMB dye solution

DMB dye solution was prepared by dissolving 16 mg 1,9 dimethylene blue into 5 ml ethanol and 2 ml formic acid. Following stirring, 2 g sodium formate was added and the solution was made up to 1 L using distilled water. The solution was then adjusted to pH 3.0 using formic acid. The solution was stored at room temperature for up to three months.

GAG assay buffer

GAG assay buffer was prepared by combining 137 ml 0.1 M sodium di-hydrogen orthophosphate and 63 ml 0.1 M di-sodium hydrogen orthophosphate, and then adjusted to pH 6.8. The solution was stored at room temperature for up to three months.

Papain digestion solution (50 $U.ml^{-1}$)

Papain digestion solution was prepared by dissolving 1250 U papain in 25 ml digestion buffer. The solution was used immediately.

2.4.1.2 Method

Following maceration and lyophilisation 15 mg of dry weight tissue was digested in 5 ml of papain digestion solution and incubated in a water bath at 60 °C for 36-48 hours, until fully digested. A negative control of papain digestion solution-only was included. Primary standard solutions of chondroitin sulphate B were diluted in GAG assay buffer to produce nine standard concentrations of 0, 3.125, 6.25, 12.5, 25, 50, 100, 150 and 200 $\mu g.ml^{-1}$. Optimisation of samples was performed at 1:10, 1:25 and 1:50 dilutions in GAG assay buffer. Standards, diluted samples, and negative controls (40 µl) were added to a clear, flat-bottomed 96 well plate in triplicate, to which 250 µl DMB dye was added. Plates were shaken for 5 min at 200 rpm on a plate shaker before the optical density of each well was measured at 525 nm using a micro plate spectrophotometer. Following deduction of blank values from all standard and sample values, a standard curve was plotted of chondroitin sulphate B vs. absorbance. Linear regression analysis was performed to interpolate the GAG concentration of the samples as a result of their absorbance. Dilution factors were reversed and the GAG concentration was determined for the dry weight of the tissue.

2.4.2 Hydroxyproline quantification

Hydroxyproline is an amino acid which is found almost exclusively in collagen proteins and hence can be used in assays to determine the collagen content of a tissue (Reddy & Enwemeka 1996). This assay was adapted from the method devised by Edwards & O'Brien (1980) where acid hydrolysis is used to breakdown the collagen to release hydroxyproline residues. Collagen content can be determined from hydroxyproline quantification by a conversion factor of 7.14, determined by its repeatability within collagen fibrils.

2.4.2.1 Reagents

The below is a list of chemical solutions used in the hydroxyproline assay and the methods used to prepare them.

Chloramine T

Chloramine T was prepared by dissolving 1.41 g chloramine T in 100 ml distilled water. The solution was used within one hour.

Ehrlich's reagent

Ehrlich's reagent was prepared by combining 7.5 g p-dimethylaminobenzaldehyde, 30 ml propan-1-ol, 13.4 ml 60 % (v/v) perchloric acid and 6.6 ml distilled water. The solution was used immediately.

Hydroxyproline assay buffer

Assay buffer was prepared by combining 13.3 g citric acid, 3.2 ml glacial acetic acid, 32 g sodium acetate (3 H_2O), 9.1 g sodium hydroxide and 80 ml propan-1-ol, and then made up to 300 ml using distilled water. The solution was the adjusted to pH 6.0 and made up to 400 ml using distilled water. The solution was stored at 4 °C, in the dark, for up to two months.

2.4.2.2 Method

Following maceration and lyophilisation 15 mg of dry weight tissue was placed in a glass test tube with 6M hydrochloric acid (5 ml) and incubated in a bench-top autoclave at 120 °C for 4 hours to hydrolyse. Samples were then neutralised using 6M sodium hydroxide. Primary standard solutions of trans-4-hydroxy-L-proline were diluted in hydroxyproline assay buffer to produce standard concentrations of 0, 2, 4, 6, 8, 10, 15, 20, 25 and 30 $\mu g.ml^{-1}$. Optimisation of samples was performed at 1:10, 1:25 and 1:50 dilutions in hydroxyproline assay buffer. Samples and standards (50 µl) were added to a clear, flat-bottomed 96 well plate in triplicate, to which chloramine T (100 µl) was added and the plate was shaken for 5 min at 200 rpm. Ehrlich's reagent (100 µl) was then added to each well and the plate was incubated in a water bath for 45 min at 60 °C. Following incubation the optical density of each well was measured at 570 nm using a micro plate spectrophotometer. A standard curve of concentration vs. absorbance was plotted and linear regression analysis was performed to interpolate the hydroxyproline concentration of the samples as a result of their absorbance. Dilution and neutralisation factors were reversed and the hydroxyproline concentration was determined for the dry weight of the tissue. The hydroxyproline concentration was then multiplied by 7.14 to determine the total collagen content within the tissue.

2.5 Basic histological & immunohistochemical techniques

In order for structures and constituents to be visualised within tissues, using histology or immunohistochemistry, the tissues must be fixed to ensure no constituents are washed out or structures are damaged during sample preparation. Any calcified tissue must first be decalcified in order for it to be soft enough to section. Tissue sections were encased in paraffin wax to enable them to hold their shape during sectioning. Following staining, sections were imaged using an upright light microscope. The following sections describe the various processes required to prepare samples for histology or immunohistochemistry.

2.5.1 Fixation

Sections to be used with histological stains were fixed in 10 % (v/v) Neutral Buffered Formalin (NBF). Immunohistochemical sections were fixed in zinc fixative solution. Sections were placed in plastic histological cassettes and labelled using a lead pencil. The plastic cassettes were immersed in fixative for 96 hours for labral sections and 48 hours for acetabular sections. Acetabular sections were then replaced in fixative for a further 48 hours following decalcification.

2.5.1.1 Reagents

0.1 M Tris solution

Tris solution (0.1 M) was prepared by dissolving 12.1 g Trizma base in 1000 ml distilled water. The solution was stored at room temperature for up to one month.

Zinc fixative solution

Zinc fixative solution was prepared by dissolving 0.5 g calcium acetate in 1000 ml 0.1 M Tris solution. The pH was adjusted to 7.0 – 7.4 and the following solution were dissolved in to the solution in order; 5.0 g zinc acetate followed by 5.0 zinc chloride. The solution was stored at room temperature for up to six months.

2.5.2 Decalcification

Acetabular sections were removed from the primary fixative and placed in 12.5 % (w/v) EDTA to decalcify until the bone was soft enough to be cut with a scalpel blade (porcine tissue approximately 2 weeks, human tissue approximately 8-10 weeks). During decalcification sections were kept at 45 ℃ in an orbital incubator to agitate the solution. The solution was changed every 2-3 days.

2.5.3 Tissue processing

Following fixation, sections were processed using an automated tissue processor by immersion in sequential pots. Sections were processed to infiltrate the structures with wax in order to maintain the shape and location of the constituents. Histology samples followed cycle 1, whilst immunohistochemistry sections followed cycle 2 to avoid submersion in NBF, as shown in Table 2-2.

Table 2-2 Tissue processing solutions and times for histology and immunohistochemistry samples. Sections were sequentially immersed in solutions following either cycle 1 or 2.

Pot Number	Reagent	Cycle 1	Cycle 2
1	10 % (v/v) NBF	1 hour	
2	70 % Alcohol	1 hour	1 hour
3	90 % Alcohol	1 hour	1 hour
4	100 % Alcohol	1 hour 10 mins	1 hour 10 mins
5	100 % Alcohol	1 hour 10 mins	1 hour 10 mins
6	100 % Alcohol	3 hours 20 mins	3 hours 20 mins
7	Xylene	4 hours 20 mins	4 hours 20 mins
8	Xylene	1 hour	1 hour
9	Xylene	1 hour 30 mins	1 hour 30 mins
10	Molten Wax	2 hours	2 hours
11	Molten Wax	2 hours 30 mins	2 hours 30 mins
12	Molten Wax	2 hours	2 hours

2.5.4 Paraffin wax embedding of sections

Sections were removed from the automated tissue processor and placed into metal moulds with the cross section surface on the base (Figure 2-12). The moulds were filled with molten wax and left to set over night at room temperature. Once the wax had hardened, the blocks were removed from the mould and excess wax was removed. The wax blocks were stored at room temperature until use. Prior to sectioning the wax blocks were cooled to -20 °C for a minimum of 1 hour and in between sectioning wax blocks were kept on ice to retain their temperature.

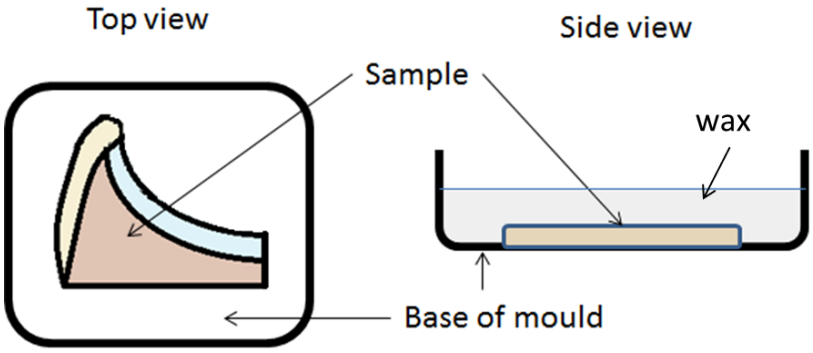

Figure 2-12 Embedding of tissue sections. Tissue sections were placed with the cross-section faced down on the base of the mould.

2.5.5 Sectioning of wax blocks

Wax blocks were sectioned on a manual microtome to a thickness of 6 µm and at an angle of 2 ° to the blade. Sections were cut from the acetabular apex down to the subchondral bone. Cut sections were then transferred to a paraffin section mounting water bath at 40 °C to be transferred onto Superfrost Plus slides. Slides were left to dry on a hot plate at 45 °C for a minimum of 3 hours.

2.5.6 Dewaxing and rehydration

Prior to staining and labelling, sections were dewaxed in two consecutive solutions of xylene, for 10 minutes in each. Following dewaxing, sections were dehydrated in three successive pots of 100 % (v/v) ethanol, for 3 minutes, 2 minutes, and 2 minutes, followed by 2 minutes in 70 % (v/v) ethanol. The sections were then rehydrated by placing under running tap water for 3 minutes.

2.5.7 Dehydration and mounting

Following staining and labelling, sections were dehydrated for 5 seconds in 70 % (v/v) ethanol, followed by three pots of 100 % (v/v) ethanol for 1 minute, 2 minutes and 3 minutes. Sections were then immersed in two pots of xylene for 10 minutes each. The slides were then mounted using a drop of DPX and glass cover slip, ensuring no bubbles were left under the glass. Slides were left in the fume hood to dry for a minimum of four hours before visualisation under a microscope.

2.6 Histological staining methods

The following reagents and methods were used to stain tissue sections in order to visualise key structures and constituents within a tissue. Haematoxylin and eosin (H&E) were used to visual general tissue architecture and cell nuclei, alcian blue identified GAGs, and sirius red and millers elastin identified collagen and elastin within the tissue, respectively.

2.6.1 Reagents

0.1 % (w/v) Sirius red

Sirius red (0.1 % w/v) was prepared by dissolving 0.1 g sirius red into 100 ml saturated picric acid solution.

1 % (v/v) acid alcohol

Acid alcohol (1 % v/v) was prepared by combining 5 ml conc. hydrochloric acid with 495 ml 70 % (v/v) ethanol.

1 % (w/v) oxalic acid

Oxalic acid (1 % w/v) was prepared by dissolving 1 g oxalic acid into 100 ml distilled water.

5 % (w/v) potassium permanganate

Potassium permanganate (5 % w/v) was prepared by dissolving 15 g potassium permanganate into 300 ml distilled water.

Scott's tap water

Scott's tap water was prepared by diluting 50ml of 10x Scott's tap water in 450 ml distilled water.

Weigerts haematoxylin

Weigerts haematoxylin was prepared by combining 2 parts of solution A with 1 part of solution B.

2.6.2 Haematoxylin and eosin

H&E staining was used to visualise general tissue architecture and cell nuclei of cartilage and labral tissue. Eosin binds to most proteins in the cytoplasm and the ECM due to their negative charge, staining them red or pink, whilst negatively charged nuclei bind to haematoxylin staining them dark blue or violet.

Following dewaxing and rehydration, slides were immersed in Mayer's haematoxylin for 1 minute then rinsed under running tap water until clear. Slides were then immersed sequentially in Scott's tap water and eosin for 3 minutes before being dehydrated and mounted.

2.6.3 Sirius red and Miller's elastin

Sirius red and Miller's elastin staining was used to visualise the collagen and elastin structure within cartilage and labral tissue. Miller's elastin binds to elastin fibrils staining them black. Sirius red binds to collagen fibres parallel to their long axis staining them red under brightfield illumination or giving them an enhanced birefringence under polarised light.

Following dewaxing and rehydration, slides were immersed in potassium permanganate for 5 minutes then rinsed using distilled water. Sections were then immersed in oxalic acid for 2 minutes followed by two rinses in distilled water for 1 minute and 4 minutes. Sections were sequentially immersed in 70 % (v/v) ethanol for 1 minute, 95 % (v/v) ethanol for 1 minute before staining with Miller's elastin for 1 hour. Following staining, sections were rinsed in 95 % (v/v) ethanol until clear, 70 % (v/v) ethanol for 1 minute, followed by tap water for 2 minutes. Sections were then stained using Weigerts haematoxylin for 10 minutes then rinsed in tap water for 1 minute. Sections were then differentiated in acid alcohol for 1 minute before being rinsed in distilled water for 30 seconds and immersed in picro sirius red for a further hour. Before dehydration and mounting, sections were rinsed in distilled water and blotted dry.

2.6.4 Alcian blue

Alcian blue was used to visualise GAGs in the labral tissue. Alcian blue stains acid mucins (including GAGs) within the tissue whilst a counter stain of periodic acid and Schiff's reagent (PAS) was used to stain the neutral mucins. Gills III haematoxylin was used to stain cell nuclei. Alcian blue stain could not be used on acetabular sections as decalcification with EDTA removes proteoglycans from the tissue.

Following dewaxing and rehydration slides were immersed in alcian blue for 15 minutes followed by running tap water for 1 minute then rinsed in distilled water. Slides were then immersed in periodic acid for 5 minutes then rinsed in distilled water three times before being immersed in haematoxylin for 90 seconds. Before dehydration and mounting, sections were rinsed in tap water until clear.

2.7 Immunohistochemical staining methods

Immunohistochemistry was used to identify the main collagen types present in the acetabular labrum and cartilage. Antibodies bind specifically to the antigens present in the collagen fibres. A secondary antibody, tagged with a stain, attaches to the primary antibody to allow the visualisation of the antigen. The secondary antibody must be raised against the IgG of the same animal in which the primary antibody has been raised.

2.7.1 Immunohistological reagents

The following reagents are used during immunohistochemical analysis:

Antibody diluent (TBS, 0.1 % (w/v) Bovine Serum Albumin, 0.1 % (w/v) sodium azide)

Antibody diluent was prepared by combining 6 ml sodium azide (1 % (w/v)), 300 µl 5 % (w/v) bovine serum albumin (BSA) and 40 ml TBS. The solution was adjusted to pH 7.6 and made up to 60 ml with TBS. The solution was stored at 4 °C for up to three months.

Bovine Serum Albumin solution (5 % (w/v) BSA)

BSA solution was prepared by dissolving 2.5 g (BSA) into 50 ml PBS and passing through a 0.2 µm filter. The solution was stored frozen for up to six months.

Hydrogen peroxide solution (3 % (v/v))

Hydrogen peroxide solution was prepared by combining 20 ml hydrogen peroxide (30% (v/v)) with 180 ml PBS. The solution was used immediately.

Pepsin working solution (0.5 % (w/v) in 5mM HCL)

Pepsin stock solution was prepared by diluting 100 mg pepsin into 10 ml 10mM HCL (pH 2.0). The solution was diluted to a working concentration by combining 1 ml pepsin stock solution with 1 ml distilled water. The solution was used immediately.

Substrate Chromogen

Substrate chromogen was prepared by combining 20 µl 3,3-diaminobenzidine (DAB) chromogen and 1 ml substrate buffer. The solution was used immediately.

Sodium chloride solution (3 M)

Sodium chloride solution was prepared by dissolving 175.32 g sodium chloride into 1 L distilled water. The solution was stored at room temperature for up to one month.

TBS containing 0.05 % (w/v) Tween 20 (TBS-T)

TBS Tween was prepared by combining 500 µl Tween 20 with 1 L TBS and adjusted to pH 7.6. The solution was stored at room temperature for up to three month.

Tris buffered saline (TBS)

Tris buffered saline was prepared by combining 25 ml 2 M tris solution with 50 ml 3 M sodium chloride and made up to 1 L using distilled water. The solution was stored at room temperature for up to one month.

Tris solution (2 M)

Tris solution was prepared by dissolving 242.26 g trizma base into 500 ml distilled water and adjusted to pH 7.6. The solution was then made up to 1 L using distilled water. The solution was stored at room temperature for up to one month.

2.7.2 Immunohistochemical methods

Following dewaxing and rehydration of specimens (section 2.7.2.1), antigen retrieval was carried out if required. Sections were then immersed in hydrogen peroxide for ten minutes followed by running tap water for three minutes. All tissue sections were circled using a hydrophobic marker, to minimise the volume of solutions required, then rinsed in TBS for ten minutes. Sections were incubated in dual endogenous enzyme block at room temperature for ten minutes, then washed twice in TBS for ten minutes each. Sections were incubated in 50µl of diluted primary antibody, in a humidified chamber, for one hour, followed by two TBS-T washes and two TBS washes, for ten minutes each. Sections were labelled with polymer horseradish by incubation for thirty minutes in the dark followed by two-ten minute TBS-T and TBS washes. Each section was covered in chromogen DAB (50µl) and incubated for ten minutes, then washed four times using distilled water. Sections were counterstained in haematoxylin for ten seconds then rinsed using tap water until it ran clear. Sections were placed into Scott's tap water for three minutes then returned to running tap water for a further three minutes, before being dehydrated and mounted.

2.7.2.1 Antigen retrieval

Antigen retrieval was carried out to unmask hidden antigens by breaking the protein cross-links formed during fixation.

Proteinase K

Proteinase K was added dropwise to each section and incubated at room temperature for twenty minutes. Sections were then rinsed in TBS for five minutes.

Pepsin

Sections were covered with pepsin working solution (0.5 % (w/v)) and incubated for fifteen minutes at 37 ℃ in a humidified chamber. Sections were allowed to cool for ten minutes then rinsed twice in TBS-T for two minutes.

2.8 Statistical analysis

Statistical analysis of numerical, percentage, and interpolated data was carried out using the methods listed below. Numerical data was statistically analysed to find significant differences between data groups. Prior to statistical analysis, percentage data was arcsine transformed and photometric data was interpolated from standard graphs.

2.8.1 Parametric numerical data

Parametric numerical data was analysed using OriginPro software, version 9.1 and/or Microsoft Office Excel 2013, including the descriptive statistical package. Data was presented as the mean ± 95 % confidence limit (CL), $\alpha = 0.05$. Two way repeated analysis of variance (ANOVA) was used for comparison of means of two or more groups. Tukey's multiple comparison test was used to identify significant differences between the groups. Data was accepted as significantly different when $\alpha \leq 0.05$.

2.8.2 Percentage data

In order to fulfil the assumption of normally distributed data in two-way ANOVA, percentage data was initially tested for normality using histograms. Data not normally distributed was then arcsine transformed. Statistical analysis was carried out as previously described (section 2.8.1) on arc sine data then values were back transformed for graphical representation. Data was presented as the arithmetic mean ± 95% CL of arcsine values.

2.8.3 Interpolated data

For data which required interpolation, linear regression analysis was performed on standard curves.

2.9 Summary

To conclude, various methods within this study use generic methods to prepare tissue, equipment, and solutions which have been detailed in this chapter. Tissue acquisition methods have been developed to produce samples for mechanical characterisation including compression and tensile testing, as well as biological characterisation including assays, histology, and immunohistochemistry. Specific methodology including specimen sizes, orientation, and location are detailed in the subsequent chapters.

Chapter 3

Biological and biochemical characterisation of porcine and human acetabular labrum and articular cartilage

3.1 Introduction

The purpose of the study detailed in this chapter was to investigate the morphology of the acetabulum and the biological constituents and structure of the porcine and human labrum and cartilage. As discussed in Chapter 1, diseases of the hip, such as FAI and DDH, are associated with damage to the acetabular labrum and are thought to be an initiator of OA (Leunig et al. 2009). During damage, the labrum can become torn and/or separated from the adjacent articular cartilage, resulting in a reduction of the functional ability of the tissues. Scientific understanding of the acetabular labrum is limited and hence, the etiology of damage in diseases such as FAI or DDH is relatively unknown. In order to fully understand how the acetabular labrum becomes damaged, it is important to understand the structure of the tissue and its interaction with the articular cartilage, from which it can become separated.

In this part of the study, the composition and structure of the labrum and cartilage were compared to identify structural and functional differences between the two tissues. The function of the hip joint is to support load and provide stability during movement, which is possible due to the tissue's composition and structure. GAGs and water are responsible for the compressive strength of the tissue, by reducing fluid flow, where as collagen provides stability due to its tensile strength (Lohmander 1988; Bader et al. 1992; Kadler et al. 1996). Porcine tissue is often used to model less readily available human tissue however, in order for porcine tissue to model human tissue, it must be structurally similar in order to provide the same function. This chapter also compared the constituents and structure of porcine and human tissue to ensure porcine tissue is a suitable model for future chapters for *in vitro* simulation of the human hip. Previous studies have been performed to characterise bovine and human acetabular labrum (Ferguson et al. 2001; Petersen et al. 2003), however, porcine tissue is more readily available and more closely corresponds in size to the human hip (Taylor et al. 2011). To the author's knowledge, no studies exist on the biological characterisation of the porcine labrum.

In order to assess the composition of the tissues, biochemical analysis was used to identify water, GAG, and collagen concentrations and the distribution of the constituents was analysed using histology and immunohistochemistry, which provided detailed knowledge of the structure and transition of the tissues. In order to identify changes in structure around the hip joint, biochemical analysis was performed on both load-bearing and non-load-bearing regions of the labrum, acetabular cartilage and femoral cartilage. Histology and immunohistochemistry was carried out on the superior, posterior, and anterior regions of the acetabulum for porcine tissue and compared to the anterior region of the acetabulum of human tissue. Differences in constituents or structure could result in varying mechanical properties; therefore it was important to identify any differences for future mechanical testing studies.

3.2 Aims and objectives

Aims:

The aim of the study presented in this chapter was to characterise the morphology, structure, and constituents of the labrum, acetabular cartilage, and femoral cartilage and the transition between the tissues in the human and porcine hip. It was also the intention to determine any differences between load-bearing and non-load-bearing regions of tissues or between femoral and acetabular cartilage for future mechanical studies.

Objectives:

- To characterise the hip joint including morphology and size.
- To quantify biochemical components, including water, GAG, and collagen content of the labrum, in comparison to cartilage.
- To quantitatively assess differences in biochemical constituents in load-bearing and non-load-bearing regions and between acetabular and femoral cartilage.
- To qualitatively assess and compare the tissue structure using histology; to determine general histoarchitecture, as well as collagen and GAG distribution.
- To identify and compare collagen types and distribution within the tissues using immunohistochemistry
- To qualitatively assess the labral-cartilage junction and identify the transition from one tissue to another.

3.3 Biochemical characterisation materials

Labral and osteochondral pins were extracted from the femoral head, acetabulum, and labrum as described in Section 2.3.5 and lyophilised as described in Section 2.3.8. Femoral osteochondral pins were extracted from a load-bearing region at the mid point between the ligamentum teres and cartilage-femoral neck junction, in the superior direction (Taylor et al., 2011, Figure 3-1). Non-load-bearing pins were extracted from the furthest point posterior to the load-bearing pin without crossing the cartilage-femoral neck junction. Acetabular osteochondral pins were taken from mirrored locations to the femoral head. Labral pins were extracted above the acetabular pin locations in the radial direction. Porcine tissue was used to evaluate the difference in load-bearing and non-load-bearing regions for femoral cartilage, acetabular cartilage, and labrum. Human tissue from a load-bearing region was compared to porcine tissue from a load-bearing region for water, GAG, and collagen concentrations.

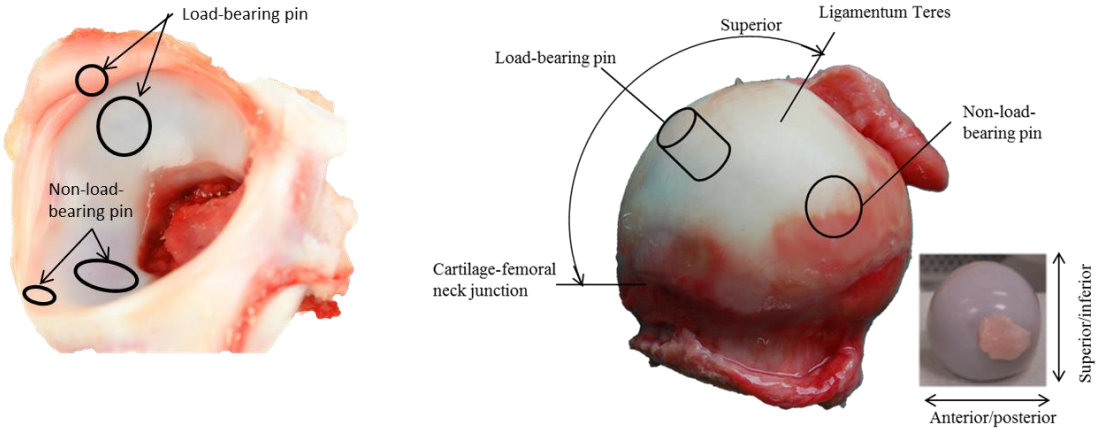

Figure 3-1 Femoral head osteochondral pin extraction. Diagram detailing the locations of femoral osteochondral pin extractions. Load-bearing and non-load-bearing pin extraction locations are shown. Figure adapted from https://en.wikipedia.org/wiki/Femoral_head and Taylor et al. 2011.

3.4 Biochemical characterisation methods

3.4.1 Determination of water content method

The water content of a tissue was calculated from the difference between the wet and dry weight of the tissue (before and after lyophilisation) and presented as a percentage of the wet weight of the tissue. Porcine tissue (n=6) was used to identify differences in water content for acetabular labrum, acetabular cartilage, and femoral cartilage for load-bearing and non-load-bearing regions. Porcine and human tissue (n=6) was used to calculate the water content in acetabular cartilage and labrum.

3.4.2 Determination of GAG content method

GAG content was determined using the DMB assay, as described in Section 2.4.1. Porcine tissue (n=6) was used to identify differences in GAG content for acetabular labrum, acetabular cartilage, and femoral cartilage for load-bearing and non-load-bearing regions. GAG content was determined for porcine and human samples (n=6) in acetabular cartilage and labrum. GAG content was determined by measuring the optical density of the tissue, using a spectrophotometer at a wavelength of 525 nm, following incubation in DMB dye. Prior to incubation in DMB dye, the tissue was lyophilisation, digested in papain, and diluted in assay buffer. A dilution factor of 1 in 25 was found to be optimal for all porcine tissue and human cartilage however, due to the low volumes of GAGs in the human labrum, the highest dilution factor of 1 in 2 was selected (section 3.4.2.1). GAG content was determined for the dry weight of the tissue.

3.4.2.1 GAG sample dilution factor

Before tissue samples were assayed they required diluting in assay buffer to ensure they fell within the linear region of the standard curve (3.0125 to 50 $\mu g.ml^{-1}$) to allow for accurate absorbance readings (Figure 3-2). In order to determine the dilution factor, a range of concentrations were investigated including 1 in 10, 1 in 25, and 1 in 50 and repeated on three samples for both cartilage and labrum using human tissue, as porcine tissue had been previously optimised within the institution. At the highest linear standard concentration of 50 $\mu g.ml^{-1}$ the absorbance was 0.285 for cartilage and 0.289 for labrum, at the lowest linear standard concentration of 3.125 $\mu g.ml^{-1}$ the absorbance was 0.0.25 for cartilage and 0.019 for labrum. Therefore, a dilution factor which gave an absorbance reading between these values was suitable. For cartilage tissue a dilution factor of 1 in 25 was found to be most suitable, as a dilution of 1 in 10 lay close to the top of the linear region and sample a dilution of 1 in 50 lay close to the bottom of the linear region. All labral samples fell below the linear region of the standards graph therefore; the highest dilution factor of 1 in 2 was selected for human labral samples (Table 3-1).

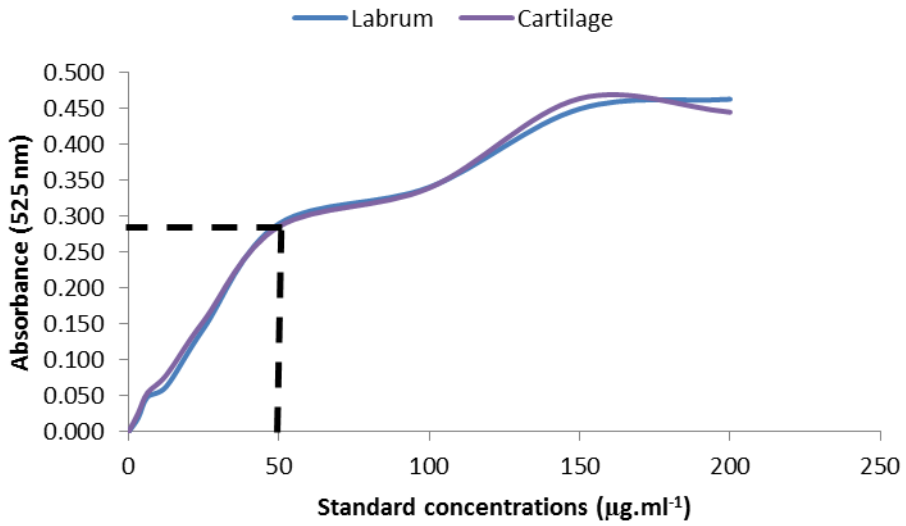

Figure 3-2 GAG assay standards. Absorbance at 525 nm of chondroitin sulphate B standards; 0, 3.125, 6.25, 12.5, 25, 50, 100, 100, 150 and 200 µg.ml^{-1}. Dashed box encloses the linear region.

Table 3-1 Absorbency readings for GAG assay dilution factor. Three samples were tested at three dilution factors for both human cartilage and labrum. The absorbency readings are shown in the below table.

Cartilage	Sample 1	Sample 2	Sample 3	Mean
1 in 10	0.11	0.28	0.21	0.20
1 in 25	0.05	0.13	0.09	0.09
1 in 50	0.02	0.06	0.05	0.05

Labrum	Sample 1	Sample 2	Sample 3	Mean
1 in 10	0.00	-0.02	0.00	-0.01
1 in 25	0.00	0.00	0.00	0.00
1 in 50	0.00	0.00	0.00	0.00

3.4.3 Determination of collagen content method

Hydroxyproline content was determined as described in Section 2.4.2 and expressed as collagen content using a conversion factor of 7.14 due to its repeatability within collagen fibrils (Edwards & O'Brien 1980). Porcine tissue (n=6) was used to identify differences in collagen content for acetabular labrum, acetabular cartilage and femoral cartilage for load-bearing and non-load-bearing regions. Porcine and human tissue (n=6 and n=5, respectively) were used to determine the collagen content in acetabular cartilage and labrum. Following lyophilisation, the tissue was hydrolysed in hydrochloric acid and diluted by 1 in 50 for porcine tissue and 1 in 10 for human tissue (Section 3.4.3.1). Chloramine T and Ehrlich's reagent were then added to measure the optical density using a spectrophotometer at a wavelength of 750 nm.

3.4.3.1 Collagen sample dilution factor

As with the GAG assay, before tissue samples were assayed they required diluting in assay buffer to ensure they fell within the linear region of the standards graph (Figure 3-3). In order to determine the dilution factor, a range of concentrations were investigated including 1 in 5, 1 in 10, 1 in 25, and 1 in 50 and repeated on three samples for both cartilage and labrum using human tissue, as porcine tissue had been previously optimised within the institution. At the highest linear standard concentration of 25 the absorbance was 1.7 and at the lowest linear standard concentration of 2 the absorbance was 0.2. Therefore, a dilution factor which gave an absorbance reading between these values was suitable. For both tissue types a dilution factor of 1 in 10 was found to be most suitable, as cartilage sample 2 for a 1 in 5 dilution lay close to the top of the linear region and all samples at 1 in 50 and labral samples at 1 in 25 lay close to the bottom of the linear region (Table 3-2).

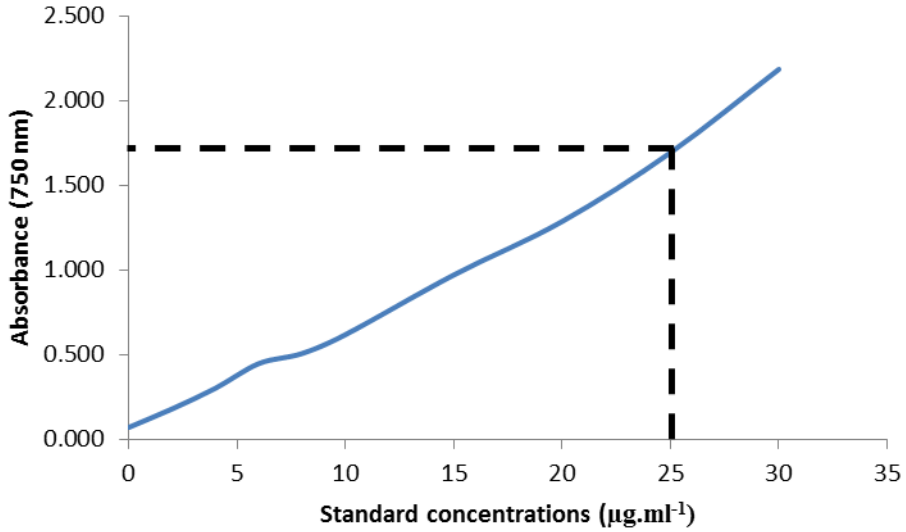

Figure 3-3 Collagen assay standards. Absorbance at 750 nm of trans-4-hydroxy-L-proline standards; 0, 2, 4, 6, 8, 10, 15, 20, 25, and 30 (µg.ml^{-1}). Dashed box encloses the linear region.

Table 3-2 Collagen tissue dilution absorbencies. Three samples were tested at four dilution factors for both human cartilage and labrum. The absorbency readings are shown in the below table.

Cartilage	Sample 1	Sample 2	Sample 3
1 in 5	1.478	1.633	0.948
1 in 10	0.964	0.839	0.641
1 in 25	0.473	0.502	0.438
1 in 50	0.284	0.246	0.251

Labrum	Sample 1	Sample 2	Sample 3
1 in 5	1.058	0.977	0.880
1 in 10	0.599	0.541	0.495
1 in 25	0.279	0.297	0.269
1 in 50	0.210	0.191	0.182

3.5 Biological characterisation methods

The following methods were used to prepare and stain acetabular tissue for histological and immunohistochemical analysis to determine the distribution of GAGs and collagen within labral and cartilage tissues and to identify the transition between the two tissue types.

3.5.1 Histological evaluation

Acetabular and labral sections were prepared as described in Section 2.3.7. Sections were taken from three regions around the acetabulum; anterior, posterior, and superior for porcine tissue (n=6 in 3 regions, Figure 3-4) and from the anterior region for human tissue (n=5 acetabular, n=6 labrum). Acetabular sections were stained using H&E or sirius red and Miller's elastin as described in Sections 2.6.2 and 2.6.3, respectively. Labral sections were stained using alcian blue as described in Section 2.6.4. Labral sections were prepared without the subchondral bone to avoid the need for decalcification, which was found to remove GAGs from the tissue, identified during a pilot study.

3.5.2 Immunohistochemical evaluation

Acetabular sections were prepared as described in Section 2.3.7. Sections were taken from three regions around the acetabulum; anterior, posterior and superior for porcine tissue (n=6 in 3 regions, Figure 3-4) and from the anterior region for human tissue (n=6). The tissue was incubated with markers for collagen types I and II. The general immunohistochemical methods used in this study are described in Section 2.7.

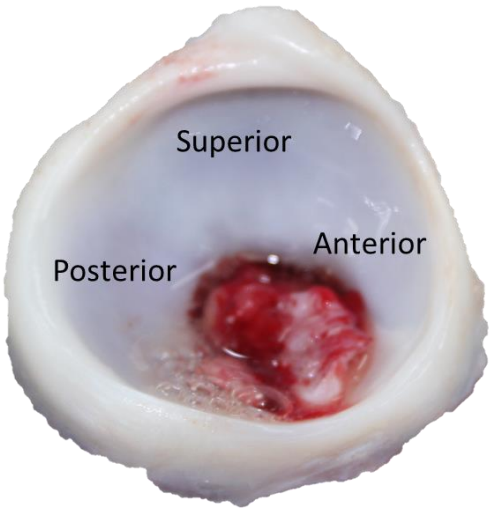

Figure 3-4 Anatomical locations of the acetabulum. The acetabulum, including the labrum and cartilage, is split into three regions, the posterior, superior and anterior. The inferior region of the acetabulum contains the transverse acetabular ligament and the acetabular fossa. Image shown is a right porcine hip.

3.5.2.1 Antibody labelling optimisation

All antibodies used throughout this study are presented in Table 3-3. Alongside the antibodies are the isotypes, dilutions, antigen retrieval method, and the control tissues. Prior to labelling tissue sections with antibodies, the methods and concentrations were optimised. Optimisation was required for the primary antibody type and duration as well as the antigen retrieval type and time. The final antibodies and retrieval methods used in this study are highlighted in green, alongside the conditions used. Unsuccessful methods were rejected due to either staining on the negative control tissue or lack of staining on the positive control tissues.

Table 3-3 Table of antibodies and antigen retrieval methods optimised for staining of human tissue. Final antibodies and conditions used are highlighted in green.

Primary Antibody	Isotype Control / Control Tissue	Antigen Retrieval	Optimised porcine/human
AB34710 Collagen I 1:500 1hr room temperature	Rabbit IgG 1hr, room temperature Tendon	Antigen unmasking solution 30 min 60 °C	Human Unsuccessful
AB34710 Collagen I 1:100 1hr room temperature	Rabbit IgG 1hr, room temperature Tendon	Pepsin 20 min 37°C humidified chamber	Porcine unsuccessful
AB34710 Collagen I 1:100 1hr room temperature	Rabbit IgG 1hr, room temperature Tendon	Proteinase K 20 min room temperature	Human unsuccessful
MAB3391Collagen I 1:50 1hr, room temperature	Mouse IgG1 1hr, room temperature Tendon	Proteinase K 20 min room temperature	Porcine successful
MAB3391 Collagen I 1:100 1hr, room temperature	Mouse IgG1 1hr, room temperature Tendon	Proteinase K 20 min room temperature	Porcine successful Human Unsuccessful
MAB3391 Collagen I 1:150 1hr, room temperature	Mouse IgG1 1hr, room temperature Tendon	Proteinase K 20 min room temperature	Porcine successful

MAB3391 Collagen I 1:200 1hr, room temperature	Mouse IgG1 1hr, room temperature Tendon	Proteinase K 20 min room temperature	Porcine successful
MAB3391 Collagen I 1:100 1hr, 37 ° C	Mouse IgG1 1hr, room temperature Tendon	Proteinase K 20 min room temperature	Porcine successful
MAB1330 Collagen II 1:50 1hr, room temperature	Mouse IgG1 1hr, room temperature Trachea	Proteinase K 20 min room temperature	Porcine unsuccessful
MAB1330 Collagen II 1:100 1hr, room temperature	Mouse IgG1 1hr, room temperature Trachea	Proteinase K 20 min room temperature	Porcine unsuccessful Human unsuccessful
MAB8887 Collagen II 1:100 1hr, room temperature	Mouse IgG1 1hr, room temperature Trachea	Pepsin 20 min 37 °C humidified chamber	Porcine successful Human successful
MAB8887 Collagen II 1:150 1hr, room temperature	Mouse IgG1 1hr, room temperature Trachea	Pepsin 20 min 37 °C humidified chamber	Porcine successful
MAB8887 Collagen II 1:200 1hr, room temperature	Mouse IgG1 1hr, room temperature Trachea	Pepsin 20 min 37 °C humidified chamber	Porcine successful

3.6 Results

3.6.1 Macro scale observations

Following dissection and measurements (section 2.3.4), macroscopic differences between the porcine and human hip joint were observed (Figure 3-5 and Table 3-4). The human acetabulum was 22 % larger in diameter than the porcine acetabulum (Figure 3-5 A and E) and had a deeper labrum (Figure 3-5 C and G). Within both species, the labrum was deepest in the superior region, followed by the posterior region, then the anterior region. The human acetabulum had a deeper socket than the porcine acetabulum, creating a steeper articulating surface. The porcine hip joint also had a larger greater trochanter but a shorter femoral neck length (Figure 3-5 B and F). The femoral head of the human joint appeared rounder than the porcine femoral head, which was elongated in the medial-lateral direction (Figure 3-5 D and H). The cartilage surfaces of the human tissue appeared duller and the joint more yellow in colour, due to the production of advanced glycation end products, in comparison to the glossy blue-white porcine cartilage and white labrum (Figure 3-5). Glycation of proteins causes disruption to the molecular conformation, the enzymatic activity and receptor function, which affects the protein's function and results in damage to the tissue and yellowing.

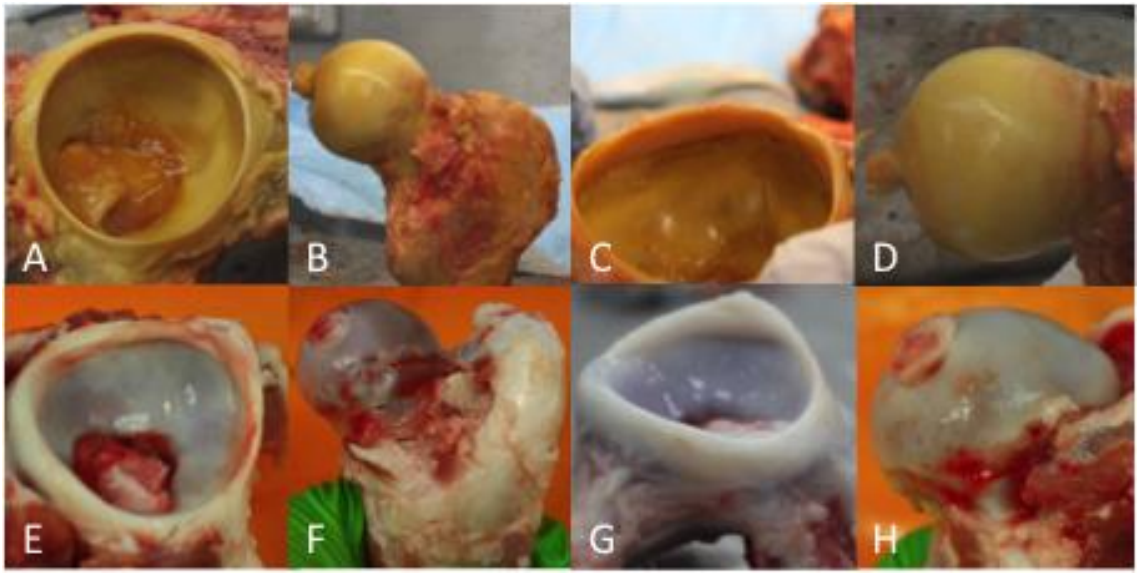

Figure 3-5 Macroscale observation of the human and porcine hip joint. A – Human acetabulum. B – Human femoral head, femoral-neck, and greater trochanter. C- Human Labrum. D – Human femoral head. E – Porcine acetabulum. F – Porcine femoral head, femoral-neck and greater trochanter. G – Porcine labrum. H – Porcine femoral head.

Table 3-4 Summary of human and porcine specimen geometry. Data represented as the mean ± 95 % CL.

	Cup diameter (mm)	Cup depth (mm)	Labrum depth (mm)		
			Superior	Anterior	Posterior
Porcine	38.17 ± 2.14	20.23 ± 1.82	4.90 ± 0.90	1.16 ± 0.18	2.75 ± 0.75
Human	48.86 ± 3.36	30.23 ± 5.62	11.02 ± 1.85	4.97 ± 1.36	7.85 ± 5.62

3.6.2 Determination of water content

3.6.2.1 Water content comparison between load-bearing and non-load-bearing regions and femoral and acetabular cartilage and acetabular labrum for porcine tissue

The water content of the acetabular labrum was significantly lower ($p<0.05$, two-way ANOVA) in comparison to femoral and acetabular cartilage however, no significant difference was observed between load-bearing and non-load-bearing regions within a tissue type or between acetabular and femoral cartilage (Figure 3-6). All cartilage types tested had a mean water content of between 75 % and 76 % and labrum between 67 % and 70%. As no significant differences were found ($p>0.05$, two-way ANOVA) between load-bearing and non-load-bearing regions and between femoral and acetabular cartilage, only acetabular cartilage and labrum from a load-bearing region was analysed for human tissue.

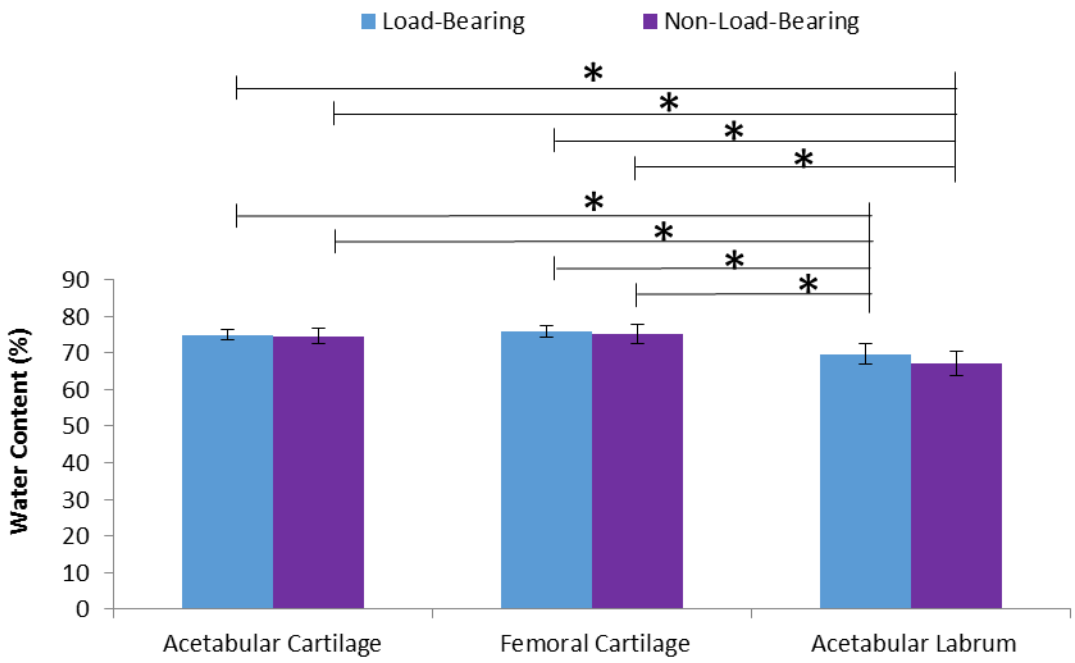

Figure 3-6 Water content of porcine acetabular cartilage, femoral cartilage, and acetabular labrum, from load-bearing and non-load-bearing regions. Data is expressed as a percentage of the wet weight for a given tissue and represented as the mean (n=6) ± 95 % CL. Data was subject to arcsine transformation prior to data analysis and expressed as the back transformed mean. Data was analysed by two-way ANOVA and individual means compared by a Tukey test. * indicates $p<0.05$.

3.6.2.2 Determination of water content in human and porcine tissues

Porcine cartilage had a significantly higher water content of ~75 % compared to human cartilage, ~69 %; however no significant difference was observed between species for the labrum. Within a species the water content varied significantly between the tissues types for porcine tissue, however no significant differences were observed between human cartilage and labrum ($p<0.05$, two-way ANOVA). Although significant differences were observed between tissue types and species, overall, all tissue types had a mean water content between 69 % and 75 % (Figure 3-7).

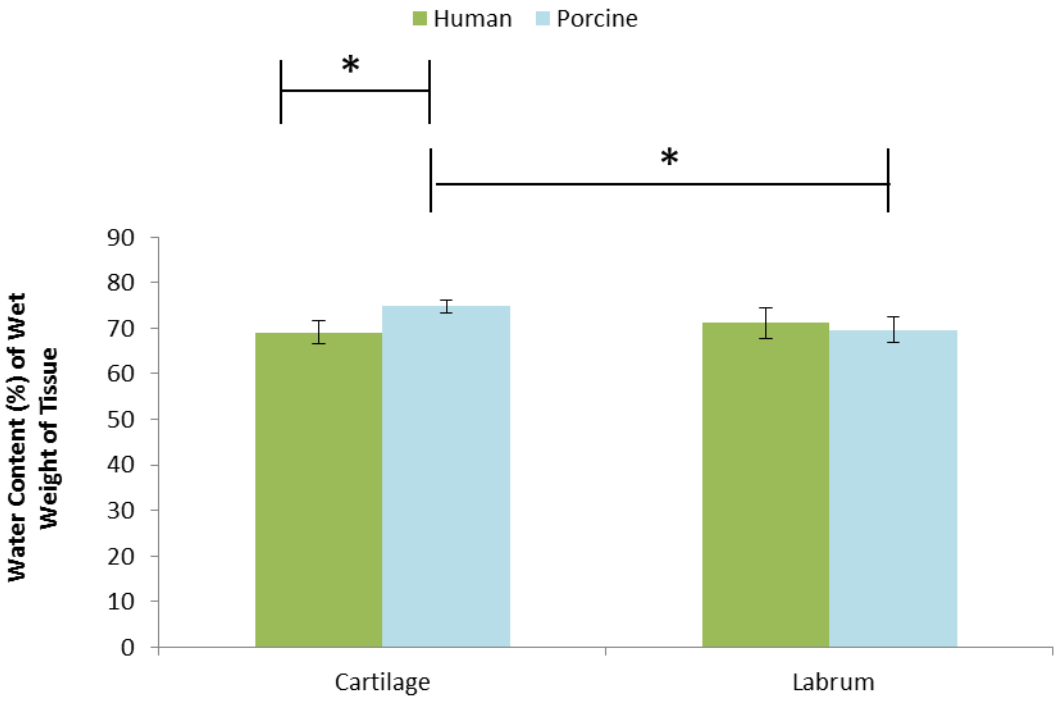

Figure 3-7 Water content of human and porcine cartilage and labrum. Water content shown as a percentage of the wet weight for a given tissue and represented as the mean ± 95 % CL (n=6). Data was subject to arcsine transformation prior to data analysis and expressed as the back transformed mean. Data was analysed by two-way ANOVA and individual means compared by a Tukey test. * indicates $p<0.05$.

3.6.3 Determination of GAG quantification

3.6.3.1 GAG quantification comparison between load-bearing and non-load-bearing regions and femoral and acetabular cartilage and acetabular labrum for porcine tissue

GAG concentration was significantly lower in labral tissue compared to cartilage tissue however; no significant differences were observed between load-bearing and non-load-bearing regions and between acetabular and femoral cartilage (Figure 3-8). All cartilage tissue types had a mean GAG concentration between 176 and 197 $\mu g.mg^{-1}$, whereas the labrum GAG concentration was between 29 and 67 $\mu g.mg^{-1}$. As no significant differences were found ($p>0.05$ two-way ANOVA) between load-bearing and non-load-bearing regions or between femoral and acetabular cartilage, only acetabular cartilage and labrum from a load-bearing region will be analysed for human tissue.

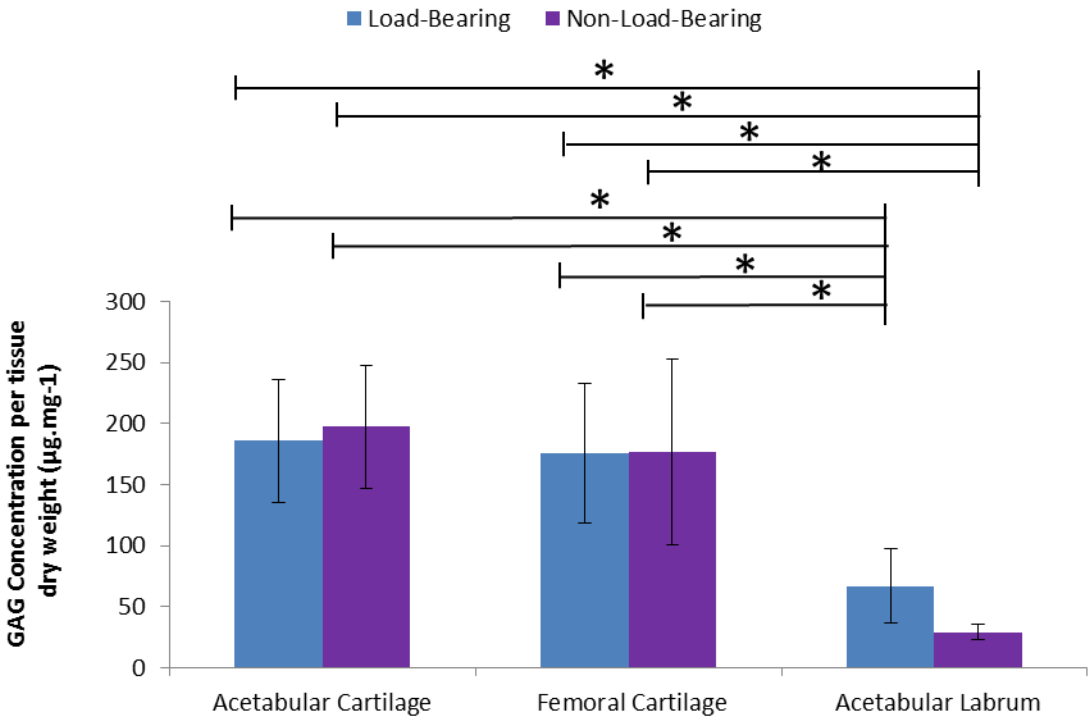

Figure 3-8 GAG quantification of porcine acetabular cartilage, femoral cartilage, and acetabular labrum, from load-bearing and non-load-bearing regions. Data is expressed as the mean (n=6) ± 95 % CL. Data was analysed by two-way ANOVA and individual means compared by a Tukey test. * indicates $p<0.05$.

3.6.3.2 Determination of GAG concentration in human and porcine tissues

Analysis of GAG quantification results for labral and cartilage tissue, in both species, showed large variations in the quantities of GAGs in different tissue types (Figure 3-9). The GAG content of the labrum was significantly lower than that of cartilage for both human and porcine species ($p<0.05$, two-way ANOVA). The concentration of GAGs in the labral tissue was 67 $ug.mg^{-1}$ and 4 $ug.mg^{-1}$ for porcine and human tissue, respectively, compared to 186 $ug.mg^{-1}$ and 70 $ug.mg^{-1}$ in the cartilage tissue. A trend was also identified across the species, with porcine tissue having significantly higher concentrations of GAGs compared to human for both tissue types. Human tissue contained approximately 94 % less GAGs in labral tissue and 62 % less GAGs in cartilage tissue compared to porcine tissue.

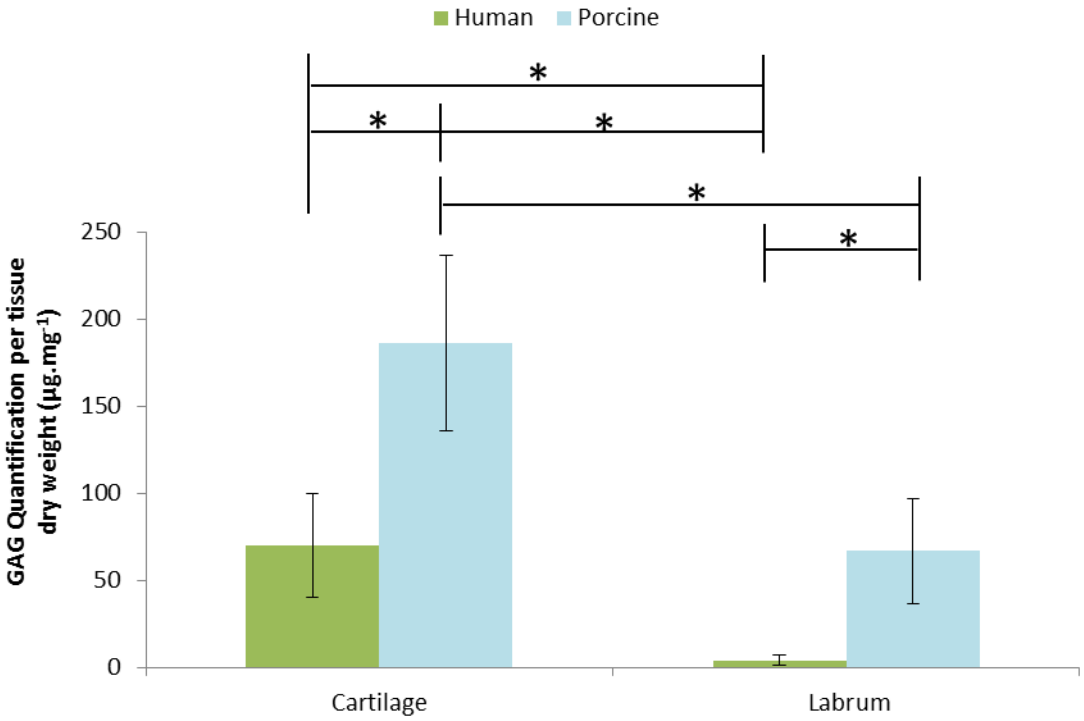

Figure 3-9 GAG quantification of human and porcine cartilage and labrum. Data is expressed as the mean (n=6) ± 95 % CL. Data was analysed by two-way ANOVA and individual means compared by a Tukey test. * indicates $p<0.05$.

3.6.4 Determination of collagen quantification

3.6.4.1 Collagen quantification comparison between load-bearing and non-load-bearing regions and femoral and acetabular cartilage and acetabular labrum for porcine tissue

Collagen concentration was significantly higher in labral tissue compared to cartilage tissue however; no significant differences were found between load-bearing and non-load-bearing regions or between acetabular and femoral cartilage (Figure 3-10). As no significant differences were found ($p>0.05$ two-way ANOVA) between load-bearing and non-load-bearing regions or between femoral and acetabular cartilage, only acetabular cartilage and labrum from a load-bearing region will be analysed for human tissue.

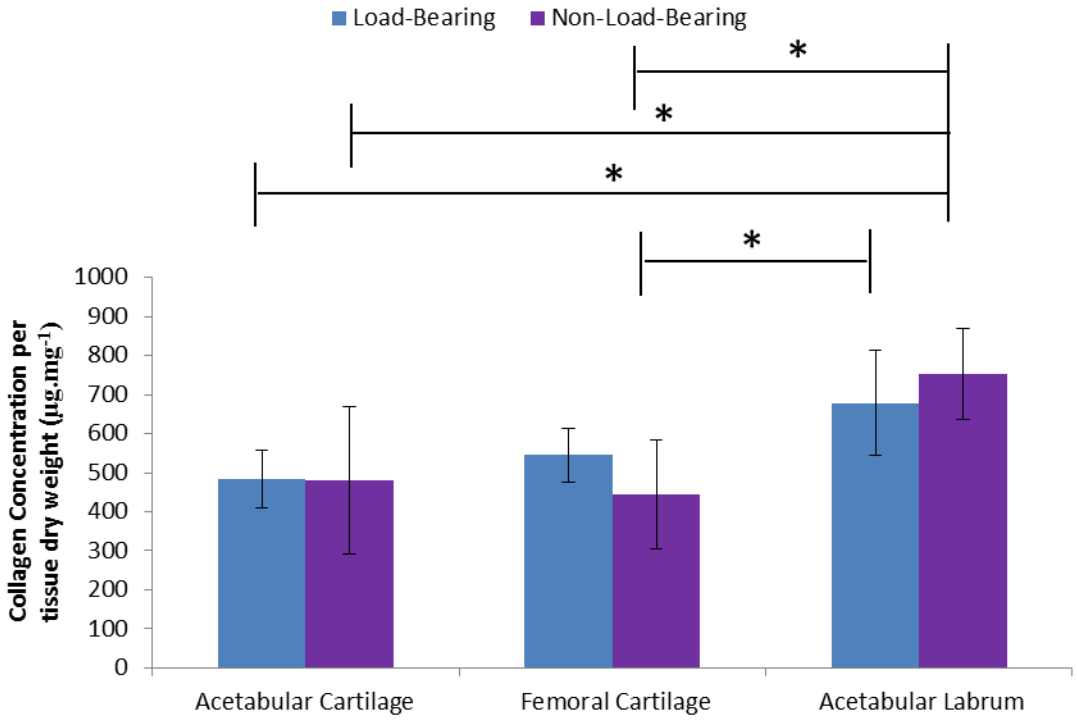

Figure 3-10 Collagen quantification of porcine acetabular cartilage, femoral cartilage, and acetabular labrum, from load-bearing and non-load-bearing regions. Data is expressed as the mean (n=6) ± 95 % CL. Data was analysed by two-way ANOVA and individual means compared by a Tukey test. * indicates $p<0.05$.

3.6.4.2 Determination of collagen quantification in human and porcine tissues

Analysis of collagen concentration for human and porcine tissues showed a variation between species and tissue types (Figure 3-11). An overall trend was observed for labral tissue which, contained more collagen than cartilage tissue and for porcine tissue which, had a higher collagen content than human tissue. Porcine labrum contained 679 µg.mg^{-1} of collagen, where as the collagen content of the human labrum was significantly lower with 506 µg.mg^{-1} ($p<0.05$ two-way ANOVA). Human cartilage collagen content was approximately 25 % lower than that of the porcine cartilage, although this was not significant, with 362 µg.mg^{-1} and 484 µg.mg^{-1} of collagen, respectively.

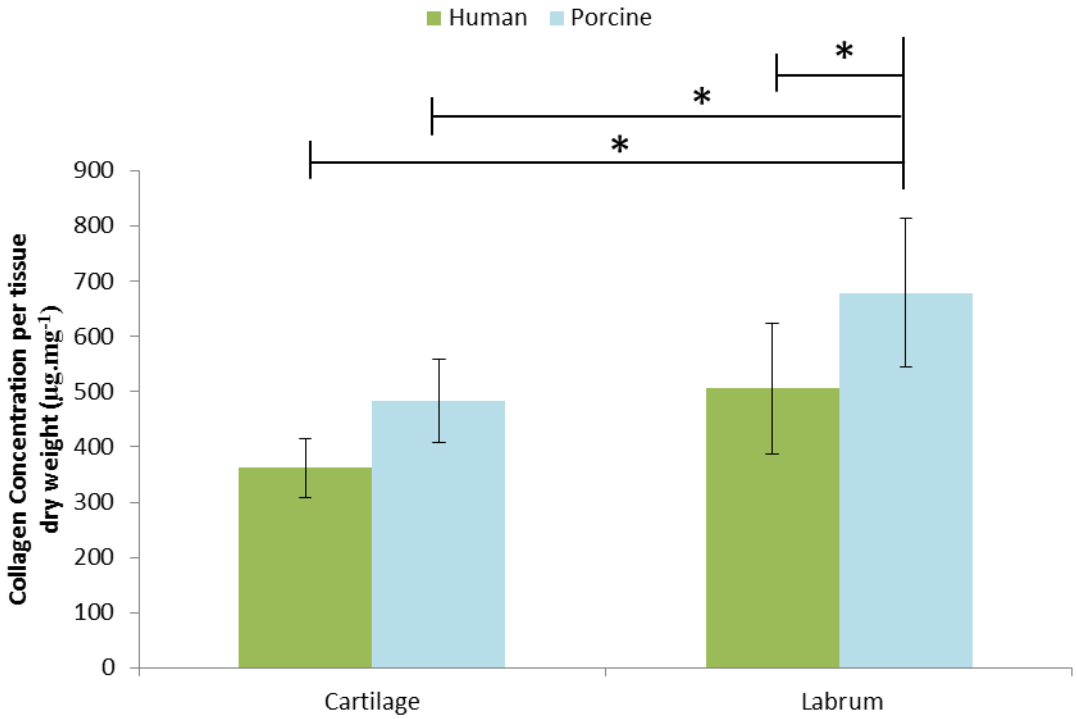

Figure 3-11 Collagen quantification of human and porcine cartilage and labrum. Data is expressed as the mean (n=6) ± 95 % CL. Data was analysed by two-way ANOVA and individual means compared by a Tukey test. * indicates $p<0.05$.

3.6.5 Histological evaluation of labrum, cartilage, and the labral-cartilage junction

Qualitative histological analysis of the acetabulum was used to identify variations in structure and morphology across three different regions within the porcine acetabulum and between human and porcine tissue. H&E was used to visualise tissue histoarchitecture and sirius red and Miller's elastin was used to identify collagen and elastin structures. Alcian blue was used to indicate the distribution of GAGs within the tissues.

3.6.5.1 Morphology of the anterior, superior, and posterior region of the porcine acetabulum

H&E staining of the anterior, superior, and posterior porcine acetabulum showed slight variation in the morphology of the acetabulum (Figure 3-12 A-C). In the posterior region, (Figure 3-12 A) the labral apex of the acetabulum was rounded in comparison to the triangular anterior region (Figure 3-12 C). The apex of the superior region varied between samples. In three out of the six hips the apex was larger, with an overhang onto the articular surface (Figure 3-12 B) and in the remaining three hips the apex was rounded, similar to the posterior region

(Figure 3-12 C). The labral base in the porcine superior region was thicker from the articulating surface to the external wall, compared to the other regions. The curvature of the articulating surfaces varied around the porcine acetabulum from the concave superior surface to the steeper and flatter anterior surface.

H&E staining of the human acetabulum identified similar structures to the porcine acetabulum. In both species, the labrum formed an apex from the top of the articulating surface, over the subchondral bone to the exterior side of the acetabulum. However, in the human acetabulum, the labrum stopped just below the apex of the subchondral bone on the external side where as the labrum continued down the external side to almost the base of the acetabulum in the porcine tissue (Figure 3-12 D). The morphology of the anterior human apex varied between samples, with three out of the five samples having a rounded apex (Figure 3-13A) and the remaining two samples having a triangular apex (Figure 3-13B). The curvature of the human anterior articulating surface was steep, similar to that of the porcine anterior surface.

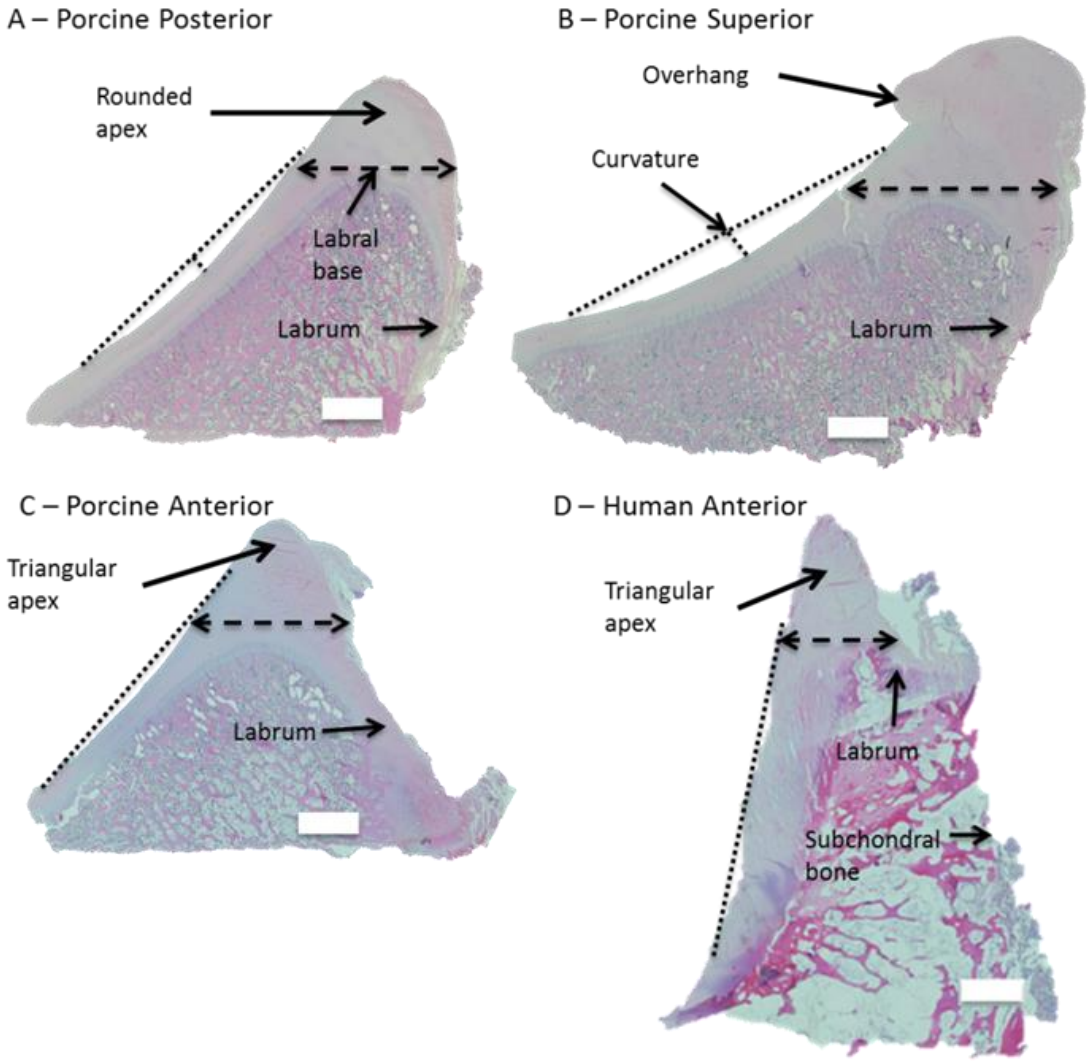

Figure 3-12 H&E staining of the acetabular cross-sections from three regions around the porcine acetabulum and the anterior human acetabulum. A – Porcine posterior region. B – Porcine superior region. C – Porcine anterior region – D – Human anterior region. Images x 2.5 magnification, scale bars represent 2000 µm.

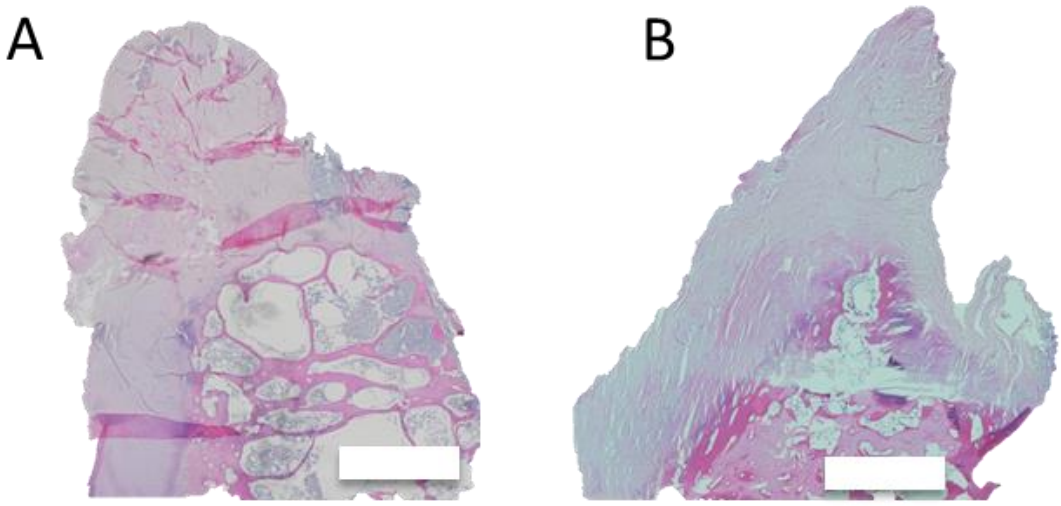

Figure 3-13 Variation in labral morphology of the human acetabulum. H&E staining of the human acetabulum. A – rounded labral apex. B – Triangular labral apex. Images x 2.5 magnification, scale bars represent 2000 µm.

3.6.5.2 General tissue histoarchitecture of the acetabulum

The overall morphology of the porcine and human acetabulum and the tissue locations are shown in Figure 3-14. H&E staining of acetabular cross sections identified slight variation in tissue structure between the posterior, superior, and anterior regions of the porcine acetabulum however; larger variations between the two species were identified. Within the porcine labrum there were two main regions identifiable with respect to tissue structure; the internal region, covering the articulating surface of the acetabulum and the middle of the apex, and the external region forming a thin band from the top of the apex and around the exterior side of the acetabulum (Figure 3-14 A). In the human acetabulum, the junction between the internal and external labrum was less distinct than in porcine tissue. The internal region of the human labrum was curved on the articulating surface, forming a slight overhang and cleft from the cartilage. The main region of the internal labrum, within the human labrum, was supported from behind by the subchondral bone however, a thin band continued up the articulating surface of the apex. The external labrum comprised the majority of the apex and transitioned gradually into the internal labrum (Figure 3-14 B). Cartilage covered the majority of the articulating surface of the porcine acetabulum, where as in the human acetabulum the internal labrum extended further down the articulating surface into the acetabular cup.

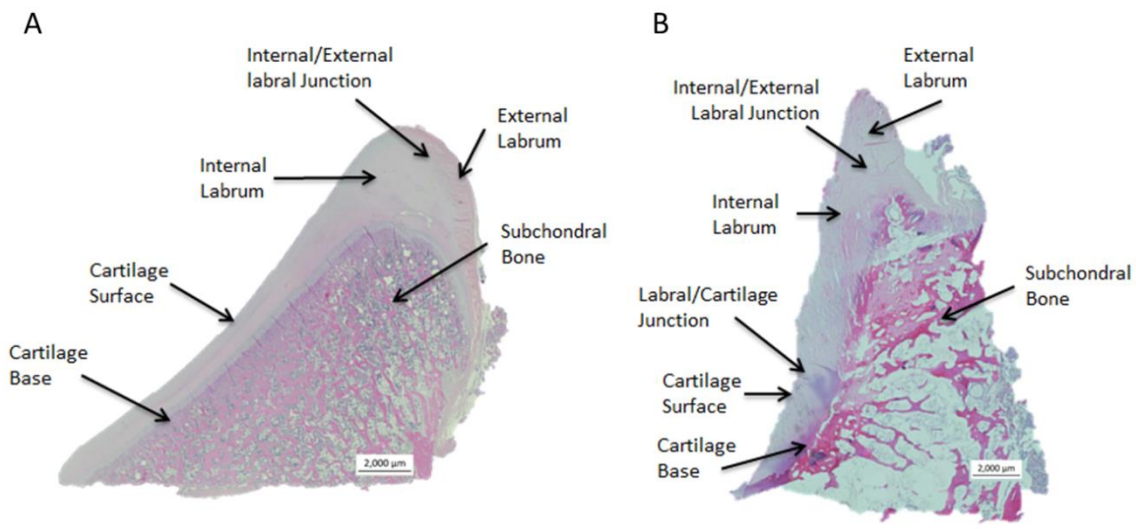

Figure 3-14 H&E staining of the porcine and human acetabulum. A – Porcine acetabulum. B – Human acetabulum. Image x 2.5 magnification, scale bar represents 2000 µm.

The internal region of the porcine labrum was cartilage-like with a smooth surface, randomly orientated cells located in lacunae, and blood vessel-like structures (Figure 3-15 A-C). There was a distinct junction between the internal and external porcine labrum (Figure 3-15 E-G). The external porcine labral region was thinner than the internal labrum in most locations around the acetabulum however, the ratio of the two tissue regions varied between samples. The exception was the superior region where, in the three rounded apices, the connective tissue structure composed the entire labral apex including the overhang area above the cartilage. The external region was a dense regular connective tissue with flattened cells located in clusters between fibre bundles (Figure 3-15 I-K). In the human labrum there were two regions, less distinct than in the porcine labrum (Figure 3-15 H), both regions were fibrous but contained little or no cells (Figure 3-15 D & L). The internal labrum was mainly composed of fibrocartilage (Figure 3-15 D) and the external labrum was a combination of dense regular and irregular connective tissue (Figure 3-15 L).

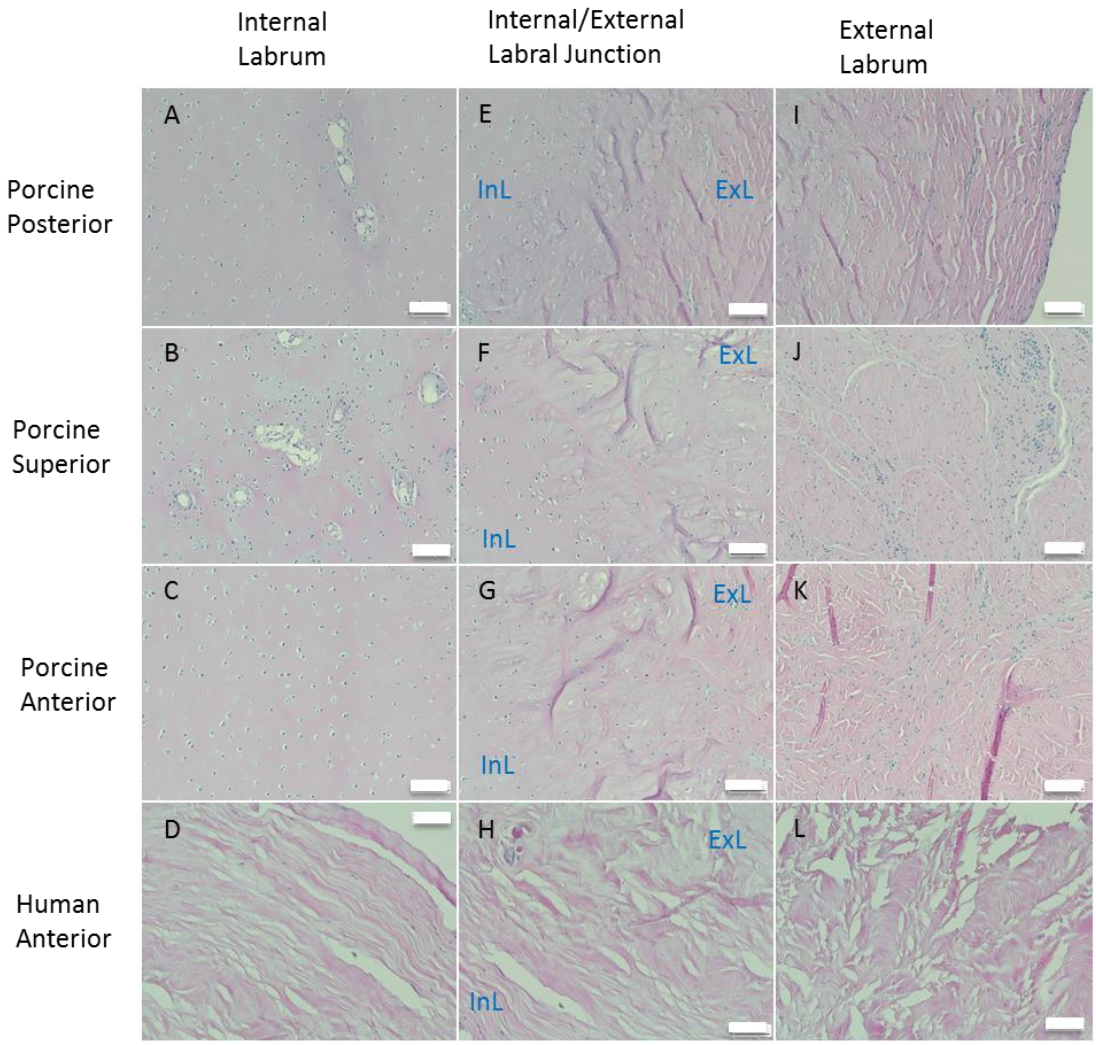

Figure 3-15 H&E staining of labrum. Staining of the porcine posterior, anterior & superior regions and the human anterior region. InL – Internal labrum. ExL – External labrum. Images x 10 magnification, scale bar represents 100µm.

H&E staining of porcine cartilage tissue identified typical cell orientations within the tissue. The cells formed linear columns perpendicular to the subchondral bone above the calcified cartilage, morphing to round randomly distributed cells in the middle zone and smaller flatter cells in the superficial zone (Figure 3-16 A-C & E-G). The human cartilage had fewer cells in comparison, which were randomly orientated throughout the tissue with no zones visible (Figure 3-16 D & H). The surface of the porcine cartilage was smooth and intact compared to the rough irregular human cartilage surface (Figure 3-16 A-D). Although the tidemark of the human cartilage was more defined compared to the porcine tissue, it showed signs of thickening, associated with damage (Figure 3-16 E-H). Within the human tissue the junction between the cartilage and labrum could be clearly identified, with the smooth surface of the cartilage transitioning into the fibrous labrum, unlike the porcine tissue where both tissue types appeared smooth and cartilage-like. The location of the labral-cartilage junction varied between samples within human tissue.

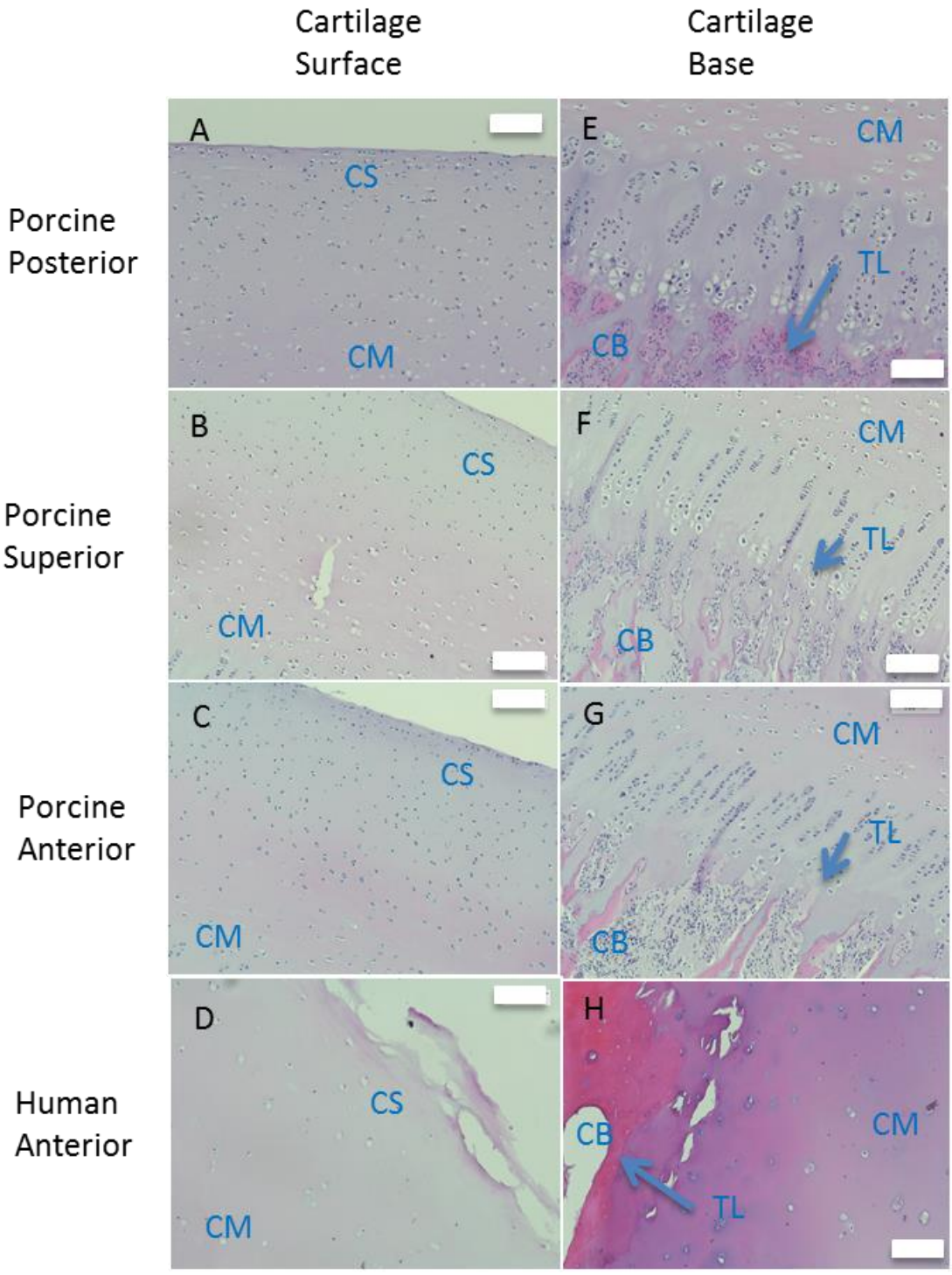

Figure 3-16 H&E staining of cartilage. Staining of the porcine posterior, anterior & superior regions and the human anterior cartilage region. CS – Cartilage surface. CM – cartilage middle. CB – cartilage base. TL – tide line. Images x 10 magnification, scale bar represents 100µm.

3.6.5.3 Collagen and elastin structure of labral and cartilage tissue

Sirius red and Miller's elastin staining of acetabular cross-sections, under brightfield illumination and polarised light, allowed the visualisation of collagen and elastin fibres. Under normal Kohler illumination both porcine and human acetabular tissue samples stained positively

throughout for collagen, as seen by their red colour (Figure 3-17). Elastin was found to be present around the lacunae and in the blood vessels of the porcine tissue samples (Figure 3-17 C-E), identified by the positive dark purple staining however, no elastin was observed in the human tissue samples.

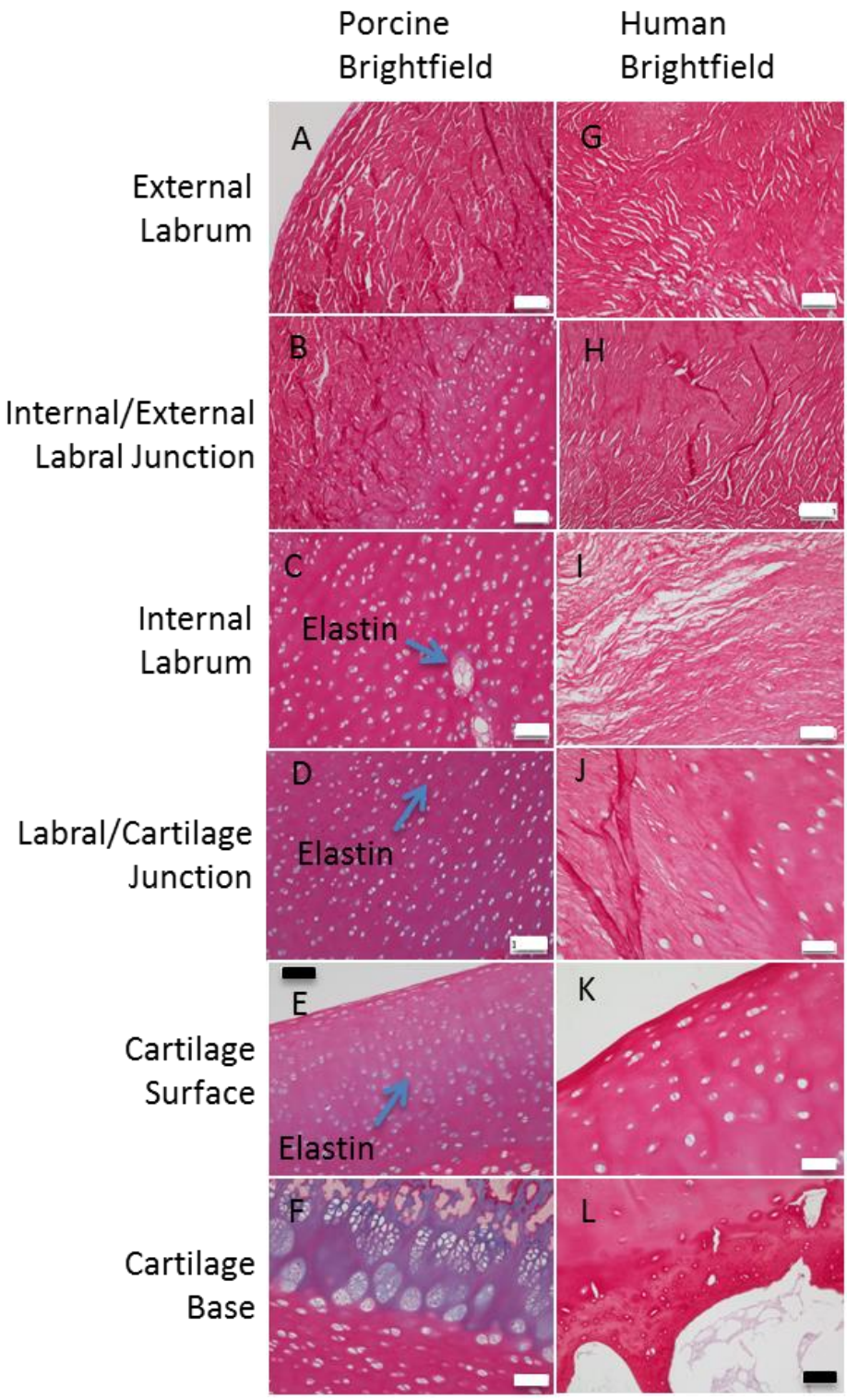

Figure 3-17 Brightfield illumination of sirius red & Miller's elastin stained porcine and human labral and cartilage tissue. Images x10 magnification, scale bar represents 100µm.

Circularly polarised illumination of sirius red and Miller's elastin stained tissue samples allowed estimation of collagen fibre diameter and orientation, within porcine and human labrum and cartilage (Figure 3-18). Fibre diameter was identified by the colour of birefringence, where small fibres appeared green under polarised illumination, medium fibres yellow or orange, and larger fibres red.

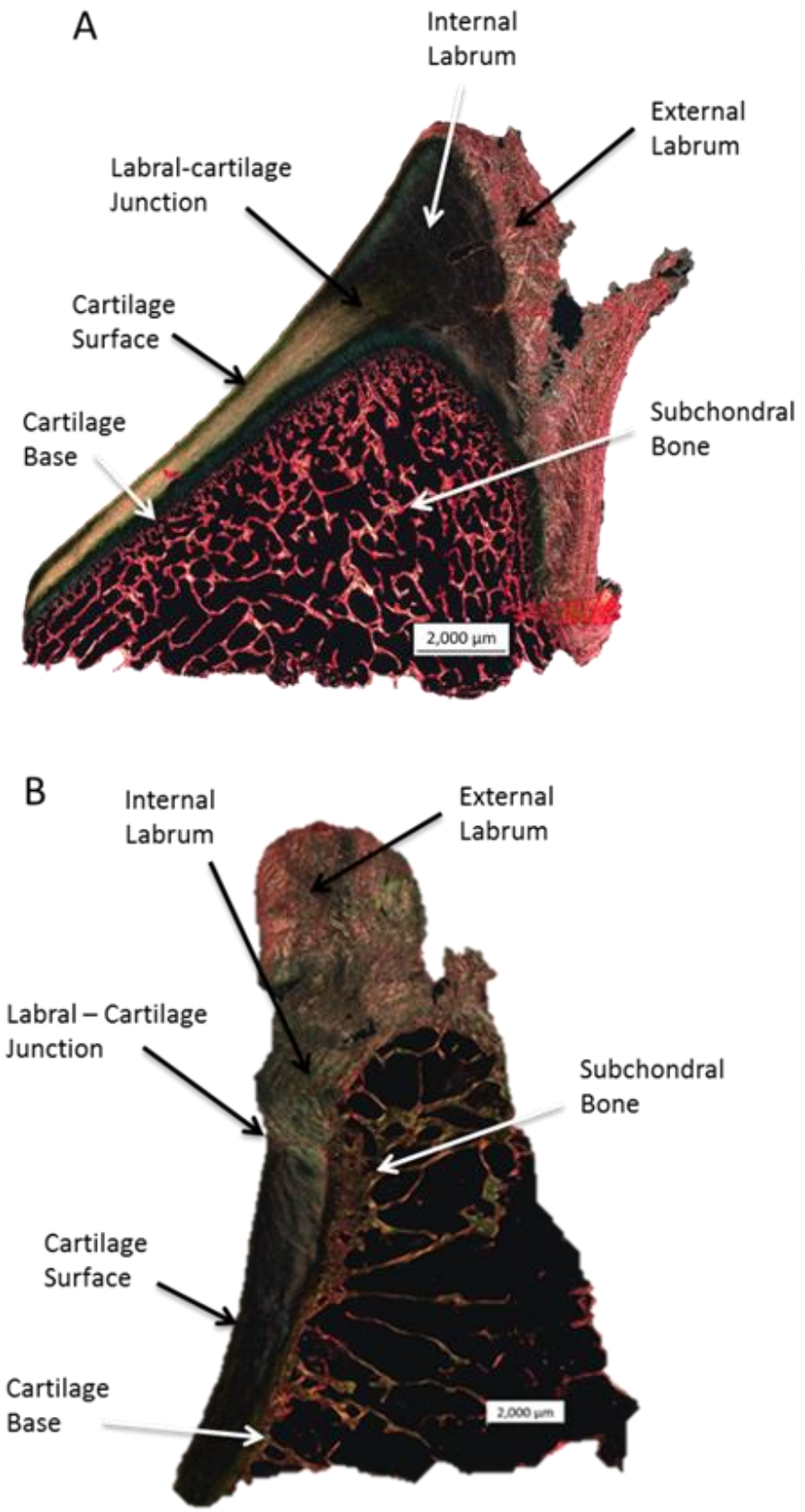

Figure 3-18 Polarised illumination of sirius red and Miller's elastin stained porcine and human acetabulum. A – Porcine acetabulum. B – Human acetabulum. Image x 2.5 magnification, scale bar represents 2000 µm.

In the porcine acetabulum, sirius red staining identified the external labrum to be mainly composed of a tight mesh of large fibres running radially around the socket of the acetabulum which could be seen end-on in the cross-sections. At the exterior edge of the external labrum, fibre bundles became aligned with the external surface in a thin superficial band (Figure 3-19 A). At the internal/external labral junction, fibre bundles in the external labrum changed alignment from radial to perpendicular to the junction, highlighted by a change in colour under polarised light (Figure 3-19 B). The main body of the internal labrum was found to be composed of medium sized fibres fanned outwards towards the articulating surface of the tissue, from the point where the internal labrum met the external labrum and subchondral bone. Towards the articulating surface the fibre bundles decreased in size below the superficial layer, indicated by green birefringence (Figure 3-19 C). At the labral-cartilage junction, the fibres stretched from the cartilage into the internal labrum, parallel to the articulating surface, highlighted in yellow (Figure 3-19 D). In porcine cartilage, medium sized fibres ran parallel to the surface in a thin superficial region along the cartilage surface, separated from the middle zone by small randomly distributed fibres (Figure 3-19 E). In the cartilage middle zone, medium sized fibres were mainly observed to be parallel to the subchondral bone (Figure 3-19 F). A thin band of calcified cartilage ran above the subchondral bone, with small fibres aligned perpendicularly to the surface (Figure 3-19 F). No differences in collagen structure were observed between the anterior, superior, and posterior porcine regions.

In the human acetabulum, the external region of the labrum was more heterogeneous than the internal labrum with primarily large collagen fibres. Similar to the porcine external labrum, fibres within the human external labrum appeared radially aligned around the acetabulum (Figure 3-19 G). At the articulating surface there was evidence of a thin superficial band with fibres aligned parallel to the surface. The junction between the internal and external labrum was less clear and uniform than in the porcine tissue however, it was identified by the change in birefringence and collagen fibre alignment (Figure 3-19 H). When stained using sirius red, the internal labrum was identified by a region of primarily small green birefringent collagen fibres, curved to form a slight overhang above the cartilage surface on the articulating side (Figure 3-19 I). In comparison to the porcine acetabulum, the labral-cartilage junction was clearer in human tissues. At the junction, the fibres from the labrum diffused into the cartilage and there was a smooth transition between the two tissues (Figure 3-19 J). Similar to porcine tissue, the labral-cartilage junction was below the top of the subchondral bone, and the labrum continued around the top of subchondral bone to the external side of the acetabulum. The cartilage superficial zone was identified by a band of medium and large fibres running parallel to the surface (Figure 3-19 K). Below the superficial zone, the middle of the cartilage was composed of randomly orientated fibres of small and medium diameter (Figure 3-19 K). Like the porcine acetabulum, the cartilage deep zone within the human acetabulum was identified by a band of

small fibres adjacent to the subchondral bone however, the collagen fibres ran parallel to the surface (Figure 3-19 L). The zones within the human cartilage were less clear than in the porcine cartilage, with the deep zone of the human cartilage varying greatly in thickness between subjects. Overall the mesh-like network of collagen fibres were less tightly packed in the human acetabulum compared to porcine samples.

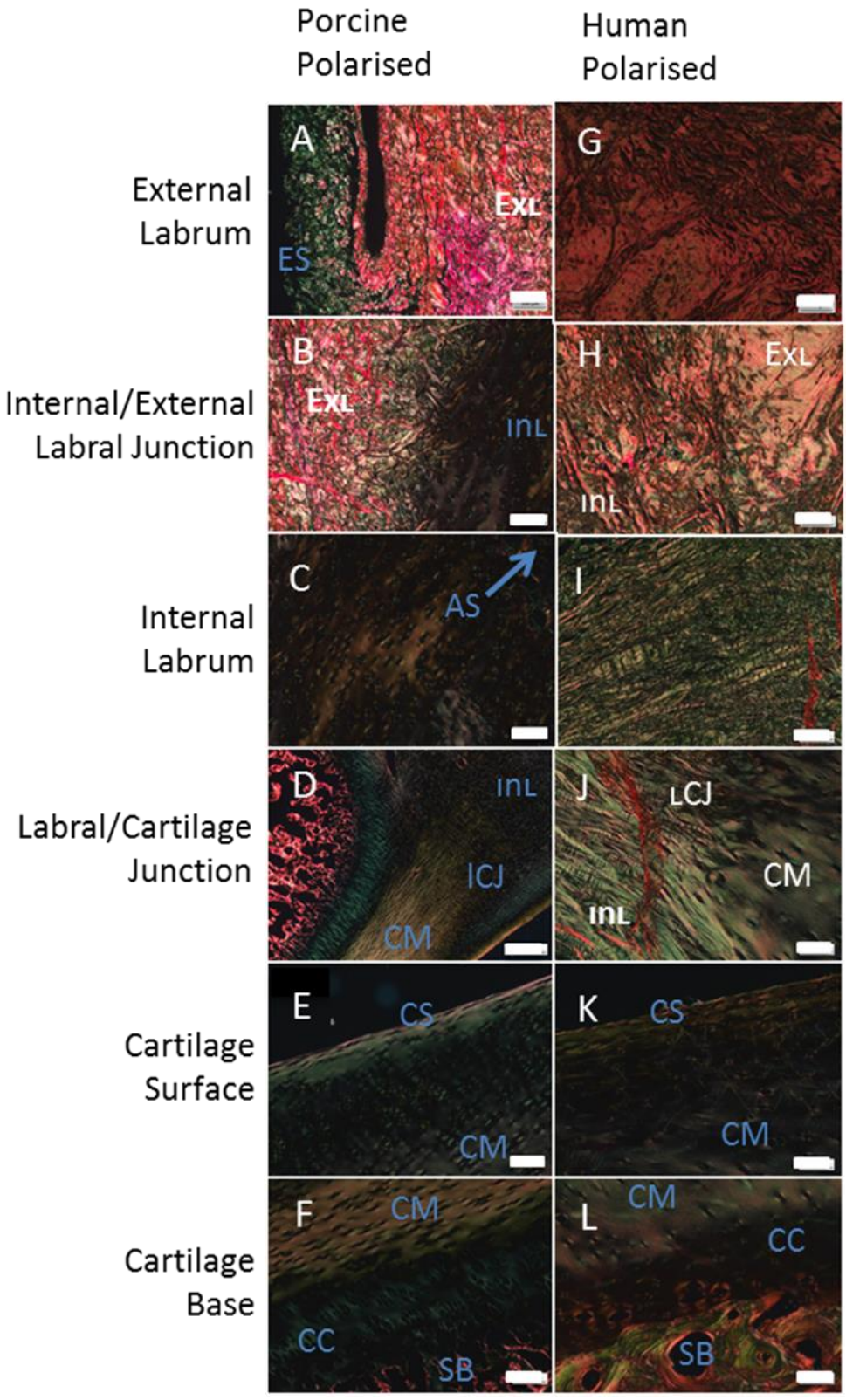

Figure 3-19 Polarised illumination of sirius red & Miller's elastin stained porcine and human labral and cartilage tissue. AS – Articular surface.CC – Calcified cartilage. CM – cartilage middle. CS – Cartilage surface. ES – External surface. ExL – External labrum. InL – Internal labrum. LCJ – Labral-cartilage junction. SB – subchondral bone. Images x 10 magnification, scale bar represents 100µm.

3.6.5.4 GAG dispersion within the human and porcine labrum

Alcian blue staining of labral sections showed the presence of GAGs in the internal porcine labrum, identified by the positive blue staining (Figure 3-20 A-C). The porcine external labrum and the human labrum showed little or no presence of GAGs highlighted by the presence of pink periodic acid-Schiff counterstaining in these regions (Figure 3-20 A-D). At the porcine internal/external labral junction GAGs could be seen dispersing from the internal labrum to the external labrum (Figure 3-20 A-C).

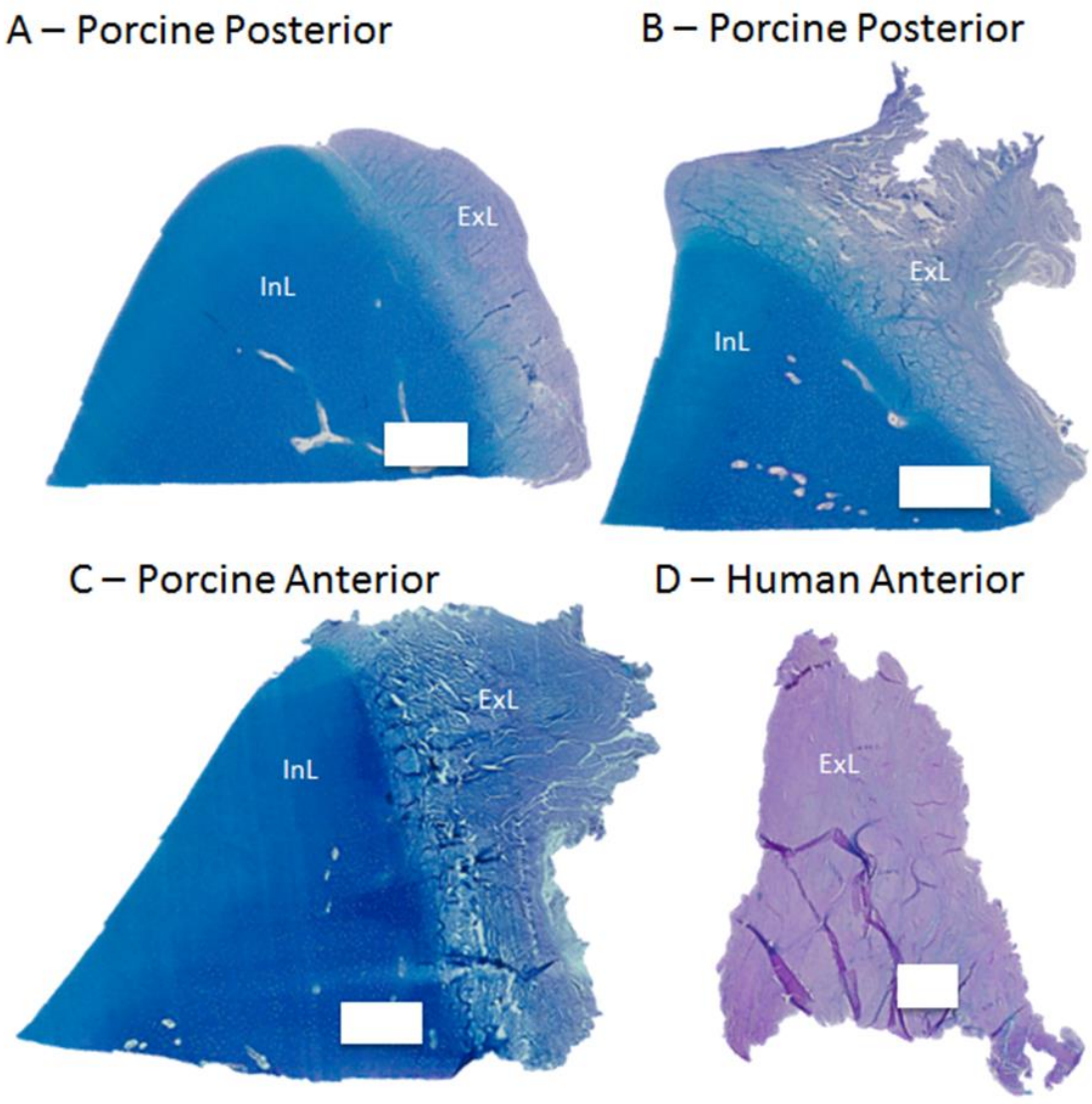

Figure 3-20 Alcian blue stained porcine and human labral sections. A – Posterior porcine labrum. B – Superior porcine labrum. C - Anterior porcine labrum. D – Anterior human labrum. InL – Internal labrum. ExL – External labrum. Images x 2.5 times magnification, porcine scale bars represents 1000 µm, human scale bar represents 500µm.

3.6.6 Immunohistochemical evaluation of labrum, cartilage, and the labral-cartilage junction

Immunohistochemistry was used to identify the different collagen types present in the acetabulum and to highlight the transition between different tissue types. The main collagen types, I and II, were determined.

3.6.6.1 Distribution of collagen types

Immunohistochemical staining of acetabular sections identified two main collagen types present in the acetabulum; type I collagen and type II collagen. Collagen type II was identified in both the porcine and human acetabulum however, collagen I was only identified in porcine tissue due to unsuccessful optimisation of antibody labelling of the human samples. In the porcine acetabulum the external labrum stained positive throughout for collagen I and the cartilage and internal labrum stained positive throughout for type II collagen, for all three regions, with a clear junction between the two. In the human acetabulum the cartilage and internal labrum stained positive for type II collagen (Figure 3-21).

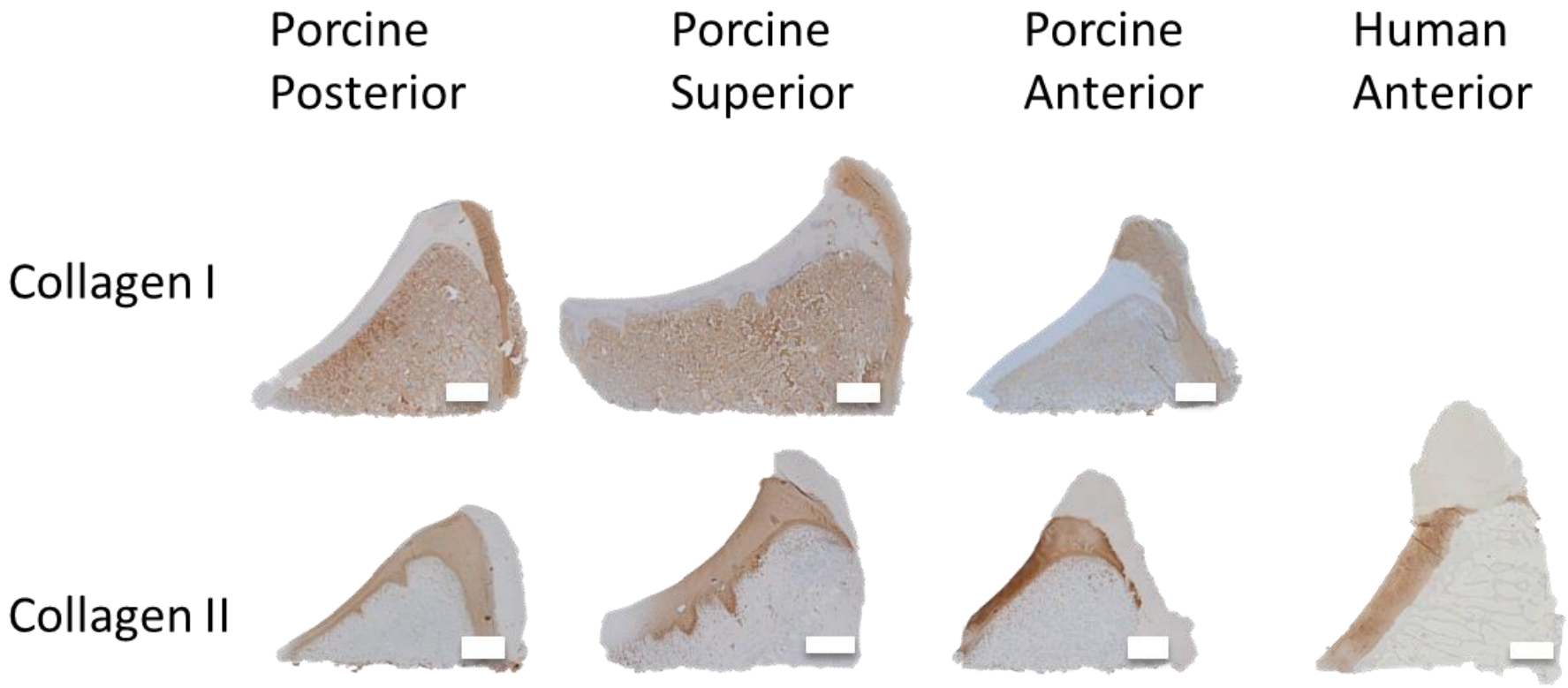

Figure 3-21 Immunohistochemistry staining of acetabular cross-sections for collagen I and II. Cross-sections were stained for collagen I (top row) and collagen II (bottom row). Positive staining of collagen is brown. Images x 2.5 magnification, scale bars represent 1000µm.

3.7 Discussion

The aim of this chapter was to analyse the biological characteristics of the soft tissues within the hip and compare porcine and human tissue for use in a subsequent *in vitro* simulation model. This included; analysing the hip on both a macroscopic and microscopic scale, to compare the morphology, structure, and constituents within the tissues. Tissues were analysed from the femoral head and acetabulum in two regions; load-bearing and non-load-bearing. As damage to soft tissues in the hip is commonly associated with a loss of GAGs and degeneration of the collagen matrix which affects the function of the tissue (Arokoski et al. 2000) the analysis focused on these constituents. In addition, due to subsequent mechanical testing requirements, different regions were analysed using the same methods to determine any differences and to eliminate the need to mechanically test multiple regions and the femoral head cartilage. Currently no such study exists in the literature to the author's knowledge.

Initial macroscopic analysis identified that the human acetabulum was larger than the porcine acetabulum, in both diameter and depth, with the human acetabulum having a much steeper articulating surface. The larger human labrum additionally increased the depth of the socket, which has been noted in literature to increase the stability of the hip (Ferguson et al. 2001; Grant et al. 2012). The labrum was found to be deepest in the superior region as well as having a more rounded apex in the posterior region compared to the triangular anterior region. These results corresponded with the findings presented in studies by Seldes et al. 2001 and Narvani 2003. The human hip also varied in morphology from the porcine hip with a smaller greater trochanter and longer femoral neck, as well as having a rounder femoral head. Although the porcine hip was smaller than the human hip, it is the closest in size compared to other readily available tissues, such as ovine or bovine (Taylor et al. 2011) and it is large enough for use in *in vitro* simulation systems, used to simulate tissue damage. The acetabular morphology of the two species did not vary significantly enough to cause concern for the use of porcine hips as an *in vitro* simulation system of the human hip.

Cartilage and labral tissue in the human hip showed signs of degeneration by their yellowed appearance, associated with older tissue. The cartilage surface appeared duller in comparison to the glossy porcine cartilage (Altman 1987) and the human tidemark showed signs of thickening, associated with damage (Seldes et al. 2001).These degenerative changes have been reported in the literature to have an effect on the mechanical properties of the tissue due to increased stiffness (Bank et al. 1998; Verzijl et al. 2002). Degeneration of the human tissue was also identified in the present study using H&E staining, where the cartilage surface appeared roughened with loose collagen fibrils present and cells were less densely populated and disorganised throughout. This supports the work by Stockwell (1967), who stated that the cellularity of cartilage decreases with age in humans. As the porcine tissue was skeletally

immature at six months old (Reinwald & Burr 2008) and the human tissue was damaged, it will be important to take this into account during mechanical testing and *in vitro* simulation.

Microscopic analysis of the porcine acetabulum revealed little variation in structure between the anterior, superior, and posterior regions within the hip, with the exception of the labrum in the superior region having an overhang above the articular cartilage and a larger area of connective tissue in half of the samples analysed. The overhang of the porcine and human superior labrum and its overall larger size may make it more susceptible to impingement and hence damage, as observed in a study by Seldes et al. (2001).

The water content of tissues is responsible for the viscoelastic behaviour of a tissue and hence by its confinement, enables the tissue to support load (Pereira et al. 2013). The water content of the labrum and cartilage from human and porcine species was assessed quantitatively using tissue lyophilisation. Overall, water content accounted for approximately three quarters of the tissues wet weight for all tissue types, which fell within the range reported for human cartilage samples, of 68-85 % and meniscus in the knee (a similar structured tissue to labrum) of 60-75 % (Speer 2005; Link 2011). The porcine labrum was found to have significantly lower water content (70 %) than porcine cartilage (75 %) however, no significant differences were found for human tissue, this could be a result of the age and level of damage in the human tissue, which has been associated with water reduction (O'Hara et al. 1990). It is likely that cartilage had higher water content due to its load-bearing function as opposed to the labrum's supportive function, which assists in load sharing (Lu & Mow 2008; Grant et al. 2012).

GAGs have been identified as having important functions in load-bearing tissues due to their ability to retain water within the tissue matrix (Lohmander 1988; Bader et al. 1992). GAG content of porcine and human cartilage and labral tissue was assessed quantitatively using a colourimetric assay with DMB dye, as well as GAG distribution in the porcine and human labrum being assessed qualitatively using alcian blue staining. Quantitatively, GAG concentrations followed a similar trend to water content, with porcine cartilage tissue having a significantly higher concentration of GAGs than the labrum; this was also seen in human tissue for GAGs and as mentioned previously is likely to be due to the tissues load-bearing function. Porcine tissue was also found to have a significantly higher GAG concentration than human tissue for both the labrum and cartilage, likely due to the immaturity of the porcine tissue. This is supported by a study carried out by Roughley & White (1980) who reported GAG concentration decreased with age. Although the same overall trend was seen between GAG and water content, the significant differences were greater for GAG concentrations, with the human labrum containing almost negligible GAGs. The histology results supported the quantitative results in this study, with human labrum containing very low concentrations of GAGs and the porcine labrum staining strongly for GAGs. Within the porcine labrum, GAGs were mainly

confined to the internal region, with a small amount dispersing across the labral junction into the external region.

Collagen fibre bundles provide structure to a tissue and their formation is related directly to the stress placed on it, with fibrils orientated in the direction of the greatest tension (Petersen et al. 2003). Collagen content and distribution was analysed quantitatively using a hydroxyproline assay and qualitatively using a sirius red stain under brightfield illumination and polarised light. Quantitatively, the measured collagen content showed an inverse relationship to water and GAG content, with labral tissues containing the lowest water and GAG content but the highest collagen content. Porcine labral tissue had significantly higher collagen content compared to porcine cartilage and although human tissue followed the same trend as porcine tissue, the difference was not found to be significant. Porcine tissue had a higher trend of collagen content than human tissue for both the labrum and cartilage, however, the difference was only found to be significant for labral tissue. The values for cartilage collagen content fell within the range reported in literature of 320 to 620 $ug.mg^{-1}$ (Fermor 2013; Taylor 2013). The higher collagen content within the labral tissue may be due to its supportive function, where the collagen fibres provide strength to the tissue. Qualitative analysis of the acetabulum revealed the presence of collagen throughout both labral and cartilage tissues with no elastin detected in human tissue and confined to the lacunae and blood vessels in porcine tissue. Cartilage tissue primarily stained positive for type II collagen and typical regions could be seen under polarised light with sirius red staining. Within porcine cartilage the superficial, middle, and deep zones appeared more pronounced and uniform in thickness in comparison to human cartilage. The labral-cartilage junction within human tissue had a clear transition zone, with the tissue type changing from cartilage to a fibrocartilage labrum. At the junction, the fibres from the labrum diffused into the cartilage and there was a smooth transition between the two tissues, as seen in a scanning electron microscopy (SEM) study by Owen et al 1999. In the porcine acetabulum the collagen structure across the cartilage-labral junction did not appear to alter and both tissues appeared cartilage-like. The junction could only be identified under polarised light by a change in fibre alignment and size. Fibre diameter was identified by the colour of birefringence, where small fibres appeared green under polarised light, medium fibres yellow or orange, and large fibres red (Junqueira et al. 1982; Cole & Malek 2004). A junction between two tissue types could result in a weakness in the tissue and a possible reason for labral-cartilage separation during damage, as seen in Type 1 tears in a study by Seldes et al. (2001). Both the cartilage and main internal labral region stained positively for type II collagen in both species. The external labral region for porcine tissue stained positively for type I collagen and although collagen I staining was unsuccessful for human tissue in the present study, the literature has reported the labrum to be comprised primarily of collagen type I (Narvani 2003; Petersen et al. 2003). Due to the negative staining of type II collagen, the external labrum can be assumed to be type I

collagen in this study. The external labral region of the porcine tissue was only found as a thin band in the majority of specimens however, in human tissue the external labrum region comprised the majority of the labral apex. The porcine internal labrum may be cartilage-like in structure due to its immaturity, and it may later develop into a fibrocartilage however, further investigation would need to be performed to confirm this. The human labral zones and fibre size were consistent with the findings by Petersen et al. 2003.

Similar to the labrum the adjacent TAL's function is to provide support to the acetabulum by resisting stretching by the femoral head and completes the circumference of the acetabulum by bridging the labrum across the acetabular notch. The support is provided by two densely packed twisted collagen fibre bundles, of which the upper part connects directly to the labrum and the lower part to the outer surface of the bone. The fibre bundles within the main region of the labrum and the TAL are uniform in direction allowing the tissues to resist tensional stresses and strains (Lohe et al. 1996).

Quantitative results for water, GAGs, and collagen content showed no significant differences between load-bearing and non-load-bearing regions or between femoral cartilage and acetabular cartilage. As a result, it was not thought necessary to mechanically test femoral tissue and the region (load-bearing or non-load-bearing) was not thought to have an effect on further results.

Characterisation of labral tissue was carried out to gain a better understanding of the tissue's constituents and structure, as well as its transition with articular cartilage, in order to help future understanding of labral function and damage etiology and patterns. Comparison of porcine and human acetabular tissues was also carried out with the aim of determining the suitability of porcine tissue as a human tissue model. The differences observed between porcine and human tissue in this study appeared to be a result of tissue immaturity, due to the young age of the porcine tissue.

Small human sample numbers were also a limitation of this study. Larger sample numbers may have provided a clearer illustration of the tissue boundaries when there was variation between samples. Tissue damage was also observed in human histological samples with tears in the tissue and no cells present. This damage could be a result of under decalcification and fixation as cells were documented in human labral tissue in a study by Audenaert et al. (2012). However, overall the two species were found to be similar in structure and constituents, with the labrum containing higher collagen content than cartilage but a lower GAG and water content. Although a more mature porcine tissue would be beneficial, the age of the tissue was limited due to the availability of animals used in the food chain for human consumption. Based on the aims of this chapter greater knowledge of the labrum has been identified and porcine hips will be suitable to use to represent human hips.

Key findings:

- The human hip is larger than the porcine hip; with a greater diameter, deeper socket and larger labrum.
- Human tissue showed signs of degeneration which needs to be taken into account for subsequent mechanical characterisation results and *in vitro* simulation models.
- The structures around the hip did not vary in porcine tissue, with only a slight variation in labral morphology in the superior region. No differences were found between femoral and acetabular cartilage or between load-bearing and non-load-bearing regions of labral and cartilage tissue.
- All tissues had a water content of around 75 %, however porcine cartilage contained slightly higher water content than porcine labrum.
- GAG content followed a similar trend to water content with cartilage having a higher GAG content than the labrum in both species. Negligible GAGs were present in the human labrum and the majority of GAGs present in the porcine labrum were located in the internal labrum.
- Collagen content had an inverse relationship to water and GAG content with labral tissue containing more collagen than cartilage tissues. The difference in collagen content was more pronounced in porcine tissues.
- Cartilage and internal labral tissue stained positive for collagen II in both species. The porcine external labrum stained positive for collagen I.
- In the human acetabulum a clear transition between the cartilage and labrum could be identified, unlike the porcine acetabulum. However, the porcine labrum had a clear transition between the internal and external labrum, unlike in the human labrum.
- The main structural difference identified between the two species was in the labrum. The human labrum was primarily comprised of external labral tissue as opposed the porcine labrum which was primarily comprised of internal labral tissue.

Chapter 4

Biomechanical characterisation of porcine and human acetabular labrum and cartilage

4.1 Introduction

In order to gain an understanding of how the acetabular labrum functions and how it becomes damaged, it is necessary to understand the mechanical properties of the tissue. The labrum's main functions are to stabilise the hip joint by deepening the socket and protect the articulating surface by forming a seal against the femoral head and preventing fluid flow (Ferguson et al. 2001; Petersen et al. 2003). Collagen within the labrum is responsible for withstanding stretching from the tensile forces placed on it by the femoral head pushing against the labrum as it articulates within the socket. As opposed to normal function, during labral damage the tissue's structure is altered compromising its mechanical properties and preventing it from functioning efficiently. The labrum becomes damaged when abnormal contact mechanics and force patterns occur in the hip joint, in instances such as FAI, when the labrum undergoes compression and shear stresses when it is impinged by the bony growth.

The purpose of the study undertaken in this chapter was to investigate the mechanical properties of the porcine and human acetabular labrum. Previously, limited mechanical studies of the acetabular labrum have focused on human or bovine tissue however, porcine tissue is frequently used as a substitute for less readily available human tissue during characterisation studies (discussed in Chapter 3) hence it is important to know the differences between the tissues (Ferguson et al. 2001; Ishiko et al. 2005).

A further aim of this study was to investigate and compare the mechanical properties of labral and cartilage tissue. A common area of labral damage is the junction between the labrum and articular cartilage, where longitudinal peripheral tears occur. Here it is proposed that this could be an area of weakness as a result of a change in tissue structure and hence mechanical properties in order to support the varying functions of the tissues (as discussed in Chapter 3). Therefore, the work in this chapter aimed to determine the porcine acetabular labrum's compressive and tensile properties in comparison to human and cartilage tissue.

Established methods have previously been used to characterise the compressive properties of soft tissues such as the meniscus in the knee and cartilage. These methods have included; indentation, unconfined compression and confined compression (Mow et al. 1998; Ferguson et al. 2001; Abdelgaied et al. 2015). Within this study indentation and unconfined compression tests were used to investigate the mechanical properties of the porcine and human labrum and cartilage. The rationale for using these two methods over confined compression was decided due to the small nature of the porcine labrum and the reduced accuracy this resulted in when preparing the tissue pins. Confined compression tests rely on the ability to fully confine the tissue, to ensure fluid flow only occurs in one direction, hence this could not be guaranteed with the porcine samples used within this study.

Tensile testing has been carried out successfully on various soft tissues to determine their tensile properties (Tissakht & Ahmed 1995; Goertzen et al. 1997; Williamson et al. 2003). The intrinsic tensile properties of the solid matrix of a tissue can be identified using tensile testing under quasi-static test conditions which minimises the effect of interstitial fluid (Proctor et al. 1989; Herbert et al. 2016). In this study tensile testing under quasi-static test conditions were carried out to determine the tensile properties of the porcine and human acetabular labrum.

4.2 Aims and objectives

Aims:

The aim of the research presented in this chapter was to mechanically characterise the acetabular labrum in terms of its compressive and tensile strength for porcine and human tissue.

Objectives:

- Determine the compressive properties of labral tissue in comparison to articular cartilage, including; creep and strain, equilibrium aggregate modulus, and permeability. Labral compressive properties were determined across the width of the tissue (perpendicular to the main fibre orientation), the direction in which the tissue is primarily loaded in compression.
- Determine the tensile properties of the acetabular labrum, including; initial Young's modulus, equilibrium Young's modulus, transition stress, transition strain, stress at failure, and strain at failure. Labral tensile properties were determined along the main fibre orientation, in which the tissue is primarily loaded in tension to determine the highest tensile properties.

4.3 Compressive biomechanical materials and methods

Indentation and unconfined compression tests under a high and low load were carried out on porcine labral pins to identify the method which would produce minimal deformation. In order to determine the compressive properties of a tissue, minimal deformation is assumed during analysis of the data as a result of the variation in permeability with deformation. As the tissue is compressed the pore sizes within the tissue are reduced, hence decreasing the permeability (Oatis & Mansour 2009). Therefore for soft tissues low loads are required to ensure minimal deformation.

Following indentation and unconfined compression tests on porcine labral tissue the method which produced the least deformation was carried out on porcine and human labrum and cartilage pins to compare the time-dependent deformation under a constant compressive load.

A summary of the loads applied to the porcine labrum during indentation and unconfined compression can be seen in Table 4-1. The loads applied and diameters of the loaded area were used to determine the compressive stress applied to the tissue.

Table 4-1 Indentation and unconfined compression applied loads. Table of the loads applied during indentation and unconfined compression using the high load and low load shaft.

	Indentation			**Unconfined**		
	Diameter of indenter tip (mm)	**Load (N)**	**Stress (MPa)**	**Diameter of specimen (mm)**	**Load (N)**	**Stress (MPa)**
High Load	1.5	0.22	0.13	5	0.53	0.03
Low Load	1.5	0.11	0.06	5	0.11	0.006

4.3.1 Experimental approach

To investigate the compressive properties of labral and cartilage tissue, mechanical creep tests were undertaken using cylindrical tissue pins (Section 2.3.5) to determine the tissue's elastic modulus and permeability. The tests were conducted using an indentation rig (Figure 4-1), which allowed an instantaneous (within 40ms), constant load to be applied to the tissue's surface until the creep deformation reached equilibrium. The indentation rig was manufactured in house and included a linear variable differential transformer (LVDT) to measure displacement with a sensitivity of 0.4 µm at a range of 10 mm. Data was recorded at a sampling rate of 10 Hz, using LabView 2012 software, after being adapted using an analogue to digital converter. The load applied to the tissue was determined by the weights of the free moving

components, dependent on the test being carried out, as resistive friction was assumed to be negligible (Taylor et al., 2011).

Creep testing was undertaken for indentation and unconfined compression using an indenter tip or flat plate respectively to apply a load. Two shafts were used during testing; a heavy weight shaft and a light weight shaft, to adjust the load applied to the tissue for both indentation and unconfined testing. During testing pins were secured inside a PBS filled specimen holder to maintain tissue hydration (Figure 4-1 A). The holder height was altered so that the specimen was as close to the tip or plate as possible before testing, to minimise impact on contact. Creep tests were carried out using 5 mm diameter labral pins and 6 mm diameter cartilage pins, with the weight of the shaft adjusted to maintain an equal compressive stress for both pin sizes. The collet was then placed in the indentation rig holder and filled with PBS (Figure 4-1 B). The sample was constrained on the bottom surface only using superglue and fluid flow was allowed in all other directions. To apply the load, the shaft was released and allowed to fall freely onto the sample.

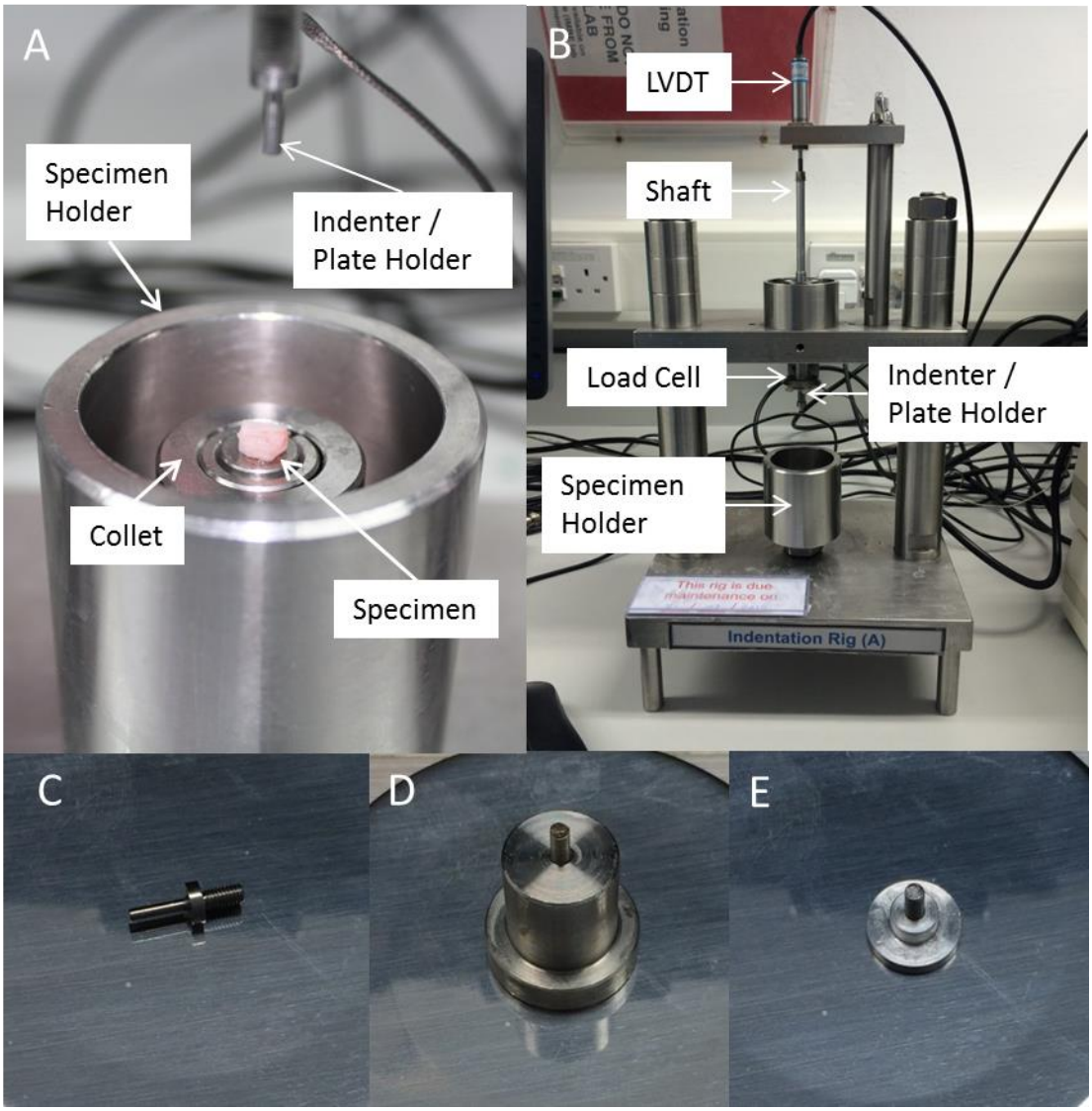

Figure 4-1 Indentation rig. The equipment used during creep testing for labral and osteochondral pins. A - Specimen holder mounted with specimen. B - Indentation rig. C - Indenter tip, D - large plate. E - Small plate.

4.3.2 Creep indentation testing

A 1.5 mm diameter impermeable flat stainless steel indenter tip was used to apply a load to the tissue surface (Figure 4-1 C). The diameter was selected so that the tip was less than a third of the tissue diameter to minimise the edge effect of the tissue. The total compressive stress applied by the heavy weight set up was 0.13 MPa and the lightweight set up was 0.06 MPa. Indentation testing was carried out using porcine labral tissue only (n=6).

4.3.3 Creep unconfined testing

An impermeable flat stainless steel plate was used to apply a load to the tissue surface during unconfined compression. The heavy weight shaft was used with a larger diameter plate; the total compressive stress applied by the heavy weight set up was 0.03 MPa (Figure 4-1 D, Table 4-1). The lightweight shaft was used with a smaller diameter plate; the total compressive stress applied by the lightweight set up was 0.006 MPa (Figure 4-1 E). The lightweight plate diameter was selected to be as small as possible to reduce the weight but still larger than the specimen diameter (9 mm) to ensure the full tissue surface was load-bearing. Heavy weight testing was carried out on porcine labrum (n=6), light weight testing was carried out on porcine and human labrum and cartilage (n=6 porcine, n=5 human).

4.3.4 Tissue thickness measurements

Specimens for compressive testing were extracted as described in Section 2.3.5 for labral and osteochondral pins. Tissue thickness was measured in order to normalise data for each pin, using high magnification photography for cartilage thickness and a digital thickness gauge for labral tissue (a thickness gauge could not be used for cartilage tissue because the thickness was measured with the subchondral bone attached).

4.3.4.1 Labral thickness measurements

Labral pins were measured prior to testing, using a digital thickness gauge (accuracy ± 0.005 mm). Samples were measured three times and average thickness calculated (Figure 4-2).

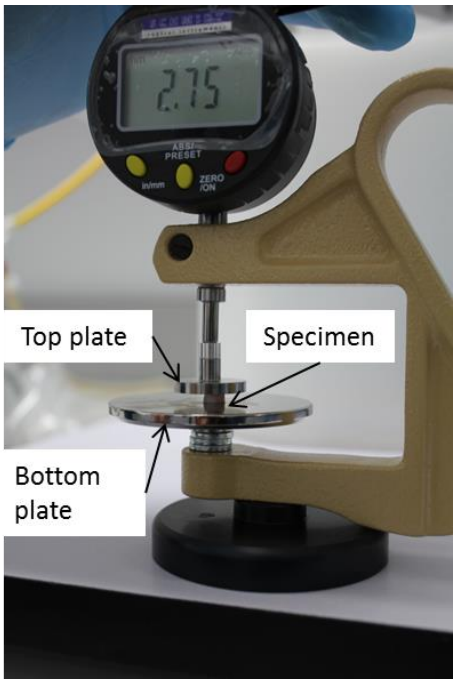

Figure 4-2 Labral tissue thickness measurement. Labral pins were placed on to the bottom plate and the top plate lowered until it touched the labral surface.

4.3.4.2 Cartilage thickness measurements

Following creep testing, cartilage pins were allowed to stress-relax for one hour then cut in half and photographed from a side view adjacent to a ruler (Ferguson et al. 2003). Using ImageJ, the measurement points on the ruler were calibrated with the computer program to measure the cartilage thickness. Cartilage thickness measurements were taken from three locations along the cartilage surface and the average thickness calculated (Figure 4-3).

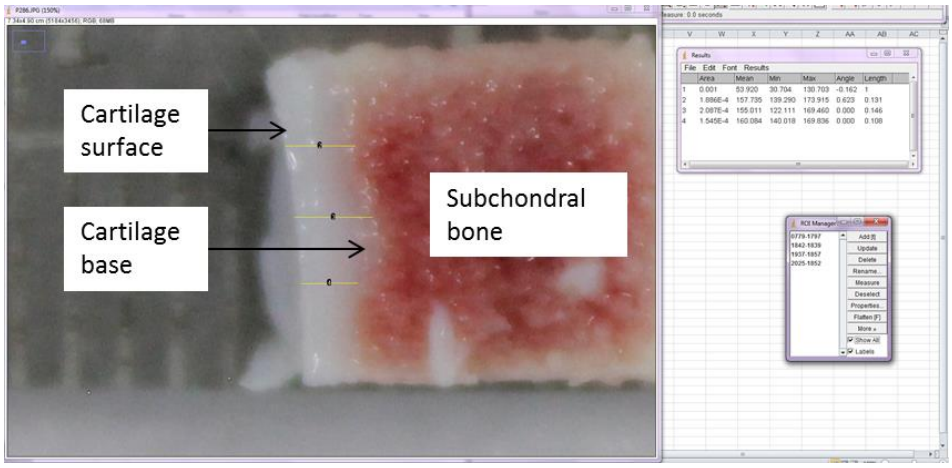

Figure 4-3 Cartilage thickness measurement. Photo of half a cartilage pin uploaded into Image J. Cartilage thickness measurements were taken at three locations across the tissue surface, represented as yellow lines.

4.3.5 Compressive data analysis

When processing the data for compression testing the first few data points were removed from the analysis shown in Figure 4-4 region A. This was the time from when the test recording started to the moment the shaft was released hence, no displacement is seen in this period. A rapid change in displacement can be identified in Figure 4-4 region B. This was when the shaft was falling through the air prior to impact with the tissue. A second rapid change in displacement can be seen when the indenter tip or plate contacted the tissue surface at the beginning of region C in Figure 4-4. In standard compression testing this is the point in which displacement data is analysed from as it is the repose from the tissue under load. However, during testing it was shown that this method was appropriate only for cartilage and not labral tissue, as the labrum was too soft for the machine to discern an accurate point when the indenter or plate came in to contact with the tissue. In Figure 4-5 it can be seen that labral tissue produces a similar curve to cartilage tissue however, in the labral tissue the second change in displacement point is identified after a higher deformation than in cartilage, meaning that the tissue has already compressed before the machine can identify when contact has been made with the surface. Therefore, for labral tissue, two analysis methods were adopted. 1. The displacement from the moment the shaft was released (DSR), identified from the point any

change in displacement was registered and 2. The displacement when an instantaneous response was identified (DIR), identified from the point a second large change in displacement was registered, the two analysis scenarios are explained in Figure 4-4 and Figure 4-5.

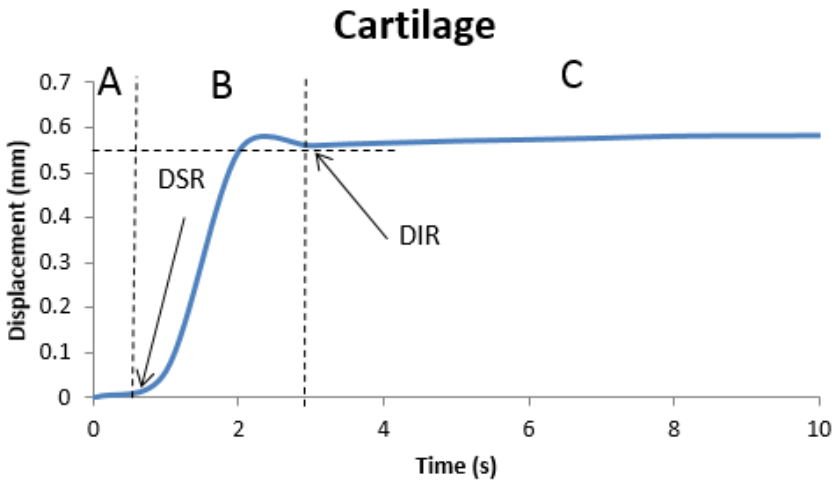

Figure 4-4 Time-displacement graph of displacement from shaft release and displacement from instantaneous response analysis for cartilage tissue. DSR (displacement from shaft release) analysis includes all data following the moment of shaft release. DIR (displacement from instantaneous response) analysis does not include DSR data and begins when a second rapid change in displacement is identified.

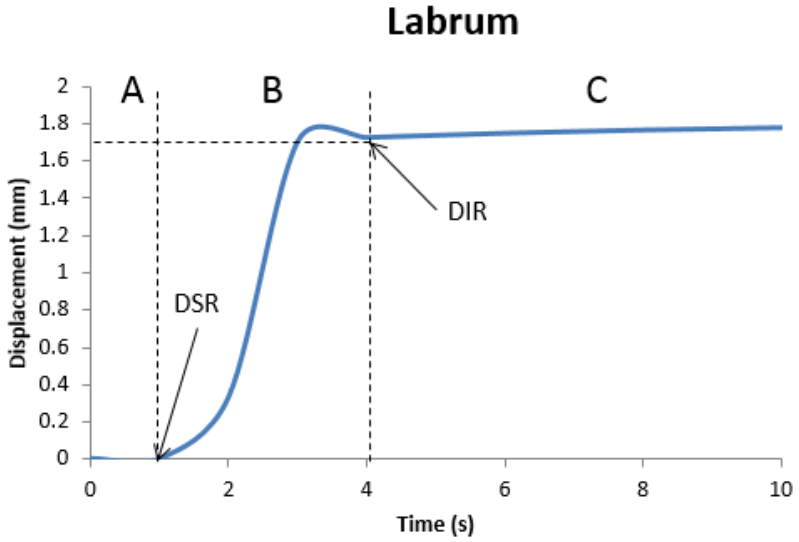

Figure 4-5 Time-displacement graph of Displacement from Shaft Release and Displacement from Instantaneous Response analysis for labral tissue. DSR (displacement from shaft release) analysis includes all data following the moment of shaft release. DIR (displacement from instantaneous response) analysis does not include DSR data and begins when a second rapid change in displacement is identified.

A limitation to using the DSR analysis method is that it will overestimate the deformation of the tissue as it will take into account the displacement from the shaft starting point to the point of contact with the tissue. However, in an attempt to reduce the error within this study, the indenter or plate was placed as close to the tissue surface as possible, without making contacting.

Overall, when analysing the DSR compression test data, high deformations meant that it was not possible to determine the mechanical properties of the tissues; including the elastic modulus and permeability, using a computational and analytical model. As mentioned previously, in order to determine these properties minimal deformation is assumed, as large deformations compress the pores in the tissue matrix which affects the permeability of the tissue. Therefore only DIR analysis of cartilage tissue (human and porcine) was possible using the computational and analytical model. Labral tissue analysed under DIR was disregarded as this was not an accurate measure of the tissues response to compressive load.

4.3.5.1 Calculation of equilibrium modulus from time-displacement data

The equilibrium modulus was determined from the time-displacement data and the initial stress applied to the tissue. Stress (σ) was calculated as the force divided by the original cross-sectional area. Strain (ε) was calculated as the deformation divided by the original sample thickness. Equilibrium modulus was calculated as the stress divided by the strain.

4.3.5.2 Biphasic poroelastic computational model

Cartilage deformation curves generated from low load unconfined compression tests along with tissue thickness measurements (section 4.3.4.2) were used to derive the equilibrium aggregate modulus and permeability of porcine and human articular cartilage using a computational and analytical model (Figure 4-6). The axisymmetric biphasic poroelastic finite element model (ABAQUS, version 6.9-1 Dassault Systems, Suresnes Cedex, France) used in this study was provided by Dr Abdellatif Abdelgaied in iMBE, University of Leeds (Abdelgaied et al. 2015). Cartilage was modelled as a poroelastic material and meshed using four-node bilinear displacement and pore pressure axisymmetric elements (CAX4P). Bone was meshed using four-node bilinear elastic axisymmetric elements (CAX4). Tissue properties were assigned to the model; a Poisson's ratio of 0 was used for cartilage and bone to maximise the biphasic effect (Jin et al. 2000), cartilage water content was determined from section 3.6.2 and an elastic modulus of 17 GPa was used for bone.

In the computational model the load was increased from 0 - 0.11 N over a 2 s period and applied for 1800s to match the experimental model. The model produced a time-displacement graph derived by the elastic modulus and permeability, which were incrementally changed, to match the experimental results (Figure 4-7). The material properties that provided the highest R^2 value

were taken as the material properties of the specific tissue. The closeness of fit of the two graphs was analysed using MATLAB (version 7.4, MathWorks Inc, Boston, USA) and a R^2 value of 0.6 or higher was accepted as significant for biological tissue.

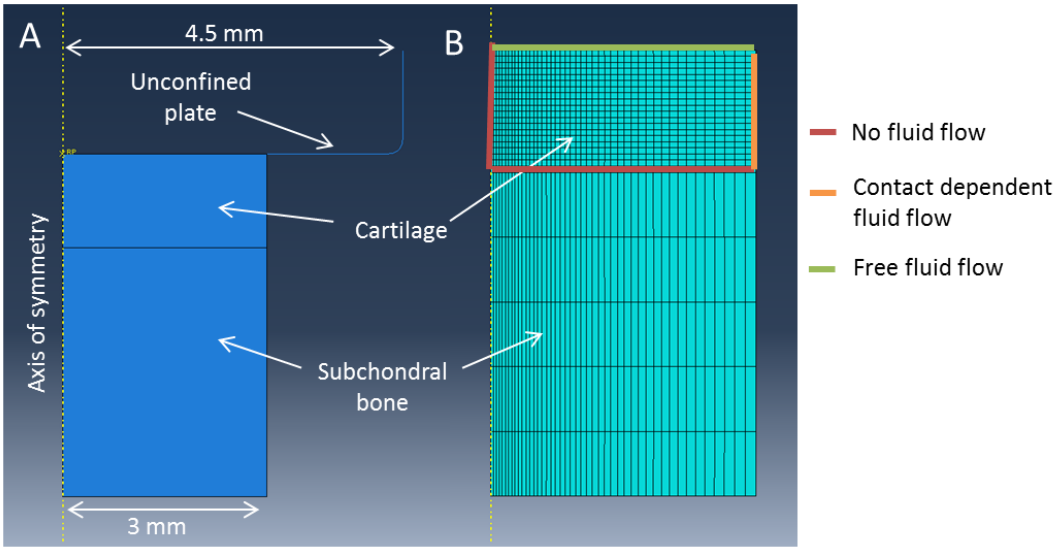

Figure 4-6 Finite element analysis model of a osteochondral pin. A – shows the axis of symmetry and the load application. B – shows the boundary conditions to impose fluid flow within the model.

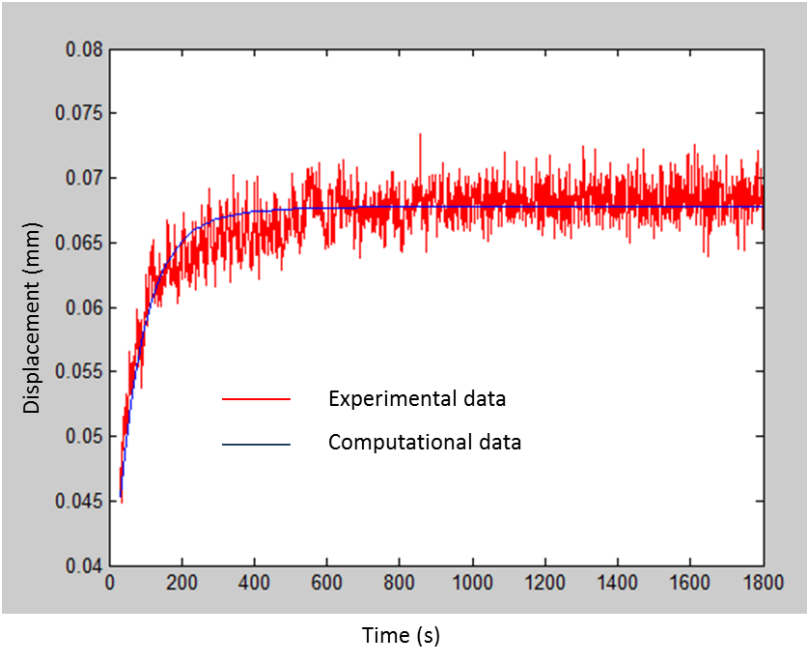

Figure 4-7 Experimental and computational time displacement curves. The elastic modulus and permeability were altered until the computational model matched the experimental model to the best fit possible.

4.3.6 Indentation rig calibration

Before each set of tests, the indentation rig was calibrated to convert voltage outputs of the LVDT into millimetres. The voltage was recorded for a range of heights, from 0 to 2.5 mm, using slip gauges. Slip gauge height was increased sequentially and the voltage output recorded, the slip gauge height was the decreased sequentially and the average of the two readings taken for each height. A linear trend line was determined from the displacement-height graph (Figure 4-8) and the equation was used to calibrate the test results.

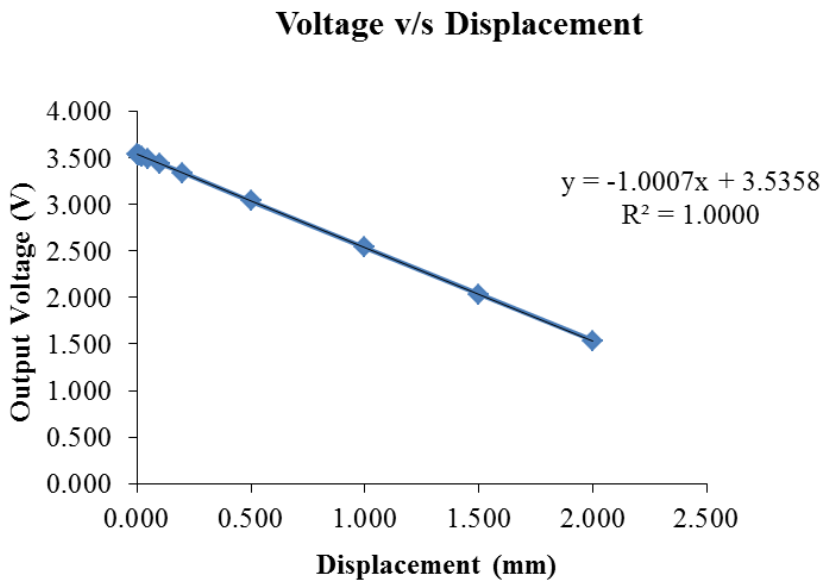

Figure 4-8 Displacement calibration. An example of a calibration graph for the LVDT to convert voltage to displacement.

4.4 Tensile biomechanical materials and methods

Tensile properties of labral tissue were determined using an Instron uniaxial testing machine and a 500 N load cell (± 0.25%, calibrated annually by Denison Mayers Group, Figure 4-9). Specimens were stretched until failure at a constant rate of 0.6 mm/min with a gauge length of 10 mm (strain rate of 0.001^{-1} s). Specimens were pre-loaded with a 0.1 N load and allowed to stress-relax for two minutes to precondition the tissue and align the collagen fibres.

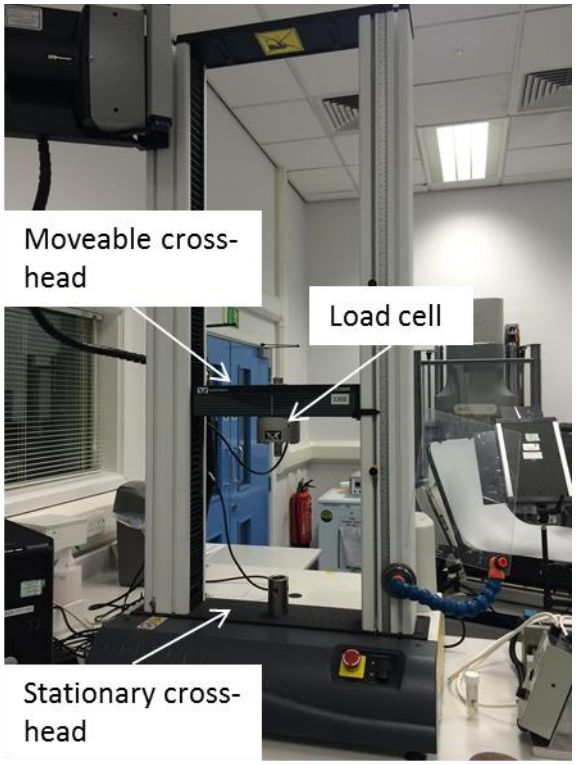

Figure 4-9 Instron testing machine. Instron testing frame with a moveable and fixed cross-head and mounted load cell.

Prior to testing, specimens were prepared as discussed in Section 2.3.6. Specimen dimensions were measured three times, using callipers (accuracy ±0.005mm), and the average taken. The specimen was then clamped in an in house built tissue holder (Figure 4-10 A & C). The tissue holder comprised two base clamps attached to a brace and two top clamps to fix the specimen in place (Figure 4-10 B). The tissue holder was then attached to the testing machine via two clamp holders, attached to a fixed cross-head at the bottom of the machine and a moveable cross-head at the top (Figure 4-10 D). Tissue hydration was maintained throughout the test using a PBS spray and slippage was monitored after testing using the grove imprints of the clamp on the tissue.

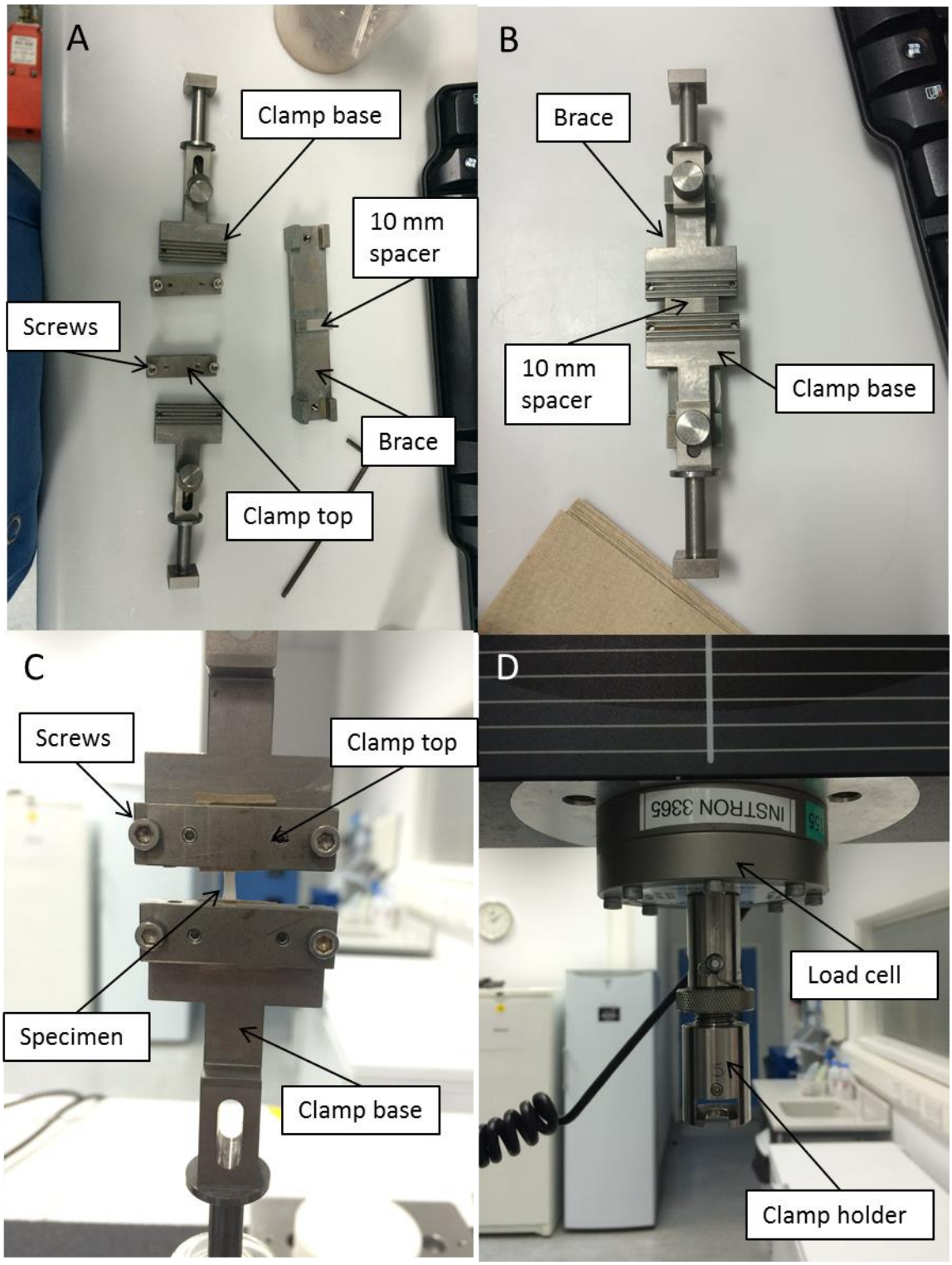

Figure 4-10 Tensile specimen set up for labral tissue. A – Deconstructed clamp set up. B – Constructed clamp set up. C – Clamp with specimen. D – Clamp holder attached to the load cell on top cross-head.

Force (N), extension (mm) and time (s) data was recorded at a sampling rate of 10 Hz, using inbuilt software and converted into engineering stress (σ_{eng}) and engineering strain (ε_{eng}), normalised to the initial specimen dimensions. Stress was calculated as the force divided by the original cross-sectional area (width x thickness) and strain was calculated as the cross-head displacement divided by the sample gauge length.

Data was analysed for each specimen by fitting the Gaussian function to the stress-strain curve from the zero to failure point, using non-linear least squares regression with a Matlab script. The script was provided by Dr Anthony Herbert in iMBE, University of Leeds and detailed in Herbert et al., 2016. The following parameters were used for the bi-linear model;

$$\sigma = E_0.\varepsilon \quad \text{for } \varepsilon \leq \varepsilon_* \quad \text{and} \quad \sigma = E_1.\varepsilon + c \quad \text{for } \varepsilon > \varepsilon_*$$

where E_0 is the moduli of the toe region, E_1 is the moduli of the linear region and ε^* is the strain at which the two linear regions intersect, c is a constant to be determined. An R^2 value of 0.99 or higher was accepted for the curve fitting model. The model iteratively optimised the transition point (ε^*,σ^*). For each tissue the initial Young's modulus, equilibrium Young's modulus, transition stress, transition strain, stress at failure, and strain at failure were calculated (Figure 4-11).

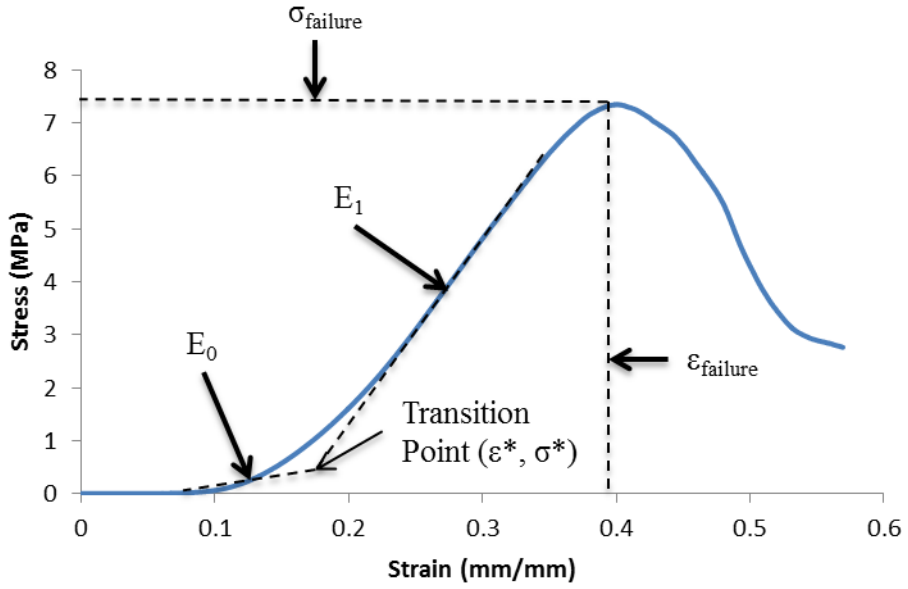

Figure 4-11 Typical stress-strain curve for labral tissue. Load and extension data was converted into stress and strain and the data plotted. From the stress-strain graphs labral mechanical properties were determined. The graph shows a stress-strain graph from a porcine labrum specimen.

During preliminary testing, using porcine tissue, the majority of samples slipped or were cut by the grips; therefore various methods were investigated to determine the optimal method to secure the specimen in the clamps. Two different grip sizes were investigated; a narrow grip, with one screw to hold the tissue in place, and a wide grip, with a screw either side of the tissue, to evenly distribute the pressure (Figure 4-12 A & B. respectively). Various gripping materials were also analysed including; surgical suturing, superglue glue, sandpaper and paper towel, as well as a range of specimen dimensions (2 x 1 mm, 2 x 2 mm, 3 x 1 mm, 3 x 2 mm, 3 x 3 mm) and shape (dumbbell and rectangle, Figure 4-12 C). Surgical sutures were tied in a knot around the ends of the specimen and bottom clamp, sand paper and paper towels were folded around each end of the specimens (Figure 4-12 D) and specimens were adhered to sandpaper using superglue.

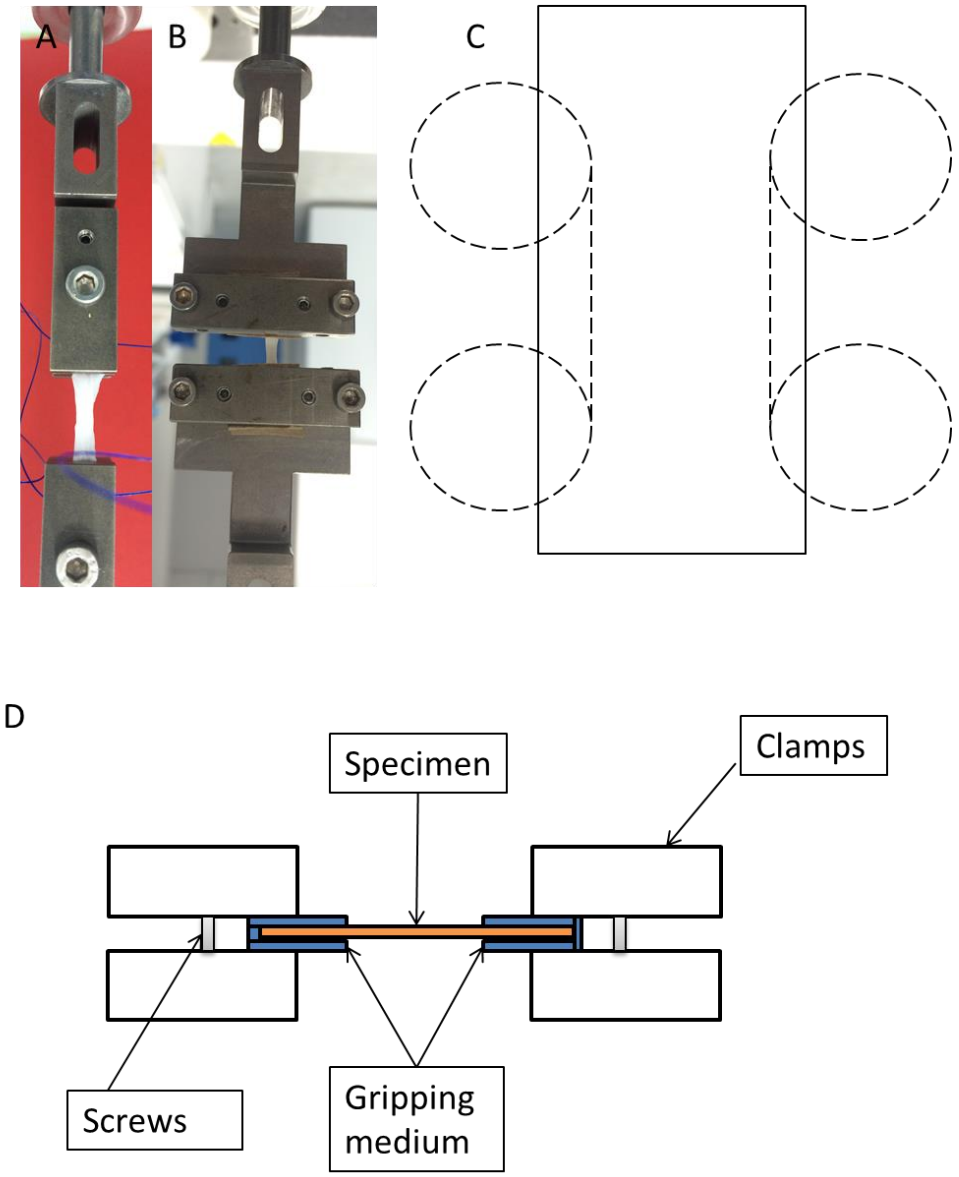

Figure 4-12 Tensile testing gripping methods and specimen shaping. A – narrow grip set up. B – wide grip set up. C – Dumbbell shaping. D – Gripping medium for various materials.

4.5 Results

4.5.1 Compressive results

4.5.1.1 Compressive specimen dimensions

Porcine and human labrum and cartilage tissue thickness was measured in order to normalise the deformation data. The mean thickness of each tissue type can be seen in Table 4-2. Human cartilage was significantly thicker than porcine cartilage, however no significant difference was identified between labral tissue ($p<0.05$ two-way ANOVA).

Table 4-2 Specimen thickness for tissue used in creep testing. Labral and cartilage thickness for porcine and human tissue.

	Human (mm)		Porcine (mm)	
	Labrum	Cartilage	Labrum	Cartilage
Mean	3.4	1.9	3.1	1.3
95% CL	0.8	0.3	0.2	0.6

4.5.1.2 Creep and percentage deformation for all compression test types

Creep and strain properties of labral tissue were determined under four conditions; indentation high load, indentation low load, unconfined high load, and unconfined low load. Data was analysed using two methods; DSR and DIR. The mean time-displacement curves for porcine labrum are shown in Figure 4-13 and the strain results are shown in Figure 4-14.

Data analysed with DSR resulted in overall higher deformations than data analysed from DIR, with all strain values above 50 %. Data analysed from DIR resulted in much lower deformations with the highest strain of 28 % for high load indentation and the lowest value of 17 % for low load unconfined deformation.

Results for both DIR and DSR showed unconfined compression to result in lower creep and strain in labral tissue than indentation. DSR analysis showed low load unconfined compression to produce lower deformation than the high load set up. Therefore future experiments within this study were continued with low load unconfined compression. As the results did not allow the impact point to be identified for labral tissue, DIR analysis for labral tissue was not analysed when comparing human and cartilage data in future studies.

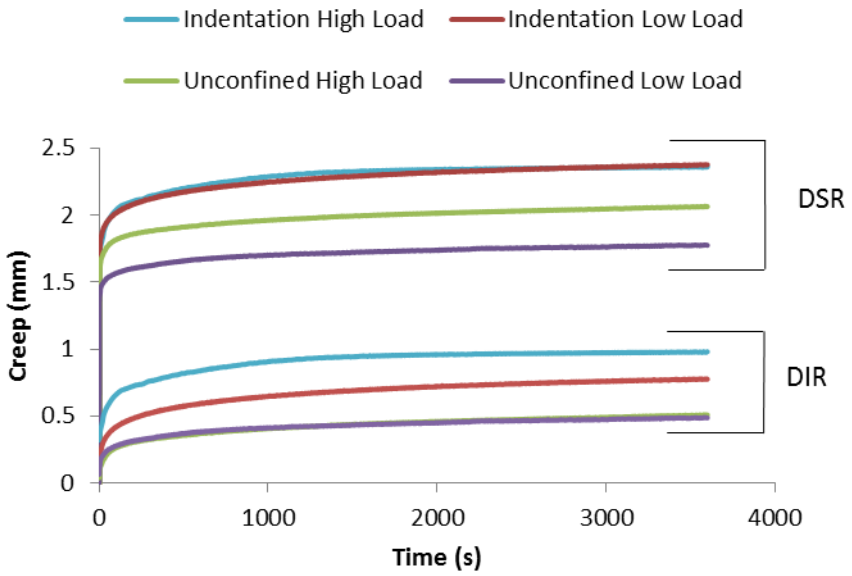

Figure 4-13 Time-displacement curves for labral tissue under four conditions. Mean average time-displacement curves for indentation high load, indentation low load, unconfined high load, and unconfined low load (n=6).

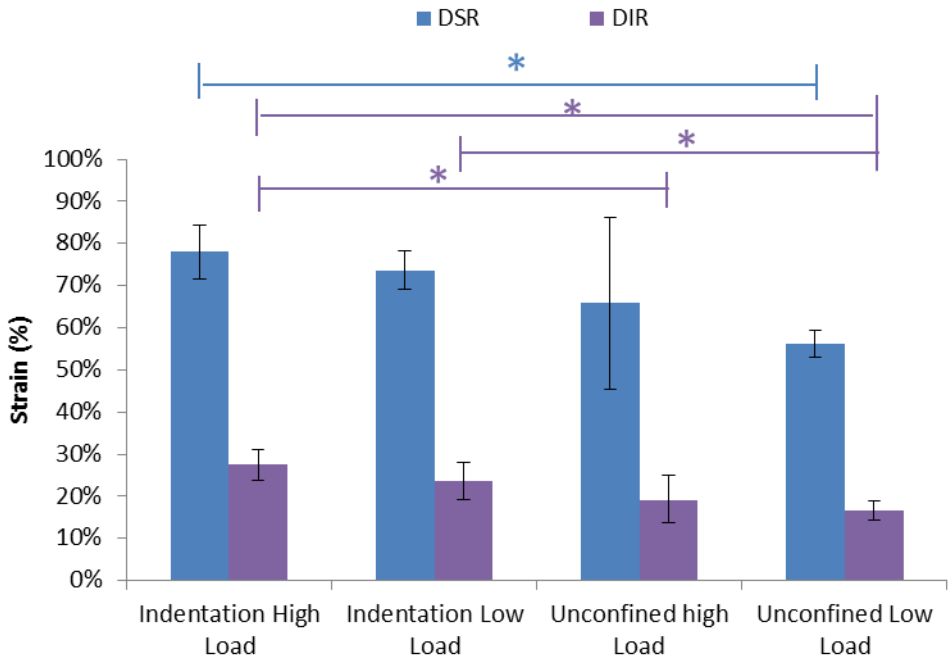

Figure 4-14 Labral strain under four test conditions. Strain for indentation high load, indentation low load, unconfined high load, and unconfined low load. Data is the mean ± 95 % CL (n=6). Data was analysed by two-way ANOVA and individual means compared by a Tukey test. * indicates $p<0.05$.

4.5.1.3 Compressive properties of porcine and human labral and cartilage tissue

Creep and strain results for unconfined low load test conditions showed significant differences between cartilage and labral tissue, in both porcine and human species. Labral tissue took longer to reach equilibrium compared to cartilage tissue (approximately 3600 s and 1800 s respectively, Figure 4-15). Deformation results for porcine and human cartilage showed the tissue to have an average strain of 7 % (DIR), where as porcine and human cartilage analysed under DSR artificially increased the strain to 47 %. Porcine and human labral tissue had an average strain of 50% when analysed under DSR (Figure 4-16). Overall a trend could be identified with higher levels of strain in porcine tissue than human tissue in all three groups, however the differences were not found to be significant (P>0.05 two-way ANOVA).

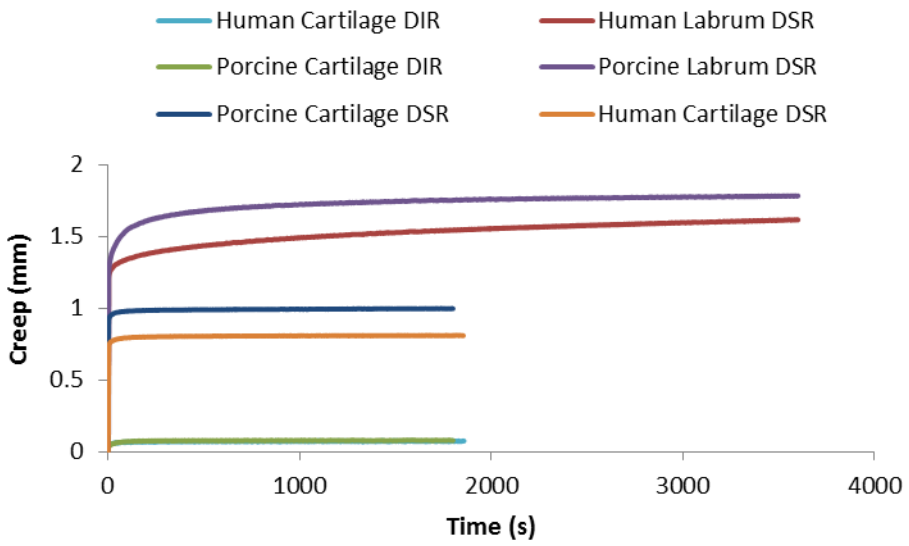

Figure 4-15 Compression testing of porcine and human labrum and cartilage. Time-displacement data of porcine and human labrum in comparison to cartilage. Cartilage tissue analysed from DIR and DSR results and labral tissue analysed from DSR results (n=6 porcine labrum and porcine and human cartilage, n=5 human labrum).

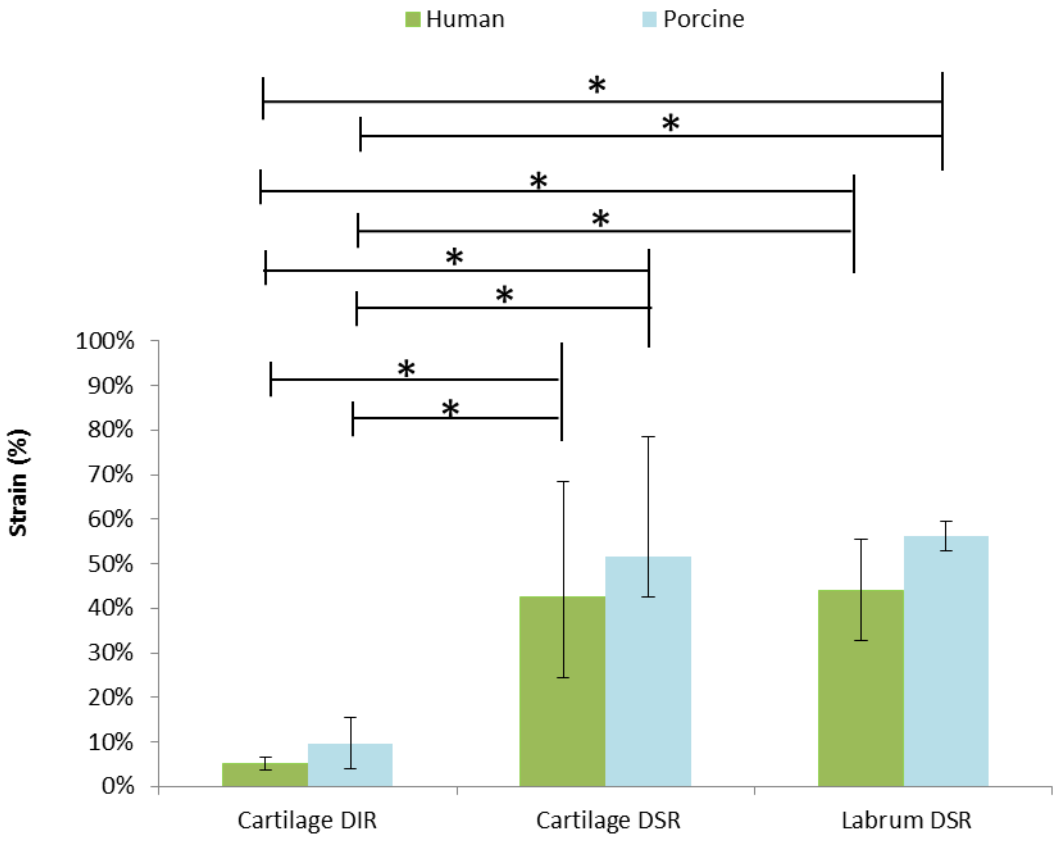

Figure 4-16 Deformation percentage of porcine and human cartilage and labral tissue. Cartilage tissue analysed from DIR and DSR results and labral tissue analysed from DSR results. Data is the mean ± 95 % CL (n=6 porcine labrum and porcine and human cartilage, n=5 human labrum). Data was analysed by two-way ANOVA and individual means compared by a Tukey test. * indicates $p<0.05$.

4.5.1.4 Determination of mechanical properties of porcine and human labrum and cartilage from time-displacement data

The equilibrium modulus of porcine and human cartilage and labrum were determined under DSR and DIR analysis for a compressive stress of 0.006 MPa from the time-displacement data (Table 4-3). DSR analysis produced higher values of equilibrium modulus than DIR analysis for all tissue types except for porcine cartilage. A trend was seen with cartilage tissue having a higher equilibrium modulus than labral tissue, except for porcine cartilage and labrum analysed under DSR where the equilibrium modulus was similar for both tissues.

Table 4-3 Equilibrium Young's modulus determined from time-displacement data. Data is shown at the mean ± 95 % CL. HC – Human Cartilage, HL – Human Labrum, PC – Porcine Cartilage, PL – Porcine Labrum

	Mean	95 % CL
HC DSR	0.0043	0.0009
HC DIR	0.0033	0.0006
HL DSR	0.0021	0.0005
HL DIR	0.0019	0.0005
PC DSR	0.0021	0.0102
PC DIR	0.0058	0.0022
PL DSR	0.0023	0.0002
PL DIR	0.0020	0.0001

4.5.1.5 Determination of material properties of porcine and human articular cartilage from the computational model

The material properties of porcine and human cartilage under DIR analysis were determined using the computational and analytical model. An R^2 value of 0.6 or higher was accepted. Of the remaining samples (porcine cartilage n=1 and human cartilage n=4) the equilibrium aggregate modulus and permeability were determined (Table 4-4). Porcine and human cartilage had similar equilibrium aggregate moduli of 0.12 MPa and 0.13 MPa respectively where as human cartilage had a higher permeability than porcine cartilage. The experimental results produced a large amount of noise deformation during the test (Figure 4-17).

Table 4-4 Material properties of porcine and human cartilage (DIR) determined from the computational model. Data presented as the mean ±95 % CL.

	Aggregate modulus (MPa)	95 % CL	Permeability (m^4/N s)	95 % CL	R^2
Porcine Cartilage	0.120	-	1.205E-15	-	0.66
Human Cartilage	0.127	0.053	2.134E-13	1.487E-13	0.8

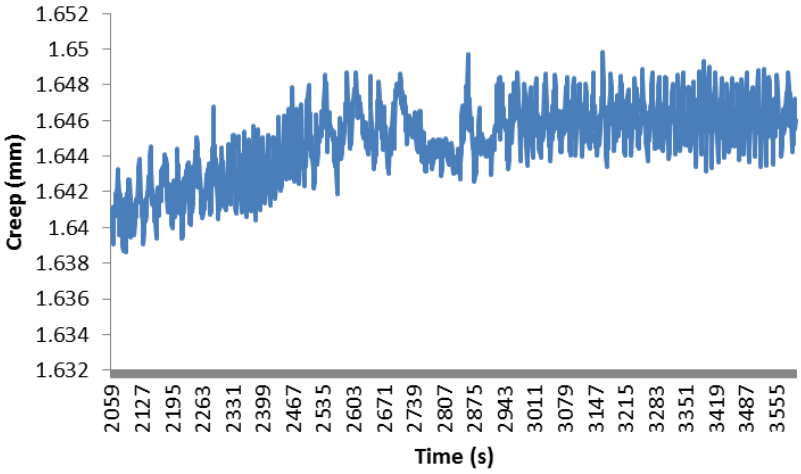

Figure 4-17 Human cartilage time-displacement graph. An example end region of a time-displacement graph of human cartilage showing the noise deformation.

4.5.2 Tensile results

4.5.2.1 Findings of pre-tests

A pilot study was carried out to determine the best test set up for securing specimens within the grips and the dimensions of the specimens, using approximately 100 samples (data not presented). Wide grips were found to be the most successful for tensile testing as the majority of specimens slipped during testing using narrow grips. Dumbbell shaping of the specimen was investigated but was unsuccessful due to the small size of the specimen. Repeats of sample cutting were inaccurate and the dumbbell shape was either uneven or off-center. Specimens wrapped in paper towel were found to be the most effective, with the least number of samples slipping, compared to superglue, sand paper and suturing. Specimens shaped to 3 mm were also found to be difficult to cut as it was nearing the maximum dimension of the specimen; therefore producing inaccuracies. Specimens shaped to 2 mm were found to be optimal for cutting and specimens cut to 2 x 2 mm in cross sectional area were found to perform better during testing than specimens cut to 2 x 1 mm due to the smaller samples slipping in the grips. Therefore rectangle specimens, 2 x 2 mm, in wide grips were used to determine the tissues mechanical properties during tensile testing. Results from any specimens showing evidence of slipping were rejected.

4.5.2.2 Tensile specimen dimensions

Tensile specimen width and thickness data is presented in Table 4-5. Labral samples were cut with parallel blades with a 2 mm spacer to produce samples 2 x 2 mm. Upon measuring the sample dimensions porcine labral samples were 2.5 x 2.5 mm and human samples were 1.5 x 1mm. Sample dimensions were normalised to stress-strain data and all samples were large enough to include whole collagen fibrils, therefore these dimensions were acceptable for tensile testing.

Table 4-5 Tensile specimen dimensions. Porcine and human labral specimen dimensions.

	Human (mm)		Porcine (mm)	
	Width	Thickness	Width	Thickness
Mean	1.7	1.0	2.4	2.5
95% CL	0.1	0.2	0.2	0.2

4.5.2.3 Tensile mechanical properties

The material properties of porcine and human tissue were in investigated under uniaxial tension to determine the tissues initial and equilibrium Young's modulus, transition stress and strain, and stress and strain at failure. Following tensile testing until failure, all specimens showed similar stress-strain behaviour, as seen in Figure 4-18. Three clear regions were identified within the stress-strain graphs; an initial non-linear toe-region, a linear region, and failure point. During tensile testing of human specimens, one specimen was identified as damaged from decalcification and one sample slipped in the grips and were therefore discarded from the study (original count n=6). The tensile properties for porcine and human labral tissue and their failure method can be seen in Table 4-6. The main failure mechanism observed for labral tissue was tearing at the grip interface with the tissue.

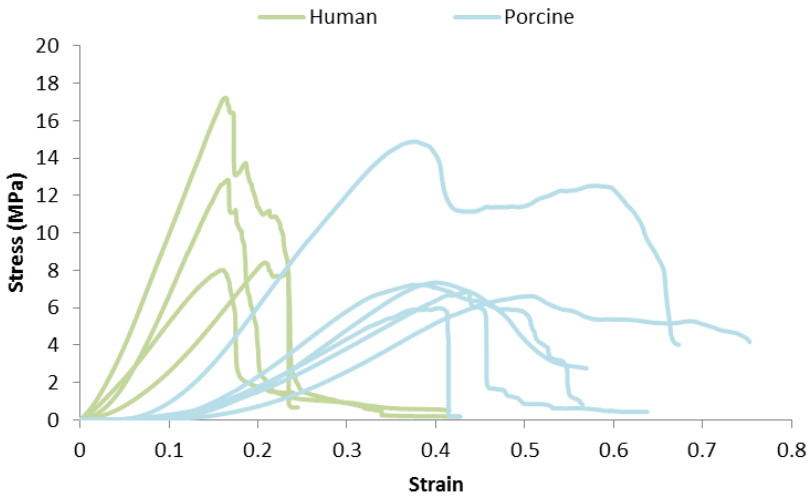

Figure 4-18 Tensile stress-strain graphs. Tensile stress-strain graphs for all human and porcine samples when tested at 0.6mm/min (n=6).

Table 4-6 Tensile properties of porcine and human labrum. Tensile properties include the initial Young's modulus (E_0), equilibrium Young's modulus (E_1), transition stress (σ^*) and strain (ε^*), and the stress (UTS) and strain ($\varepsilon_{failure}$) at failure. * indicates significant difference between porcine and human tissue.

Species	Specimen	E0 (MPa)	E1 (MPa)	σ* (MPa)	ε* (%)	UTS (MPa)	$\varepsilon_{failure}$ (%)	Failure Location
Porcine	1	1.8	32.6	22.9	13	7.2	37.3	grips
	2	2.1	31.3	33.7	16	7.4	40.0	grips
	3	1.8	23.3	36.8	20	6.6	50.7	grips
	4	3.8	24.0	63.2	16	6.9	43.7	middle
	5	5.5	58.8	58.1	11	14.9	37.8	grips
	6	2.4	23.8	32.5	14	6.0	40.3	grips
	Mean	2.9*	32.3*	41.3*	15*	8.2	41.6*	
	95% CL	1.6	14.3	16.6	4	3.5	5.3	

Species	Specimen	E0 (MPa)	E1 (MPa)	σ* (MPa)	ε* (%)	UTS (MPa)	εfailure (%)	Failure Location
Human	1	66.9	120.3	267.5	4	17.2	16.3	grips
	2	30.2	102.3	151.1	5	12.8	16.6	middle
	3	40.5	59.5	161.8	4	8.0	16.0	grips
	4	17.6	54.4	140.4	8	8.4	20.8	grips
	Mean	38.8*	84.1*	180.2*	5*	11.6	17.4*	
	95% CL	33.3	51.4	93.7	3	6.9	3.6	

During tensile testing, human tissue withstood higher stresses than porcine tissue for all parameters calculated (initial and equilibrium Young's modulus, transition stress and ultimate tensile stress (UTS)) and lower strains (transition strain and strain at failure). All stresses and strains were significantly different between the two tissue types except for UTS which was similar for the two tissues (11.6 MPa for human tissue and 8.2 MPa for porcine tissue). Human tissue had an equilibrium Young's modulus approximately 2.5 fold higher than porcine tissue (84.1 MPa compared to 32.3 MPa), however the strain at failure was almost three fold lower than porcine tissue with strains of 5 % and 14 %.

4.6 Discussion

In this chapter the mechanical properties of the labrum were investigated under compressive and tensile forces for both human and porcine tissue. Compressive properties were determined from the time-displacement response and deformation of the labrum in comparison to cartilage. Tensile testing determined the labrum's Young's modulus as well as transition and failure properties.

Low load unconfined compression testing of porcine labral tissue produced the least amount of creep compared to indentation testing and high load unconfined compression. Labral tissue was extremely soft in compression and even under low load unconfined compression produced deformations of 56 % for DSR analysis and 17 % for DIR analysis. During compression, a tissues deformation is a result of the fluid flow from the tissue. The matrix of a tissue, including its permeability and its GAG content, governs fluid flow. As the matrix becomes compressed the pore sizes within the tissue decrease trapping fluid within the tissue. GAGs are also responsible for holding water within the matrix due to their opposite charge to water. When an instantaneous load is applied to a tissue, initially, fluid is rapidly squeezed from the tissue. Once a large volume of fluid has escaped from the tissue, the rate of fluid flow decreases until equilibrium is reached, when fluid flow ceases (Oatis & Mansour 2009). Under compressive load, cartilage tissue reached equilibrium faster than labral tissue suggesting that the labrum has a lower permeability than cartilage as the fluid took longer to flow out of the matrix. Cartilage tissue took on average approximately 1800s to reach equilibrium compared to 3600s for labral tissue.

During compression testing a limitation was identified as a result of the soft nature of labral tissue. The analysis of the test relied on identification of the moment the tip/plate came into contact with the tissue surface. However, for labral tissue it was not possible to identify this point and therefore two analysis methods were used. DSR analysis was thought to be more accurate than DIR for labral tissue, as the plate starting position was as close to the tissue surface as possible. Although DSR values included movement of the shaft without labral deformation and therefore over estimated the deformation, this analysis method resulted in lower systematic error in comparison to DIR analysis. DIR analysis was most accurate for cartilage tissue as it was possible to identify the moment of impact on the tissue. Hence, DSR analysis of cartilage was included in the results in order to make comparisons between the two tissues. DSR analysis produced deformations approximately two to three times higher than DIR analysis for labral tissue and up to ten times higher for cartilage tissue.

Oatis & Mansour, (2009) found the Young's modulus of cartilage to be in the range of 0.5 to 0.8 MPa and Ferguson et al., (2001) found the bovine labrum to have a compressive modulus of 0.2 MPa. Oatis & Mansour, (2009) found that tissues with a higher aggregate modulus, a measure

of stiffness, deformed less. Therefore it was hypothesised that labrum would undergo a higher deformation than cartilage tissue within this study, however the DSR results for cartilage and labrum showed similar deformations for both tissues. This was likely a result of the systematic error mentioned previously and the size of the tissue. Due to the small nature of the tissue any slight error in placing the indenter/plate close to the tissue surface produced significant deformation errors.

High deformation using DSR analysis meant that it was not possible to determine the tissue's material properties using the computational and analytical model and labral DIR results were not accurate; therefore, only the material properties of human and porcine cartilage were analysed under DIR using this method. Following analysis using the computational method it was identified that the R^2 value was particularly low in a large number of samples. Upon investigation a large range of noise was identified from the time-displacement data in comparison to deformation and this was a result of the low loads chosen to compare to labral tissue. Under this load cartilage tissue did not provide a sufficient amount of deformation to gain a true understanding of the tissues response to compressive loads. Therefore, further work would be required in order to determine the material properties of the labrum in comparison to cartilage tissue using this experimental set up. Optimisation of the method to get the plate closer to the tissue at the start of the experiment would make the test more accurate or a measure of the distance between the plate and the tissue surface would allow an accurate deformation to be calculated. Although the study did not provide definitive material properties it still provided and insight into the general responses of the tissues under compressive load.

Any slight differences between species could also be a result of the age of the human tissue, as degenerative changes seen in the macroscopic analysis of human tissue in Chapter 3, are associated with increased stiffness and therefore reduced deformation, as reported by Bank et al. (1998) and Verzijl et al. (2002). Although an overall trend could be seen between porcine and human tissue, the compressive properties for both labrum and cartilage tissue were very similar between species, therefore porcine tissue would be suitable to use for *in vitro* simulation of the natural hip, in terms of its compressive properties.

A further limitation to this study when comparing labral and cartilage tissue was the use of osteochondral pins. Cartilage tissue was attached to bone; hence to mimic these boundary conditions and constrain the expansion of the labrum at the base, the tissue was superglued to the specimen holder. Although this limited the fluid flow from the base of the labrum, fluid flow was possible across the cartilage-bone interface.

Preliminary tensile testing of labral tissue found specimens of target cross-section 2 x 2 mm, wrapped in paper towel, between wide grips produced the least amount of slippage in test specimens (data not presented). However, although consistent between samples, desired sample

sizes were not accurate with actual sample sizes and future work should look at more reliable methods for cutting samples. During testing, the majority of specimens failed at the grips rather than at the centre. Although some studies (Ferguson et al. 2001; Abdelgaied et al. 2015) reject samples which fail at the grips, a study by Ng, Chou, & Krishna, 2005 found that failing at the grips as opposed to the centre did not have an effect on the material properties of the tissue. As well as the study by Ng et al., 2005, within the present study, specimens that failed in the middle produced stress and strain values within the range of specimens that failed at the grips. Stress-strain data will not be affected by failure location; however future work should confirm that failure location does not affect the UTS for labral tissue. Prior to testing, tensile specimens were preconditioned to align the sample (Proctor et al. 1989; Smith et al. 2008).

Porcine and human labral samples produced similar stress-strain curves, with a clear toe-region, linear region and failure point. The non-linear toe-region of the stress-strain curve is formed by collagen fibres un-crimping (Miller et al. 2012), which provided a much lower Young's modulus compared to the linear region where collagen fibres were being stretched. The difference between the toe-region and linear region was ten fold greater in porcine labrum compared to only two fold in human with the transition point occurring at approximately 15% strain for porcine labrum but only 5 % strain for human labrum. Human labrum was stiffer than porcine labrum and had UTS of 11.6 MPa compared to 8.2 MPa meaning it can withstand higher forces without failing compared to porcine labrum, which undergoes higher deformation under lower loads. Within the present study human labral tensile properties fell within the range found by Ishiko, Naito, & Moriyama, (2005) for human labrum for equilibrium Young's modulus and UTS but were lower in terms of strain at failure. The human tensile properties were also similar to those reported by Ferguson et al., (2001) for bovine labrum. Porcine tissue had a lower Young's modulus than the bovine and human labrum, a similar UTS and a strain at failure similar to the human labrum of Ishiko et al., (2005). These differences seen between the species could be due to variations in the collagen fibre alignment as discussed in Chapter 3.

Collagen fibres within the labrum are predominantly orientated in the circumferential direction, orientated along the direction of greatest load; hence the labrum functions by resistance to forces around the circumference of the acetabulum. As the labrum has been found to have low stiffness under compression and higher stiffness under tension its function is to resist stretching and may aid in supporting the hip joint by securing the femoral head within the acetabulum, minimising the risk of dislocation. Studies by Ferguson et al. (2001) and Petersen et al. (2003) also found the labrum to provide a sealing function against the femoral head aiding in load support by minimising fluid flow as well as stabilising the hip by creating a deeper socket. Opposed to the labrum, cartilage tissue is stiffer in compression which allows it to function by supporting load. As the labrum is stiffer in tension it is most likely that damage occurs whist the tissue is in compression, in instances such as impingement, where the labrum becomes

compressed by a bony extension of the hip joint. When looking at creating labral damage in *in vitro* simulation of the hip, compression of the labrum should be induced to cause damage to the tissue. Although bovine tissue would be a more suitable match to human tissue based on its tensile properties, the hip joints are too large for use in *in vitro* simulation using a single station hip simulator. Porcine tissue shows some differences to human tissue and these will need to be taken into consideration when looking at damage methods as lower forces maybe required, however the main damage mechanism occurs during compression where there is little difference between porcine and human tissue.

Key findings:

- Low load unconfined compression produced the lowest deformation in porcine labral tissue.
- Cartilage tissue reached equilibrium faster than labral tissue which would suggest the labrum has a lower permeability than cartilage tissue.
- Labral tissue deformed more than cartilage tissue which would suggest the labrum has a lower aggregate modulus compared to cartilage tissue.
- Porcine and human tissue were found to have similar compressive properties
- Labral tissue had a similar stress-strain to other soft tissues including a toe-region, linear-region and failure point.
- The human tissue transitioned from the toe-region to the linear-region at a lower strain than porcine tissue suggesting the collagen in the human labrum is less crimped.
- The human labrum was stiffer than the porcine labrum, with a higher Young's modulus.
- The labrum was found to be weaker in compression than tension, therefore making it more susceptible to damage under compressive forces.

Chapter 5

In vitro simulation of the natural hip joint

5.1 Introduction

Due to increased knowledge of the acetabular labrum's function, research into labral treatment has increased, specifically into procedures that aim to preserve and fix the tissue rather than remove it. Therefore, the properties and function of the labrum has become an area of interest. Previous studies that have investigated the properties and functions of the labrum have provided important advances in the knowledge of the tissue however, all previous *in vitro* studies have largely simplified *in vivo* test conditions (Ferguson et al. 2003; Safran et al. 2011; Smith et al. 2011; Cadet et al. 2012; Song et al. 2012; Philippon et al. 2014). Previous studies were carried out over short periods of time, with reduced motion and/or load, which may result in severe limitations with regards to clinically relevant conclusions. When investigating the effects of labral damage on the hip joint, the full gait cycle should be considered to gain a full understanding of the effects of labral damage.

During a standard gait cycle, the hip undergoes large ranges of motion as well as a complex loading cycle with two main peaks at heel-strike and toe-off. An ISO (International Organisation for Standardization) standard has been developed to outline the full human gait cycle, which is widely accepted during testing of artificial joints. However, it must be noted that although this standard is an average representation of a gait cycle, it is still simplified from clinical reality. The ISO standard dictates the "relevant angular movement between articulating components, the pattern of the applied force, the speed and duration of the testing, the sample configuration, and the test environment to be used". ISO14242 suggests a standard gait cycle for the hip which dictates the abduction-adduction (AA), flexion-extension (FE), and internal-external rotation (IE) motion with simultaneous axial loading to replicate the simplified motion and loading of the hip during walking (BSI 2014, Figure 5-1).

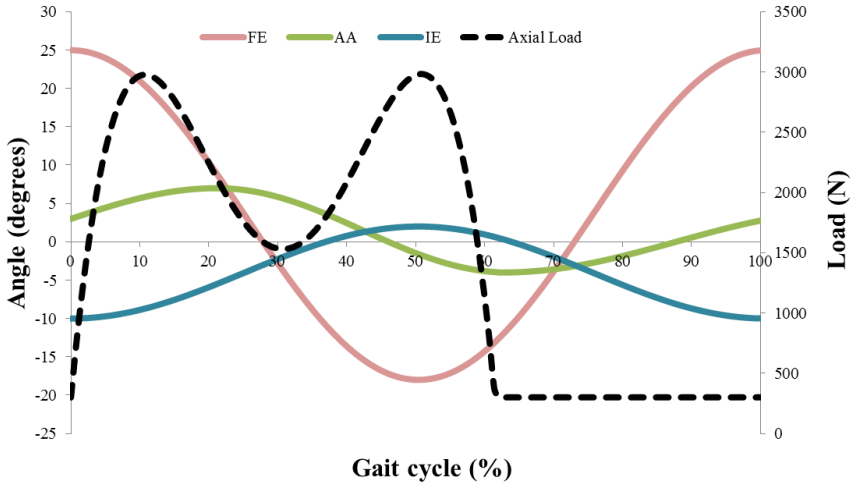

Figure 5-1 ISO standard 14242 hip joint gait cycle. A full gait cycle of the human hip during walking, showing flexion-extension (FE), abduction-adduction (AA), internal-external rotation (IE), and axial load (adapted from BSI 2014).

Hip simulators have been extensively used to assess the wear of total hip replacement components under normal or extreme conditions. The simulators allow the components to be tested over prolonged periods of time using a continuous gait cycle to replicate long term *in vivo* conditions. During testing, new components are run under a standard set of conditions (ISO 14242) to investigate the wear rate and hence likely life span of the prostheses (Saikko et al. 2001; Scholes et al. 2001; Dowson et al. 2004). Studies also exist to investigate the possible causes of damage in hip joint prostheses that have prematurely failed. Extreme conditions such as adverse loading, increased cup angle, and medial-lateral (ML) displacement have been identified as possible causes for hip joint replacement failure, including rim damage (Fisher 2011; Stewart & Hall 2006). An increased cup inclination angle or ML displacement in total hip replacements has been shown to move the position of loading closer to or on to the acetabular rim (Figure 5-2). This can result in an increased load, as a result of non conformity and initiate or accelerate damage (Lizhang et al. 2013; Fisher 2011). It was hypothesised that labral damage could be replicated *in vitro* by adversely loading the natural hip joint during a continuous gait cycle, in a hip simulator. To the author's knowledge, *in vitro* testing of whole natural hip joints have not been conducted under the full gait cycle (ISO 14242) in a hip simulator prior to this study. By developing a natural hip simulation study, the soft tissues in the hip could be assessed in situ or the effects of labral damage on hip joint function could be investigated more accurately. To date the most advanced natural hip joint simulation study was developed by Groves, (2016) however, the study was carried out using a pendulum simulator, limited to one axis of motion and a simplified loading profile.

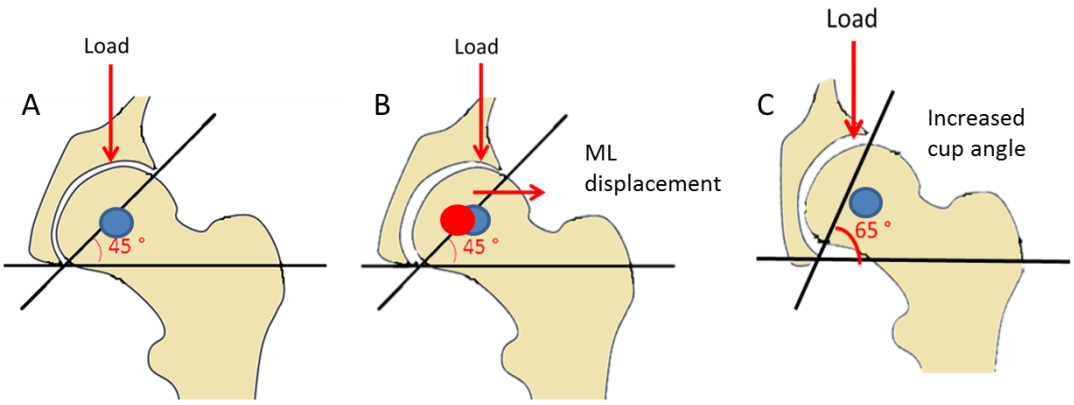

Figure 5-2 Adverse loading conditions in hip joint replacements. A – natural *in vivo* set up. B – ML displacement. C – Increased cup inclination angle. Blue dot – femoral head CoR. Red dot – Acetabular cup CoR. Image adapted from Wikipedia https://en.wikipedia.org/wiki/Hip

Therefore, the aim of this chapter was to develop two novel *in vitro* simulation systems of the natural hip; the first an *in vitro* simulation of the natural hip functioning without damage under a full range of motion and the second, a labral damage model to replicate damage associated with diseases such as FAI and DDH where the labrum becomes damaged, torn and/or separated from the articular cartilage. Both the natural hip joint and labral damage model were to function under normal gait conditions identified by ISO 14242, for FE, IE and AA, with a scaled down load for porcine tissue. Various methods were investigated for developing a labral damage model including; increased cup angle, increased load, and ML displacement to alter the contact position and area and size of the load.

5.2 Aims and objectives

Aims:

The aim of this chapter was to develop an *in vitro* natural hip and labral damage model using a single station hip simulator. The aim of the labral damage model was to replicate labral damage as seen in morphologically abnormal hip joints such as FAI and DDH.

Objectives:

- Develop an *in vitro* simulation of the natural hip using a single station hip simulator to function without damage under normal gait motion.
- Develop an *in vitro* labral damage model of the natural hip using a single station hip simulator under normal gait and abnormal loading conditions.
    - Investigate the effects of increased cup inclination angle on the hip joint
    - Investigate the effect of increased load on the hip joint
    - Investigate the effect of medial lateral displacement of the femoral head on the hip joint

5.3 Overview

To develop an *in vitro* natural hip simulation system, development of specific methods were required as this was the first study to test a natural hip in a hip simulator. The processes involved in the development of a natural hip and labral damage model are outlined in Figure 5-3. The initial stages of this study focused on the methodology to develop a natural hip model which was then advanced to a labral damage model. The first stages included the method development to anatomically align the CoR of the hip to the simulator in order to eliminate external forces on the joint. This was carried out by primarily aligning the CoR of the acetabular cup to the CoR of the simulator, followed by aligning the femoral head to the acetabulum. Prior to testing, the hip joint was disarticulated in order to assess the articulating surfaces for damage, therefore the femoral head required realigning to the acetabular cup. The natural hip model was set up under normal *in vivo* conditions as explained in Section 5.7. The labral damage model was then developed by investigating the effects of increased cup inclination angle, increased load and ML displacement, as described in Section 5.11.2.

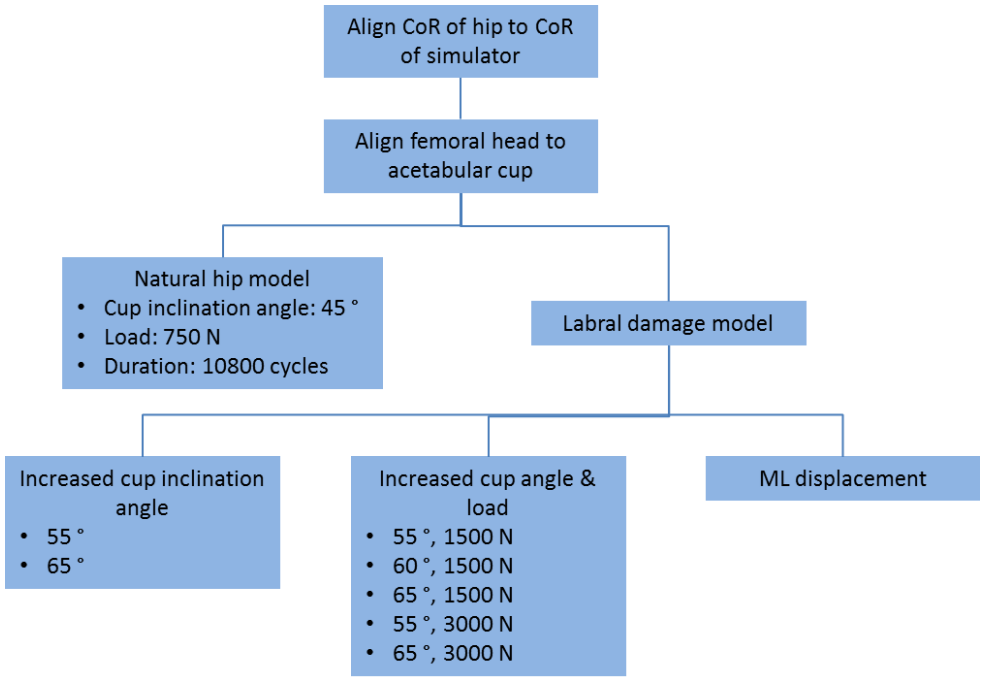

Figure 5-3 Flow chart of the method development for the *in vitro* simulation models. This flow chart shows the process of how the *in vitro* simulation models were developed.

5.4 Simulator overview

To develop an *in vitro* natural hip and labral damage model a single station anatomical hip simulator was used (Figure 5-4 A). The simulator was used to apply an ISO standard (ISO 14242) walking cycle to a whole porcine hip joint (femoral head and acetabulum). The walking cycle was applied using a demand wave cycle and its accuracy was monitored via a feedback wave cycle. The machine was designed specifically to allow the natural hip to be tested in a physiological and anatomical configuration. The simulator's three degrees of motion (FE, AA, and IE) and axial load were driven by electro-mechanical actuators and the simulator was capable of displacement in the ML and AP directions (either free-floating for natural alignment or locked at a set displacement, Figure 5-4 A & B). Motions in the FE, AA, and IE direction were accurate to ± 0.03 °, ML and AP direction to ± 0.2 mm and the axial load was accurate to ± 50 N. The natural hip was secured in the simulator via holders manufactured in-house (Section 5.6) with the acetabular cup mounted below a six-axis load cell and the femoral head to a moveable cradle. The simulator had a working height of 205 mm and was programmable through the ranges of motion described in Table 5-1.

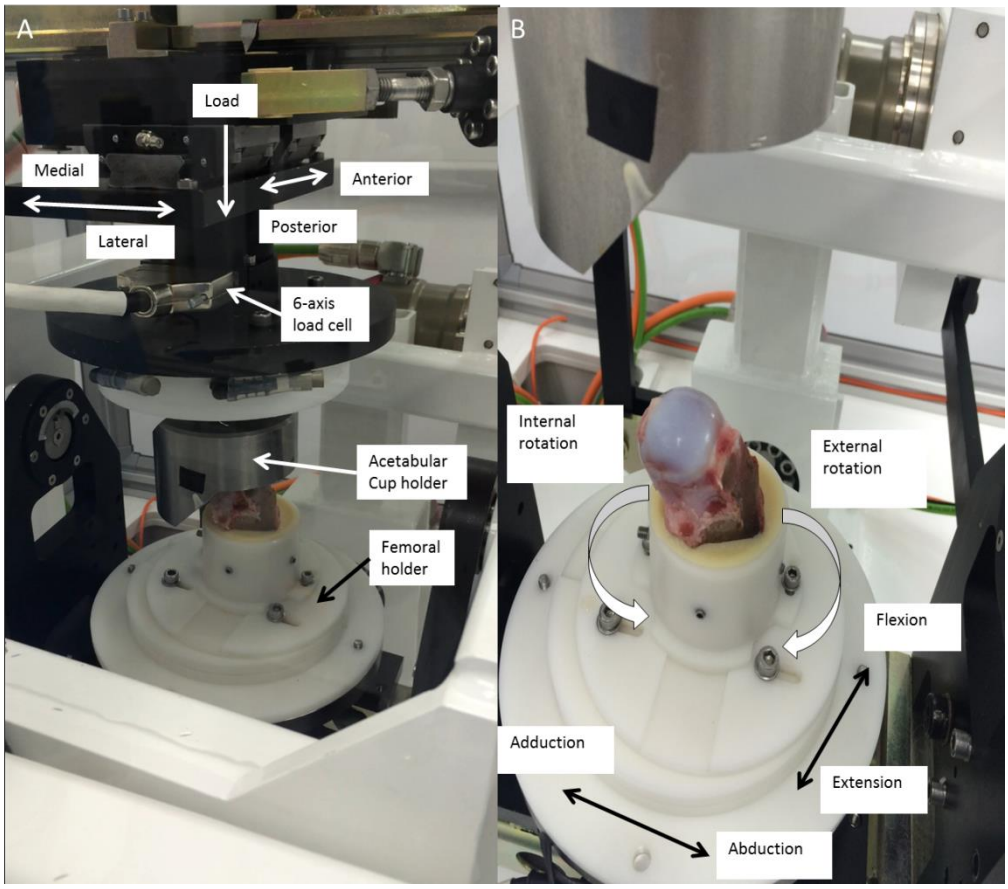

Figure 5-4 Single station hip simulator set up and axes. A – Mounted natural porcine hip (acetabulum & femoral head). B – Simulators three degrees of motion.

Table 5-1 Hip simulator programmable ranges. The table shows the ranges in which the simulator is cable of for each direction of motion or load as well as the location it is driven from.

Load/Motion	Programmable Range	Applied through
Load	4500 N	Cup
Flexion/Extension	± 60 °	Head
Internal/External Rotation	± 25 °	Head
Abduction/Adduction	± 25 °	Head
Medial-Lateral	± 5 mm and ± 1kN	Head
Anterior-Posterior	± 10 mm	Head

5.4.1 Simulator calibration

Prior to specimen testing the simulator was calibrated for load and displacement using an external load cell (calibrated by Denison Mayers Group) and calibrated slip gauges respectively. The six axis load cell was capable of measuring axial, ML and AP loads as well as torques around the FE, IE and AA axes. The simulator was allowed to warm up for 30 minutes prior to calibration to avoid drift in the load cell signal. The axial force, ML, FE and AA load cells were calibrated via the automatic load calibration file provided within the simulator software (Prosim Hip Simulator Application Program). The external load cell was mounted onto the simulator at seven set locations consistent with the axial load, flexion, extension, abduction, adduction, internal and external rotation positions (Figure 5-5 A). A series of five loads were applied to the external load cell and the readings were recorded for each load and input into the software to produce a calibration constant.

To calibrate the ML displacement sensor, an automatic displacement calibration file provided with the simulator software was used alongside a series of slip gauges. The slip gauges were pressed against the ML slide by rotating the ML motor by hand and the actual positions input into the software (slip gauges of 4.1, 6.1, 8.1, 10.1, 12.1 mm representing actual positions of -4, -2, 0, 4, and 4 were used as directed by the manufacturer (Figure 5-5 B). The ML motor demand position was then calibrated against the actual position as determined by the calibrated position sensor.

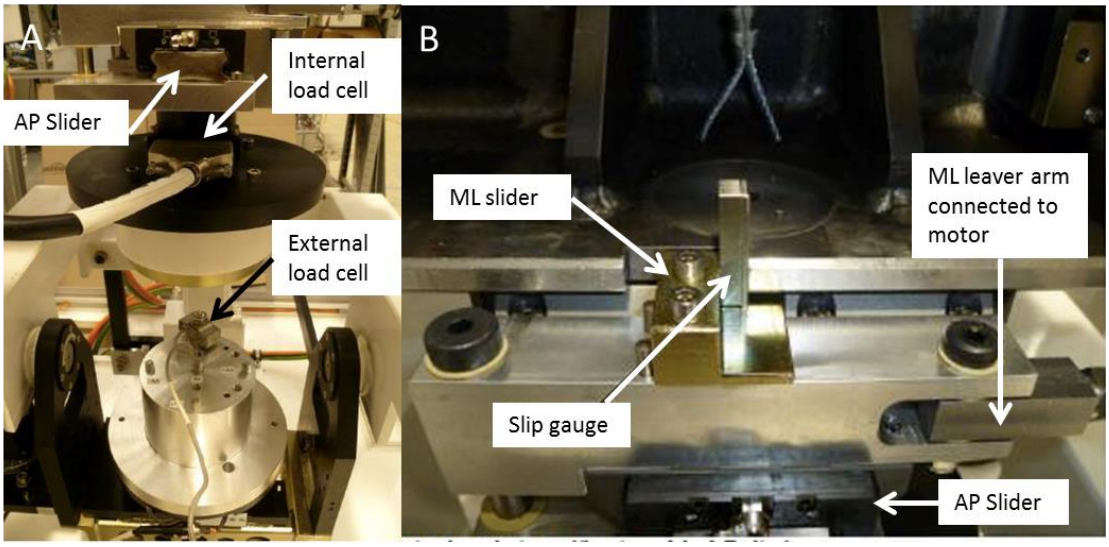

Figure 5-5 Simulator calibration. A – load calibration using an external load cell, load cell in negative FE position. B –Calibration of ML displacement. Imaged adapted from the Hip Simulator Hardware Manual.

5.5 General methodology

5.5.1 Lubrication

Prior to testing, cartilage and labral tissue hydration was maintained throughout the study by covering exposed surfaces with a PBS soaked tissue. *In vitro* tests of the whole natural joint were carried out with the joint surfaces submerged in 25 % bovine serum, defrosted at room temperature 24 hours prior to testing. The serum was used to lubricate the joint by replicating synovial fluid and closely mimicking *in vivo* lubrication regimes. The serum was contained within a gaiter secured by a top and bottom jubilee clip. Concentrated bovine serum was diluted in distilled water to produce 25 % bovine serum.

5.5.2 Specimen fixation

The alignment of the hip joint was maintained during testing by fixing the porcine acetabulum and femoral head into custom designed holders using non-sterile Polymethylmethacrylate (PMMA) bone cement. PMMA bone cement was provided as a two-component mixture; consisting of a liquid and powder. During curing the viscosity of the cement thickened due to the exothermic reaction. For femoral potting, the cement was used immediately after mixing to maintain its liquid state where as, for acetabular potting, the cement was used once it formed a dough-like consistency to support the weight of the cup. Bone cement took approximately 10 minutes to part-set when it became un-workable and non-adhesive and approximately 30 minutes to fully harden.

5.5.3 Specimen dissection

Porcine specimens were dissected, as discussed in Section 2.3.2, to separate the acetabular cup and femoral head. Following dissection, excess pubis, ischium, and ilium bone were removed from the acetabulum, the femur was shortened to 75 mm, and the greater trochanter was removed (Figure 5-6). Specimens were reduced in size to ensure they fit within the working distance of the simulator and to prevent impingement of protruding bony structures on the surrounding cement in the pots. The femoral head diameter of each specimen was measured using digital callipers across the largest articulating direction of the hip (AP) and assumed to be spherical.

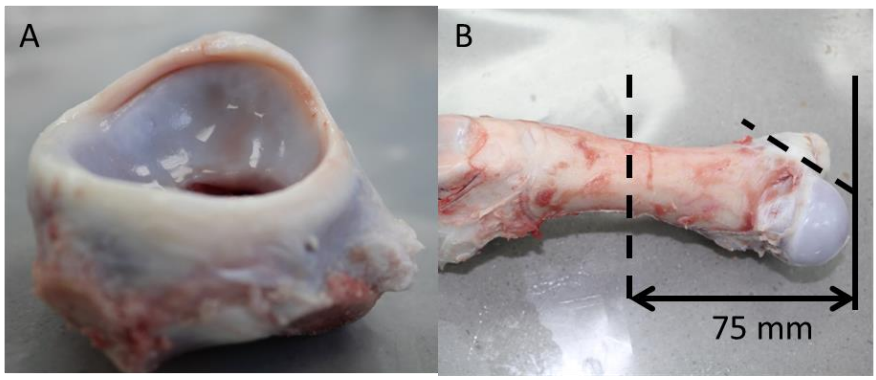

Figure 5-6 Acetabular cup and femoral head dissection. A - Excess pelvic bone was removed from around all sides of the acetabular cup. B – The femur was cut 75 mm from the superior of the femoral head and the greater trochanter removed. Dashed lines represent cutting locations.

5.6 Development of specimen holders and fixtures

Dynamic *in vitro* testing of whole natural joints had not been conducted in a hip simulator prior to this study, hence designing and manufacturing of new specimen holders and alignment fixtures were required. To maintain simplicity, the specimen holders and alignment fixtures used throughout this study were adapted from designs used in a pendulum simulator for whole natural joints (Groves 2016) and were manufactured from Delrin® (polyoxymethylene plastic). Adaptations were required to account for the new CoR position of the simulator, a larger working area, and the attachment of the holders to the simulator. Design drawings for the new holders can be seen in Appendix B.

The acetabular cup holder was composed of two parts; the cup base and the stainless-steel cup (Figure 5-7). The cup base was designed to attach to both the hip simulator and the stainless-steel cup. The cup base had two serum inlets/outlets to fill the gaiter once the hip was in the simulator, a groove to ensure the acetabular cup was centred within the simulator, a ridge to seal the gaiter, as well as screw holes on the top and bottom to attach the fixture to the simulator and cup holder, respectively (Figure 5-7 A). The stainless-steel cup was the original design from the pendulum simulator which had two side cement grub screws to hold the cement within the holder once it had set (Figure 5-7 B).

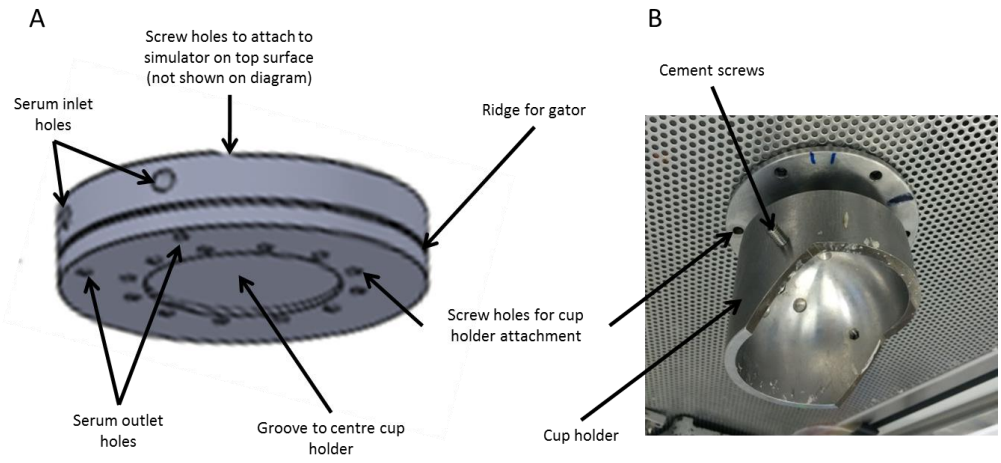

Figure 5-7 Acetabular cup holder. A – Cup base. B – Stainless-steel cup. Orientation shown as inserted into the simulator.

The femoral holder was composed of three separate plates, secured together using screws; the base plate, FE plate, and AA plate including the femoral pot (Figure 5-8). The screws could be loosened for the plates to move along the groves independently of each other to centralise the femur in the pot for different specimens. The femoral pot and AA plate were from the original pendulum design and the new FE and base plate took into account the new dimension of the hip

simulator with a total height of 110 mm from the lower mounting surface to the CoR of the femoral head. The femoral holder attached directly to the simulator via two screws in the base plate, which were also used to centralise the holder in the femoral alignment rig. Additionally there were four cement grub screws, from the internal to the external of the holder, to secure the cement in the cup once it had set.

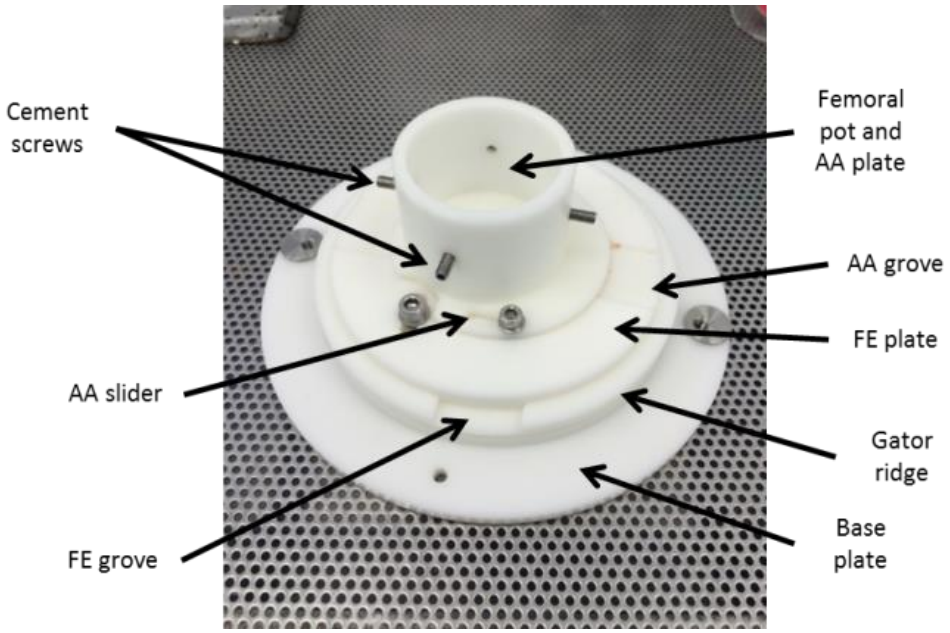

Figure 5-8 Femoral holder. Femoral holder for specimen alignment and attachment to the hip simulator.

5.7 Specimen alignment

The samples were aligned to each other and to the CoR of the simulator using two separate devices; a clamp and a femoral potting rig with a method adapted from Lizhang 2010 and Groves 2016 (Figure 5-9).

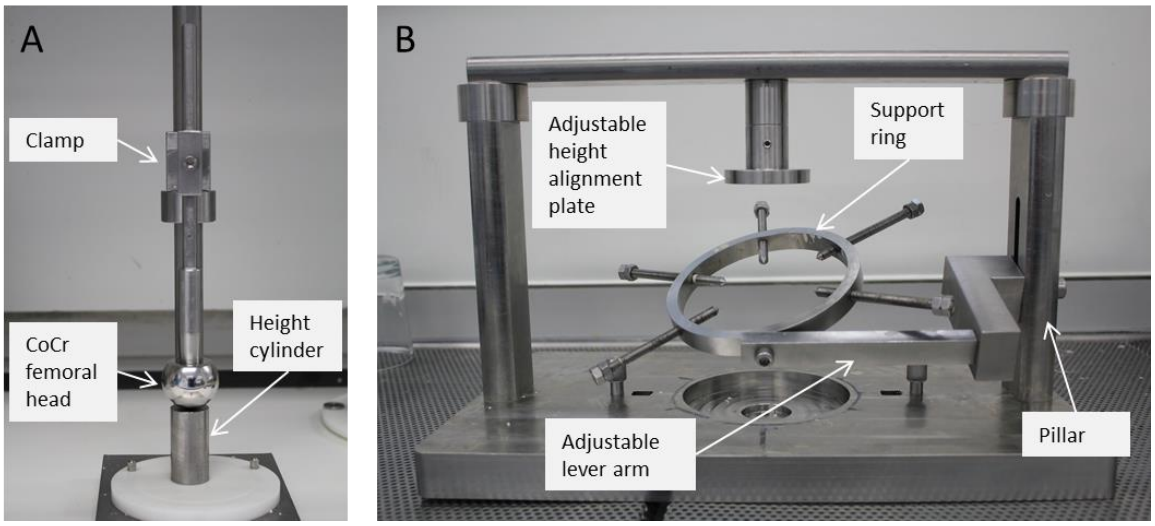

Figure 5-9 Alignment rigs. A – Clamp for acetabular cup alignment. B – Femoral potting rig for femoral head alignment

5.7.1 Acetabular cup alignment

The clamp set up was used to align the height of the acetabular cup and consisted of a series of cobalt-chromium (CoCr) femoral heads and a series of height cylinders. The diameter of the CoCr femoral heads matched the diameter of the natural femoral head (to the nearest millimetre) and the height of the cylinders matched the CoR of the simulator with the radius of the femoral head deducted. For each specimen the device was adapted to ensure the correct CoR for each specimen. The height cylinder was placed on the bottom of the clamp stand and the CoCr femoral head was lowered on top and its height secured (Figure 5-9 A).

The height cylinder was replaced by the stainless-steel cup (Figure 5-10 A), which was filled with cement. Once the cement had semi-cured and became dough-like, the acetabular cup was anatomically inverted and positioned in the cement with TAL facing upwards. The CoCr femoral head was used to push the acetabular cup into the cement until it reached its predefined height (Figure 5-10 B). An inclinometer was placed across the superior-inferior face of the acetabulum and was used to set the desired inclination angle of the cup (Figure 5-10 C). Any excess cement close to the edge of the acetabular rim was pushed away from the cup, to replicate *in vivo* conditions, ensuring the tissues were free to move. The side grub screws were tightened into the cement, which was left to cure for 30 minutes.

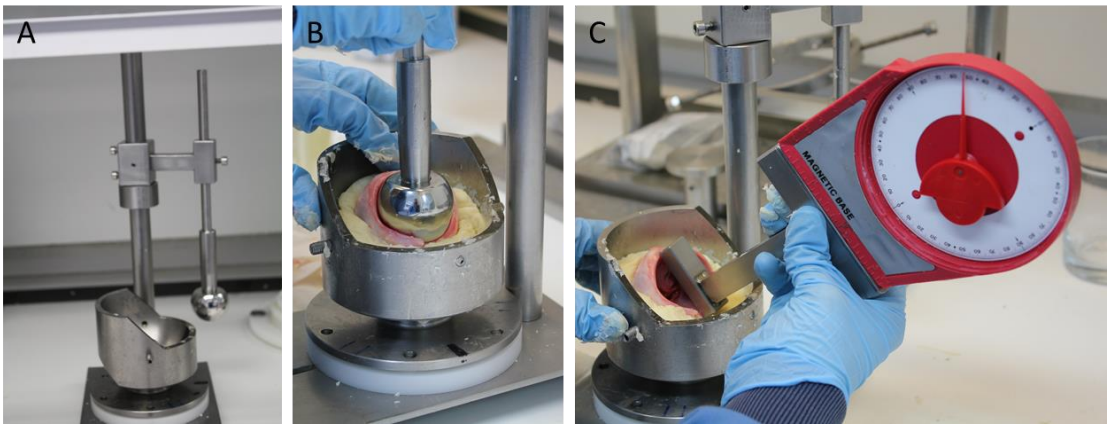

Figure 5-10 Acetabular cup alignment. A – Stainless-steel cup. B – Acetabular cup height alignment. C – Acetabular cup inclination angle alignment.

5.7.2 Femoral head alignment

The stainless-steel pot was transferred onto the base of the femoral potting rig and the femoral head was inverted (relative to its natural anatomy) and lowered into the socket of the acetabulum (Figure 5-11 A). The adjustable lever arm was lowered until the support ring was a close to the femoral-head neck junction as possible. The notch on the femoral-head neck junction was aligned to the centre of the TAL, and the fovea capitis of the femoral head was aligned to the ligamentum teres to minimise the clearance between the femoral head and acetabular cup. Once in alignment the surrounding screws on the support ring were tightened to hold the femur in position. The angle of the adjustable lever arm was recorded, prior to inverting it 180 ° (Figure 5-11 B). In the process of inverting the femur the stainless-steel pot was removed and replaced with the femoral holder and the adjustable height alignment plate (Figure 5-11 C). The femoral head was gently raised until it came into contact with the alignment plate, whilst maintaining the angle of the lever arm (Figure 5-11 D). Once the femur was in position the lever arm was locked in place and the femoral holder filled with cement. The four surrounding grub screws were tightened to secure the cement. Once the cement had set the screws on the support ring were loosened and the femoral pot was removed from the rig.

For increased cup inclination angle specimens, the same procedure was followed as described in Section 5.7.1 for the acetabular cup. The femoral head was aligned following the method described above, however prior to tightening the support ring screws the femur was adducted by the increased angle, measured using the inclinometer on the medial side of the femur. For example if the cup inclination angle was increased from 45 ° to 55 ° the femur was lowered by 10 °.

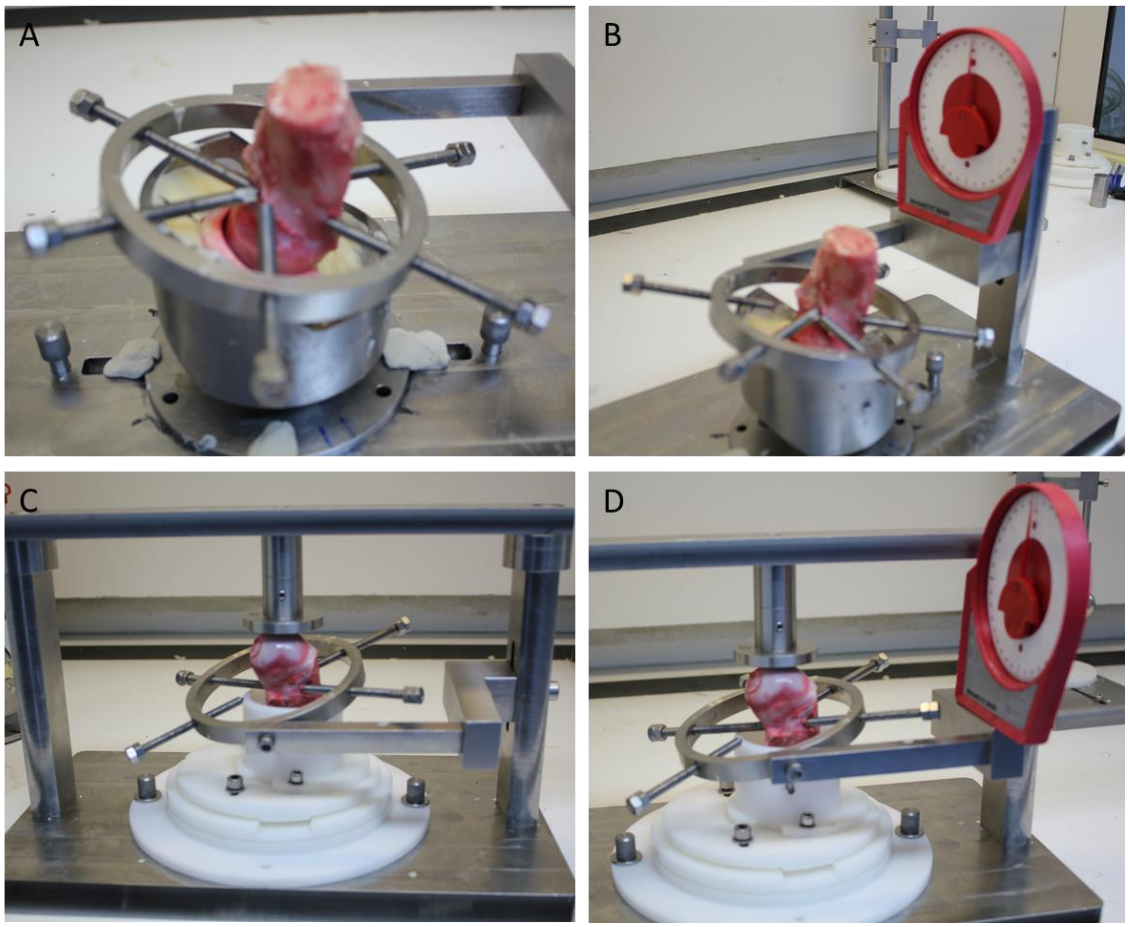

Figure 5-11 Femoral head alignment. A – femoral head aligned with acetabular cup. B – Angle of lever arm measured. C – Femoral head height alignment. D – lever arm inverted by 180 °.

5.7.3 Specimen mounting

The stainless-steel cup was fixed to the cup base and attached to the upper mounting surface of the simulator (Figure 5-12 A). A gaiter was secured around the base of the femoral holder using a jubilee clip and the holder was attached to the lower mounting surface of the simulator (Figure 5-12 B). The upper mounting surface was lowered until the femoral head relocated inside the acetabular cup (Figure 5-12 C). The acetabular cup was held in position via a loaded spring above the upper mounting surface. The gaiter was secured around the acetabular holder using a jubilee clip and filled with 1500 ml of 25 % bovine serum via the serum inlet valves (Figure 5-12 D).

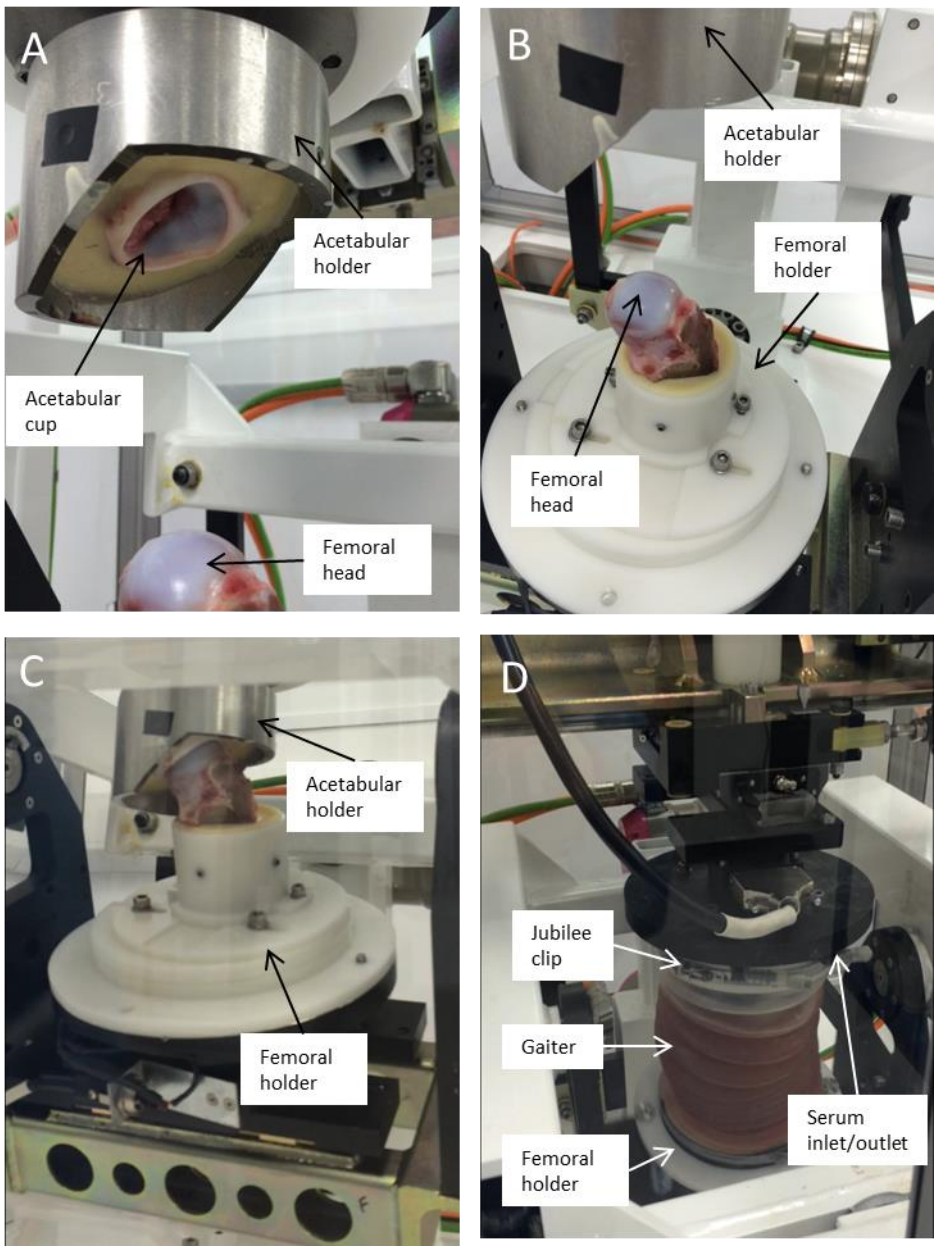

Figure 5-12 Hip simulator set up. A – Acetabular cup inverted and fixed to upper mounting surface. B – Femoral head fixed to lower mounting surface. C – Hip joint relocation with gaiter removed. D – Simulator set up with gaiter filled with bovine serum.

5.8 Test analysis

All specimens were assessed visually and the results were documented using photography and written analysis. Specimens were assessed prior to, during* and post testing for morphology, colour, and surface changes. Changes to the articulating surfaces of the femoral cartilage, acetabular cartilage and acetabular labrum were analysed from photos taken using a standard camera set up to obtain 9 images of the surfaces from the same locations before, during and after testing. For each test, the set-up (including number of cycles, cup angle, load and ML displacement) and cause of failure if applicable, were documented in an Excel spreadsheet.

*it was discovered part way through testing that it was not possible to identify the precise moment when damaged occurred as the joints were enclosed in gaiters. Hence during the final stages of testing when successful labral damage was observed, tests were paused every hour and the specimens photographed.

5.8.1 Sample imaging

Morphological surfaces of the hip were imaged before and after testing to document any changes to the labrum and cartilage tissues. Images were taken of the superior acetabulum and femoral head from above using a camera stand and of the side surfaces of the acetabulum (five) and femoral head (four) using a tripod (Figure 5-13). The tripod and stand were set at specific heights and distances from the samples to ensure before and after pictures were of similar locations. A reference marker was placed on the base of the camera stand with circles to match the base diameters of the holders to ensure the samples were placed in identical locations (Figure 5-14). When the image was taken the camera was set to full zoom and the specimen was rotated to set positions. Exact degrees of rotation were achieved using marks to match the screw holes in the holders.

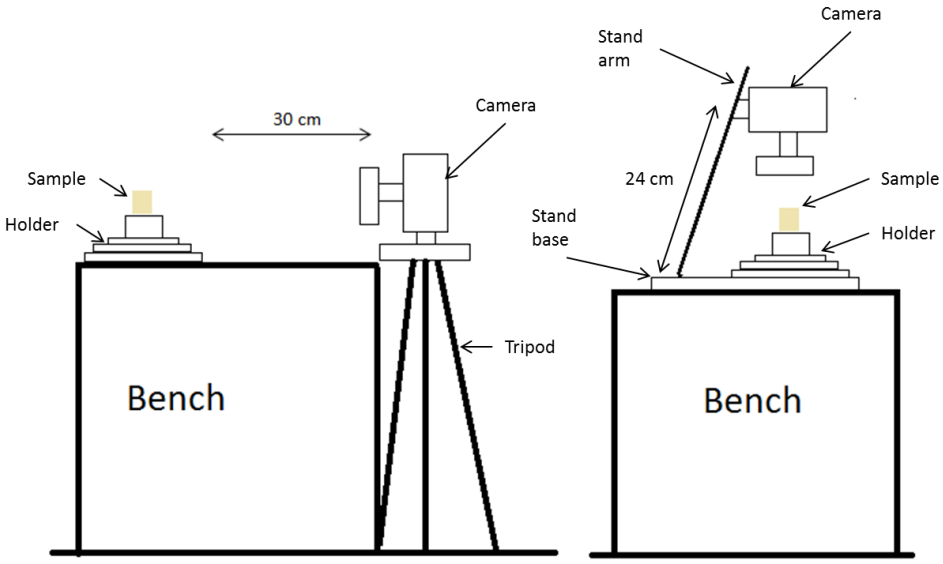

Figure 5-13 Camera set up. Left - set up for anterior, posterior, medial and lateral imaging of acetabulum and femoral head. Right - set up for superior imaging of acetabulum and femoral head.

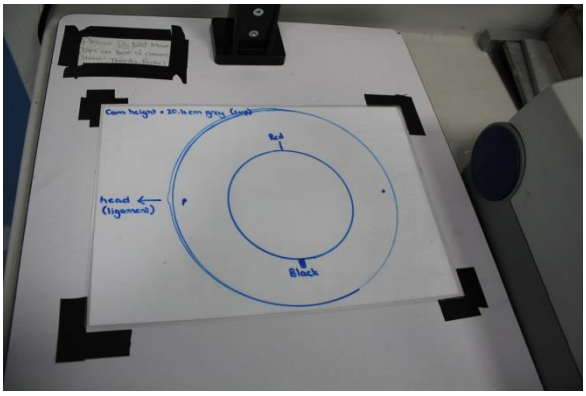

Figure 5-14 Sample alignment markers for photography. Markers were placed on the base of the camera stand to position the samples during photography.

5.8.2 Sample analysis

Damage to specimens was assessed in terms of labral damage (LD) and cartilage damage (CD) and documented in a table using a yes (Y) or no (N) analysis initially. Any damage observed was then classified using either the Lage or Outerbridge scale for labral and cartilage damage respectively. Any changes in colour and / or morphology were also documented and the cause of test failure if applicable.

5.8.2.1 Labral analysis

Labral damage was classified visually using the Lage scale (Lage et al. 1996). Damage was specified by the type and location using the Lage classification scale listed in Table 5-2.

Table 5-2 Lage classification system of labral damage. Table adapted from Lage et al,. (1996).

Labral damage type	Definition
Radial flap	Disruption of the free margin of the labrum with the consequent formation of a discrete flap
Radial fibrillated	Generally of a hairy appearance at the free margin of the labrum
Longitudinal peripheral	Tears of variable length along the labral-cartilage junction
Unstable	Abnormal labral function, as opposed to shape

5.8.2.2 Cartilage analysis

Cartilage damage was classified visually using the Outerbridge scale (Cameron et al. 2003). Damage was specified by the type and depth using the Outerbridge scale listed in Table 5-3.

Table 5-3 Outerbridge classification system of cartilage damage. Table adapted from Cameron et al., (2003).

Cartilage Grade	Definition
0	Normal cartilage
I	Cartilage with softening and swelling
II	Partial thickness defect with fissures on the surface that do not reach the subchondral bone or exceed 1.5 cm in diameter
III	Fissures to the level of subchondral bone in an areas with a diameter of more than 1.5 cm
IV	Exposed subchondral bone

5.9 Test inputs

To develop an *in vitro* simulation system of the natural hip, the hip must function under natural motion without resulting in damage. In order to progress the *in vitro* simulation system into a labral damage model, the damage must mimic that seen in abnormal hip morphology diseases such as FAI or DDH. Damage associated with these diseases includes labral tears and/or separation from the articular cartilage.

5.9.1 Natural hip joint model

In vitro simulation of the natural hip was undertaken with the acetabular cup set at a 45 ° inclination angle (or Sharp's angle) to represent *in vivo* alignment (Harrison et al. 2014, Figure 5-15). Sharp's angle is the angle formed by a line through the superior to inferior acetabular rim and the horizontal plane from an AP view of the hip. An inclination angle of 45 ° represents *in vivo* loading where the load is applied above the superior surfaces of the acetabular cup and femoral head, which are protected by articular cartilage (Figure 5-15). The hip joint motion (FE, AA and IE) was determined by ISO 14242 and ran for 10,800 cycles, the equivalent of 3 hours at 1Hz (n=6), as this was considered long enough for damage to occur if the joint was functioning under abnormal conditions. Previous studies running natural hip joints or hemiarthroplasties have used a maximum cycle time of two hours (Lizhang 2010; and Groves 2016). During testing the ML displacement was locked to zero to prevent the hip from dislocating due to the lack of external ligaments and muscles, the AP displacement was left free to self align any slight mismatch in the joint.

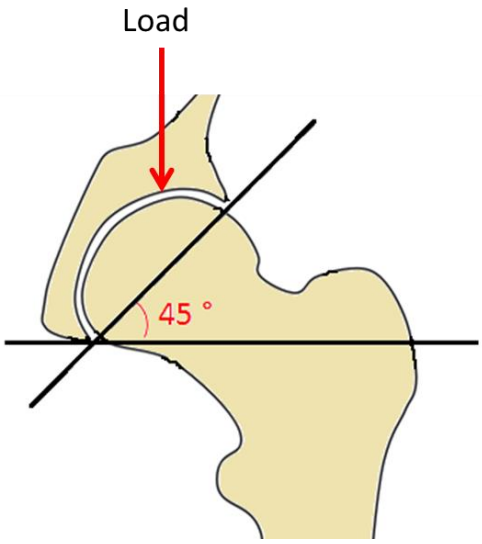

Figure 5-15 Cup inclination angle. The porcine acetabular cup was cemented at 45 ° to represent *in vivo* alignment. Image adapted from Wikipedia https://en.wikipedia.org/wiki/Hip

The human load cycle (ISO 14242) was scaled down to accommodate for the physiological loading of the pig. In previous studies, when testing the natural porcine hip, a maximum dynamic load of 800 N was applied to the joint, equivalent to the pig's whole body weight, which was approximately 25 % of the human load cycle (Lizhang 2010 and Groves 2016, Figure 5-16). This load was used to replicate normal loading through the hip for the natural hip model.

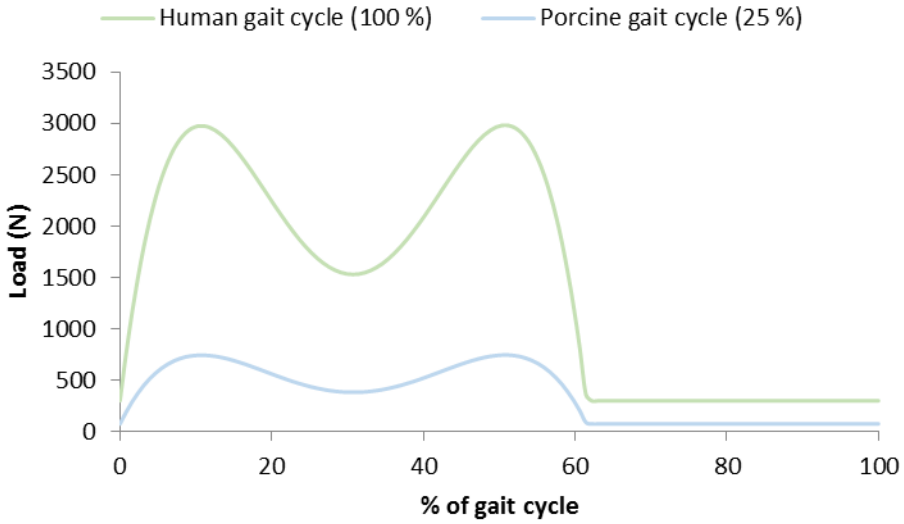

Figure 5-16 Porcine and human gait cycle. The load within the human gait cycle was scaled down by 25 % for the porcine hip.

5.9.2 Labral damage model

The labral damage model was advanced from the previously developed natural hip model and used the same initial set up for joint alignment and simulator alignment and tests were ran for a minimum of 10,800 cycles. A number of input variables were additionally investigated to replicate labral damage, which determined the cup inclination angle, ML displacement and load applied to the specimen. The individual variable set ups are discussed in the following sections and a summary of the test conditions investigated can be seen in Table 5-4.

Table 5-4 Method development for labral damage model. The combinations of test inputs investigated to create a labral damage model. Left table – increased angle and load. Right table – ML displacement with increased angle and load.

Load (N)	Angle		
	55°	60°	65°
750	X		X
1500	X	X	X
3000	X		X

Additional ML Displacement			
Load (N)	Angle		
	45°	55°	60°
1500	X	X	
2250		X	X

Increased cup inclination angle

The inclination angle of the cup was increased to move the area of loading from the superior acetabular cartilage surface around to the labral-cartilage junction (Figure 5-17). An increased cup angle in artificial joints has been shown to move the area of loading closer to the edge of the acetabular cup (Fisher 2011 and Stewart & Hall 2006). This can result in damage around the rim, where the labrum is located in a natural joint. Increased cup angles of 55 °, 60 °, and 65 ° were investigated and the method for setting the cup inclination angle was described in section 5.7.1.

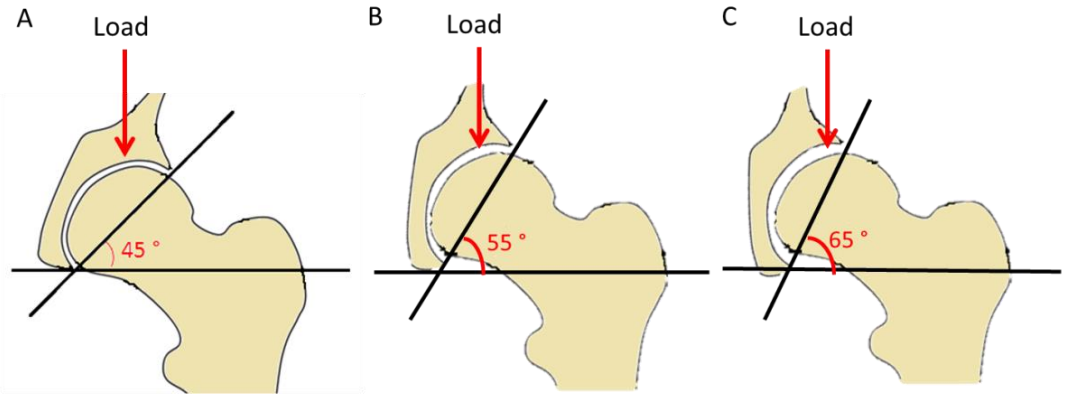

Figure 5-17 Increased cup inclination angle for labral damage model. A – *In vivo* inclination angle. B – Middle increased cup inclination angle. C – Maximum increased cup inclination angle.

Increased load

The load placed on the hip was increased to replicate increased contact stresses associated with abnormal hip joint morphology, which can be a direct result of contact or as a result of non conformity within the joint. The hip was placed under three elevated peak loads; 1500 N, 2200 N, and 3000 N, which represented 50 %, 75 %, and 100 % of the human gait cycle, dependent on the test method carried out. The three different load cycles can be seen in Figure 5-18. The increased loads were also ran in combination with increased cup inclination angles

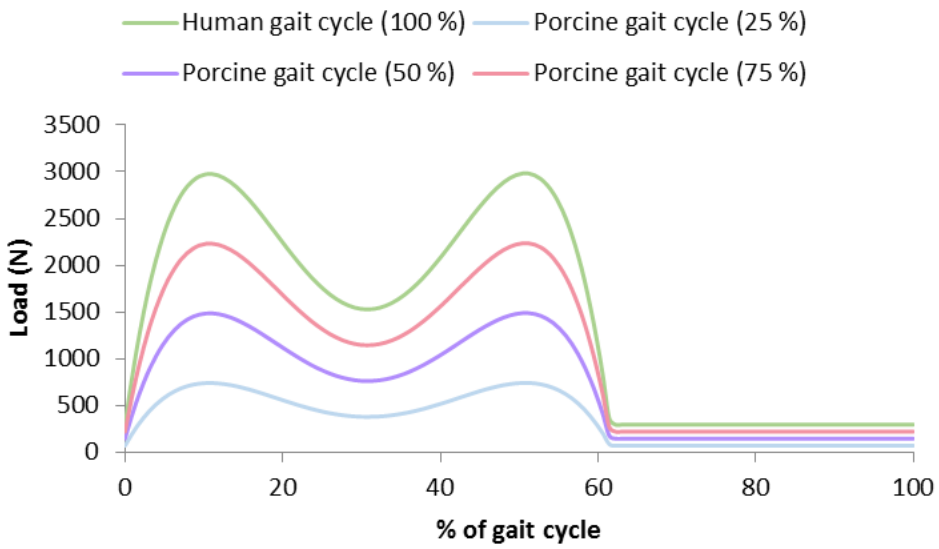

Figure 5-18 Load cycle for labral damage model. Four loading profiles for labral damage model, scaled down from the human gait cycle.

ML displacement

The femoral head was offset in the ML direction to replicate impingement on the labral-cartilage junction (Figure 5-19). The femoral head was offset in the lateral direction by its maximum displacement, the point at which the femoral head came into contact with the labral-cartilage junction (approximately 4 mm). The femoral head was displaced once it was aligned in the simulator by laterally translating the AA plate and femoral pot. The femoral displacement was recorded for each sample using a ruler attached to the FE plate and marker attached to the AA plate. The ML displacement on the simulator remained locked in position to prevent the hip from self-aligning after the femoral head had been displaced. ML displacement was also ran in combination with increased cup inclination angles and increased loads.

ML displacement tests were carried out for this study as part of an undergraduate project. A MEng Master's student (Aimee Cheesbrough) is acknowledged as conducting the tests under the candidate's supervision.

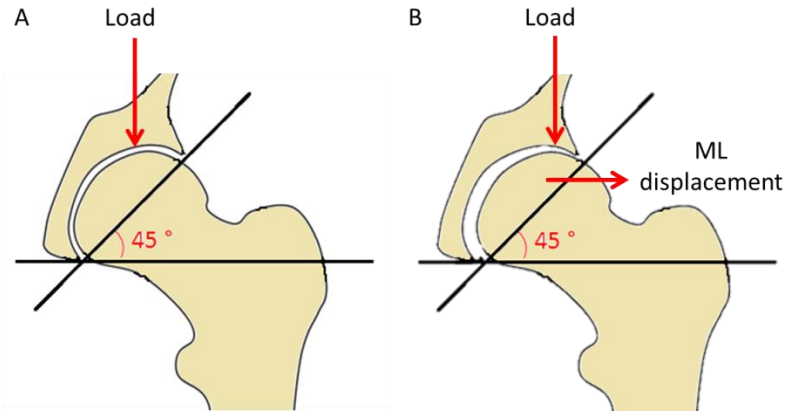

Figure 5-19 Medial-lateral displacement for labral damage model. A - Original (*In vivo*) set up. B – Femoral head displaced laterally until the head came into contact with the labral-cartilage junction.

5.10 Results

5.10.1 Natural hip joint model

Under normal joint set up, with a peak load of 750 N and an acetabular cup inclination angle of 45 ° no damage to either the articular cartilage or labrum was identified. An Outerbridge score of 0 was given to all cartilage surfaces and a Lage score was not applicable. Overall, seven specimens were tested with only one specimen failing due to a cement particle trapped between the articulating surfaces, resulting in artificial damage to the cartilage surfaces. After testing, a change in colour of the cartilage and labrum surfaces was noted in all specimens. The colour change was a result of blood leaking from the joint into the bovine serum, which subsequently became darker in colour. An example specimen can be seen in Figure 5-20 with before and after images of the acetabulum and femoral head (superior images of the specimen, taken using the camera stand set up).

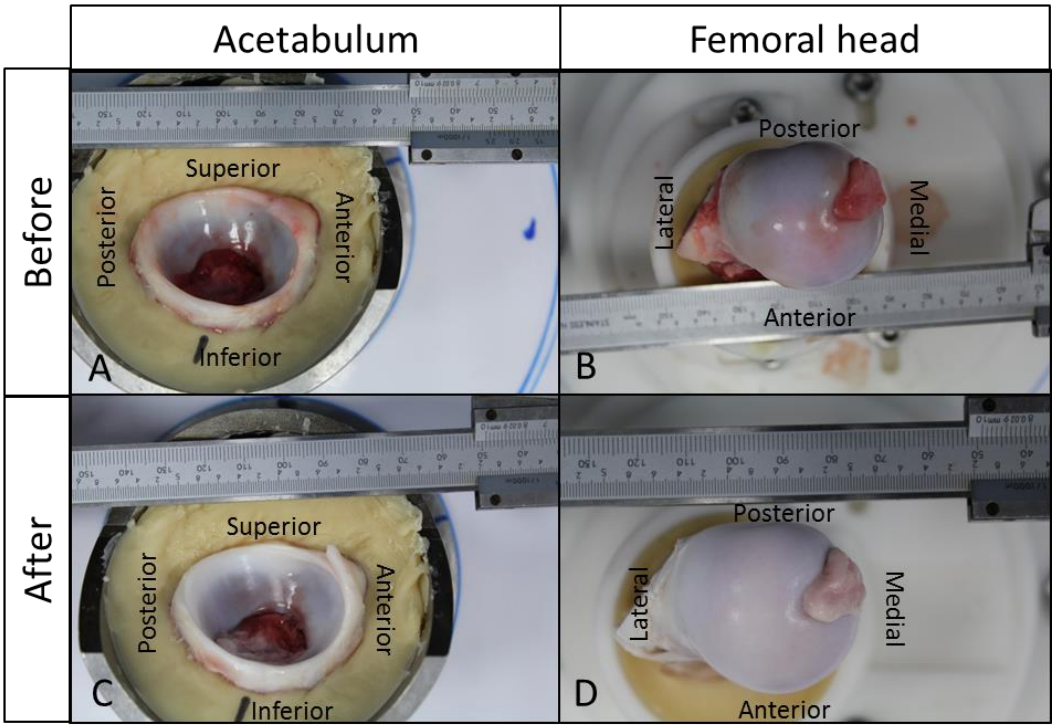

Figure 5-20 Natural hip joint model results. Superior images of acetabular cup and femoral head before and after testing.

5.10.2 Labral damage model

5.10.2.1 Increased cup inclination

The set up and analysis for each test specimen used in this study group are outlined in Table 5-5. The left side of the table outlines the set up conditions and the right side documents the results and analysis for each specimen. In some cases, the test failed due cement damage (Ce/D) either as a result of set up error or specimen dislocation; these tests were discarded and are identified in grey. Initial test findings, including labral damage (L/D), cartilage damage (C/D), cement damage (Ce/D), and colour change (C/C) were documented using a yes/no (Y/N) system, whilst specific details were documented in the additional notes and classification columns.

Table 5-5 Summary of increased angle test results and analysis for labral damage model specimens. L/D – labral damage, C/D – cartilage damage, Ce/D – cement damage, C/B – cartilage bruising, S/W – stripe wear, L/F – labral flattening, R/F – radial fibrillation, L/P - labral peripheral.

Repeat	Cup angle (°)	Load (N)	Cycle count	ML Displacement	L/D	C/D	Ce/D	C/B	Additional notes	Lage score	Outer-bridge score
1	55	750	10800	N			Y		cement particle		
2	55	750	10800	N	N	N	N	Y		N/A	0
3	55	750	10800	N	N	N	N	Y		N/A	0
1	65	750	10800	N			Y		dislocation		
2	65	750	10800	N	N	N	N	Y		N/A	0
3	65	750	10800	N			Y		cement particle		
4	65	750	10800	N			Y		dislocation		
5	65	750	10800	N	N	N	N	Y		N/A	0
6	65	750	10800	N			Y		dislocation		
7	65	750	10800	N	Y	N	Y	Y		L/F	0
8	65	750	10800	N	Y	N	N	Y		L/F	0
9	65	750	10800	N	Y	N	N	Y		L/F	0

Although an inclination angle of 55° caused the point of load to move closer to the labral-cartilage junction it remained mainly on the cartilage surface. However, it is believed that as a result of the load being dispersed around the cup, it would have resulted in an increased load on the labrum. An inclination angle of 65° caused the point of load to move further around to the labral-cartilage junction which would have directly increased the load on the labrum.

Increasing the cup inclination angle by 10 ° to give an inclination angle of 55 ° was found to have no effect on the hip joint. The labrum remained rounded in shape and no damage to the cartilage surface was identified (Figure 5-21). A Lage classification was not available as no damage was seen and an Outerbridge score of 0 was given to all cartilage surfaces. Of the three

hip joints tested one failed due to a cement particle becoming trapped between the articulating surfaces. The cement particle caused scratches to the acetabular and femoral cartilage; however no further damage was identified. As seen in the natural hip model, blood leaked from the tissues into the serum giving the tissues a whiter appearance.

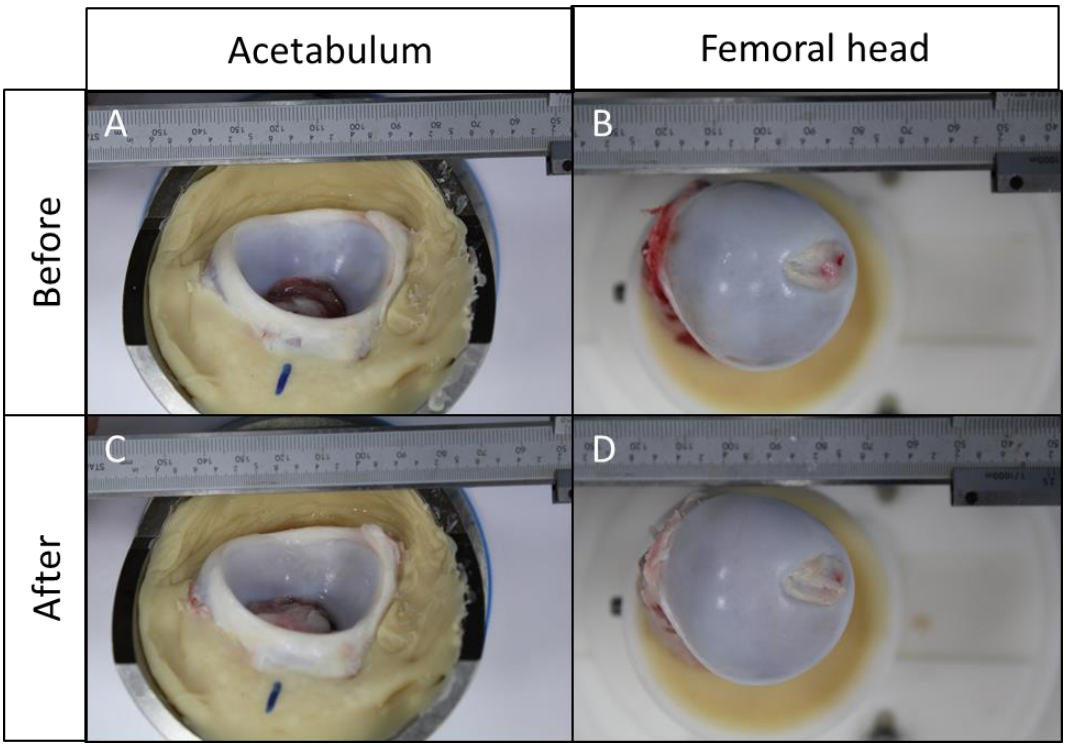

Figure 5-21 Increased cup angle of 55 ° for labral damage model. Porcine acetabulum and femoral head before and after testing (750 N, 55 °). Images taken of the superior region of the porcine hip. Image showing repeat 2 in Table 5-5.

An increased cup inclination angle of 65 ° resulted in no damage to the cartilage surfaces, giving an Outerbridge score of 0 (Figure 5-22). Labral flattening in the superior region was observed in 60 % of the specimens tested (highlighted in red, Figure 5-22 D and E) with the others showing no labral damage. Labral flattening was not documented in the Lage classification and therefore a score was unavailable. In total nine porcine hips were tested with three failing due to the sample dislocating and one due to a cement particle trapped between the articulating surfaces. It was noted that an increase in cup angle of 20 ° resulted in a high failure rate of testing due to dislocation of the specimens. A colour change was also documented due to blood leaking from the joint into the surrounding serum.

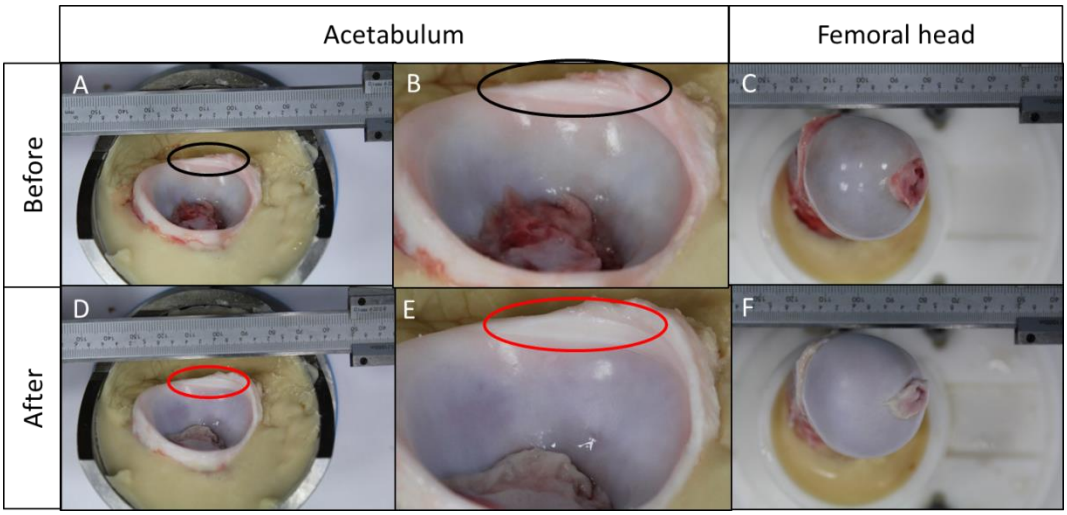

Figure 5-22 Increased cup angle of 65 ° for labral damage model. Porcine acetabulum and femoral head before and after testing (750 N, 65 °). Images B and E show enlarged images of the circled areas in A and D respectively. Images taken of the superior region of the porcine hip. Images taken of the superior region of the porcine hip. Image showing repeat 8 in Table 5-5.

As damage associated with abnormal hip joint morphology was not identified as a result of increased cup inclination angle, it was decided that the model would be further developed to incorporate either an ML displacement and/or increased load.

5.10.2.2 ML displacement

The set up and analysis for each test specimen used in this study are grouped and outlined in Table 5-6. The left side of the table outlines the set up conditions and the right side documents the results and analysis for each specimen. In some cases, the test failed due cement damage (Ce/D) either as a result of set up error or specimen dislocation; these tests were discarded and are identified in grey. Initial test findings, including labral damage (L/D), cartilage damage (C/D), cement damage (Ce/D), and colour change (C/C) were documented using a yes/no (Y/N) system, whilst specific details were documented in the additional notes and classification columns.

Table 5-6 Summary of ML displacement test results and analysis for labral damage model specimens. L/D – labral damage, C/D – cartilage damage, Ce/D – cement damage, C/B – cartilage bruising, S/W – stripe wear, L/F – labral flattening, R/F – radial fibrillation, L/P - labral peripheral.

Repeat	Cup angle (°)	Load (N)	Cycle Count	ML Displacement	L/D	C/D	Ce/D	C/C	Additional notes	Lage score	Outer-bridge score
1	45	1500	10800	Y	N	Y	N	Y	C/B & S/W	N/A	1
1	60	2250	10800	Y					dislocation		
2	60	2250	10800	Y					dislocation		
1	55	2250	10800	Y					dislocation		
2	55	2250	10800	Y					dislocation		
1	55	1500	10800	Y					Femur snapped		
2	55	1500	10800	Y	Y	Y	Y	Y	C/B & S/W	R/F	1
3	55	1500	10800	Y					dislocation		
4	55	1500	10800	Y	Y	N	N	Y	C/B & S/W	L/P	1
5	55	1500	10800	Y	N	N	N	Y	C/B & S/W		1

For maximum medial lateral displacement, four test set ups were investigated. The initial test was run with an increased load of 1500 N and *in vivo* inclination angle of 45 °. Following testing, slight cartilage bruising was observed on both the femoral head and acetabular cartilage with an Outerbridge score of 1. In order to move the area of loading closer to the labral-cartilage junction, the angle was increased to 60 ° to allow for an increased lateral offset of the femoral head as well as the load increased to 75 % of the human gait cycle (2250 N peak load). This test set up resulted in dislocation of the joint and cartilage delamination as a result of impingement on the surrounding bone cement. To prevent dislocation, the acetabular cup inclination angle was reduced to 55 °, however with the same peak load of 2250 N it was concluded that the increased load was causing the joint dislocation as opposed to the increased cup angle. A lower peak load of 1500 N with a combined increased cup angle of 55 ° was then investigated with some damage observed. In one specimen more predominant cartilage bruising was identified over a larger area than in all other groups (Figure 5-23) and in a second specimen labral flattening and radial fibrillation was observed. However, a further three tests resulted in two specimen failures and one specimen where no damage was observed.

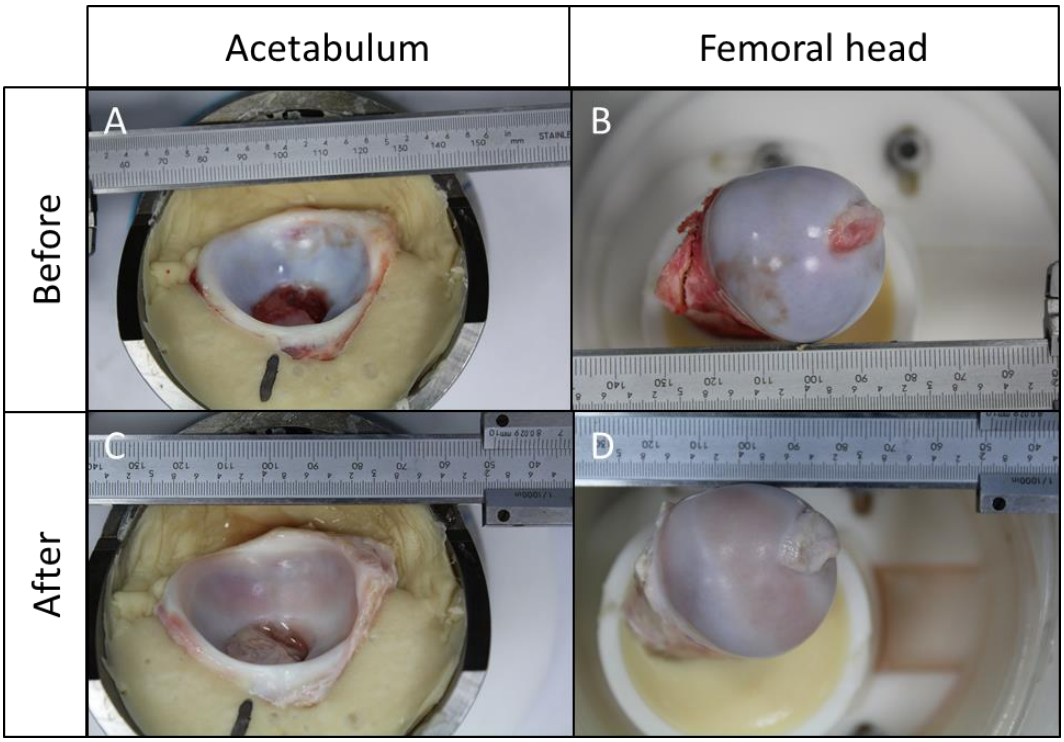

Figure 5-23 Medial lateral displacement for labral damage model. Porcine acetabulum and femoral head before and after testing (maximum ML displacement, 1500 N, 55 °). Images taken of the superior region of the porcine hip. Images taken of the superior region of the porcine hip. Images taken of the superior region of the porcine hip. Image showing repeat 5 in Table 5-6.

Damage as a result of ML displacement was not consistent between samples therefore, it was identified that ML displacement was not a reliable method to develop a labral damage model and it was decided that the model would be further developed to incorporate increased loads.

5.10.2.3 Increased load

The set up and analysis for each test specimen used in this study are grouped and outlined in Table 5-7. The left side of the table outlines the set up conditions and the right side documents the results and analysis for each specimen. In some cases, the test failed due cement damage (Ce/D) either as a result of set up error or specimen dislocation; these tests were discarded and are identified in grey. Initial test findings, including labral damage (L/D), cartilage damage (C/D), cement damage (Ce/D), and colour change (C/C) were documented using a yes/no (Y/N) system, whilst specific details were documented in the additional notes and classification columns.

Table 5-7 Summary of increased load test results and analysis for labral damage model specimens. L/D – labral damage, C/D – cartilage damage, Ce/D – cement damage, C/B – cartilage bruising, S/W – stripe wear, L/F – labral flattening, R/F – radial fibrillation, L/P – labral peripheral.

					Increased load						
Repeat	Cup angle (°)	Load (N)	Cycle Count	ML Displacement	L/D	C/D	Ce/D	C/C	Additional notes	Lage score	Outer-bridge score
1	55	1500	36000	N	Y	Y	N	Y	C/B & S/W	L/F	1
1	60	1500	10800	N	Y	Y	N	Y	C/B & S/W femoral Ce/D following failure	R/F & L/P	3
2	60	1500	18000	N	Y	Y	N	Y		R/F & L/P	3
3	60	1500	10800	N			Y		Femur snapped		
4	60	1500	10800	N			Y		dislocation		
5	60	1500	28800	N	Y	Y	N	Y	C/B & S/W	L/F	1
6	60	1500	10800	N			Y		acetabulum loosened		
7	60	1500	28800	N	Y	N	N	Y	C/B & S/W femoral Ce/D following failure	R/F	1
8	60	1500	16200	N	Y	Y	N			L/F & R/F	1
1	65	1500	10800	N	Y	Y	N	Y	femoral Ce/D following failure	R/F & L/P	3
2	65	1500	10800	N			Y		dislocation		
3	65	1500	10800	N			Y		dislocation		
4	65	1500	10800	N	Y	Y	N	Y	femoral Ce/D following failure	R/F & L/P	3
1	55	3000	10800	N	Y	Y	N	Y	C/B & S/W	L/P	4
1	65	3000	13	N			Y		dislocation		

Increased loads of 3000 N and 1500 N were tested in this section combined with a range of increased cup inclination angles. Initial tests, with a peak load of 3000 N and cup inclination angles of 55 ° and 65 ° were found to cause catastrophic damage to the specimens. The immature porcine tissue was too soft and resulted in the failure of the subchondral bone, followed by delamination of the cartilage as a result of contact with the bone cement (Figure 5-24).

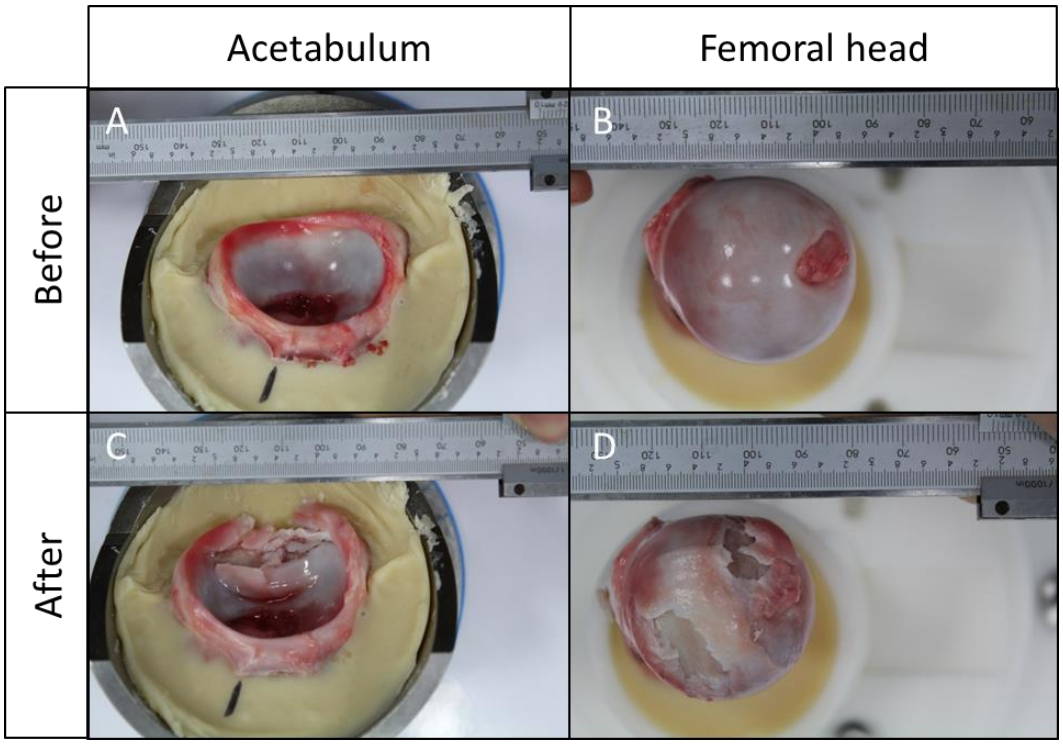

Figure 5-24 Increased load of 3000 N (55 °) for labral damage model. Porcine acetabulum and femoral head before and after testing (3000 N, 65 °). Images taken of the superior region of the porcine hip. Image showing repeat 1 in Table 5-7.

An increased load of 1500 N was found to be less aggressive over a range of increased cup inclination angles. An increased load of 1500 N combined with an increased cup angle of 55 ° resulted in slight labral and cartilage damage after a prolonged cycle count of 36,000 cycles. Damage observed included labral flattening and cartilage bruising identifying the contact area and path of the acetabular cup and femoral head (Figure 5-25). Bruising was observed in the superior region of the cup as a circular scar and across the femoral head as a stripe in the AP direction. Bruising was identified by a darkening and reddening of the cartilage tissue, which gradually faded around the impact area and was given an Outerbridge score of 1. Although damage was observed in this test, it was not consistent with damaged observed in abnormal morphology hip diseases.

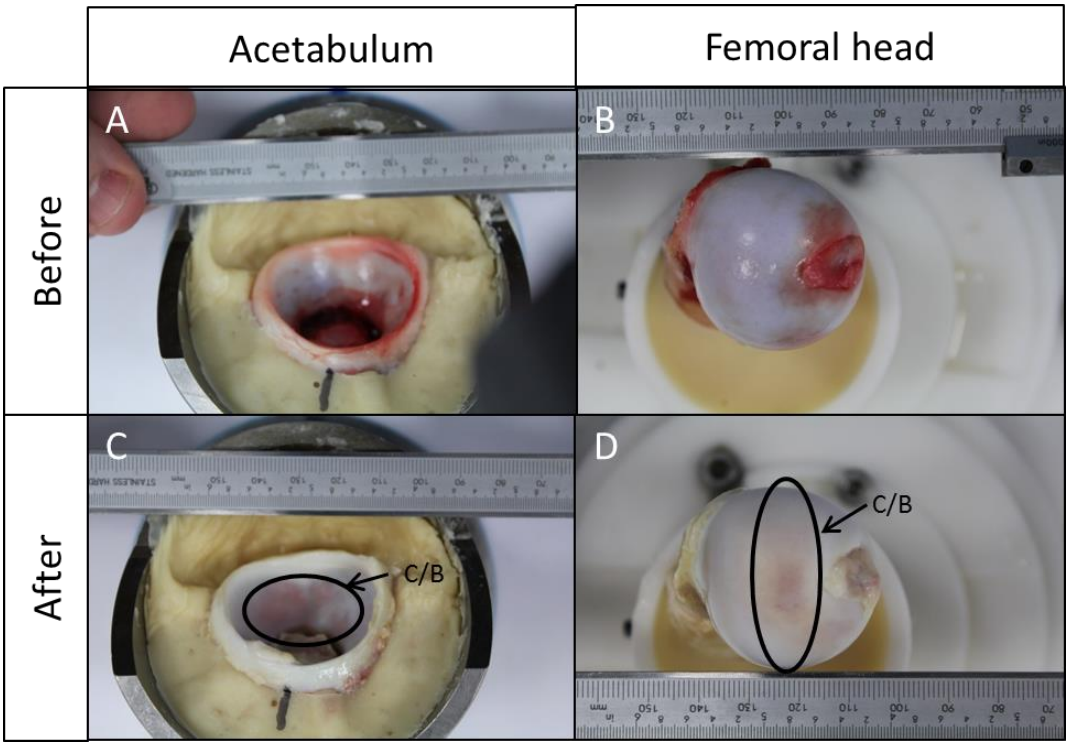

Figure 5-25 Increased load of 1500 N (55 °) for labral damage model. Porcine acetabulum and femoral head before and after testing (1500 N, 55 °). Images taken of the superior region of the porcine hip. Image showing repeat 1 in Table 5-7.

An increased load of 1500 N combined with an increased cup angle of 65 ° resulted in damage associated with abnormal hip joint diseases, including labral fibrillation at the tissue apex and longitudinal peripheral tears across the labral-cartilage junction (Figure 5-26 E), however the test had a 50 % failure rate due to specimen dislocation. Following longitudinal peripheral tears the labrum and cartilage separated causing the femoral head to dislocate and impinge on the surrounding bone cement, resulting in rapid cartilage delamination and exposure of the subchondral bone. As these tests were run over a long time period and damage times varied between specimens it was difficult to identify the moment the longitudinal peripheral tear occurred to terminate the simulator before further femoral damaged. Damage to the acetabular cartilage was given with an Outerbridge score of 3 as a result of large areas of damage and cuts to the cartilage surfaces. Following these tests it was decided the simulator would be paused every hour and the specimens imaged to identify the damage sequence.

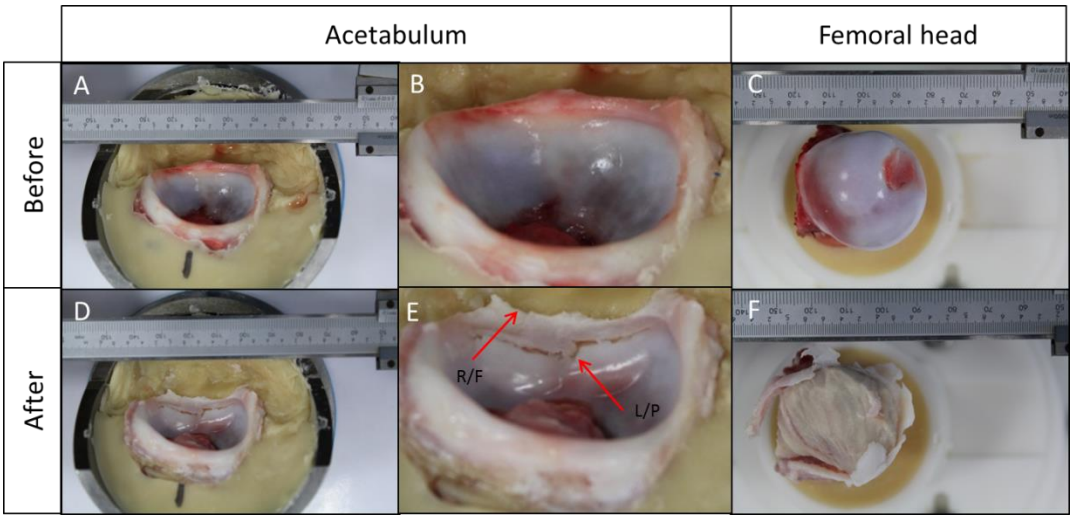

Figure 5-26 Increased load of 1500 N (65 °) for labral damage model. Porcine acetabulum and femoral head before and after testing (1500 N, 65 °). Images taken of the superior region of the porcine hip. Image showing repeat 1 in Table 5-7.

To minimise the risk of dislocation the inclination angle was reduced to 60 ° and used with an increased load of 1500 N. Labral flattening was observed in 100 % of the hips, radial fibrillation in 80 % of the hips, cartilage bruising including femoral stripe wear in 60 % of the hips and longitudinal peripheral tears along the labral-cartilage junction in 40 % of the samples (Figure 5-27). Of the samples where specimens were imaged at multiple time points (4 out of 5) labral flattening occurred prior to radial fibrillation which occurred before the longitudinal tear was formed. Cartilage bruising was observed early in the tests, within the first three hours of the four specimens which were imaged at multiple time points. Samples where longitudinal peripheral tears did not occur within the first three hours were left to run for more cycles, however no further damage was observed. Samples where only cartilage bruising occurred were given an Outerbridge score of 1, where as sample where longitudinal tears were observed were given an Outerbridge score of 3. In total eight tests were run with three of the tests failing, however only one of the tests failed as a result of specimen dislocation. As noted in the natural hip joint model a change in colour was also seen in all specimens ran at increased loads as a result of blood loss into the surrounding serum.

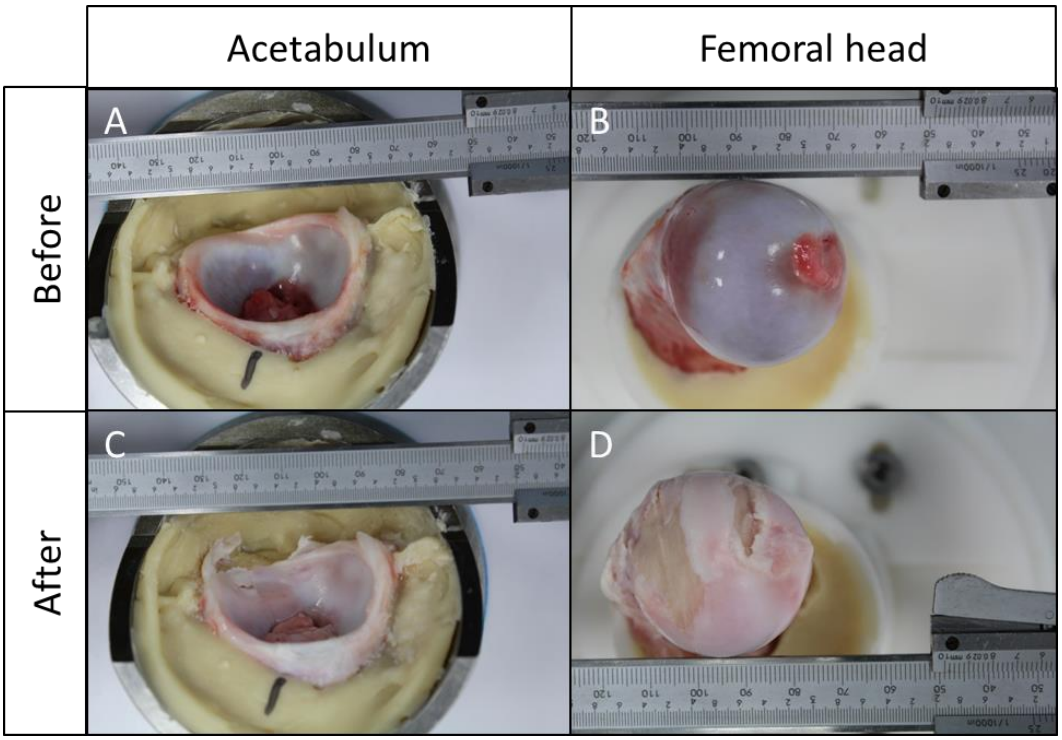

Figure 5-27 Increased load of 1500 N (60 °) for labral damage model. Porcine acetabulum and femoral head before and after testing (1500 N, 60 °). Images taken of the superior region of the porcine hip. Image showing repeat 2 in Table 5-7.

5.11 Discussion

5.11.1 Natural hip joint model

The main aim of this study was to develop a novel natural hip model, which functioned under a full range of motion and load cycle. The first stage of the method development was to anatomically align the acetabular cup and femoral head. This was successfully achieved using a rig designed in house. There was low clearance between the acetabular cup and femoral head as seen *in vivo* and the acetabular cup provided sufficient overcoverage of the femoral head. The second stage involved aligning the CoR of the hip to the CoR of the simulator. This was successfully achieved using a custom made rig which aligned the CoR of the acetabular cup to the CoR of the simulator, the femoral head was then aligned to the acetabular cup and its height determined using a second custom made rig. This was confirmed when the specimen was placed in the simulator and the joints realigned at the CoR of the simulator. After the hip joint was aligned within the simulator it was successfully ran for a period of three hours under the full ISO14242 gait cycle with a peak load of 750 N, without any labral or cartilage damage identified. This natural hip model could be used in future studies to assess the mechanical properties of the tissues in the hip in situ. This model was then used as the basis for a labral damage model.

5.11.2 Labral damage model

Research into abnormal hip joint diseases, such as FAI or DDH, has rapidly increased in recent years. Improved knowledge of the acetabular labrum has identified it as an active tissue in hip joint function; aiding in hip joint stability and protecting the articular surfaces (Song et al. 2012; Ferguson et al. 2001). Simulator studies have been used to assess the function and characteristics of natural tissues, however they are limited to small areas of tissue, partial loading or motion, and mainly to cartilage, ligaments or meniscus. There is very limited knowledge of the labrum under dynamic testing. Song et al. 2012 recently investigated the effect of a focal or complete labrectomy utilising a servohydraulic materials testing machine to apply an axial load and angular displacement and Groves 2016 developed an *in vitro* hip simulation model to assess tribological properties of natural porcine tissue, however neither model applied the full range of motion of the hip during walking.

The main aim of this study was to develop a novel natural hip model, which functioned under a full range of motion and load as well as a labral damage model to replicate damage seen in diseases such as FAI and DDH. To develop a labral damage model, increased Sharp's angle, increased load and ML displacement were investigated. Increased cup angle and ML displacement has been found to cause failure or damage in artificial hip joints due to concentrated loads, hence these methods were investigated to cause damage to the natural

tissues of the hip (Al-Hajjar et al. 2016). By applying a standard gait cycle (ISO 14242) and using a standard alignment method, tests are repeatable and can be easily adapted to investigate further experimental set ups.

Complete porcine natural hips were tested *in vitro* in a single station anatomical hip wear & friction simulator with 25 % bovine serum lubricant and under a full load and gait cycle (ISO 14242). An *in vivo* hip set up was utilised for the natural hip model, where the acetabular cup was cemented with a Sharp's angle of 45 ° and a peak load of 750 N was applied. Each test was run for a minimum of three hours in order to provide sufficient time for damage to develop. As reported in section 5.9.2 no damage was evident after running the hip joint under natural joint conditions (n=6). Discolouration of the tissues was observed as a result of blood leaking out of the joint into the surrounding serum however; it was not associated with damage. It was therefore evident this set up provided a successful *in vitro* simulation of the natural hip which could be used for future tribological investigations of the acetabular labrum.

Labral and cartilage damage has been observed in patients with hip joint disease as a result of abnormal joint morphology. Abnormal joint morphology alters the loading pattern through the hip, causing damage to the tribological interface. Soft tissue damage of the labrum includes tears, fibrillations and/or separation from the adjoining articular cartilage and has been classified by surgeons using a Lage scale. Cartilage damage has also been classified using the Outerbridge scale to document the size and type of damage. In order to develop a successful *in vitro* damage model, the model must closely mimic damage seen in diseases such as FAI and DDH. Three different test set ups were investigated to develop labral damage; increased cup angle, increased load and ML displacement. By altering the test set up the loading area of the hip joint was translated closer to the labral-cartilage junction and damage was accelerated by increasing the load.

The labral damage model set up was progressed to include a combination of increased load and increased cup angle. Overall, it was discovered that loads of 750N were too low to produce any substantial damage, whereas loads over 2250 N were too high and resulted in failure of the subchondral bone. Porcine tissue used in this study is relatively immature and is therefore softer and unable to withstand high loads. Angles less than 55 degrees did not cause sufficient damage to the joint tissues where as an angle of 65 degrees resulted in joint dislocation. ML displacement caused cartilage bruising and some labral damage, however results were not consistent between specimens and were not reliable to produce a labral damage model. Therefore, a load of 1500 N combined with an increased cup inclination angle of 60 degrees, with no ML displacement, was found to produce the ultimate test set up for a labral damage model.

Increasing the angle of the acetabular cup translates the loading area closer to the labral-cartilage junction, hence promoting damage to relatively unloaded areas. An increase in cup angle on its own resulted in labral flattening. Labral flattening was not documented on the Lage classification; however it is possible that labral flattening is a preliminary stage to labral damage which is not observed by surgeons as it is asymptomatic. An increase in inclination angle resulted in lower conformity of the hip joint and less acetabular coverage of the femoral head, hence promoting dislocation.

Cartilage bruising identified with increased loads and cup angles was allocated an Outerbridge score of 1 as it was associated with cartilage softening and swelling. Cartilage bruising on the acetabular cup was circular in dimension and predominantly in the superior region of the cup; however bruising to the femoral head formed a stripe in the anterior-posterior direction across the superior region of the head. Stripe wear has been identified in artificial hip joints by Al-Hajjar et al. 2015 as a result of edge loading. During edge loading, the contact area of the head is translated onto the rim of the cup as a result of rotational or translational mal positioning of the cup. Cartilage bruising could be a result of the intended change in alignment of the joint and could provide further information to areas of loading within the joint under various test set ups. However, this should be interpreted with caution as cartilage bruising could be a result of loss in joint conformity. When the femoral head and acetabular cup are concentrically aligned, the load is distributed across the contacting areas. Therefore, when the joint becomes misaligned the load becomes concentrated over a smaller contact area which, in turn increases the stress. Labral flattening was also observed in this test set up, however this level of damage was not significant enough to be used in a labral damage model.

Labral fibrillation at the tissue apex, longitudinal peripheral tears across the labral-cartilage junction and level 3 Outerbridge damage to the acetabular cartilage, were identified at increased cup angles and loads. Cartilage delamination was also identified in some studies where the femoral head dislocated as a direct result of the longitudinal peripheral tear. Labral tears were reported by Song et al. 2012 to reduce the stability of the hip which could result in joint dislocation.

As the joint was enclosed in a gaiter filled with opaque lubricant and was ran over a long time period it was difficult to identify the instance of joint failure to terminate the test prior to joint dislocation therefore, for future tests it was decided to pause the simulator and image the specimens every hour. As the simulator was paused every hour the stages of labral damage were identified. The first stage of labral damage included labral flattening, followed by labral fibrillation and finally longitudinal peripheral tears. Cartilage bruising was observed within the first three hours of testing in all specimens. The labral damage model could be used to assess

the various stages of labral damage, labral treatments, and the effect of labral damage on hip joint function.

A limitation to the study included the use of porcine tissue as opposed to human cadaveric tissue. Although porcine tissue is often used as an *in vivo* model due to its similar structure and mechanical properties (Chapters 3 and 4) as a whole joint model there are significant differences between the species. The pig is a quadrupedal animal therefore; the femur has a higher natural flexion position during standing than the bipedal human. This will result in a variation in the gait cycle during walking between the species as well as different loading patterns through the hip joint. Within this study porcine hips were aligned using the natural alignment of the human hip and subject to the motions of its gait cycle. Ideally the porcine hip would have been aligned and run under its natural alignment to ensure the joint was correctly loaded and to prevent extreme motion however, very little is known about the porcine gait cycle and its contact mechanics. Also, once a successful natural hip and labral damage model was developed a future aim of this project was to use human tissue in the models. In order to undertake this aim the set up and conditions would have to be identical in order to compare results, hence the porcine hips were aligned and run using human criteria.

A second limitation to this study was time. Artificial joint prostheses are often tested using a six-station simulator for minimum of 3 million cycles. As the joints are highly conforming and manufactured to a high tolerance, the joints are able to run continuously unsupervised. However, when testing natural joints they are less predictable, due to the variation between specimens and the degeneration of the tissue therefore, they need to be supervised limiting the time they can be ran for. This dictated the minimum time for testing within this study to 10800 cycles, however ideally this would have been increased, especially in the control groups to ensure no damage would occur after prolonged testing. In order to accelerate joint damage an increased load of 2250 N could have been investigated, which would have reduced the number of test cycles, however this was not possible due to time constraints.

Key findings:

- An *in vitro* hip model was successfully developed using a cup inclination angle of 45 ° and a peak load of 750 N which was run for three hours.
- Increasing the cup inclination angle did not result in labral damage.
- Increasing the load above 2250 N resulted in dislocation of the femoral head from the acetabular cup.
- Increasing the cup inclination angle above 65 ° resulted in high levels of dislocation.

- An *in vitro* labral damage model was developed using an increased cup inclination angle of 55 ° combined with an increased load of 1500 N.

Chapter 6

Overall discussion and conclusions

6.1 General discussion

Due to a lack of suitable methods for in situ assessment of soft tissues in the hip, there is a requirement for the development of a simulation system that can be used to investigate the mechanical and tribological properties of these tissues. Also, due to the simplicity of current labral damage models, there is a further requirement for the development of an advanced labral damage simulation system that can be used to investigate the effects of labral damage in a model that closely replicates *in vivo* conditions. The aims of this project were to develop methodologies for the production of an *in vitro* natural hip model as well as a labral damage model. These models could be developed to assess the mechanical properties of soft tissues in the hip, in situ, as well as investigating the etiology and progression of mechanical labral damage and current or new labral treatments. In order to gain a more detailed understanding of the labrum and potential areas of weakness for damage, biological and mechanical characterisation of the acetabular labrum was also undertaken.

The *in vitro* natural hip and labral damage simulation systems aimed to represent the clinically relevant motions and loads of the hip. The simulation systems were found to accurately produce the demand cycle and the labral damage model was also found to replicate several features of damage observed in hip joints with abnormal morphology, such as radial fibrillation and longitudinal peripheral tears. The *in vitro* natural hip model was developed by aligning the hip under normal *in vivo* conditions, with a Sharp's angle of 45 ° and a peak load of 750 N (modified for the porcine hip), whereas the labral damage model was developed by increasing the Sharp's angle to 60 ° and increasing the load to 1500 N. The natural hip model accurately represented *in vivo* conditions with no damage to the labrum or cartilage identified whereas the labral damage model identified key stages of labral damage.

A fully functioning labral damage model for the mechanical assessment of labral damage and repair techniques would provide a means to assess the long term clinical outcomes of current and new repair methods. Current repair methods have generally evolved from short term outcomes, rather than scientific research so may not be optimised and the long term outcomes remain uncertain. Attempts have been made in the past to develop *in vitro* labral damage models, to assess the effects of labral damage and repair techniques, however, to date they are limited to partial ranges of motion, reduced loading, and relatively short durations. The studies outlined in the literature are summarised in Table 6-1, which details the type of tissue used, the load and motion applied to the tissue, and the duration of testing. Studies by Ferguson et al., (2003); Cadet et al., (2012); Philippon et al., (2014) used whole hip joints to investigate the effect of labral tears on the labral seal and Smith et al., (2011) used a labral damage model to assess the effect on labral strain and hip joint stability. These methods did not accurately replicate *in vivo* test conditions due to the limited load, loading cycle, motion or duration (Table

6-1). Song et al., (2012) and Safran et al., (2011) used an *in vitro* hip joint model to assess the effects of a full and partial labrectomy on cartilage friction and strains across the labrum during hip motion, respectively. Song et al., (2012) applied a rotational motion to the hip joint during loading where as Safran et al., (2011) moved the hip through a range of 36 positions (comprised of a combination of extreme or partial FE, AA, and IE positions) however, no axial load was applied during testing. All tests were carried out for a short time period, with Ferguson et al., (2003) applying the longest load for 1 hour (Table 6-1). The most advanced hip joint model was developed by Groves, (2016) using a whole natural hip joint in a simulator to apply a dynamic load during motion. Although the dynamic load was applied to the joint over a period of two hours, motion was limited to one plane (flexion-extension), the loading pattern was greatly simplified and the hip joint was anatomically inverted. As these tests do not closely mimic *in vivo* conditions, there is a requirement for an advanced *in vitro* natural hip and labral damage model that would allow tests to be carried out, under the full gait cycle and loading pattern for a prolonged period of time.

The advantages of a more advanced labral damage model, using a full gait and load cycle, would provide more representative results, as the effect of localised labral tears may only be seen under specific joint movement. Most frequently patients complain of hip pain, as a result of labral tears, when the hip is flexed and internally rotated, however this could vary depending on the location of the labral tear. During natural motion the hip moves in a combination of flexion-extension, abduction-adduction, and internal-external rotation throughout the load cycle. Therefore, to test the hip joint in a stationary position, *in vivo* conditions are sacrificed and the true effect of labral tears, the labral seal and labral strain are not fully analysed. By developing an *in vitro* simulation model using a full gait cycle, the full effect on the labrum could be investigated more accurately. The only study to apply an *in vivo* load was Philippon et al., (2014), at higher loads the effects on the labrum would likely differ from lower loads tested within the other studies however, all loads applied within these studies did not mimic the full loading cycle within the hip. The hip undergoes various loads throughout the gait cycle, with two peak loads at heel strike and toe-off and a significantly reduced load during the swing phase. During periods of loading, interstitial water is squeezed out of the tissues therefore, the periods of lower loading are required to allow the tissue to recover when the water is drawn back into the tissue. The current model developed in this study, applies a full loading cycle to the hip joint, therefore more accurately modelling *in vivo* conditions.

Table 6-1 Summary of tissue models in literature and current study. Table includes the author, the type of tissue used, the load or pressure applied during the test, and the motion applied during the test. BW - Body weight.

Study	Tissue	Load/pressure	Motion	Duration
Ferguson 2003	Whole hip joint Human	Static & dynamic 0.25-0.75 x BW (~200 – 550 N)	Stationary	1 hr
Cadet 2012	Whole hip joint Human	2-4 psi	Stationary	2 mins
Smith 2011	Whole hip joint Human	10-40 N	Anterior translation to dislocation	N/A
Song 2012	Whole hip joint Human	Static 700 N	9 ° rotation position prior to testing, stationary during test	13 s
Philippon 2014	Whole hip joint Human	Static 2118 N (~2.7 x BW)	Stationary	300 s
Safran 2011	Whole hip joint Human	No load	Extreme or partial FE, AA, IE	N/A
Groves 2016	Whole hip joint Porcine	25-750 N dynamic	FE dynamic	2 h
Current model	Whole hip joint Porcine	750 N dynamic	FE, AA, IE dynamic	3 h

A further advantage of the development of a labral damage simulation system, using a whole hip joint under the full gait cycle, would be in the development of new techniques and therapies. A major disadvantage to the development of surgical techniques is the use of *in vivo* animal models however, there is an ethical desire to reduce, replace or refine the number of animals used within these studies (Guhad, 2005). The simulation system would provide a means of testing a wide range of methods early in the development cycle and reduce the number of *in vivo* animal models required.

One of the major barriers to the successful treatment of labral damage is the limited knowledge of the tissues biological and mechanical properties as well as the damage process. Therefore, a detailed understanding of the labrum's structure and constituents, as well as compressive and tensile properties will aid in the understanding of how the tissue becomes damaged. This knowledge will also help tailor the successful development of suitable damage methods for *in vitro* simulation. Improvements in *in vitro* testing will lead to more accurate testing of treatment

methods, which can be translated directly to the patient. Therefore, an improved knowledge of the labrum and its damage will provide earlier and better interventions and approaches to repairing the tissue, using novel or existing techniques.

Carrying out the tests within this study allowed limitations to be identified, which could have an effect on the result obtained in this study. The limitations discovered in the previous chapters (Chapter 3-5) and the implication they could have on the results will be discussed further in this chapter.

6.2 Tissue selection

Within this study, animal tissue was used due to the limited availability and ethical issues associated with human tissue. The pig hip was chosen as it had previously been reported in the literature to be similar in dimension and geometry to the human hip (Taylor et al., 2011) and previously been used to develop a natural hip joint model (Groves, 2016). However, a limitation of porcine tissue was the age of the tissue, which was determined by the age of the pig available in the commercial food chain. Porcine legs, provided as a product of the meat industry were approximately six months old at slaughter. Immature tissue was identified during sample preparation, where the bone was found to be soft. Immature cartilage has also been reported in the literature to have a different structure to the equivalent mature tissue (Julkunen et al., 2007) and the presence of growth plates were identified in the immature porcine hip by Taylor et al., (2011). Variations in the collagen structure as well as the distribution and concentration of water and GAGs could have an effect on the mechanical properties of the tissue. The mechanical properties of a tissue are governed by its intrinsic structure; including its permeability and GAG content which are responsible for fluid retention and hence, load support (Mow & Huiskes, 2004). Fluid flow governs the load support of a tissue, where fluid becomes trapped within the matrix upon initial loading and slowly squeezes out over time. Therefore, the maturity of the tissue could have an effect on the structure and constituents identified in Chapter 3 and the mechanical properties identified in Chapter 4.

6.3 Biological characterisation

Collagen is the main structural protein in the ECM and accounts for a large portion of the acetabular labrum. GAGs bind to the collagen structure and due to their negative charge, attract interstitial water molecules into the tissue. The structure of collagen was effectively observed using microscopy alongside sirius red histological staining. This part of the study developed one of the first examples of whole labral tissue sections to be visualised in situ, alongside the adjacent cartilage and subchondral bone. Sirius red had previously been used to visualise the structures within cartilage tissue (Kim et al., 2014), however, it had not been used to investigate the microscopic structure of the labrum and its transition to articular cartilage and subchondral bone. The results of the study identified two tissue types within the acetabular labrum; a fibrocartilage inner labral region and a connective tissue outer labral region, which correlated with the findings of Petersen et al., (2003). However, within the present study the junction between the two tissues types was not easily identifiable in the human labrum, especially in comparison with the porcine labrum. As well as an unclear junction in the human tissue, there was more variability between the samples making an overall summary of the tissue regions complex. A study by Owen et al., (1999) used SEM to examine the collagen network at the interfaces between the cartilage, labrum, and bone in sheep acetabula. The interfaces were clearly visible using SEM, however the tissues required multiple fixation methods to image the three interfaces. A limitation to the present biological study was the use of a standard fixation and processing method across all three tissues. Acetabular sections, containing three different tissue types, of both hard and soft material, proved difficult to process using one standard method. This may have resulted in artefacts or reduced visualisation in areas of the tissue. Although the fixation process was optimised for porcine tissue, to improve this study a pilot sample group could have been used to optimise the fixation process for human tissues. This highlighted a further limitation of the study, in relation to sample size. Due to the costs and difficulties in obtaining human tissue, the sample size of each group was limited to six repeats. Reduced sample sizes may have masked patterns in the structures analysed within the tissue as well as preventing the optimisation of tissue processing. A futher limitation of the human samples was the patient demographics, the tissue was harvested from unhealthy patients and therefore may not be representative of typical labral structure.

The results of the quantitative assays were also novel as water, GAG and collagen content had not previously been quantified within the acetabular labrum, to the author's knowledge. It was observed overall that water and GAG content were lower in the acetabular labrum in comparison to the adjacent articular cartilage however, contained higher collagen content. These constituents may indicate the functional properties of the labral tissue to play a supportive role, rather than a load-bearing role as seen in articular cartilage. Further results showed the content of GAGs within the human labrum were significantly lower compared to porcine labrum, with

human labrum almost devoid of GAGs. These results were confirmed by histological staining, using alcian blue dye. Staining of GAGs within the labrum showed the majority of GAGs within the porcine labrum to be contained within the inner fibrocartilage region with slight diffusion into the external labrum, where as human tissue mostly stained negatively for GAGs. Regrettably, it was not possible to analyse the transition of GAGs between the labrum and articular cartilage using histological staining within this study. Pilot studies showed the decalcification process of subchondral bone, using EDTA, removed GAGs from the tissue therefore, prior to staining the labrum was removed from the bone and subsequently from the articular cartilage. To improve this study, alternative processes could have been investigated to either decalcify the tissue, or use fixation methods which would allow calcified bone to be sectioned and stained, such as resin embedding. A study by Donath & Breuner, (1982) identified a method to section calcified bone with soft tissues attached which successfully preserved the soft tissue in situ. If sufficient equipment was available, this method could have been applied to labrum, cartilage and subchondral bone sections within this study.

6.4 Mechanical characterisation

Three methods were primarily considered to determine the compressive properties of the porcine acetabular labrum; indentation, unconfined compression, and confined compression. Ferguson et al., (2001) studied the compressive properties of the bovine labrum using confined compression, where circular discs of labral tissue 3.20 ± 0.06 mm were placed inside a 3.3 mm diameter impermeable stainless steel confining chamber. In this study, labral discs were cut to the required dimension whilst frozen, using a razor cutting die and hollow coring tool. During preliminary tests within the current study, a limitation was identified due to the small size of the porcine labrum. During the cutting process, the tissue became partially defrosted, resulting in reduced consistency in specimen dimensions. Confined compression testing required low clearance between the specimen and chamber to prevent fluid flow from the sides of the specimen therefore, this method was discarded. Indentation and unconfined compression methods were investigated within this study. The methodology used was adapted from a study by Abdelgaied et al., (2015) who investigated the compressive properties of the meniscus in the knee using indentation and unconfined compression. Within this study the compressive properties of labral tissue were analysed in comparison to articular cartilage using indentation and unconfined compression under a high and low load. Initial results using porcine tissue identified unconfined compression under a low load to produce the lowest amount of deformation. Therefore, this method was carried forward for human and cartilage tissue. Although the compressive properties of the bovine labrum had been previously investigated by Ferguson et al 2003, compressive properties of porcine and human tissue were novel to this study. Very little difference was seen in the compressive responses between the porcine and human labrum, however, labral tissue was found to be softer than cartilage resulting in higher deformations. A limitation to the compressive testing of labral tissue was the size and shape of the tissue. The porcine and human labrum are much smaller than the bovine labrum, tested by Ferguson et al., (2003) and hence, due to their triangular shape the size of samples for testing were limited. Small samples require a smaller compressive load in order to maintain the assumption of minimal deformation and hence, the Young's modulus and permeability could not be calculated using this method. Ideally, in future studies a method should be investigated to test the labrum in situ, to remove the effect of loading at the edge in small tissue sections. A lighter load should also be investigated to minimise the deformation of the tissue, so that the assumptions of the computer model can be maintained.

A further novel finding to this part of the study was the tensile properties of the porcine labrum. Although the tensile properties of the human and bovine labrum had previously been investigated by Ferguson et al., (2003) and Ishiko et al., (2005), the porcine labrum has never been studied. Within this study, the porcine labrum was identified to be weaker than the human labrum, with a lower UTS and Young's modulus. Although tensile testing was successfully

carried out within this study, limitations to the method used were identified. Quasi-static test conditions were used in this study to determine the intrinsic properties of the ECM. This required lower strain rates, compared to those seen *in vivo* in order to eliminate the effect of frictional drag as a result of interstitial fluid. Quasi-static test conditions are often used for tensile testing therefore enabling the comparison of results between tissues. Ideally tensile testing should be determined for both quasi-static and *in vivo* test conditions. A further limitation mentioned previously was the failure location of the tensile specimens. Due to the small size of the porcine labrum, dumbbell shaping of the specimens was not possible with the cutting method used in this study. Therefore, further methods should have been investigated for sample preparation that enabled the shaping of the specimens in order to promote centre failure and reduce any effect of the grips on the results. Ferguson et al., (2003) used a cryotome to produce thin sections of labral tissue. Although, this method was attempted in a pilot study using porcine tissue, only one freezing medium and cutting blade was investigated.

6.5 *In vitro* simulation

The aim of the *in vitro* simulation systems was to successfully replicate *in vivo* motion and loading using a whole hip joint in either a standard or abnormal anatomical set up. The standard cup inclination angle was determined from the literature as 45 degrees and the motion and loading patterns were replicated from ISO 14242, which is used during the testing of artificial hip joint replacements (BSI 2014; Harrison et al., 2014). These parameters were identified based on the average human being therefore, a limitation of this study was the use of porcine tissue. The pig is a quadrupedal animal, walking on four legs, hence the natural position, motion and loading of the hip will significantly vary compared to that of the bipedal human. The human gait cycle has been extensively researched however, in comparison, very little is known regarding the porcine gait and load cycle. An assumption can be made from the pig's natural stance position, that the porcine femoral head is greater in flexion in comparison to the human hip. Hence by aligning the hip joint using the average human cup inclination angle the kinematics and kinetics of the hip may be altered. Within this study human parameters were applied to the porcine hip as they were more fully understood and future models using human tissue can be directly compared.

During the preparation process, excess bone and tissue was removed from around the joint and the hip joint was disarticulated to allow the specimens to be cemented within the pots and the surfaces to be inspected for potential damage. Any samples with damage identified prior to testing were discarded from the study. A method was successfully developed to re-align the hip joint using a rig designed in-house. Key features of the hip joint, such as the TAL and ligamentum teres were used to accurately align the hip joint as well as minimising the clearance between the articulating surfaces. A study by Lizhang et al., (2013) identified that an increased clearance of as little as 1 mm approximately doubled the contact stresses within a hemiarthroplasty. Therefore, although the hips appeared successfully aligned a slight mis-alignment, not detectable to the eye, could have significant effects on the stresses within the hip. Studies in the literature using whole hip joint utilise bony landmarks of the pelvis and femur to align the joints (Safran et al., 2011; Smith et al., 2011; Cadet et al., 2012; Song et al., 2012), and Philippon et al., (2014) further aligned the hip using pins however, all the studies also remove the excess tissue around the joint losing natural alignment of the hip. Safran et al., (2011) developed a method using MRI to identify labral damage without removing the joint capsule and disarticulating the joint and a study by Van Arkel et al., (2015) investigated the contributing factors of the external hip ligaments on restraint to hip rotation. It was identified that each capsular ligament acted as a restraint to rotation at some point in the gait cycle. Therefore, in order to improve this study a method should be investigated to keep the hip intact, allow damage to be identified prior to testing and maintain as much of the external bones and soft tissue as possible. By maintaining an intact joint capsule, natural joint lubrication will also be

improved due to the encapsulated synovial fluid, hence, mimicking *in vivo* conditions more accurately.

Cartilage damage has been extensively assessed *in vivo* and various grading systems have been developed including the Outerbridge, Bentley, Casscells, and insall grading systems. The grading systems are used to identify various types of damage and produce a more consistent method for comparing damage between patients and diseases. More recently a grading system has been developed to assess damage found in the acetabular labrum (Lage et al., 1996). Grading systems were used within this study, to identify the stages and extent of labral and cartilage damage, within the natural hip and labral damage models. Not only was labral damage successfully replicated, stages of labral damage were also identified in the form of labral flattening, followed by labral fibrillation and finally longitudinal peripheral tears. These results were novel, as stages of labral damage have not previously been identified to this level of detail. A study by Beck et al., (2005) identified damage patterns associated with the type of impingement found in the hip but did not identify the progressive stages of damage. Although these grading systems were successful in identifying key stages and types of damage, limitations exist as they are subjective to the grader analysing the damage. The grades assigned may vary between graders particularly when the level of damage is close to the boundary of two criteria, even if previous training has been undertaken. This was evident in initial analysis of ML displacement data when grading was carried out by a separate grader. Therefore the data was reanalysed by the author so all data was consistently analysed. Although all data was consistently analysed within this study making comparisons between various set ups consistent, variations between this study and the literature could still exist, especially when compared with a clinical specialist who would be more familiar with the types of tears. In order to improve the accuracy of grading, a larger number of graders could have been used and an average score taken. In future studies of this nature, ideally three or four graders should analyse the samples and if possible the graders should be familiar with acetabular damage.

The observation of damage was assessed using the Outerbridge and Lage classification system from a series of images taken of the specimens. The protocol developed for imaging the specimens was successful in allowing all the tissues surface to be visualised in detail. However, the uses of a more advanced method, such as surface metrology, in addition to the classification systems, would have provided quantitative analysis of damage and possible identification of smaller damage not easily visible to the eye. Groves, (2016) developed a method for assessing surface damage using Microset® replicas and 2D contact profilometry with Talymap Gold software.

As discussed previously, the *in vitro* labral damage simulation system successfully replicated types of damage observed clinically. However, a major limitation to this study was the location

of the damage identified. Within the literature, it has been reported that the majority of labral tears are located in the anterior region of the acetabulum (Narvani, 2003). However, the damage seen within this study was isolated to the superior region of the acetabulum. This was a result of the load directly translated to the superior edge of the acetabulum, either as a result of ML displacement or increased cup inclination angle. ML displacement and increased cup inclination angle were investigated either with or without an increased load to induce damage. These methods were chosen as ML displacement indirectly increases the load by concentrating the area of loading and increased cup inclination angle causes edge loading, which has been seen to result in damage in artificial hip replacements (Fisher, 2011; Lizhang et al., 2013). An increased load was thought to accelerate damage and hence reduce the number of cycles required to initiate damage. This resulted in a limitation to the study as these methods did not directly replicate the way in which damage is caused by abnormal hip joint morphology. Damage seen in diseases such as FAI is a result of a cam or pincer impingement which, as mentioned previously, is caused by a bony growth on either the femoral head-neck or acetabular rim (Clohisy et al., 2010). The labral damage model could have been improved by mimicking a cam or pincer impingement which may have replicated damage locations seen *in vivo*. A possible method to replicate a cam or pincer impingement would have been to use a 3D printed bony growth on either the femoral head or acetabular cup, however this would minimise the advantages of using a completely natural hip model, as seen in this study.

6.6 Future work

This study is the first, in which a whole natural hip joint has been successfully included in a simulation system *in vitro*, under a full gait and load cycle. It is also the first, in which a labral damage model has been successfully developed and which replicates various stages of labral damage, using the full gait and load cycle. This study has the potential to lead to future studies in order to gain a more in depth understanding of the acetabular labrum in situ, and more accurately replicate the effect of labral damage on the function of the hip joint.

Ideally, any future studies should include a high replicate number of at least ten repeats. This would minimise the effect of the high variability within natural tissue. In addition, the age of porcine tissue for use in tissue characterisations and *in vitro* simulation should be investigated, to determine the effect of using immature porcine tissue and potentially identify a more suitable tissue.

The biological study could be expanded to include more replicates within the quantitative assays which may have produced stronger trends either between the tissue types or between the specimens. Initial trends were identified within this study, however they were not always found to be significant due to the variation between specimens. Damaged specimens could also be investigated using the stains mentioned in this study and compared to healthy tissue to determine the effect on collagen structure as well as GAG and water content.

Additional collagen types could have been investigated, to identify the presence of additional structures within the labrum such as blood vessels and nerves. Previous studies have identified the presence of blood vessels and nerves in the perimeter of the acetabular labrum however, this has not been carried out for porcine tissue (Kelly et al., 2005).

Various microscopy methods could be used to achieve more detailed visualisation of the structure and constituents of labral tissue. Multiphoton imaging or SEM would provide a more detailed view of the collagen fibres however, they would be limited to a smaller area. Therefore a combination of multiphoton imaging or SEM as well as histology would provide a more comprehensive understanding of the collagen alignment within the labrum. Studies investigating the collagen structure within the labrum have focused on SEM (Shibutani, 1988; Owen et al., 1999; Petersen et al., 2003) however, multiphoton imaging has not been used to visual the labral structure even though it has proven successful for other soft tissues (Schenke-Layland, 2008; Mansfield et al., 2015). Schenke-Layland, (2008) used multiphoton imaging to look at the ECM of various tissues types including; cartilage, heart valve, and exocrine, where as Mansfield et al., (2015) used multiphoton imaging with two-photon fluorescence and second harmonic generation to identify the microstructural response of cartilage during loading. TEM combined

with cupermuronic blue staining could also be used to visualise the dispersion of GAGs across the labral-cartilage junction.

In order to improve the biomechanical characterisation of labral tissue in this study, compression tests with lighter loads should be investigated, which would allow the elastic modulus and permeability of the porcine and human labrum to be determined. Micro-indentation has previously been carried out to determine the mechanical properties of small and soft tissues (Mahoney et al., 2000; Zamir & Taber, 2004; Cao et al., 2006). Cao et al., (2006) determined the compressive properties of mouse articular cartilage using micro-indentation and a biphasic finite element model. Adaptations to the current compression rig should also be investigated to reduce the load of the shaft, as this was proven in this study to reduce the deformation considerably.

Additionally, methods should be investigated to more accurately cut labral tissue, in order to carry out confined compression of labral tissue, which would allow results to be directly compared to those carried out by Ferguson et al., (2003). Ferguson et al., (2003) developed a method for cutting labral tissue using a cryotome and corer, whilst the tissue was frozen. Although frozen specimens were utilised within this study during sample preparation, initial studies using a cryotome were unsuccessful and should therefore be further investigated. Using a cryotome would allow the specimen to remain frozen whilst cutting, therefore improving the accuracy of the specimen dimensions, as the tissue would be more rigid. Labral tissue cut with a cryotome could also be used for improving tensile testing of labral tissue within this study. The majority of samples failed at the grips within this study, and although this was shown to not impact on the test results on tendons by Ng et al., (2005), centre failure should be further investigated to identify the effects within labral tissue. In using a cryotome, specimens could be cut more accurately and to smaller dimensions. Thinner specimens would be easier to shape into dumbbells, which promotes centre failure.

In addition to natural labral tissue, it would also be beneficial to determine the compressive and tensile properties of damaged labral tissue. This could be implemented by placing various lengths or orientations of cuts in the labral tissue prior to testing as seen in studies by Ferguson et al., (2003); Safran et al., (2011); Cadet et al., (2012); Song et al., (2012); and Philippon et al., (2014) or by using various stages of damaged tissue from the *in vitro* labral damage model developed in this study.

In the future, it will possible for the *in vitro* natural hip model, developed in this study, to be used for analysis of the biomechanical properties of the acetabular labrum. The model could be developed to study the frictional properties as well as the compressive and tensile strengths of the labrum, in situ. Ideally in future tests, the joints would be run for a longer length of time, however due to the joint being enclosed in a gaiter filled with serum, the bones become

saturated and soft after a prolonged time. Therefore, the development of a model with an intact joint capsule would allow for natural lubrication of the joint and remove the need for artificial serum. By further including the surround soft tissues and bone, the forces on the hip joint will be more accurate. This would require further development of the model and the set up process to allow the hip to be anatomically aligned and any damage to be identified prior to testing, without the visualisation of the joint.

The labral damage model could be used to more accurately test the effects of labral damage on labral strain, cartilage friction, and hip joint stability. The tests developed by Safran et al., (2011); Smith et al., (2011); and Song et al., (2012) could be progressed to be tested with *in vivo* conditions under the full load and gait cycle of the hip, using the models produced in this study. Also, by developing a method which would keep the joint capsule intact, the effects of labral damage on the labral seal could be performed in studies similar to Ferguson et al., (2003); Cadet et al., (2012); and Philippon et al., (2014).

The *in vitro* simulation study would have been improved by including more replicates, especially in the method development stages of the labral damage model. Various set up methods were discarded after a limited number of repeats due to the samples rapid failure, however due to the variations in samples, a larger number of replicas should have been used to fully rule out each set up group. A larger number of graders would also have been advantageous to provide more accurate grading of the tissues, additionally graders more familiar with acetabular damage would be beneficial. Finally, a further development of the *in vitro* simulation systems produced in this study, would be the use of human tissue, to determine if the same damage processes occur in both species. As the human hip is larger than the porcine hip, higher cup inclination angles could also be investigated as well as higher loads to represent *in vivo* human loading conditions. It may also be possible to obtain human hips with cam or pincer growths or labral tears already present, which could be used to compare to the results determined in this study.

In the future the models developed in this study may reduce the number of animals used for testing novel repair techniques for labral tissue. In addition, the range of biological and biomechanical properties determined in this study will be useful for use in computer models of the soft tissues in the acetabulum. The study as well as highlighting the success, has also identified methods which require further development to give an even greater understanding of the labrum.

6.7 Overall conclusion

In conclusion, this study represents a major step forward in the development of natural hip models and the understanding of the labrum and labral damage. The methods presented here are currently the most advanced known for natural hip and labral modelling, with the *in vivo* conditions replicated in terms of the full gait and load cycle. However, issues with mechanical testing need to be further investigated to gain a fuller understanding of the porcine and human labrum. This study has contributed largely to the knowledge and understanding of the structure, function and damage of the labrum and the models will provide a basis for the future development of biomechanical testing of soft tissues in situ. Research into this tissue was previously very limited and much of the work carried out was related to the effect of labral tears on various functions of the hip.

Appendices

Appendix A – Materials

Equipment used and their suppliers.

Equipment	Model	Supplier
Autoclave	Tactrol 2	**Priorclave**
Automatic pipettes	12.5 ml	**Eppendorf**
Balances	GR200	**A&D Instruments**
Bench top centrifuge	Micro centaur MSE	**Sanyo**
Class II fume cabinet	Airone-R recirculating fume cabinet	**Safelab**
Digital SLR camera	EOS 550D	**Canon**
Dissection kit	Various	**Thackeray**
Fine tip stainless steel forceps	E12	**Raymond A lamb Ltd**
Freeze dryer	Savant ModulyoD	**Thermo**
Freezer (-20°C)	Electrolux 3000	**Jencons PLC**
Freezer (Human tissue)	Biomedical freezer	**Sanyo**
Fridge	Electrolux ER8817C	**Jencons PLC**
Fume hood	Recirculating fume cabinet	**SafelLab**
Fume hood (human)	Cell guard biological safety cabinet	**NuAire**
Hacksaw	N/A	**Thackray Instruments**
Hot plate	E18.1 hotplate	**Raymond A Lamb**
Material testing machine	3365	**Instron**
Indentation material testing machine	N/A	**In-house**
Linear variable differential transformer (LVDT)	RDP D5-200H	**Electrosence**
Magnetic stirrer	SB161 - 3	**Stuart scientific**

Magnetic stirrer bar	FB55593	**Fisher Scientific**
Micro-plate spectrophotometer	Multiskan Go	**Thermo Scientific**
Microscope (upright)	AX10	**Carl Zeiss**
Microscope camera	AxioCam MRc5	**Carl Zeiss**
Microtome	RM 2125 RTF	**Leica Microsystems (UK) Ltd**
Microtome blades	S35	**Raymond A Lamb Ltd**
Orbital incubator	S150	**Staurt**
OriginPro	9.1	**OriginLab**
pH meter	3510	**Jenway Ltd**
Piezoelectric force transducer	060-1896-02	**Electrosence**
Pipette boy	Integra acu	**Integra Bioscience**
Rat-toothed forceps	N/A	**Thackray Instruments**
Scales	CS series 5000 g	**Ohaus**
Scalpel holder	(4) 6091	**Swann Morton**
Hip simulator	Single station hip simulator	**ProSim**
Slide holder	E102	**Raymond A Lamb**
Surgical blades	(22) non-sterile	**Swann Morton**
Surgical scissors	N/A	**Thackray Instruments**
Standard forceps	N/A	**Thackray Instruments**
Table Shaker	802/TW	**Luckham Ltd**
Tissue processor	TP1020	**Leica Microsystems**
Vacuum pump	RV8	**Edwards**
Water bath	G352	**Grant**
Water purifier	Reservoir 75L	**ELGA**
Wax dispenser	E66	**Raymond A Lamb**
Wax oven	Windsor E18/31	**Raymond A Lamb**

Chemicals and reagents used and their suppliers.

Chemical/Reagent	Supplier
1,9 dimethylene blue	Sigma-Aldrich
Alcian blue	Atom Scientific
Aqueous periodic acid solution 0.1%	Sigma-Aldrich
Bovine serum albumin	Sigma-Aldrich
Calcium acetate	Thermo Fisher Scientific Ltd
Chloramine T	Sigma-Aldrich
Chondroitin sulphate B	Sigma-Aldrich
Citric acid	VWR International
Collagen I antibody MAB3391	Millipore
Collagen II antibody MAB 1330	Millipore
Diastase	Sigma-Aldrich
Di-sodium hydrogen orthophosphate	VWR International
DPX mountant	Thermo Fisher Scientific Ltd
Dulbecco's PBS tablets*	Oxoid
Eosin	VWR International
Ethanol	VWR International
Ethylenediaminetetraacetic acid (EDTA)	Fisher Scientific
Formic acid	Sigma-Aldrich
Glacial acetic acid	VWR International
Haematoxylin (Gills no 3)	Sigma-Aldrich
Haematoxylin (Mayers)	Thermo Fisher Scientific Ltd
Haematoxylin (Weigert's)	Atom Scientific
Histo-Clear III	National Diagnostics
Hydrochloric acid	VWR International
Hydrogen peroxide	Sigma-Aldrich
IgG1 kappa isotype	Dako
ImmEdge Hydrophobic barrier pen	Vector laboratories
L-cyceine hydrochloride anhydrous	Sigma-Aldrich
L-glutamine	Invitrogen Ltd/Lonza
Methylated spirits	Biostains Ready Reagents
Miller's stain	Raymond A Lamb
Neutral buffered formalin (10% v/v)	Sigma-Aldrich
Oxalic acid	VWR International

Papain	**Sigma-Aldrich**
Paraffin wax pellets	**Thermo Fisher Scientific Ltd**
PBS tablets	**Oxoid**
p-dimethylaminobenzaldehyde	**Sigma-Aldrich**
Pepsin (general purpose grade)	**Fisher Scientific**
Perchloric acid (60%)	**BDH**
pH standards (4, 7, 10)	**Scientific Laboratory Supplies Ltd**
Picric acid	**Sigma-Aldrich**
PMMA bone cement	**Centri-base**
Potassium permanganate	**Thermo Fisher Scientific Ltd**
Propan-1-ol	**VWR International**
Proteinase K	**Dako Ltd**
Schiffs reagent	**Sigma-Aldrich**
Scott's tap water	**Thermo Fisher Scientific Ltd**
Sirius red	**VWR international**
Sodium acetate	**Thermo Fisher Scientific Ltd**
Sodium azide	**G Biosciences**
Sodium chloride	**Thermo Fisher Scientific Ltd**
Sodium di-hydrogen orthophosphate	**VWR International**
Sodium formate	**VWR International**
Sodium hydroxide (6 M)	**VWR International**
Sodium hydroxide	**Thermo Fisher Scientific Ltd**
Sodium hydroxide pellets	**Fisher Scientific**
Superglue	**Loctite 3030**
Trans-4-hydroxy-L-proline	**Sigma-Aldrich**
TriGene disinfectant	**Scientific Laboratory Supplies Ltd**
Trizma base	**Sigma-Aldrich**
Tween 20	**Sigma-Aldrich**
UltraVision One detection system, HRP polymer (ultra V Block, Ultravision One HRP Polymer)	**Thermo Fisher Scientific Ltd**
UltraVision One large volume detection system, DAB plus substrate (DAB Plus substrate, DAB Plus chromogen	**Thermo Fisher Scientific Ltd**
Virkon disinfectant	**Scientific Laboratory Supplies Ltd**
Xylene	**Biostains Ready Reagents**

Zinc acetate	**Sigma-Aldrich**
Zinc chloride	**Fluka**

* PBS was prepared by dissolving one PBS tablet per 100 ml of sterile distilled water.

Consumables used and their suppliers.

Item	Model/Size	Supplier
Beakers	Various	Pyrex
Bijous	5ml	Bibby Sterlin Ltd
Bottles (Duran)	100 ml, 1000 ml, 2000 ml	Simax
Coplin jar	60 ml	Raymond A Lamb
Gaiter	Custom made	SimSol
Glass cover slips	No. 1 22 x 64 mm	Scientific laboratory supplies
Glass slides	J1800 AMNZ 25 x 75 x 1 mm	Thermo Scientific
Glass troughs	E105	Raymond A Lamb
Histology cassettes	M490-2	Simport
Histology moulds	E.10.8/4161	Raymond A Lamb
Jubilee clip	Stepless clamps spring/screw	Oeiker
Measuring cylinders	Vaious	Azlon
Nitrile gloves	PFR250	EcoShield
Paint brush	No 6 E6	Raymond A Lamb
Pipettes	5 ml, 10 ml, 25 ml Sterile R	Sarstedt
Pipette tips	2 µl, 20 µl, 200 µl, 1000 µl	Alpha Laboratories Ltd/Star Lab
Plastic pasteurs	2655111	VWR International
Pots	60ml, 150ml, 250ml	Bibby Sterlin Ltd
Specimen containers	60 ml, 150 ml, 250 ml	Scientific Laboratory Supplies Ltd
Test tubes		
Universals	25ml	Bibby Sterlin Ltd
Vented cap for rimless tube (Bacti-Cap)	FB51367	Fisher Scientific
Well plate, Nunc®	96-well flat bottomed	Scientific laboratory supplies

Appendix B – Mechanical drawings

Mechanical drawings of the acetabular cup holder

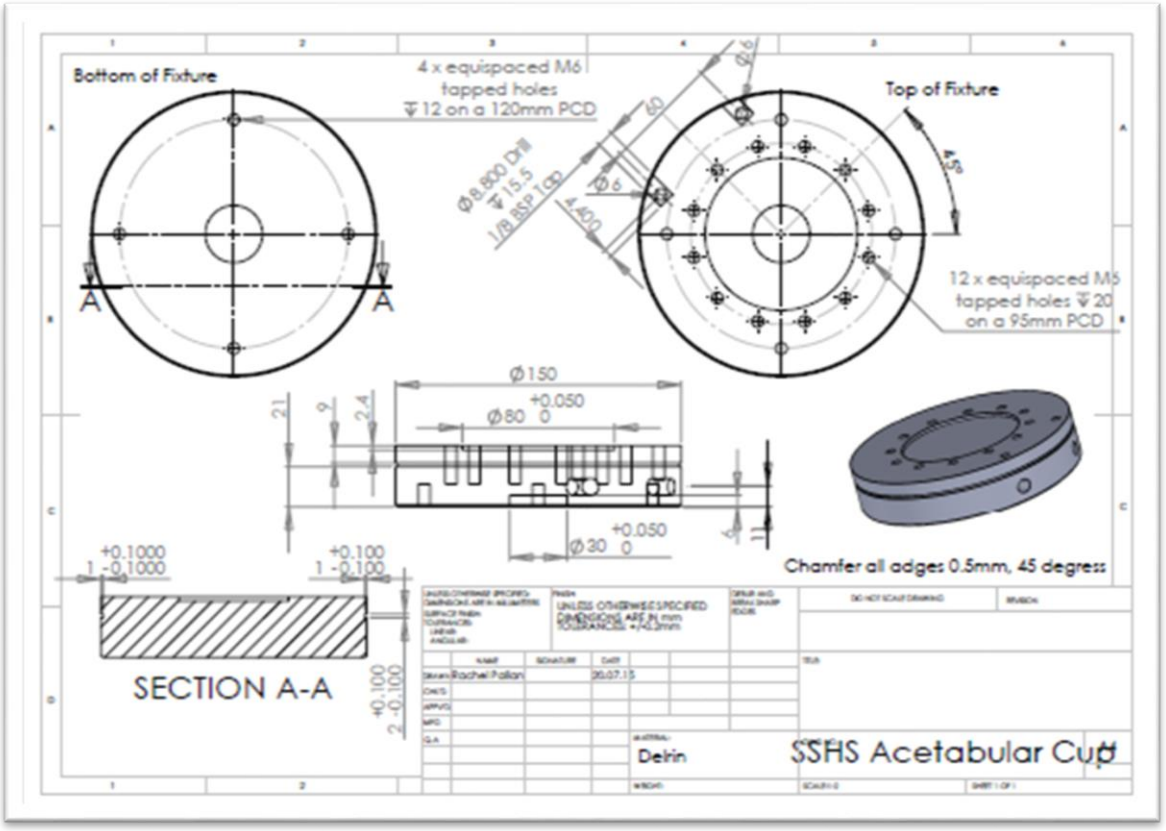

Mechanical drawings of the femoral holder

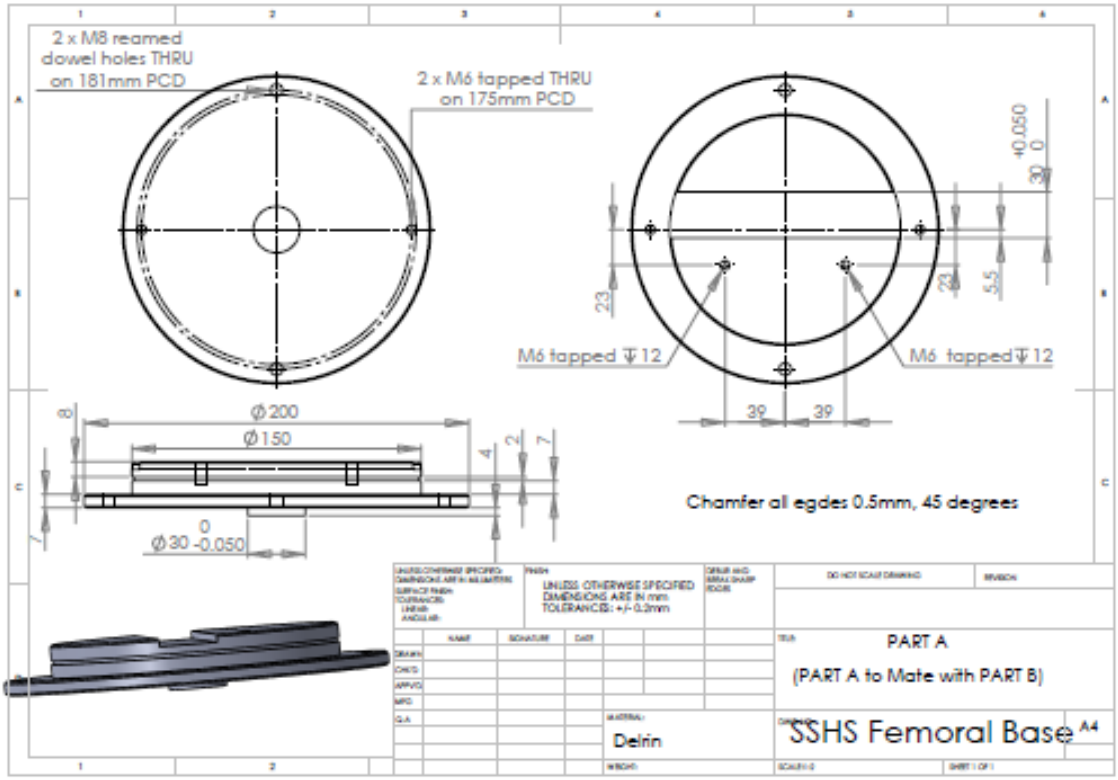

References

Abdelgaied, A. et al., 2015. Comparison of the biomechanical tensile and compressive properties of decellularised and natural porcine meniscus. *Journal of Biomechanics*, 48(8), pp.1389–1396.

Al-Hajjar, M. et al., 2016. Wear of composite ceramics in mixed-material combinations in total hip replacement under adverse edge loading conditions. *Journal of Biomedical Materials Research - Part B Applied Biomaterials*, Epub. Available at: http://doi.wiley.com/10.1002/jbm.b.33671.

Al-Obaid, Y.F., Bangash, F.N. & Bangash, T., 2007. *Trauma-An Engineering Analysis: With Medical Case Studies Investigation*, Springer.

Altman, R.D., 1987. Overview of osteoarthritis. *The American Journal of Medicine*, 83(4B), pp.65–69.

Anderst, W.J. & Tashman, S., 2009. The association between velocity of the center of closest proximity on subchondral bones and osteoarthritis progression. *Journal of Orthopaedic Research*, 27(1), pp.71–77.

Andriacchi, T.P. et al., 2004. A framework for the in vivo pathomechanics of osteoarthritis at the knee. *Annals of Biomedical Engineering*, 32(3), pp.447–457.

Andriacchi, T.P. & Dyrby, C.O., 2005. Interactions between kinematics and loading during walking for the normal and ACL deficient knee. *Journal of Biomechanics*, 38(2), pp.293–298.

Arden, N.K., Arden, E. & Hunter, D., 2008. *Osteoarthritis*, Oxford University Press.

Armstrong, C.G. & Mow, V.C., 1982. Variations in the intrinsic mechanical properties of human articular cartilage with age, degeneration, and water content. *The Journal of bone and joint surgery. American volume*, 64(1), pp.88–94.

Arokoski, J.P. et al., 2000. Normal and pathological adaptations of articular cartilage to joint loading. *Scandinavian journal of medicine & science in sports*, 10(4), pp.186–98.

Arthritisresearchuk.org, 2009. Arthritis information | Arthritis Research UK. Available at: http://www.arthritisresearchuk.org/arthritis-information.aspx?gclid=CL_Np96a6LMCFebLtAod0V0AoA [Accessed November 24, 2012].

Athanasiou, K., Darling, E. & Hu, J., 2010. *Articular Cartilage Tissue Engineering*, Morgan & Claypool Publishers.

Athanasiou, K.A., Darling, E.M. & Hu, J.C., 2010. Articular Cartilage Tissue Engineering. *Synthesis Lectures on Tissue Engineering*, 35(3), pp.411–182.

Audenaert, E.A. et al., 2012. Histologic assessment of acetabular labrum healing. *Arthroscopy - Journal of Arthroscopic and Related Surgery*, 28(12), pp.1784–1789.

Bader, D.L. et al., 1992. The effects of selective matrix degradation on the short-term compressive properties of adult human articular cartilage. *Biochimica et biophysica acta*, 1116(2), pp.147–154.

Bank, R.A. et al., 1998. Ageing and zonal variation in post-translational modification of collagen in normal human articular cartilage. The age-related increase in non-enzymatic

glycation affects biomechanical properties of cartilage. *The Biochemical journal*, 330(Pt 1), pp.345–351.

Bauer, R., Kerschbaumer, F. & Poisel, S., 1996. *Atlas Of Hip Surgery*, Thieme.

Beck, M. et al., 2005. Hip morphology influences the pattern of damage to the acetabular cartilage: femoroacetabular impingement as a cause of early osteoarthritis of the hip. *J Bone Joint Surg [Br]*, 87(7), pp.1012–18.

Berry, D.J. & Lieberman, J., 2012. *Surgery of the Hip*, Elsevier Health Sciences.

Bharam, S., 2006. Labral tears, extra-articular injuries, and hip arthroscopy in the athlete. *Clinics in sports medicine*, 25(2), pp.279–92, ix.

Blankenbaker, D.G. et al., 2007. Classification and localization of acetabular labral tears. *Skeletal radiology*, 36(5), pp.391–7.

Bowman, K.F., Fox, J. & Sekiya, J.K., 2010. A clinically relevant review of hip biomechanics. *Arthroscopy : the journal of arthroscopic & related surgery : official publication of the Arthroscopy Association of North America and the International Arthroscopy Association*, 26(8), pp.1118–29.

Bredella, M.A., 2011. *Imaging of the Hip, An Issue of Magnetic Resonance Imaging Clinics.*, Elsevier Health Sciences.

BSI, 2014. BS ISO 14242-1:2014 Implants for surgery - wear of total hip-joint prostheses. *International Standard*.

Bucholz, R.W., 2012. *Rockwood and Green's Fractures in Adults: Two Volumes Plus Integrated Content Website (Rockwood, Green, and Wilkins' Fractures)*, Lippincott Williams & Wilkins.

Buckley, M.R. et al., 2008. Mapping the depth dependence of shear properties in articular cartilage. *Journal of biomechanics*, 41(11), pp.2430–2437.

Cadet, E.R. et al., 2012. Investigation of the preservation of the fluid seal effect in the repaired, partially resected, and reconstructed acetabular labrum in a cadaveric hip model. *The American journal of sports medicine*, 40(10), pp.2218–23.

Callaghan, J.J., 2003. *The adult knee. 1*, Lippincott Williams & Wilkins.

Cameron, M.L., Briggs, K.K. & Steadman, J.R., 2003. Reproducibility and reliability of the outerbridge classification for grading chondral lesions of the knee arthroscopically. *The American journal of sports medicine*, 31(1), pp.83–6.

Cao, L. et al., 2006. Compressive properties of mouse articular cartilage determined in a novel micro-indentation test method and biphasic finite element model. *Journal of biomechanical engineering*, 128(5), pp.766–771.

Chevalier, X., 1993. Fibronectin, cartilage, and osteoarthritis. *Seminars in arthritis and rheumatism*, 22(5), pp.307–18.

Clarkson, H.M., 2005. *Joint Motion and Function Assessment: A Research-based Practical Guide*, Lippincott Williams & Wilkins.

Clohisy, J.C., St John, L.C. & Schutz, A.L., 2010. Surgical treatment of femoroacetabular impingement: a systematic review of the literature. *Clinical orthopaedics and related research*, 468(2), pp.555–64.

Cole, B.J. & Malek, M.M., 2004. *Articular Cartilage Lesions: A Practical Guide to Assessment*

and Treatment, Springer.

Conditions, N.C.G.C. for A. and C. & NICE, 2008. Osteoarthritis. Available at: http://www.nice.org.uk/CG59 [Accessed November 24, 2012].

D'Antonio, J.A. & Dietrich, M., 2006. *Bioceramics and Alternative Bearings in Joint Arthroplasty: 10th BIOLOX Symposium. Washington D.C., June 10-11, 2005.*, Springer.

Dinauer, P.A., Murphy, K.P. & Carroll, J.F., 2004. Sublabral sulcus at the posteroinferior acetabulum: a potential pitfall in MR arthrography diagnosis of acetabular labral tears. *AJR. American journal of roentgenology*, 183(6), pp.1745–53.

Donath, K. & Breuner, G., 1982. A method for the study of undeealeified bones and teeth with attaehed soft tissues *. *Journal of Oral Pathology*, 11(4), pp.318–326.

Dooley, P.J., 2008. Femoroacetabular impingement syndrome: Nonarthritic hip pain in young adults. *Canadian family physician Médecin de famille canadien*, 54(1), pp.42–7.

Dowson, D. et al., 2004. A hip joint simulator study of the performance of metal-on-metal joints: Part II: Design. *Journal of Arthroplasty*, 19(8), pp.124–130.

Drake, R.L., Vogl, A.W. & Mitchell, A.W.M., 2012. *Gray's Basic Anatomy*, Elsevier Health Sciences.

Dy, C.J. et al., 2012. Etiology and Severity of Impingement Injuries of the Acetabular Labrum : What Is the Role of Femoral Morphology ? *Orthopedics*, 35(6), pp.778–784.

Edwards, C. a & O'Brien, W.D., 1980. Modified assay for determination of hydroxyproline in a tissue hydrolyzate. *Clinica chimica acta; international journal of clinical chemistry*, 104(2), pp.161–167.

Elices, M., 2000. *Structural Biological Materials: Design and Structure-Property Relationships*, Elsevier.

Eroschenko, V.P., Ph.D. & Fiore, M.S.H. di, 2012. *DiFiore's Atlas of Histology With Functional Correlations*, Lippincott Williams & Wilkins.

Ferguson, S.J. et al., 2003. An in vitro investigation of the acetabular labral seal in hip joint mechanics. *Journal of biomechanics*, 36(2), pp.171–8.

Ferguson, S.J. et al., 2000. The acetabular labrum seal: a poroelastic finite element model. *Clinical Biomechanics*, 15(6), pp.463–468.

Ferguson, S.J. et al., 2000. The influence of the acetabular labrum on hip joint cartilage consolidation: a poroelastic finite element model. *Journal of biomechanics*, 33(8), pp.953–60.

Ferguson, S.J., Bryant, J.T. & Ito, K., 2001. The material properties of the bovine acetabular labrum. *Journal of orthopaedic research : official publication of the Orthopaedic Research Society*, 19(5), pp.887–96.

Fermor, H., 2013. *Engineering of natural cartilage substitution biomaterials*.

Fisher, J., 2011. Bioengineering reasons for the falure of metal-on-metal hip prostheses. *The bone & joint journal*, 93, pp.1001–1004.

Frankel, V.H. & Pugh, J.W., 1984. *Surgery of the Hip Joint* R. G. Tronzo, ed., New York, NY: Springer New York.

Ganz, R., 2006. Labral Refixation for Femoro-Acetabular Impingement. *Video Journal of*

Orthopaedics, 4070.

Ganz, R. et al., 2008. The etiology of osteoarthritis of the hip: an integrated mechanical concept. *Clinical orthopaedics and related research*, 466(2), pp.264–72.

Goertzen, D.J., Budney, D.R. & Cinats, J.G., 1997. Methodology and apparatus to determine material properties of the knee joint meniscus. *Medical engineering & physics*, 19(5), pp.412–419.

Goldring, M.B. & Marcu, K.B., 2009. Cartilage homeostasis in health and rheumatic diseases. *Arthritis research & therapy*, 11(3), p.224.

Grana, W.A. & Fischer, S.J., 2006. AAOS - OrthoInfo. Available at: http://orthoinfo.aaos.org/ [Accessed November 24, 2012].

Grant, A.D., Sala, D.A. & Davidovitch, R.I., 2012. The labrum: Structure, function, and injury with femoro-acetabular impingement. *Journal of Children's Orthopaedics*, 6(5), pp.357–372.

Grodzinsky, A.J. et al., 2000. Cartilage Tissue Remodeling in Response to Mechanical Forces. *Annual Review of Biomedical Engineering*, 2, pp.691–713.

Groves, D., 2016. *Geometric variances in hip oseoarthritis ad tribology of the natural hip*. Univeristy of Leeds.

Guhad, F., 2005. Introduction to the 3Rs (Refinement , Reduction and Replacement). *American Association for Laboratory Animal Science*, 44(2), pp.58–59.

Harrison, C.L. et al., 2014. Research Synthesis of Recommended Acetabular Cup Orientations for Total Hip Arthroplasty. *Journal of Arthroplasty*, 29(2), pp.377–382.

Hefti, F., 2007. *Pediatric Orthopedics in Practice*, Springer.

Henak, C.R. et al., 2011. Role of the acetabular labrum in load support across the hip joint. *Journal of biomechanics*, 44(12), pp.2201–6.

Herbert, A. et al., 2016. Bi-linear mechanical property determination of acellular human patellar tendon grafts for use in anterior cruciate ligament replacement. *Journal of Biomechanics*, 49(9), pp.1607–1612.

HipDysplasia.org, 2012. Adult Hip Dysplasia - Signs and Symptoms | International Hip Dysplasia Institute. Available at: http://www.hipdysplasia.org/adult-hip-dysplasia/adult-signs-and-symptoms/ [Accessed November 24, 2012].

Hochberg, M.C. et al., 1995. Guidelines for the medical management of osteoarthritis. Part I. Osteoarthritis of the hip. American College of Rheumatology. *Arthritis and rheumatism*, 38(11), pp.1535–40.

Ikada, Y., 2006. *Tissue Engineering: Fundamentals And Applications (Google eBook)*, Academic Press.

Ishiko, T., Naito, M. & Moriyama, S., 2005. Tensile properties of the human acetabular labrum - The first report. *Journal of Orthopaedic Research*, 23(6), pp.1448–1453.

Jaberi, F.M. & Parvizi, J., 2007. Hip pain in young adults: femoroacetabular impingement. *The Journal of arthroplasty*, 22(7 Suppl 3), pp.37–42.

Jin, Z.M. et al., 2000. Frictional behaviour of bovine articular cartilage. *Biorheology*, 37(1,2), pp.57–63.

Johnson, D.H. et al., 2007. *Practical Orthopaedic Sports Medicine & Arthroscopy*, Lippincott Williams & Wilkins.

Johnson, K. et al., 2004. *Spotlight Science: 9, Book 9*, Nelson Thornes.

Joshi, M.D. et al., 1995. Interspecies variation of compressive biomechanical properties of the meniscus. *Journal of biomedical materials research*, 29(7), pp.823–8.

Julkunen, P. et al., 2007. Characterization of articular cartilage by combining microscopic analysis with a fibril-reinforced finite-element model. *Journal of biomechanics*, 40(8), pp.1862–70.

Junqueira, L.C.U., Montes, G.S. & Sanchez, E.M., 1982. The influence of tissue section thickness on the study of collagen by the picrosirius-polarization method. *Histochemistry*, 74(1), pp.153–156.

Kadler, K.E. et al., 1996. Collagen fibril formation. *The Biochemical journal*, 316(Pt 1), pp.1–11.

Katta, J. et al., 2008. Biotribology of articular cartilage--a review of the recent advances. *Medical engineering & physics*, 30(10), pp.1349–63.

Kelly, B.T. et al., 2005. Vascularity of the hip labrum: a cadaveric investigation. *Arthroscopy : the journal of arthroscopic & related surgery : official publication of the Arthroscopy Association of North America and the International Arthroscopy Association*, 21(1), pp.3–11.

Kennon, R., 2008. *Hip And Knee Surgery: A Patient's Guide to Hip Replacement, Hip Resurfacing, Knee Replacement, & Knee Arthroscopy*, Lulu.com.

Khurana, J.S., 2009. *Bone Pathology*, Springer.

Kim, T. et al., 2014. An in vitro comparative study of T2 and T2* mappings of human articular cartilage at 3-Tesla MRI using histology as the standard of reference. *Skeletal Radiology*, 43(7), pp.947–954.

Knahr, K., 2011. *Tribology in Total Hip Arthroplasty*, Springer.

Komistek, R.D. et al., 2005. Knee mechanics: a review of past and present techniques to determine in vivo loads. *Journal of biomechanics*, 38(2), pp.215–28.

Konrath, G.A. et al., 1998. The role of the acetabular labrum and the transverse acetabular ligament in load transmission in the hip. *The Journal of bone and joint surgery. American volume*, 80(12), pp.1781–8.

Lage, L. a, Patel, J. V & Villar, R.N., 1996. The acetabular labral tear: an arthroscopic classification. *Arthroscopy : the journal of arthroscopic & related surgery : official publication of the Arthroscopy Association of North America and the International Arthroscopy Association*, 12(3), pp.269–272.

Leunig, M. et al., 2005. Femoroacetabular Impingement: Etiology and Surgical Concept. *Operative Techniques in Orthopaedics*, 15(3), pp.247–255.

Leunig, M., Beaule, P.E. & Ganz, R., 2009. The concept of Femoroacetabular impingement: Current status and future perspectives. *Clinical Orthopaedics and Related Research*, 467(3), pp.616–622.

Lewis, C.L. & Sahrmann, S.A., 2006. Acetabular labral tears. *Physical therapy*, 86(1), pp.110–21.

Link, T.M., 2011. *Cartilage Imaging: Significance, Techniques, and New Developments*, Springer.

Little, C.J., Bawolin, N.K. & Chen, X., 2011. Mechanical properties of natural cartilage and tissue-engineered constructs. *Tissue engineering. Part B, Reviews*, 17(4), pp.213–27.

Lizhang, J. et al., 2013. Effect of clearance on cartilage tribology in hip hemi-arthroplasty. *Proc Inst Mech Eng H, J Engineering inMedicine*, 227(12), pp.1284–1291.

Lizhang, J., 2010. *Tribology of the hemiarthroplasty*. University of Leeds.

Lohe, F. et al., 1996. Structure, Strain and Function of the Transverse Acetabular Ligament. *Acta Anatomica*, 157, pp.315–323.

Lohmander, S., 1988. Proteoglycans of joint cartilage. *Baillière's Clinical Rheumatology*, 2(1), pp.37–62.

Loudon, J.K. et al., 2013. *Clinical Mechanics and Kinesiology*, Human Kinetics.

Lu, X.L. & Mow, V.C., 2008. Biomechanics of articular cartilage and determination of material properties. *Medicine and Science in Sports and Exercise*, 40(2), pp.193–199.

Mahoney, E. et al., 2000. The hardness and modulus of elasticity of primary molar teeth : an ultra-micro-indentation study. *Journal of Denistry*, 28(8), pp.589–594.

Manaster, B. & Zakel, S., 2006. Imaging of Femoral Acetabular Impingement Syndrome. *Clinics in sports medicine*, 25(4), pp.635–657.

Mansfield, J.C., Bell, J.S. & Winlove, C.P., 2015. The micromechanics of the superficial zone of articular cartilage. *Osteoarthritis and Cartilage*, 23(10), pp.1806–1816.

Maquet, P.G.J., 1985. *Biomechanics of the Hip*, Berlin, Heidelberg: Springer Berlin Heidelberg.

Martin, R.B., Burr, D.B. & Sharkey, N.A., 1998. *Skeletal Tissue Mechanics*, Springer.

McDermott, I., 2010. Acetabular labral tears. Available at: http://www.sportsortho.co.uk/left-navigation/conditions/hip/acetabular-labral-tears [Accessed November 24, 2012].

McGinnis, P.M., 2005. *Biomechanics Of Sport And Exercise*, Human Kinetics.

McGinty, J.B. et al., 2002. *Operative Arthroscopy*, Lippincott Williams & Wilkins.

Mechlenburg, I. et al., 2007. Cartilage thickness in the hip joint measured by MRI and stereology – a methodological study. *Osteoarthritis and Cartilage*, 15(4), pp.366–371.

Mellon, S.J. et al., 2011. The effect of motion patterns on edge-loading of metal-on-metal hip resurfacing. *Medical engineering & physics*, 33(10), pp.1212–20.

Miller, K.S. et al., 2012. Characterizing local collagen fiber re-alignment and crimp behavior throughout mechanical testing in a mature mouse supraspinatus tendon model. *Journal of Biomechanics*, 45(12), pp.2061–2065.

Mirzayan, R., 2006. *Cartilage Injury in the Athlete*, Thieme.

Monkhouse, W.S., 2007. *Master Medicine: Clinical Anatomy*, Elsevier Health Sciences.

Mononen, M.E. et al., 2012. Effect of superficial collagen patterns and fibrillation of femoral articular cartilage on knee joint mechanics-a 3D finite element analysis. *Journal of biomechanics*, 45(3), pp.579–87.

Morcuende, J.A. & Weinstein, S.L., 2002. Developmental dysplasia of the hip: natural history,

results of treatment, and controversies. *Oxford Univeristy Press*, pp.1–20. Available at: http://fds.oup.com/www.oup.com/pdf/13/9780192631619.pdf [Accessed November 24, 2012].

Mow, V.C. et al., 1998. Effects of fixed charges on the stress–relaxation behavior of hydrated soft tissues in a confined compression problem. *International Journal of Solids and Structures*, 35(34-35), pp.4945–4962.

Mow, V.C. & Huiskes, R., 2004. *Basic Orthopaedic Biomechanics and Mechano-Biology*, Lippincott Williams & Wilkins.

Müller-Gerbl, M., Schulte, E. & Putz, R., 1987. The thickness of the calcified layer of articular cartilage: a function of the load supported? *Journal of anatomy*, 154, pp.103–11.

Naal, F.D. et al., 2011. Surgical hip dislocation for the treatment of femoroacetabular impingement in high-level athletes. *The American journal of sports medicine*, 39(3), pp.544–50.

Narayan, R., 2009. *Biomedical Materials*, Springer.

Narvani, A.A., 2003. Acetabular labrum and its tears. *British Journal of Sports Medicine*, 37(3), pp.207–211.

Ng, B.H., Chou, S.M. & Krishna, V., 2005. The Influence of Gripping Techniques on the Tensile Properties of Tendons. *Proceedings of the Institution of Mechanical Engineers, Part H: Journal of Engineering in Medicine*, 219(5), pp.349–354.

Nissi, M., 2008. *Magnetic Resonance Parameters in Quantitative Evaluation of Articular Cartilage*. Kuopio.

Nordin, M. & Frankel, V.H., 2001. *Basic Biomechanics of the Musculoskeletal System*, Lippincott Williams & Wilkins.

O'Hara, B.P., Urban, J.P. & Maroudas, A., 1990. Influence of cyclic loading ion the nutrition of articular cartilage. *Annals of the Rheumatic Diseases*, 49(7), pp.536–539.

Oatis, C.A. & Mansour, J., 2009. *Kinesiology The mechanics & pathomechanics of human movement* 2nd ed. E. J. Lupash & A. M. Klingler, eds., Glenside, Pennsylvania: Lippincott Williams & Wilkins.

OpenStax College, 2013. Multiaxial Joint. Available at: http://cnx.org/content/m46383/latest/ [Accessed July 24, 2013].

Ottenbrite, R.M., Park, K. & Okano, T., 2010. *Biomedical Applications of Hydrogels Handbook*, Springer.

Owen, G.R., Kaab, M. & Ito, K., 1999. Scanning Electron Microscopy Examination of Collagen Network Morphology At the Cartilage , Labrum , and Bone Interfaces in the Acetabulum. *Scanning Microscopy*, 13(1), pp.83–91.

Parvizi, J. et al., 2006. Management of arthritis of the hip in the young adult. *The Journal of bone and joint surgery. British volume*, 88(10), pp.1279–85.

Parvizi, J., Rothman, R.H. & Wiesel, S.W., 2012. *Operative Techniques in Adult Reconstruction Surgery*, Lippincott Williams & Wilkins.

Patient.co.uk, 2012. Patient.co.uk. Available at: http://www.patient.co.uk/editorial_disclaimer.asp [Accessed November 24, 2012].

Paul, J.P., 1976. Force actions transmitted by joints in the human body. *Proceedings of the*

Royal Society of London. Series B, Containing papers of a Biological character. Royal Society (Great Britain), 192(1107), pp.163–72.

Paul, J.P., 1966. Section of Orthopsedics Biomechanics. *Section of Orthopaedics*, 59, pp.31–36.

Pereira, H. et al., 2013. The meniscus: Basic science. In *Meniscal Transplantation*.

Petersen, W., Petersen, F. & Tillmann, B., 2003. Structure and vascularization of the acetabular labrum with regard to the pathogenesis and healing of labral lesions. *Archives of orthopaedic and trauma surgery*, 123(6), pp.283–8.

Philippon, M.J. et al., 2007. Clinical presentation of femoroacetabular impingement. *Knee surgery, sports traumatology, arthroscopy : official journal of the ESSKA*, 15(8), pp.1041–7.

Philippon, M.J. et al., 2014. The hip fluid seal-Part I: The effect of an acetabular labral tear, repair, resection, and reconstruction on hip fluid pressurization. *Knee Surgery, Sports Traumatology, Arthroscopy*, 22(4), pp.722–729.

Pierannunzii, L. & D'ImporzanoMarco, 2007. Treatment of femoracetabular impingement: a modified resetion osteoplasty technique through an anterior approach. *Healio Othopedics*, 30(2), pp.96–102.

Proctor, C.S. et al., 1989. Material properties of the normal medial bovine meniscus. *Journal of orthopaedic research : official publication of the Orthopaedic Research Society*, 7(6), pp.771–782.

Radin, E.L., 1980. Biomechanics of the Human Hip. *Clinical Orthopaedics and Related Research*, 152(152), pp.28–34.

Reddy, G.K. & Enwemeka, C.S., 1996. A simplified method for the analysis of hydroxyproline in biological tissues. *Clinical biochemistry*, 29(3), pp.225–229.

Reinwald, S. & Burr, D., 2008. Review of nonprimate, large animal models for osteoporosis research. *Journal of bone and mineral research : the official journal of the American Society for Bone and Mineral Research*, 23(9), pp.1353–68.

Robinson, P., 2010. *Essential Radiology for Sports Medicine*, Springer.

Rolauffs, B. et al., 2008. Distinct horizontal patterns in the spatial organization of superficial zone chondrocytes of human joints. *Journal of structural biology*, 162(2), pp.335–44.

Rolauffs, B. et al., 2010. Proliferative remodeling of the spatial organization of human superficial chondrocytes distant from focal early osteoarthritis. *Arthritis and rheumatism*, 62(2), pp.489–98.

Roughley, P.J. & White, R.J., 1980. Age-related changes in the structure of the proteoglycan subunits from human articular cartilage. *The Journal of biological chemistry*, 255(1), pp.217–224.

Rydell, N., 1973. Biomechanics of the hip-joint. *Clinical Orthopadedics*, 92, pp.6–15.

Safran, M.R. et al., 2011. Strains across the acetabular labrum during hip motion: a cadaveric model. *The American journal of sports medicine*, 39(Suppl), pp.92–102.

Saikko, V. et al., 2001. Wear simulation of total hip prostheses with polyethylene against CoCr, alumina and diamond-like carbon. *Biomaterials*, 22, pp.1507–1514.

Schenke-Layland, K., 2008. Non-invasive multiphoton imaging of extracellular matrix structures. *Journal of Biophotonics*, 1(6), pp.451–462.

Scholes, S.C., Green, S.M. & Unsworth, A., 2001. The wear of metal-on-metal total hip prostheses measured in a hip simulator. *Proceedings of the Institution of Mechanical Engineers. Part H, Journal of engineering in medicine*, 215(H), pp.523–530. Available at: http://pih.sagepub.com/lookup/doi/10.1243/0954411011536118.

Seibel, M.J., 2006. *Dynamics of Bone And Cartilage Metabolism*, Academic Press.

Seldes, R.M. et al., 2001. Anatomy, histologic features, and vascularity of the adult acetabular labrum. *Clinical orthopaedics and related research*, 382, pp.232–240.

Shapiro, F., 2002. *Pediatric Orthopedic Deformities*, Gulf Professional Publishing.

Shibutani, N., 1988. Three-dimensional architecture of the acetabular labrum--a scanning electron microscopic study. *Nihon Seikeigeka Gakkai zasshi*, 62(4), pp.321–9.

Singh, H. & Neutze, J.A., 2011. *Radiology Fundamentals: Introduction to Imaging & Technology*, Springer.

Smith, C.D. et al., 2008. Tensile properties of the human glenoid labrum. *Journal of Anatomy*, 212(1), pp.49–54.

Smith, M. V et al., 2011. Effect of acetabular labrum tears on hip stability and labral strain in a joint compression model. *The American journal of sports medicine*, 39, p.103.

Smith, S., 2012. *Act now, move now, demand more!*, Available at: http://www.arthritiscare.org.uk/LivingwithArthritis/oanation-2012.

Song, Y. et al., 2012. Articular cartilage friction increases in hip joints after the removal of acetabular labrum. *Journal of Biomechanics*, 45(3), pp.524–530.

Speer, K.P., 2005. *Injury Prevention and Rehabilitation for Active Older Adults*, Champaign: Sheridan Books.

Stewart, T.D. & Hall, R.M., 2006. (iv) Basic biomechanics of human joints : Hips , knees and the spine. *Current Orthopaedics*, 20, pp.23–31.

Stockwell, R. a., 1967. The cell density of human articular and costal cartilage. *Journal of anatomy*, 101(Pt 4), pp.753–763.

Stockwell, R.A., 1979. *Biology of Cartilage Cells*, CUP Archive.

Talmage, J.B., 2009. Hip Dysplasia - Medical Disability Guidelines. Available at: http://www.mdguidelines.com/hip-dysplasia [Accessed November 24, 2012].

Taylor, C., 2013. *Development and characterisation of mechanical and enzymatic models of cartilage degeneration*. University of Leeds.

Taylor, S.D. et al., 2011. Comparison of human and animal femoral head chondral properties and geometries. *Proceedings of the Institution of Mechanical Engineers, Part H: Journal of Engineering in Medicine*, 226(1), pp.55–62.

Tissakht, M. & Ahmed, A.M., 1995. Tensile stress-strain characteristics of the human meniscal material. *Journal of Biomechanics*, 28(4), pp.411–422.

Van-Arkel, R.J. et al., 2015. The capsular ligaments provide more hip rotational restraint than the acetabular labrum and the ligamentum teres: An experimental study. *Bone and Joint Journal*, 97(B), pp.484–491.

Verzijl, N. et al., 2002. Crosslinking by Advanced Glycation End Products Increases the Stiffness of the Collagen Network in Human Articular Cartilage. *Arthritis and*

rheumatism, 46(1), pp.114–123.

Whiting, W.C., Ph.D. & Rugg, S., 2006. *Dynatomy: Dynamic Human Anatomy, Volume 10*, Human Kinetics.

Whiting, W.C. & Zernicke, R.F., 2008. *Biomechanics Of Musculoskeletal Injury*, Human Kinetics.

Williamson, A.K. et al., 2003. Tensile mechanical properties of bovine articular cartilage: Variations with growth and relationships to collagen network components. *Journal of Orthopaedic Research*, 21, pp.872–880.

Yanagishita, M., 1993. Function of proteoglycans in the extracellular matrix. *Acta pathologica japonica*, 43(6), pp.283–93.

Yannas, L. V, 2005. *Regenerative Medicine II: Clinical and Preclinical Applications*, Springer.

Zamir, E.A. & Taber, L.A., 2004. On the effects of residual stress in microindentation tests of soft tissue structures. *Journal of Biomechanical Engineering*, 126(2), pp.276–283.

Zhang, D. et al., 2012. Lubricin Distribution in the Menisci and Labra of Human Osteoarthritic Joints. *Cartilage*, 3(2), pp.165–172.

Zhang, Y. et al., 2012. Analysis of the mineral composition of the human calcified cartilage zone. *International journal of medical sciences*, 9(5), pp.353–60.

Zhu, W. et al., 1993. Viscoelastic shear properties of articular cartilage and the effects of glycosidase treatments. *Journal of orthopaedic research : official publication of the Orthopaedic Research Society*, 11(6), pp.771–81.